Exploring the role of $CD8^+$ T-cells in Chronic Lymphocytic Leukaemia

Lauren K. Elston

Division of Cancer and Genetics
School of Medicine
Cardiff University

Supervisors: Dr. Stephen Man
Prof. Chris Pepper

A dissertation submitted to Cardiff University in candidature for the degree of Doctor of Philosophy

December 2016

DECLARATION

This work has not been submitted in substance for any other degree or award at this or any other university or place of learning, nor is being submitted concurrently in candidature for any degree or other award.

Signed ……(candidate) Date……..

STATEMENT 1

This thesis is being submitted in partial fulfilment of the requirements for the degree of ……(insert MCh, MD, MPhil, PhD etc., as appropriate)

Signed ……(candidate) Date……..

STATEMENT 2

This thesis is the result of my own independent work/investigation, except where otherwise stated, and the thesis has not been edited by a third party beyond what is permitted by Cardiff University's Policy on the Use of Third Party Editors by Research Degree Students. Other sources are acknowledged by explicit references. The views expressed are my own.

Signed ……(candidate) Date……..

STATEMENT 3

I hereby give consent for my thesis, if accepted, to be available online in the University's Open Access repository and for inter-library loan, and for the title and summary to be made available to outside organisations.

Signed ……(candidate) Date……..

STATEMENT 4: PREVIOUSLY APPROVED BAR ON ACCESS

I hereby give consent for my thesis, if accepted, to be available online in the University's Open Access repository and for inter-library loans after expiry of a bar on access previously approved by the Academic Standards & Quality Committee.

Signed ……(candidate) Date……..

Acknowledgements

Firstly I would like to thank both of my supervisors, Dr. Steve Man and Prof. Chris Pepper, both for giving me the opportunity to undertake this project, and for their continuous guidance and support throughout.

I would also like to thank Prof. Chris Fegan for providing CLL patient blood samples in addition to giving essential advice and information on treated patient samples. I am also grateful to Dr Ceri Jones and Dr Guy Pratt for providing additional CLL samples, and anyone in the department who donated blood for the cause. Without these samples, this project would not have been possible. My thanks and appreciation go to Prof. Duncan Baird, Dr. Rhiannon Robinson and the rest of the STELA group for patiently teaching me the way of the telomere.

I want to extend my gratitude to everyone in the lab for their advice and support throughout my project, in particular Sophie, Rosária, Julia and Marie for making me feel so welcome when I first joined the team and providing constant laughter and emotional support. An especially big thank you to Mel for her kindred companionship, I could not have asked for a greater friend to spend the latter half of my PhD with.

Thank you to all my family and friends for always being there to offer words of encouragement and providing fun distractions when they were very much needed. I am particularly grateful for the support of my Mum, who has always been there with her hugs and words of wisdom throughout my life and even traversed across the borders to visit me during my writing lockdown.

Finally I would like to thank my dear husband Matt for joining me on this perilous journey of pitfalls and successes, for carrying me when I felt I could go no further and for providing the endless cups of tea to help me through the thesis writing. None of this would have been possible without you.

This research was funded by Cancer Research Wales.

Abstract

Although chronic lymphocytic leukaemia (CLL) is a B-cell malignancy, T-cells from CLL patients often display abnormal characteristics when compared to age-matched healthy donors. One example is the preferential expansion of $CD8^+$ T-cells within a subgroup of CLL patients resulting in an inverted CD4:CD8 ratio (CLL^{IR}). This thesis describes a detailed analysis of the T-cell compartment with an emphasis on $CD8^+$ T-cells. It confirms that CLL patients have abnormal memory T-cell subset distributions, with skewing to more differentiated memory subsets (EM/EMRA $CD8^+$ T-cells) and an increase in a replicative senescent phenotype ($CD57^+$). Furthermore, CLL^{IR} patients demonstrated significantly inferior prognosis compared to their normal ratio counterparts (CLL^{NR}). The aim of this thesis was to further characterise the expanded $CD8^+$ T-cells within the CLL^{IR} subgroup to define more precise prognostic markers and to understand the role of these T-cells in CLL disease.

Polychromatic phenotyping of CLL patients (n = 99) was carried out using 8-colour flow cytometry, testing for markers associated with senescence (CD57/KLRG-1), exhaustion (PD-1) and activation (HLA-DR/CD38). This allowed the identification of multiple discrete subsets of T-cells, with a greater complexity of subsets seen in CLL patients compared to healthy donors. There was also an increase in senescent phenotypes within CLL^{IR} patients, confirming previous results. However, the use of additional markers identified increased frequencies of an 'activated senescent' phenotype ($CD8^+CD57^+HLA\text{-}DR^+$) within CLL^{IR} patients. This phenotype was shown to have a prognostic effect on progression-free survival in both multivariate and univariate analysis, with higher frequencies conferring inferior prognosis.

Multivariate analyses also revealed $CD4^+$ subsets, including those with a $CD4^+HLA\text{-}DR^+PD\text{-}1^+$ phenotype, to be of prognostic value. This prompted a phenotypic assessment of the $CD4^+$ T-cell compartment. Like the $CD8^+$ population, $CD4^+$ T-cells showed increased frequencies of senescent phenotypes within CLL^{IR} patients. There was also an exacerbation of $CD57^+HLA\text{-}DR^+$ and $HLA\text{-}DR^+PD\text{-}1^+$ phenotypes within the CLL^{IR} subgroup, the latter being the strongest prognostic phenotype identified by multivariate analysis within the entire study.

To further evaluate the prognostic potential and stability of the CD4:CD8 ratio in CLL, preliminary phenotypic analysis was performed on a small cohort of treated and untreated patients. These results showed a disproportionate number of patients with inverted ratio in the treated patient group. Furthermore, the prognostic phenotypes $CD8^+CD57^+HLA\text{-}DR^+$ and $CD4^+HLA\text{-}DR^+PD\text{-}1^+$ were over represented within the treated subgroup.

Finally, single telomere length analysis (STELA) of $CD8^+$ T-cells in CLL was performed to explore potential changes in the replicative history between CLL^{NR} and CLL^{IR} patients. Overall, the mean telomere lengths of T-cells from CLL^{IR} patients was similar to that of CLL^{NR} patients, suggesting that the expanded $CD8^+$ compartment does not necessarily arise from a long-lived population that has undergone multiple rounds of division. The STELA did reveal two additional subgroups of CLL patients that had either “short” or “long” telomeres within their T-cell memory subsets. This observation may provide an additional molecular marker that could be investigated either in combination or alone for prognostic relevance.

Overall the results from the phenotypic analysis and STELA suggest that there is an active ongoing T-cell response in CLL, but the nature of the stimulus is unclear. The expanded T-cells in CLL are unusual and do not follow the patterns of T-cell exhaustion and senescence seen in chronic viral diseases and other cancers. Importantly, this study has defined two phenotypes ($CD8^+CD57^+HLA\text{-}DR^+$ and $CD4^+HLA\text{-}DR^+PD\text{-}1^+$) that have greater prognostic power than the inverted CD4:CD8 ratio. These may be useful in identifying patients who are likely to develop more aggressive clinical disease.

Contents

Abbreviations

ADCC	Antibody dependent cell-mediated cytotoxicity
APC	Antigen presenting cell
BCL-2	B-cell lymphoma 2
BCR	B-cell receptor
BSA	Bovine serum albumin
CARs	Chimeric antigen receptors
CD	Cluster of differentiation
CD40L	CD40 ligand
CLL	Chronic lymphocytic leukaemia
CLLIR	CLL inverted ratio patient
CLLNR	CLL normal ratio patient
CM	Central memory (T-cells)
CMV	Cytomegalovirus
CSR	Class switch recombination
CTL	Cytotoxic T-lymphocytes
DC	Dendritic cell
DMSO	Dimethyl sulfoxide
DN	Double negative (cells)
DP	Double positive (cells)
EBV	Epstein-Barr virus
EDTA	Ethylenediaminetetraacetic acid
EM	Effector memory (T-cells)
EMRA	Effector memory CD45RA+ (T-cells)
FACS	Fluorescence-activated cell sorting
FC	Fludarabine and cyclophosphomide
FCR	Fludarabine, cyclophosphomide and rituximab
Foxp3	Forkhead Box P3
HD	Healthy donor
HIV	Human immunodeficiency virus
IFN-γ	Interferon gamma
Ig	Immunoglobulin
IGHV	Immunoglobulin heavy chain variable region
IL	Interleukin
IL7Rα	Interleukin-7 receptor α
KLRG-1	Killer cell lectin-like receptor 1
LPS	Lipopolysaccharides
mAbs	Monoclonal antibodies
MACS	Magnetic-activated cell sorting
MHC	Major histocompatibility complex
MPEC	Memory precursor effector cell
NETs	Neutrophil extracellular traps
NF-κB	Nuclear Factor-κB
NK cells	Natural killer cells
NKT cells	Natural killer T-cells

PAMPs	Pathogen-associated molecular patterns
PBMC	Peripheral blood mononuclear cells
PBS	Phosphate buffer saline
PD-1	Programmed cell death receptor 1
PFA	Paraformaldehyde
PFS	Progression-free survival
PRRs	Pattern recognition receptors
RER	Rough endoplasmic reticulum
RPMI	Roswell Park Memorial Institute
SHM	Somatic hypermutation
SLEC	Short-lived effector cell
SP	Single positive (cells)
STELA	Single telomere length analysis
TCR	T-cell receptor
Tfh cell	T follicular helper cells
TGF	Transforming growth factor
Th cell	T helper cell
TILs	Tumour infiltrating lymphocytes
TLRs	Toll-like receptors
TNF	Tumour necrosis factor
Treg	Regulatory T-cell
Tscm	Stem cell memory T-cell
TTFT	Time to first treatment
Zap-70	Zeta-associated protein 70

Figures

Tables

Chapter 1
Introduction

1.1 The immune system

The immune system is a complex system of proteins, cells and organs that defend the host against pathogens. This primarily targets foreign pathogens such as viruses, bacteria and parasites, but the immune system can also play a role in non-infectious diseases such as cancer (Wood 2006; Dunn et al. 2004; Dranoff 2004). The immune system's response is usually categorised into two types: the innate immune response and the adaptive immune response (Figure 1.1). The innate response refers to pre-existing immunological mechanisms that are present in the host system prior to infection that can recognise common components that belong to pathogens. The adaptive response follows on from the innate and specifically targets pathogens to resolve infection (Kindt et al. 2007; Janeway et al. 2001; Dranoff 2004).

1.1.1 Innate immunity

A human host's primary defence against external pathogens are the physical barriers of the body, such as the skin epithelium, cilia and mucosal membranes (Kindt et al. 2007). There are also biochemical immune barriers: hydrochloric acid is secreted by the stomach; lysozyme, an enzyme found in bodily secretions such as sweat and tears and can break down bacterial walls; skin and mucosa secretions contain antimicrobial peptides e.g. defensins (Wood 2006; Kindt et al. 2007; Schauber and Gallo 2009).

If physical and biochemical barriers are unsuccessful, invading foreign pathogens or damaged/infected host cells are recognised by specialised immune cells. Specialised innate immune cells can recognise foreign pathogen associated molecules that are conserved across many pathogens, known as pathogen-associated molecular patterns (PAMPs). Innate immune cells recognise these PAMPs via pattern recognition receptors (PRRs), such as Toll-like receptors (TLRs)(Kindt et al. 2007; Wood 2006; Iwasaki and Medzhitov 2015). Various TLRs have been defined that can recognise pathogen products, one example being the Toll-like receptor 4 (TLR4), which recognises the lipopolysaccharides (LPS) found in gram-negative bacterial cell walls (Pålsson-McDermott and O'Neill 2004; Chow et al. 1999). Recognition leads these innate immune cells to initiate various downstream immunological processes, including:

phagocytosis of foreign/damaged bodies, induction of the complement system, production of immunological products such as chemokines and cytokines, mediated activation of the innate inflammatory response and, if the innate immune response fails to resolve the infection, recruitment of the adaptive immune response (Wood 2006; Kindt et al. 2007; Iwasaki and Medzhitov 2015). Examples of innate immune cells are discussed further below.

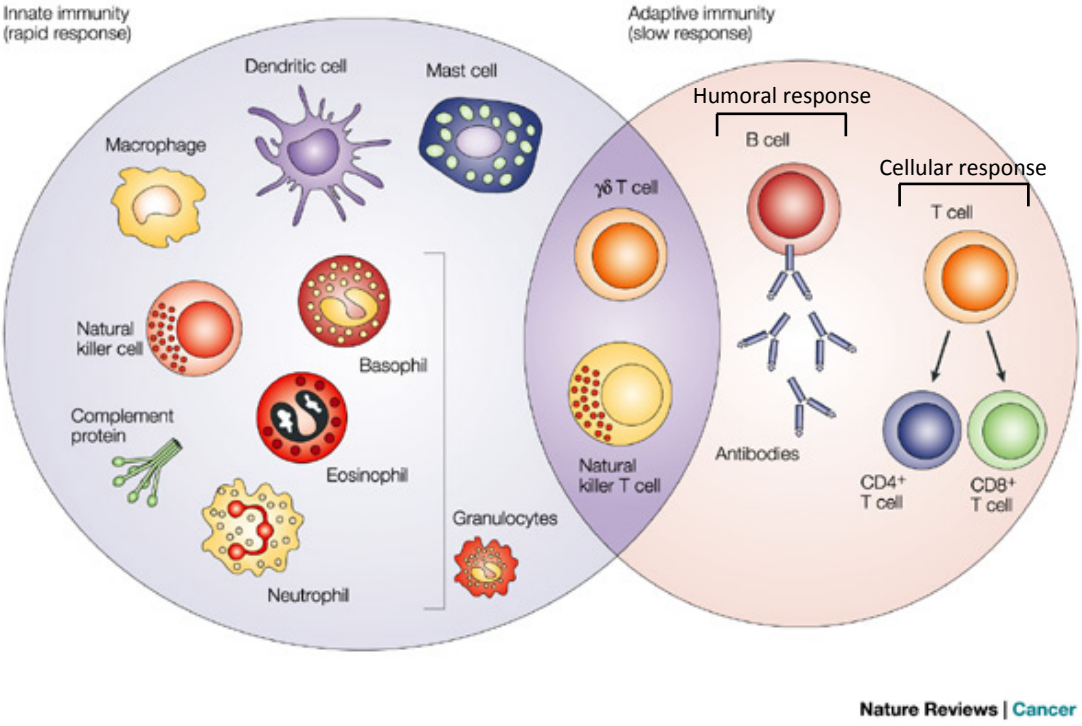

Figure 1.1. The components of the innate and adaptive immune response. The immune response can be divided into two main components. The innate response acts as the non-specific first line of defence against pathogens. The adaptive response is a later response following lack of pathogen clearance by the innate system; adaptive components are more antigen-specific and form the basis of immunological memory (adapted from Dranoff (2004)).

1.1.1.1 Neutrophils and other granulocytes

Neutrophils are bone marrow-derived granulocytic cells that circulate in the blood stream for approximately 5.4 days before migrating into tissue sites following extravasation (Pillay et al. 2010). Neutrophils are the first innate cells to be recruited to the site of infection via the secretion of chemoattractants including the cytokine IL-8 (Hammond et al. 1995). During extravasation, the neutrophil 'rolls' along and adheres to the vascular endothelium, before transmigrating between the endothelial cells and basement membrane and into the tissue towards the site of infection (Kindt et al. 2007; Wood 2006; Kolaczkowska and Kubes 2013; Janeway et al. 2001).

The predominant function of the neutrophil is the ingestion (phagocytosis) and killing of pathogens, particularly bacteria and viruses. Direct recognition of the pathogen (e.g. with TLRs) leads to extensions of the neutrophil cell membrane (pseudopodia) that surround and engulf the microorganism into a phagosome (Kindt et al. 2007; Wood 2006). Once engulfed, the neutrophils kill the pathogen by releasing anti-bacterial proteins and lytic enzymes from neutrophil granules into the lysosome. Alternatively, neutrophils kill phagocytosed microbes by producing reactive oxygen and reactive nitrogen species and/or antibacterial proteins (Wood 2006; Kolaczkowska and Kubes 2013).

In addition to phagocytosis, neutrophils can also aid the elimination of pathogens by degranulation, whereby the granular products that are used to kill phagocytosed pathogens are released into the extracellular environment to tackle extracellular pathogens (Kolaczkowska and Kubes 2013). A third, more recently described method is the employment of Neutrophil Extracellular Traps (NETs) by activated neutrophils: nuclear products with granular and cytoplasmic proteins are released by neutrophils to bind and kill extracellular pathogens (Wartha et al. 2007). Therefore, neutrophils play a key role in limiting the spread of infection.

1.1.1.2 Macrophages

Monocytes are derived from the haematopoietic lineage and are produced in the bone marrow. Upon migration from the blood stream into various tissues monocytes develop into either tissue-specific macrophages or dendritic cells (DCs) (Murray and Wynn 2011; Kindt et al. 2007). Once primed, macrophages have increased phagocytic activity in a similar way to neutrophils (Kindt et al. 2007). However, where neutrophils are

limited to ingesting smaller pathogens such as bacteria and viruses, macrophages can phagocytose much larger products, including dead cells and tissue debris. They are therefore not only able to aid in the elimination of the pathogen, but also play a role in removing the dead/dying cells and maintaining healthy tissue environments (Wood 2006; Murray and Wynn 2011).

Macrophages can also secrete complement proteins and Fc receptors that bind to pathogens and act as opsinins to enhance phagocytic activity (Murray and Wynn 2011). Opsinisation of the pathogen, where complement proteins or antibodies are attached to the pathogen to enhance recognition and binding, can boost the phagocytic activity of neutrophils, macrophage and other phagocytes, in addition to the B- and T-cells of the adaptive response (Carroll 2004): when the opsinin is an antibody this is known as antibody-dependent cell-mediated cytotoxicity (ADCC) (Wood 2006).

Activated macrophages at the site of an infection can also secrete various inflammatory factors that initiate the inflammatory response, such as the cytokines IL-1, tumour necrosis factor-α (TNF-α) and IL-6 (Nackiewicz et al. 2014; Murray and Wynn 2011). This leads to increased vascular permeability and activation of endothelial cells that upregulate adhesion molecules, leading to recruitment of more phagocytic cells to the site of infection, such as neutrophils. Vascular permeability also allows entry of further immune factors such as complement serum proteins. Furthermore, activated macrophages can bridge the innate and adaptive immune responses by presenting ingested antigenic peptides to T-cells (Kindt et al. 2007; Murray and Wynn 2011; Wood 2006).

Depending on tissue locality, microenvironment stimuli and phenotypic function, macrophages can be split into distinct subpopulations (Gordon and Taylor 2005; Shi and Pamer 2011; Martinez and Gordon 2014). Further to this, they are divided into subsets based on their polarisation upon activation. M1 macrophages are considered to be 'classically' activated by PAMPs and/or interferon-γ (IFN-γ) and play an immunological role against pathogens, as well as demonstrating anti-tumour immunity (Murray and Wynn 2011; Mantovani et al. 2004). M2 macrophages are 'alternatively' activated and play a role in immune regulation and tumour promotion. The current literature now suggests M2 can be subdivided further based on their inducible factors and functional properties (Martinez and Gordon 2014; Mantovani et al. 2004).

1.1.1.3 Natural Killer (NK) cells

The innate natural killer (NK) cells were first identified as lymphocytes displaying cytotoxicity to tumour cells (Wood 2006; Vivier et al. 2008). They play an important role in the non-specific recognition and destruction of infected host cells and are considered the first-line of defence against viral infections (Kindt et al. 2007). NK cells display various inhibitory and activating receptors that allow them to distinguish between target and non-target cells (Cerwenka and Lanier 2001). Additionally, NK cells can recognise target cells through ADCC with their CD16 receptor (Vivier et al. 2008). When recruited to inflammatory sites, NK cells are stimulated by other immune cells including macrophages and T-cells via IFNs, IL-12, IL-18, IL-15 and IL-2 (Vivier et al. 2008). NK-mediated killing can occur via Fas ligand (FasL) induced cell death, or by degranulation of cytotoxic proteins upon binding to the target cell to trigger apoptosis (Wallin et al. 2003; Kindt et al. 2007). Activated NK cells produce important cytokines including IFN-γ and TNF-α: as IFN-γ is an activating cytokine for M1 macrophages, this enables NK cells and macrophages to establish a constant activation loop during the inflammatory immune response (Wood 2006). Furthermore, both IFN-γ and TNF-α can stimulate maturation of DCs.

1.1.1.4 Dendritic cells (DCs)

DCs bridge the innate and adaptive immune responses due to their phagocytic activity during the innate stage and priming of T-cells in the adaptive response. DCs phagocytose pathogens, but they do not demonstrate the killing and digestive functions observed in macrophage and neutrophils (Steinman and Hemmi 2006). DCs instead process and present antigenic fragments on MHC class-I and MHC class-II complexes to T-cells. In this way, they act as innate sentinels within the body. DCs are also able to promote innate and adaptive cells by the production of various cytokines, including IL-12, an NK cell enhancing cytokine (Steinman and Hemmi 2006; Ferlazzo et al. 2004).

1.1.1.5 Eosinophils, basophils and mast cells

Like neutrophils, eosinophils and basophils are granulocytic cells. Eosinophils are also phagocytes, although their phagocytic activity is less prominent than that of neutrophils, whereas basophils are non-phagocytic (Kindt et al. 2007). Mast cells have similar properties and possess granules containing immunological factors. Upon activation, mast cells undergo degranulation and release histamine, heparin and proteolytic

enzymes, as well as produce various prostaglandins and leukotrienes (Marshall 2004). All these factors increase vasodilation and vascular permeability, as well as initiate recruitment of other cells such as neutrophils (Wood 2006). Where mast cells are located in either mucosal or connective tissues, eosinophils and basophils circulate in the blood and are recruited to specific locations upon infection (Medzhitov 2007).

These innate cells are all thought to play key roles in the resolution of parasitic infections (Medzhitov 2007; Meeusen and Balic 2000). Eosinophils have demonstrated anti-parasitic action *in vivo* via ADCC killing of helminth worms (Wood 2006; Kindt et al. 2007). Mast cells, eosinophils and basophils have also been considered prominent players in the allergic reaction (Wardlaw et al. 2000; Kindt et al. 2007).

1.1.2 The bridge between innate and adaptive immunity

If the innate response is unable to resolve pathogenic infection/tissue damage, the more specific adaptive immune response is launched. The innate and adaptive responses are highly interlinked. Innate recognition of a pathogen allows for a more effective adaptive immune response, as the innate immune response produces many immunological molecules that aid in the recruitment and activation of adaptive immune cells (Kindt et al. 2007).

As mentioned in Section 1.1.1.4, DCs bridge the innate and adaptive responses via their ability to ingest pathogens, migrate to the peripheral lymph nodes and present antigenic peptides alongside co-stimulatory molecules to activate naive T-cells (Steinman and Hemmi 2006). Furthermore, many DC subpopulations have been identified with different immunological properties that help determine the type of adaptive response (Iwasaki and Medzhitov 2015). In humans, the major $CD1c^+$ DC population express a wide variety of PRRs, including TLRs and lectins. $CD1c^+$ DCs play a key role in the promoting the T helper type 1 response against intracellular pathogens via the secretion of TNF-α, IL-8, IL-10, and IL-12 (Collin et al. 2013; Mittag et al. 2011). They have also been shown to produce IL-23, a key Th17 cytokine (Dillon et al. 2010). This implies $CD1c^+$ DCs help direct the adaptive immune response against intracellular pathogens (Th1 response) and extracellular pathogens such as fungi (Th17 response); interestingly, despite promoting $CD4^+$ Th1 cells, $CD1c^+$ DCs show poor cross-presentation to $CD8^+$ T-cells compared to other DC subsets (Collin et al. 2013). Alternatively, a second, smaller $CD141^+$ DC population possess enhanced phagocytosis

of dead cells, recognition of viral nucleic acids (via TLR3 and TLR8 receptors) and superior cross-presentation to $CD8^+$ T-cells (Joffre et al. 2012; Sancho et al. 2009). Langerhans cells, located in the epidermis, have been shown to secrete cytokines associated with the T helper type 2 response, thereby directing a humoral adaptive response (Iwasaki and Medzhitov 2015).

Similar to DCs, macrophages are also able to present antigen to adaptive immune cells (Murray and Wynn 2011), and the aforementioned M1 and M2 subsets promote certain adaptive responses. M1 macrophages promote the Th1 response and cellular immunity, whereas M2 macrophages help promote the Th2/humoral response (Mills 2015). In the same sense, adaptive immune cells such as T-cells can produce cytokines to promote further innate cell activation, such as macrophage activation, completing an innate-adaptive immune response loop.

1.1.3 Adaptive immunity

Where the innate system distinguishes between 'self' and 'non-self' to instigate immediate non-specific responses against foreign bodies, the adaptive immune response is the generation of highly specific lymphocytes generated against the pathogenic antigens (Kindt et al. 2007). The primary cells of the adaptive response are B-cells, which play a central role in the humoral immune response, and T-cells that initiate cell-mediated immunity, in addition to aiding the activation of the B-cell humoral response.

1.1.3.1 B-cells and humoral immunity

B-cell progenitors (pro-B-cells) arise in the bone marrow by commitment of the common lymphoid progenitor to the B-cell lineage via expression of the transcription factor Pax5 (Cobaleda et al. 2007). Consequently, pro-B-cells undergo multiple proliferation and differentiation steps within the bone marrow microenvironment to develop into precursor B-cells (pre-B-cells) and then the immature B-cell (Hoffman et al. 2016; Thomas et al. 2006). Immature B-cells are then released from the bone marrow into the periphery and home to the spleen to undergo further maturation steps and differentiate into marginal zone B-cells and follicular B-cells (Hoffman et al. 2016; Pillai and Cariappa 2009). Marginal zone B-cells remain in the spleen, whereas follicular B-cells circulate in peripheral lymphoid tissues.

During the development from pro-B-cell to immature B-cell, multiple immunoglobulin heavy- and light- chain gene rearrangements occur that are essential for B-cell development, resulting in the presentation of a mature IgM B-cell receptor (BCR), a membrane-bound antibody molecule on the B-cell surface for antigen recognition (Hoffman et al. 2016; Thomas et al. 2006) (Figure 1.2A). This rearrangement process allows for the random generation of a varied BCR repertoire that can recognise a large range of antigens, including self-antigens; therefore, to prevent self-reactive B-cells leaving the bone marrow, immature B-cells undergo negative selection for self-antigen and clonal deletion. Upon entering the periphery and maturing, B-cells express both IgM and IgD on their cell surface (Hoffman et al. 2016).

Activation and differentiation of B-cells are dependent upon the antigen type recognised by the BCR (signal 1) followed by co-stimulation (signal 2) and the cytokine microenvironment (Figure 1.2B). Canonical activation for the majority of BCR antigens requires the presence of helper T-cell (Th cell) co-stimulation (T-dependant) through receptor/ligand stimulus such as the CD40/CD40L axis, and stimulatory cytokines such as IL-4, IFN-γ and IL-21. Upon antigen recognition the B-cell ingests and processes antigenic material for MHC-II presentation to $CD4^+$ T-cells, and in this way acts as an APC similar to DCs and macrophages (Hoffman et al. 2016; Nutt et al. 2015). Activated B-cells upregulate MHC-II alongside co-stimulatory molecules CD80 and CD86, enhancing B-cell promotion of Th cell activation by the formation of the T-B link, the so-called immune synapse (Hoffman et al. 2016; Suvas et al. 2002). This in turn triggers upregulation of co-stimulatory CD40L on Th cells, as well as the production of Th cytokines to promote further B-cell activation, proliferation and differentiation.

Following BCR engagement, B-cells migrate to the germinal centres of secondary lymphoid organs to form the T-B link and undergo rapid proliferation and differentiation. During this time, further genetic rearrangements of the Ig heavy- and light chains occur to allow for affinity maturation of the antibody. Somatic hypermutation (SHM) of the heavy- and light-variable region rapidly generates a wide variety of high affinity antigen binding sites, and class switch recombination (CSR) generates other antibody isotypes (IgG, IgE, IgA) that can initiate different immunological responses. In combination, SHM and CSR produce high affinity antigen-specific antibodies with a range of specificities and isotypes to trigger various immunological reactions (Z. Li et al. 2004; Hoffman et al. 2016).

Following affinity-based positive selection, B-cells differentiate into memory B-cells or plasma cells (effector B-cells). Plasma cells have low levels of membrane bound antibody and secrete high volumes of unbound antibodies that play a vital role in the humoral effector responses, including complement activation, ADCC and opsonisation (Hoffman et al. 2016). Memory B-cells persist following the resolution of an infection and present the same BCRs as their naïve precursor, but with a much higher affinity and varying isotypes (IgD, IgE, IgA) due to SHM and CSR (LeBien and Tedder 2008). Memory B-cells and long-lived serum antibodies from plasma cells can mount an effective, rapid response to secondary antigenic challenge (Hoffman et al. 2016).

Non-canonical activation has also been identified with some antigens that are able to induce B-cell activation independently of Th cell involvement (T-independent), such as LPS/polysaccharide antigens (Figure 1.2B). T-independent co-stimulatory signals include TLRs presented by both B1 and marginal zone B-cells, such as TLR4 recognition of LPS (Hoffman et al. 2016). NKT cells, neutrophils and DCs have also demonstrated non-canonical stimulation both directly (CD40L) and indirectly (cytokines) with marginal zone B-cells (Cerutti et al. 2012).

The majority of B-cells are bone-marrow derived (B2 B-cells), but a subset of self-renewing B-cells have also been identified that originate from the foetal liver and persist past neonatal development (B1 B-cells) (Hoffman et al. 2016). The majority of evidence supporting B1 B-cells comes from mouse studies, and the significance of B1 B-cells in humans is less understood. They are thought to make up a small proportion of the human B-cell compartment and can be distinguished from B2 B-cells by the expression of marker CD5, normally found on T-cells. They are a self-renewing population, unlike other B-cells that are continuously generated from the bone marrow, and have a short life span of a few weeks unless introduced to antigen. Mature B1 B-cells present multi-specific IgM as their BCRs, recognise carbohydrate or phospholipid based antigens rather than protein antigens and activate independently of T-cells (Hoffman et al. 2016; Kindt et al. 2007; Baumgarth 2011). Therefore, the B1 B-cell subset demonstrates lower affinity for antigen and little class switching.

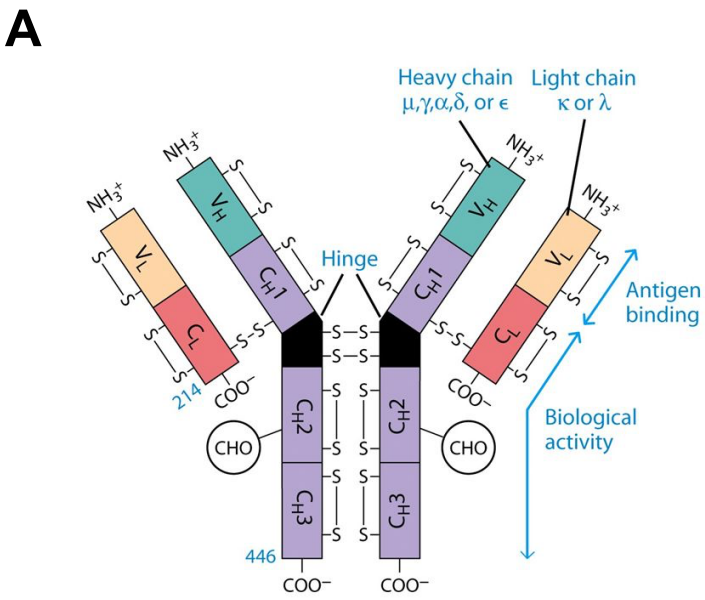

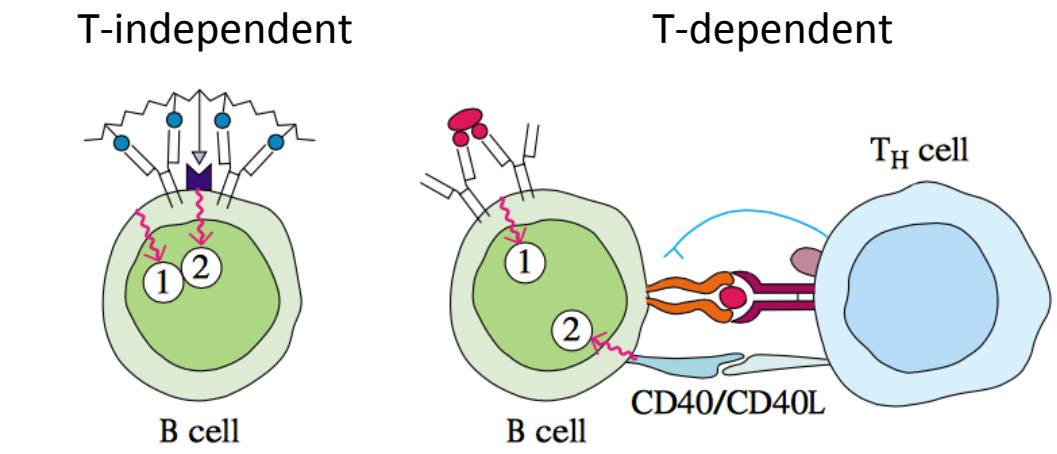

Figure 1.2. BCR structure and B-cell activation. (A) BCRs are membrane bound Ig presented B-cells. Ig molecules comprise two heavy- and two light-chains, both of which contain variable (V) and constant (C) regions. The upper region forms the antigen binding site, whereas the lower regions confer for the downstream biological activity (e.g. ADCC) (B) B-cell activation occurs via BCR signalling (Signal 1) and co-stimulation (Signal 2), which can occur in both a T-independent and T-dependant manner. T-independent involves recognition of PAMPs such LPS/polysaccharides by both BCR and PRRs. T-independent activation requires BCR recognition of antigen combined with costimulation from Th cells, such as CD40/CD40L engagement (Figures adapted from Kindt et al. (2007); Villadangos and Schnorrer (2007)).

1.1.3.2 T-cells and cell-mediated immunity

B-cells and the humoral response hold some limitations for immune defence: antibodies are not able to interact with intracellular pathogens, and the humoral response to an initial infection takes time, with a lag of 5-7 days before antibody levels increase (although the lag is greatly reduced in secondary infections, with a larger, prolonged humoral response). The cell-mediated arm of the adaptive immune response involves the activation of lymphocytes known as $CD4^+$ and $CD8^+$ T-cells. These recognise peptide antigens bound to MHC on APCs using T-cell receptors (TCRs). This recognition and activation leads to the generation of Th cells and cytotoxic T-cells (CTLs) that perform various effector functions, including killing infected/damaged cells and promoting other arms of the immune response (Kindt et al. 2007; Wood 2006).

$CD4^+$ T-cells

$CD4^+$ T-cells form a vast repertoire of different cellular subtypes that engage in different immunological functions within the immune response (Figure 1.3). Development into these subtypes depends greatly on the stimulus within the microenvironment during the time of activation and differentiation, e.g. cytokines, and can be distinguished by the cellular receptors they express and the cytokines they produce (Zhu et al. 2010).

The first $CD4^+$ subsets to be identified were the Th1 and Th2 groups. Th1 cells help the cell-mediated immune response by promoting the growth of $CD8^+$ CTLs against intracellular pathogens (Wood 2006). The Th1 cell subset development is promoted by cytokines produced during the innate phase of the immune response. IL-12, secreted by macrophages and DCs, is the main cytokine that can drive Th1 differentiation (Murray and Wynn 2011): IL-12 also stimulates IFN-γ production by NK cells that can promote Th1 (Martín-Fontecha et al. 2004; Morandi et al. 2006). Th1 cells also produce IFN-γ that then further stimulates a Th1 environment and also initiates additional macrophage activation, completing an innate-adaptive immune activation loop to fight against intracellular pathogens (Medzhitov 2007). B-cells can also stimulate Th1 differentiation via IFN-γ production (Hoffman et al. 2016).

Th2 cells help mediate responses against extracellular pathogens and promote the humoral response. Th2 development is driven by the cytokine IL-4, produced by mast cells (Wood 2006; Swain et al. 1990). DCs are also thought to play a role in the polarisation to the Th2 subset in an IL-4 environment, although how is unclear (Moser

and Murphy 2000; Banchereau and Steinman 1998). Th2 cells drive humoral responses via the secretion of IL-4, IL-5 and IL-13 cytokines, which promote eosinophil, basophil and mucosal epithelia functions. IL-4 production also encourages B-cell synthesis of IgE antibodies, which further promotes mast cell and basophil activation (Medzhitov 2007).

Th17 is a third subset of T helper cells that has been defined more recently (Zhu et al. 2010). Th17 cells help in the resolution of extracellular bacteria and fungi and are vital for inflammatory reactions in tissues (Park et al. 2005; Medzhitov 2007). Activated macrophages produce IL-23 and IL-1, cytokines that drive polarisation to the Th17 subset during infection and stimulates Th17-cell production of pro-inflammatory cytokines including IL-17, IL-6 and TNF-α (Murray and Wynn 2011). IL-17 has pro-inflammatory properties and recruits neutrophils to the site of infection and stimulates cytokine production in tissue cells (Park et al. 2005). However, the cytokines known to drive early Th17 polarisation in mice are IL-6 and TGF-β, with IL-23 as essential to mount a successful Th17-cell response (Weaver et al. 2006).

Follicular helper cells (Tfh) are another T helper cell type, identified by expression of homing receptor CXCR5 that aids localisation to the germinal centre. Here Tfh cells perform a critical role in T-B cell interactions by promoting B-cell proliferation and differentiation (C. S. Ma et al. 2012; C. S. Ma et al. 2009). Early human Tfh cell differentiation has been reported to be driven by IL-12 (C. S. Ma et al. 2009), but whether Tfh-cells are a distinct subset or linked to the another Th lineage (Th1/Th2/Th17) is still uncertain (Zhu et al. 2010; Iwasaki and Medzhitov 2015). Tfh cells are distinguished by distinct expression of IL-21, BCL-6 and surface receptors such as ICOS and PD-1 (C. S. Ma et al. 2009).

Regulatory T-cells (Tregs) are a subpopulation of $CD4^+CD25^+$ T-cells that play an important role in the negative regulation of the immune response and peripheral tolerance of T-cells (Sakaguchi et al. 1995). Tregs are further characterised by the expression of transcription factor Foxp3, which is essential for Treg differentiation (Hori et al. 2003; Josefowicz et al. 2012). Tregs can be further subdivided into natural Tregs (nTregs) and inducible Tregs (iTregs) (X. Lin et al. 2013). nTregs are developed in the thymus via high affinity MHC-II self-selection, similar to other $CD4^+$ T-cells, with the exception that $Foxp3^+$ cells with a strong affinity for self-antigens receive survival signals, whereas self-reactive $Foxp3^-$ cells are deleted (X. Lin et al. 2013; Josefowicz et

al. 2012; de Lafaille and Lafaille 2009). On the other hand, iTregs are thymus-derived $CD4^+$ Th cells that are converted to Tregs upon peripheral antigenic stimulation (de Lafaille and Lafaille 2009), such as gut microbiota or environmental pathogens (e.g. food). It has therefore been hypothesised that nTregs play more of a role in the tolerance of 'self' and the prevention of autoimmune diseases, whereas iTregs are more involved in the tolerance of commensal organisms and foreign antigens that are commonly found in the environment. This division of function has not been fully established and research to fully understand the immune-regulatory mechanisms employed by Tregs is still ongoing (Josefowicz et al. 2012; T. T. Lin et al. 2014). CTLA-4 is an important molecule on the Treg cell surface that binds with CD80 and CD86 molecules on activated $CD4^+$ T-cells and DCs to suppress T-cells (Boehmer 2005). Tregs have also been shown to produce immune-regulatory products including IL-10, IL-35, IL-9, perforin and granzyme A, and TGF-β that are thought to directly suppress activated T-cells (Josefowicz et al. 2012; Boehmer 2005).

Although Foxp3 upregulation appears to play a key role in the immune-regulatory ability of Tregs (Josefowicz et al. 2012), two $Foxp3^-$ iTregs have also been reported: IL-10 producing type 1 regulatory (Tr1) cells and TGF-β producing Th3-cells (X. Lin et al. 2013).

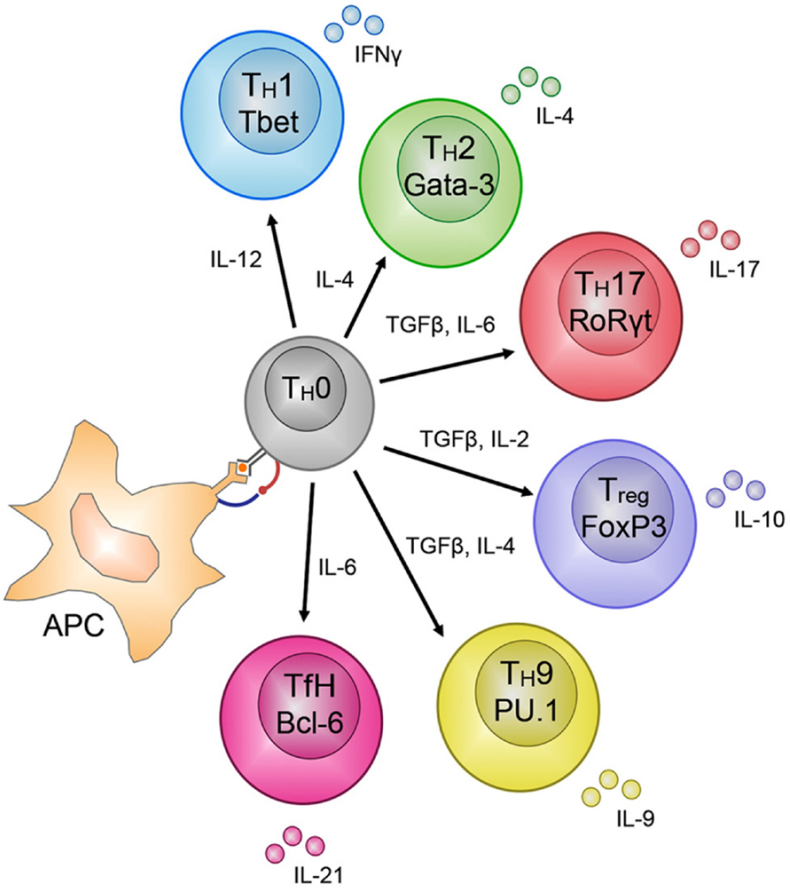

Figure 1.3. CD4$^+$ T-cell subsets. Following antigenic recognition and activation, naïve CD4$^+$ T-cells (Th0) can differentiate into various CD4$^+$ subsets depending upon the cytokine microenvironment. Th1 and Th2 were the first helper cell subsets to be identified, followed by additional helper subsets including Th17, Th9 and Tfh. CD4$^+$ T-cells can also differentiate to Tregs, which play a role in the regulation/suppression of host immunity (Figure taken from Russ et al. (2013)).

$CD8^+$ T-cells

The large majority of $CD8^+$ T-cells differentiate into cytotoxic T-cells (CTLs) that can directly kill pathogen infected or malignant target cells. $CD8^+$ T-cell activation and proliferation is stimulated by IL-2 produced by $CD4^+$ Th cells, thereby activating $CD8^+$ T-cells through a Th-dependent manner (N. Zhang and Bevan 2011). Stimulation with IL-2 along with cytokines IFN-γ, IL-4 and IL-10 promote differentiation $CD8^+$ differentiation into CTLs. $CD8^+$ T-cells can also be activated without $CD4^+$ help when activated APCs upregulate co-stimulatory molecules (Wood 2006).

Upon recognition of an infected or malignant target cell, CTLs release granules, polarised to the target cell, containing the cytotoxic effector molecules granzyme A, granzyme B, and perforin (Bossi and Griffiths 1999; Sanin and Pearce 2016). Perforin monomers insert into the target cell membrane to form polymeric pores, with the potential to cause cell death by osmotic lysis. Granzymes can enter the target cell through perforin pores, lyse cytosolic proteins and initiate programmed cell death (Wood 2006). Granzyme A and granzyme B are the most prevalent effector molecules within CTLs: one study reported 4.9×10^6 and 2.2×10^7 copies per cell, respectively, with granzyme B being one of the most common proteins produced in these cells overall (Hukelmann et al. 2016). This allows for rapid cytolytic function upon CTL activation. CTLs also secrete cytokines including IFN-γ and TNF-α that indirectly kill the target cell by initiating the effector functions of other immune cells (Sanin and Pearce 2016).

CTLs are also able to trigger target cell death by promoting Fas-mediated apoptosis. Fas (CD95) is widely expressed across all cell types, and upon activation CTLs synthesise Fas ligand (FasL) and transport FasL to the cell surface via secretory molecules during CTL degranulation (Bossi and Griffiths 1999). On the CTL surface, FasL then engages Fas on the target cell to initiate apoptosis.

$CD8^+$ T-cells have also demonstrated immune-regulatory function by producing IL-10. During the peak of the adaptive response, $CD8^+$ T-cells are the largest producers of IL-10 in peripheral infection sites, which are dramatically reduced following resolution. Interestingly, IL-10^+CD8^+ T-cells still demonstrate high cytotoxicity (granzyme B, IFN-γ, TNF-α)(N. Zhang and Bevan 2011).

T-cell development

Like B-cells, T-cell precursors arise from lymphoid progenitors within the bone marrow, which then commit to T-cell development. These progenitors exit the bone marrow and migrate to the thymus as double negative (DN) cells, i.e. expressing neither CD4 nor CD8 molecules on their surface ($CD4^{-}CD8^{-}$) (Germain 2002). DN cells undergo extensive division in the thymus cortex developing through four DN sub stages (DN1-DN4)(Germain 2002; Wood 2006). At the DN3 stage cells begin to express the pre-TCR α-chain on their surface and undergo genetic rearrangement of the β-chain, which then binds with the pre-α-chain to form a pre-TCR. Successful β-chain rearrangement resulting in pre-TCR expression, alongside CD3 and other cell surface proteins, is essential for further T-cell development. DN3 cells that fail to present pre-TCR enter developmental arrest and die by apoptosis. However, the mechanism behind the selection process is not completely understood (Wood 2006; Germain 2002). Late DN3/DN4 T-cells undergo additional rounds of cell division followed by genetic rearrangements of the pre-α-chain and low-level expression of the fully formed α/β TCR with CD3, gradually upregulating CD8 and then CD4 to become double positive (DP; $CD4^{+}CD8^{+}$).

DP thymocytes undergo rounds of both positive and negative selection to ensure that the T-cells that develop are specific for the host's own MHC molecules (self-MHC) and foreign antigens. Cortical epithelial cells within the cortex present both MHC-I and MHC-II on their cell surface: DP T-cells with TCRs specific for the self-MHC complexes are positively selected to receive survival signals. If DP T-cells fail to recognise self-MHC they die by apoptosis. At the cortico-medullary junction DP T-cells encounter DCs presenting self-peptides on MHC complexes. If a DP T-cell recognises self-antigen (via TCR) they are negatively selected to undergo apoptosis. Surviving DP cells then differentiate to mature single positive (SP) $CD8^{+}$ or $CD4^{+}$ T-cells, depending on whether they recognised MHC-I or MHC-II during the selection process, and migrate into the peripheral circulation (Germain 2002).

A third T-cell type has also been reported; γ/δ T-cells. These make up a small proportion of the total T-cell pool (1-5%) but are present in larger proportions (20-50%) within specific tissues, including the intestine, dermis, lung and womb (Silva-Santos et al. 2015; Vantourout and Hayday 2013). DN cells can mature into either α/β or γ/δ T-cells, and the γ/δ TCR is generated by genetic rearrangements of γ- and

δ-chains in a similar fashion to α/β TCRs (Germain 2002), although there are fewer variable genes at the γ or δ locus so the variation in antigen recognition is limited (Born et al. 2012). The functional role of γ/δ T-cells within the immune response is still poorly defined, although they have demonstrated recognition and cytotoxic function against tumour antigens such as phosphoantigens (Tanaka et al. 1995; Morita et al. 1995), normally produced by bacteria and parasites but also accumulated in stressed or transformed cells (Silva-Santos et al. 2015).

APC-mediated activation of T-cells

The MHC/antigen complex is recognised by the TCR on a T-cell specific for that MHC class and antigen and is an essential factor in T-cell activation. There are two classes of MHC molecules on APCs: MHC class I and MHC class II (Figure 1.4A). Although they perform similar roles for T-cell activation, they are recognised by different T-cells ($CD8^+$ and $CD4^+$, respectively) and the pathways in antigen processing differ (Figure 1.4B) (Wood 2006; Germain 2002).

MHC I molecules interact with TCRs of the $CD8^+$ T-cell and present endogenous antigens from within an infected/damaged cell. Viral infection and 'hijacking' of a host cell's intracellular processes leads to the generation of new viral proteins within the cytoplasm that are not accessible to external immune recognition. These viral antigens are degraded by the proteasome, along with other cytosolic proteins, into shorter peptide fragments. Antigenic peptides are translocated into the rough endoplasmic reticulum (RER) by transporter proteins, to bind with newly synthesised MHC I molecules. Once the MHC/antigen complex is formed it is transported to the surface of the cells where it can be presented to $CD8^+$ T-cells (Wood 2006; Villadangos and Schnorrer 2007).

MHC II differs in that it presents extracellular antigens to $CD4^+$ T-cells. Extracellular proteins are taken up by APCs into endosomes using endocytic pathways such as phagocytosis. Endosome/lysosome fusion exposes the ingested proteins to lower pH levels and proteolytic enzymes that activate in the acidic environment, resulting in degradation of the antigen into smaller peptide fragments. Both MHC I and MHC II molecules are synthesised within the RER, but formation of the MHC II/antigen complex occurs elsewhere, in a vesicle called the compartment for peptide loading (CPL). During synthesis the invariant chain binds the antigen-binding site of immature

MHC II, preventing MHC II from associating with any intracellular peptides (including self-peptides) within the RER. The invariant chain also regulates the movement of MHC II to the CPL, which then fuses with the endolysosome containing antigenic peptides. Here the invariant chain disassociates from MHC II, allowing antigenic peptides to bind, before transporting to the cell surface and presenting to $CD4^+$ T-cells (Wood 2006; Villadangos and Schnorrer 2007).

Most cell types can present antigen via MHC I to alert $CD8^+$ T-cells to intracellular damage or infection and initiate the cytotoxic response, but only APCs can present antigen and prime $CD8^+$ T-cells to differentiate into effector T-cells via co-stimulatory factors. Phagocytic APCs can ingest and present exogenous antigens to $CD8^+$ T-cells. However, the term APC normally refers to cells that can also present MHC II (Kindt et al. 2007). The main three cell types that can do this are DCs, macrophages and B-cells, and are known as professional APCs (Steinman and Hemmi 2006; Hoffman et al. 2016; Murray and Wynn 2011), although MHC II is also expressed by cortical epithelial cells (Germain 2002). DCs are the primary APCs that constitutively express MHC II and co-stimulatory receptors. Upon phagocytosis of antigen material, macrophages begin upregulation of MHC II and costimulatory receptors on their cell surface. B-cells, like DCs, constitutively express MHC II, but only upregulate co-stimulatory receptors when activated (Kindt et al. 2007). Under certain inflammatory conditions, nonprofessional APCs, such as fibroblasts or epithelial cells in the thymus, are also able to temporarily present MHC II.

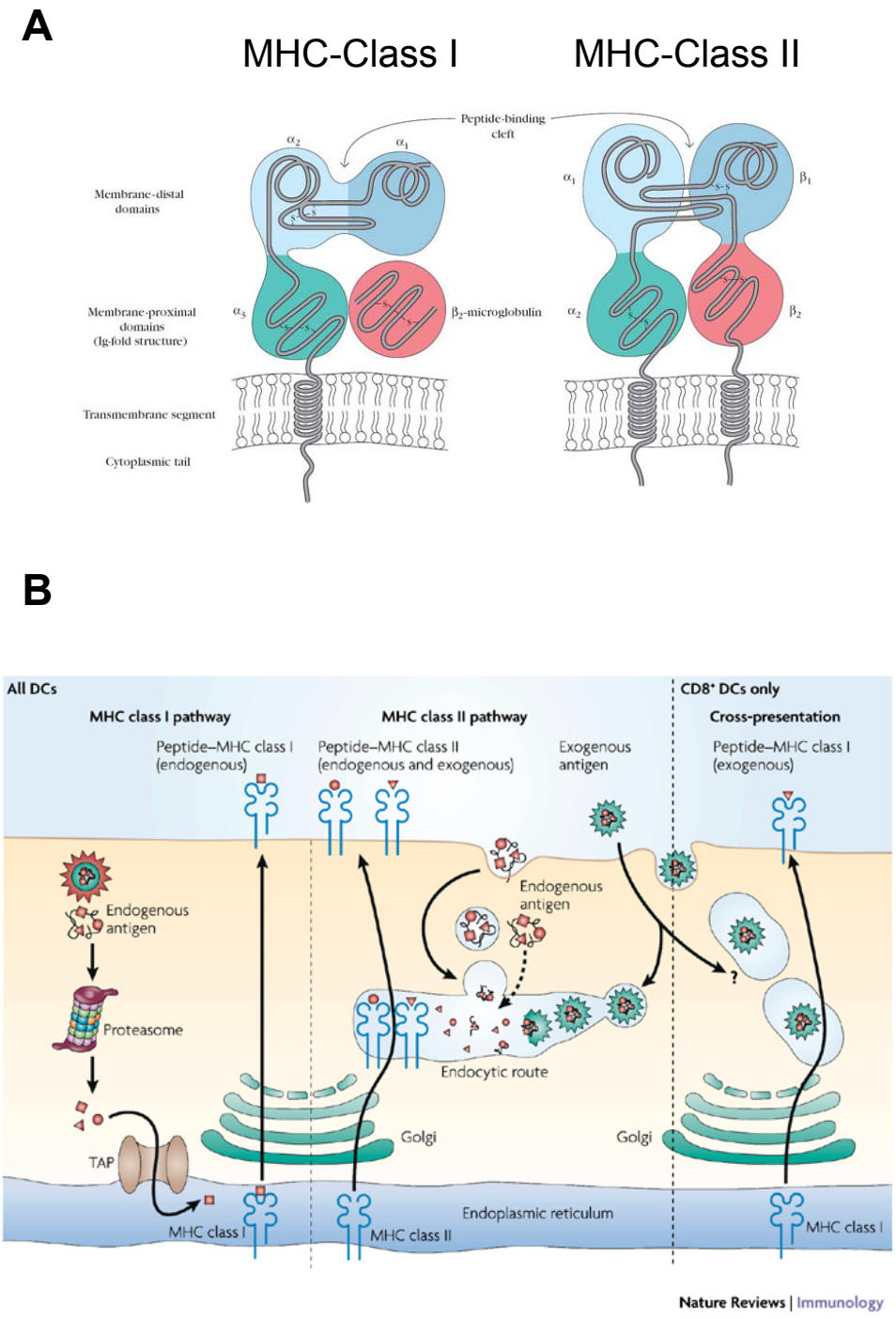

Figure 1.4. MHC structure and presentation. (A) MHC molecules are presented on APCs with antigenic peptides to be recognised by T-cell receptors (TCRs) and initiate T-cell activation. MHC I is recognised by $CD8^+$ T-cells, whereas MHC II is recognised by $CD4^+$ T-cells. (B) MHC I molecules mainly present endogenous antigen degraded in the cytosol via proteasomes, whereas MHC II presents predominantly exogenous antigen ingested by the APC, although presentation of internalised endogenous antigen can also occur. MHC I has also demonstrated exogenous presentation, although the mechanism is still unknown (Figures adapted from Kindt et al. (2007); Villadangos and Schnorrer (2007)).

T-cell memory

Following primary antigenic stimulation the majority of naïve T-cells differentiate into a heterogeneous population of short-lived effector cells (SLECs) that work to resolve the infection before undergoing apoptosis (Sarkar et al. 2008; N. Zhang and Bevan 2011). A smaller population (5-10%) develop into memory precursor effector cells (MPECs) that survive the contraction and develop into a long-lived pool of memory T-cells (Figure 1.5)(Yuzefpolskiy et al. 2015; N. Zhang and Bevan 2011). The memory pool is then able to rapidly and efficiently respond to a repeat infection (Sallusto et al. 2004).

T-cells can be initially divided into two functionally different subsets: central memory (CM) and effector memory (EM) T-cells. CM T-cells are $CD45RO^+$ and present homing receptors CCR7 and CD62L on the cell surface that aid CM homing to the lymph nodes, spleen and blood (Sallusto et al. 2004). CM T-cells have a more efficient response to antigen than naïve cells but have a slower effector response upon secondary antigen stimulation when compared to EM T-cells (Sallusto et al. 2004). $CCR7^-CD45RO^+$ EM T-cells are located in the blood, spleen and non-lymphoid tissues (Seder and Ahmed 2003), and upregulate adhesion molecules that initiate homing to inflamed tissues (Sallusto et al. 2004). EM T-cells contain large amounts of perforin and have a rapid effector function and cytokine secretion upon antigenic challenge (Sallusto et al. 2004; Seder and Ahmed 2003). However, compared to CM T-cells, EM T-cells have reduced proliferative capacity and shorter telomeres, along with a poorer response to homeostatic cytokines and reduced survival (Klebanoff et al. 2006). Normal memory subset distribution differs between $CD4^+$ and $CD8^+$ T-cells: CM T-cells are the primary memory subset in the $CD4^+$ T-cell compartment, whereas EM T-cells form a higher proportion of the $CD8^+$ T-cells (Sallusto et al. 2004).

Persistent antigen, from chronic infection or tumours, can lead to conversion of memory T-cells to a more highly differentiated memory subset (EMRA) (Klebanoff et al. 2006; Angelosanto et al. 2012). EMRA T-cells are considered ‘terminally differentiated’ and ‘exhausted’ cells with impaired effector function, poor proliferative capacity and reduced ability for cytokine production (Klebanoff et al. 2006; Nunes et al. 2012). When antigen-specific T-cells are removed from an established chronic infection they do not recover memory potential and function (Angelosanto et al. 2012), although EMRA T-cells do appear to have the potential to overcome senescence under certain stimuli (Di

Mitri et al. 2011; Chong et al. 2008), or when removed from the earlier stages of chronic stimulation (Angelosanto et al. 2012).

Due to their greater homeostatic potential, CM T-cells were thought to perform the main role of T-cell memory pool maintenance. Recent studies have now identified human $CD8^+$ and $CD4^+$ T-cells with stem cell-like properties (Tscm cells) that form approximately 2-3% of the circulating $CD8^+$ and $CD4^+$ lymphocytes of healthy donors (Gattinoni et al. 2011). Tscm-cells present similar cell surface markers as the naïve T-cell population, including memory markers CCR7 and CD45RA (and lack of CD45RO), but can be further distinguished from naïve cells by the expression of additional markers CD95 and CD122 (IL2Rβ). The functional profile of Tscm-cells differs from naïve T-cells and is more in-line with CM and EM memory subsets; they have a more rapid response to antigenic stimulation and production of effector cytokines (IFN-γ, IL-2 and TNF-α), and a proliferative capacity when stimulated by homeostatic cytokines IL-15 and IL-7. Tscm-cells appear to present the least differentiated memory subset, thereby adding to the linear model as Tscm>CM>EM>EMRA.

Gattioni et al. (2011) demonstrated superior engraftment potential of Tscm cells via adoptive transfer compared to other memory subsets: Tscm cells engrafted with 10- to 100- fold more progeny compared to naïve and CM T-cells. In addition, adoptive transfer of $CD8^+$ Tscm, CM or EM-cells (co-transferred with $CD4^+$ T-cells) into a humanised murine tumour model demonstrated that mice with Tscm cells experienced tumour regression and cure, whereas all mice with CM cells died within 40 days of transfer. EM cells did not significantly extend survival versus application of $CD4^+$ T-cells alone. This anti-tumour potential, along with the enhanced proliferative ability and longer-lived survival of Tscm cells, suggests they could be prime candidates for adoptive T-cell based cancer immunotherapy. However, the relatively low numbers of Tscm cells within the T-cell pool limits the successful application of this population in therapy.

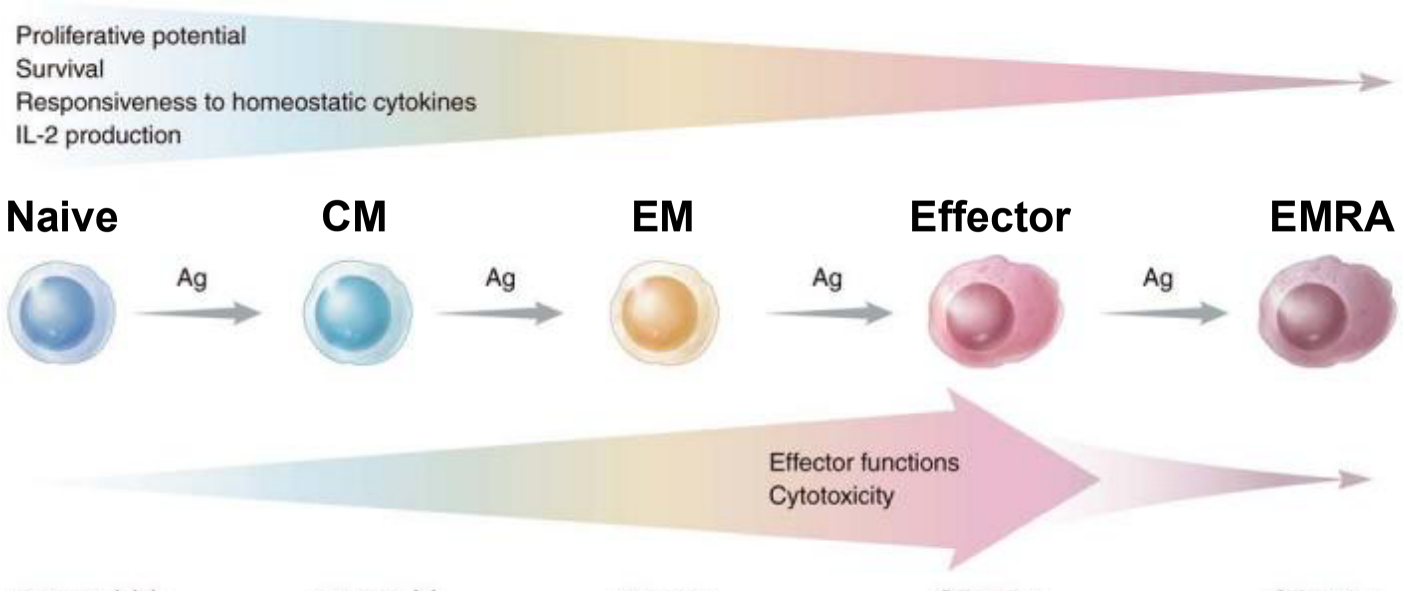

Figure 1.5. Linear T-cell memory model. Upon initial antigenic stimulation, naïve T-cells differentiate and proliferate into short-lived effector cells (SLECs) that die following disease resolution, and memory precursors (MPECs) that eventually differentiate to form the long-lived memory pool of CM and EM T-cells. Following any consequent reinfections, these memory T-cells form a more rapid, effective immune response than the primary infection. During chronic antigenic stimulation, such as chronic viral infections or tumours, the continual stimulation of the T-cells drives them to a more differentiated EMRA T-cell state with reduced proliferative capacity and effector potential (Figure adapted from Klebanoff et al. (2006)).

1.1.3.3 T-cell markers for activation, senescence and exhaustion

Several cell surface markers have been defined that aid the characterisation of T-cells and their differentiation status, some of which have demonstrated functional roles. The following markers are discussed due to their relevance in this study.

CD38

CD38 is a transmembrane glycoprotein expressed on many immune cells, including T-cells and B-cells (Malavasi et al. 2008; Dianzani et al. 1994). Ligation of CD38 on T-cells leads to the expression of additional activation markers and proliferation (Funaro et al. 1990). CD38 also appears to interact and form complexes with cell surface receptors including TCRs and BCRs (Funaro et al. 1993; Dianzani et al. 1994). This lends strength to CD38 having a functional role in cell activation, and it is now a widely accepted marker for activation (Buggert et al. 2014).

As well as being highly upregulated on activated T-cells, CD38 expression is also reported on DP thymocytes, naïve $CD4^+$ T-cells and $CD4^+$ Tregs (Tenca et al. 2003; Dianzani et al. 1994; Read et al. 1998). There is normally little or no CD38 found on memory T-cells (Malavasi et al. 2008). $CD8^+$ T-cells with high CD38 have been reported in chronic infections, although the importance of this is uncertain (Malavasi et al. 2008). CD38 expression on $CD4^+$ and $CD8^+$ T-cells is employed as a prognostic marker in HIV patients for AIDS progression (Malavasi et al. 2008).

HLA-DR

HLA-DR is a MHC class II molecule, usually expressed on APCs, that presents antigen to $CD4^+$ T-cells. Upregulation of MHC class II, including human HLA-DR, is also reported on activated T-cells. Cytokine stimulation with interleukins and IFNγ has been shown to promote HLA-DR upregulation on both $CD4^+$ and $CD8^+$ T-cells (Salgado et al. 2002; Basham and Merigan 1983), but the regulation and functional mechanisms behind T-cell MHC II presentation are still poorly understood (Holling et al. 2002).

As with CD38, HLA-DR is a commonly used marker for activated T-cells (Buggert et al. 2014). Co-expression of HLA-DR and CD38 has been reported on early effector T-cells at the peak of the primary immune response (Anichini et al. 2010). Similar to CD38, increased HLA-DR expression correlates with loss of $CD4^+$ and progression to AIDS in HIV patients (Buggert et al. 2014).

CD57

CD57 was first described as an NK glycoprotein receptor, but is also expressed by highly differentiated T-cells that have poor proliferative capacity (Koch et al. 2008; Focosi et al. 2010). Expression of CD57 on $CD4^+$ and $CD8^+$ T-cells has been shown to be directly associated with the number of cellular divisions, and inversely linked to telomere length (Focosi et al. 2010; Brenchley et al. 2003).

$CD57^+$ T-cells accumulate during the persistent antigenic stimulation of chronic infections, such as CMV and HIV, and increase with age (Focosi et al. 2010; Strioga et al. 2011; Brenchley et al. 2003). Increased frequencies of $CD57^+$ T-cells are also reported in both solid cancers and haematological malignancies (Akagi and Baba 2008; Characiejus et al. 2008; Van den Hove et al. 1998). Expansion of CMV-specific $CD8^+CD57^+$ T-cells with a more differentiated memory phenotype is often observed in the elderly (Focosi et al. 2010). However, $CD57^+$ T-cells still have the ability to produce cytokines upon activation, and have demonstrated rapid proliferation under certain stimuli (Focosi et al. 2010; Chong et al. 2008). Interestingly, $CD8^+CD57^+$ T-cells have also shown more cytotoxic potential than $CD8^+CD57^-$ T-cells, which strongly correlates with granzyme A, granzyme B and perforin expression (Chattopadhyay et al. 2008).

Programmed cell death 1 receptor (PD-1)

PD-1 is a transmembrane receptor containing an Ig superfamily domain, an immune-receptor tyrosine-based inhibitory motif (ITIM) and an immune-receptor tyrosine-based switch motif (ITSM). Various immune cells can express PD-1, including T-cells, B-cells and DCs. For T-cells, upregulation of PD-1 occurs following activation, with the immunosuppressive effects of PD-1 ligation to PD-L1/PD-L2 observed as little as a few hours following activation (Keir et al. 2008).

Ligation of PD-1 leads to the direct inhibition of the downstream signalling pathways of the TCR costimulatory molecule CD28, leading to the dampening of TCR activation and inhibition of cytokine induction (Keir et al. 2008). $CD8^+$ T-cells specific for CMV, EBV, HIV and vaccinia-virus all demonstrated varying levels of PD-1 expression thought to be related to length of antigenic exposure (Day et al. 2006). Furthermore, PD-1 upregulation on both $CD4^+$ and $CD8^+$ T-cells is associated with progressive HIV (increased viral load, reduced $CD4^+$ count), and blocking PD-1/PD-L1 ligation has been

shown to reverse immune dysfunction within the disease (Day et al. 2006; Trautmann et al. 2006). Therefore, PD-1 is one of the best described immunosuppressive markers and is commonly used to distinguish T-cells undergoing differentiation to exhaustion following chronic antigenic stimulation (Buggert et al. 2014; Anichini et al. 2010).

Killer cell lectin-like receptor G1 (KLRG-1)

KLRG-1 was initially attributed as an NK cell surface receptor, but has since been identified on T-cells with poor proliferative potential (Thimme et al. 2005). KLRG-1 is also greatly upregulated on the SLEC population during peak response of infection (Voehringer et al. 2002; Y. Li et al. 2009), as well as a subset of short-lived terminally differentiated KLRG-1^+ Tregs with enhanced immune-regulatory capabilities (Cheng et al. 2012). KLRG-1 binds to a conserved area on cadherin molecules (including E-, N- and R- cadherin), which then inhibits the proliferation of activated T-cells (Y. Li et al. 2009; Henson et al. 2009).

KLRG-1 is present at very low levels in the naïve T-cell pool, but then KLRG-1^+ T-cell frequency progressively increases through memory subset differentiation (CM<EM<EMRA)(Voehringer et al. 2002). Virus specific T-cells from resolved infections demonstrate lower expression of KLRG-1, whereas persistent antigenic stimulation leads to increased frequencies of KLRG-1^+ T-cells (Bengsch et al. 2007). Higher frequencies of KLRG-1^+ T-cells have been reported in multiple chronic viral infections, including HIV (72-89%), EBV and CMV (>92%) compared to resolved influenza (40-73%) (Ibegbu et al. 2005; Thimme et al. 2005). Furthermore, additional characterisation with CD57 has identified a 'terminally differentiated' CD57$^+$KLRG-1^+ subset (Ibegbu et al. 2005). KLRG-1 therefore represents a marker to identify more differentiated T-cell subsets under conditions of chronic antigen exposure.

Although T-cells expressing KLRG-1 demonstrate poor proliferative capacity, they are still able to maintain effector functions similar to that of T-cells with low KLRG-1, such as IFN-γ production and degranulation (Ye et al. 2012; Voehringer et al. 2002). Interestingly, KLRG-1^{high} T-cells adoptively transferred from mice with influenza infection in the lung were able to persist in the absence of antigenic stimulation, and demonstrated proliferative potential during antigen re-exposure in new hosts (Ye et al. 2012), implying some plasticity in response.

Interleukin-7 receptor α (IL-7Rα/CD127)

Homeostatic cytokines IL-7 and IL-15 maintain naïve and memory T-cell survival and population turnover (Seder and Ahmed 2003). Expression of the α-subunit of the IL-7 receptor, IL-7Rα (CD127), is critical for efficient T-cell memory development and survival (Kaech et al. 2003; Hand et al. 2007). Naïve T-cells express CD127 but during activation CD127 is downregulated (Hand et al. 2007; Sarkar et al. 2008). At 7 days post-infection, a small fraction of T-cells (MPECs) begin to re-express CD127 and the frequency of $CD127^{+}$ cells gradually increases (Bachmann et al. 2005; Sarkar et al. 2008). Presentation of CD127 could therefore distinguish antigen-specific T-cells with memory potential.

CD127 can be used in combination with KLRG-1 to characterise differentiated T-cells. Following T-cell contraction $CD62^{high}$ cells are observed within the KLRG-$1^{low}CD127^{high}$ population, implying that that CM T-cells arise from this less differentiated phenotype, whereas EM T-cells may be derived from KLRG-$1^{high}CD127^{low}$ T-cells (Kurtulus et al. 2011). Acute virus-specific T-cells present the KLRG-$1^{low}CD127^{high}$ phenotype, whereas viral-specific T-cells exposed to chronic infection are KLRG-$1^{high}CD127^{low}$ (Bengsch et al. 2007). Interestingly, IL-7-mediated signalling induces rapid internalisation of IL-7R on T-cells and down modulation of CD127 (Ribeiro et al. 2012), thereby losing the ability to respond to further IL-7 stimulation.

BCL-2

BCL-2 is an anti-apoptotic molecule that is induced by IL-7/IL-15 stimulation and performs direct interactions with pro-apoptotic molecules, such as Bim or Bax, to prevent initiation of cellular apoptosis (Kurtulus et al. 2011; Oltval et al. 1993). Formation of Bim/BCL-2 complexes are essential for naïve T-cell survival (Wojciechowski et al. 2007). Like CD127, BCL-2 is downregulated during activation. MPECs with low KLRG-1 and high CD127 expression were associated with higher expression of BCL-2 compared to SLECs, supporting a role for BCL-2 in T-cell memory development and survival (Kurtulus et al. 2011; Dunkle et al. 2013). Furthermore, BCL-2 is higher in CM T-cells than EM T-cells, suggesting increased homeostatic survival within the CM compartment (Kurtulus et al. 2011).

1.2 Cancer immunology

The immune system can identify and kill abnormal or damaged host cells. Tumour reactive T-cells have been identified in cancer patients, implying that mechanisms to recognise and resolve malignant cells are present within the immune response. However, tumour resolution is not achieved due to the tumour's ability to promote immune evasion, thereby facilitating tumour progression (Hanahan and Weinberg 2011).

1.2.1 Immune surveillance and immunoediting

The method by which the immune system regulates response to cancer is known as immune surveillance and immunoediting. Immune surveillance was first coined by (Burnet 1957), who hypothesised that lymphocytes were responsible for the removal of any malignant cells that arise. Immune surveillance is therefore vital for recognition and elimination of malignancy. Immunodeficient or immunosuppressed patients demonstrate an increased risk of both viral and non-viral malignancies, supporting the theory of immune surveillance that prevents cancer progression in normal individuals (Hanahan and Weinberg 2011; Dunn et al. 2004). Immune surveillance requires an active tumour-specific immune response, and there is evidence for autologous tumour-specific antibodies and T-cells in cancer patients. Several tumour antigens have been identified that can be recognised by $CD4^+$ and $CD8^+$ T-cells, such as differentiation antigens, mutational antigens, overexpressed/amplified antigens, viral antigens and cancer-testis antigens (Dunn et al. 2004). Tumour-infiltrating lymphocytes (TILs) within the tumour microenvironment have been shown to correlate strongly with patient survival in multiple cancers (Dunn et al. 2004; Galon et al. 2006). Specifically, $CD3^+$ TILs correlate with better prognoses in epithelial ovarian cancer with a five-year survival rate of 38% in patients with $CD3^+$ TILs versus 4.5% survival in patients without TILs (L. Zhang et al. 2003).

Research since the original outlining of immune surveillance has evolved the hypothesis to include tumour survival and escape from immunological destruction, and it is now split into three stages: elimination, equilibrium and escape (Figure 1.6)(Dunn et al. 2004). Elimination comprises the immune surveillance stage that, if successful, results in the recognition and removal of cancerous cells without tumour progression (Dunn et al. 2004). The second stage, equilibrium, occurs if the immune system is unable to eradicate the cancer completely, but can perform immune functions that prevent the

tumour from progressing. However, this form of keeping the tumour cells in check can facilitate clonal evolution of immunologically resistant tumour cells that are able to escape elimination and suppression due to reduced immunogenicity and the ability to induce immune control mechanisms (Smyth et al. 2006; Dunn et al. 2004).

In addition to tumour evasion, tumour-promoting inflammation has been reported as an enabling characteristic in cancers. Inflammation within the tumour environment was initially thought to be an immune response against the malignancy. However, a pro-inflammatory environment has since been demonstrated to benefit the tumour in aiding tumour promotion and progression. Inflammation provides recruitment of beneficial molecules to the tumour site that promote survival and growth, as well as enzymes that promote tumour angiogenesis, invasion and metastasis (Hanahan and Weinberg 2011).

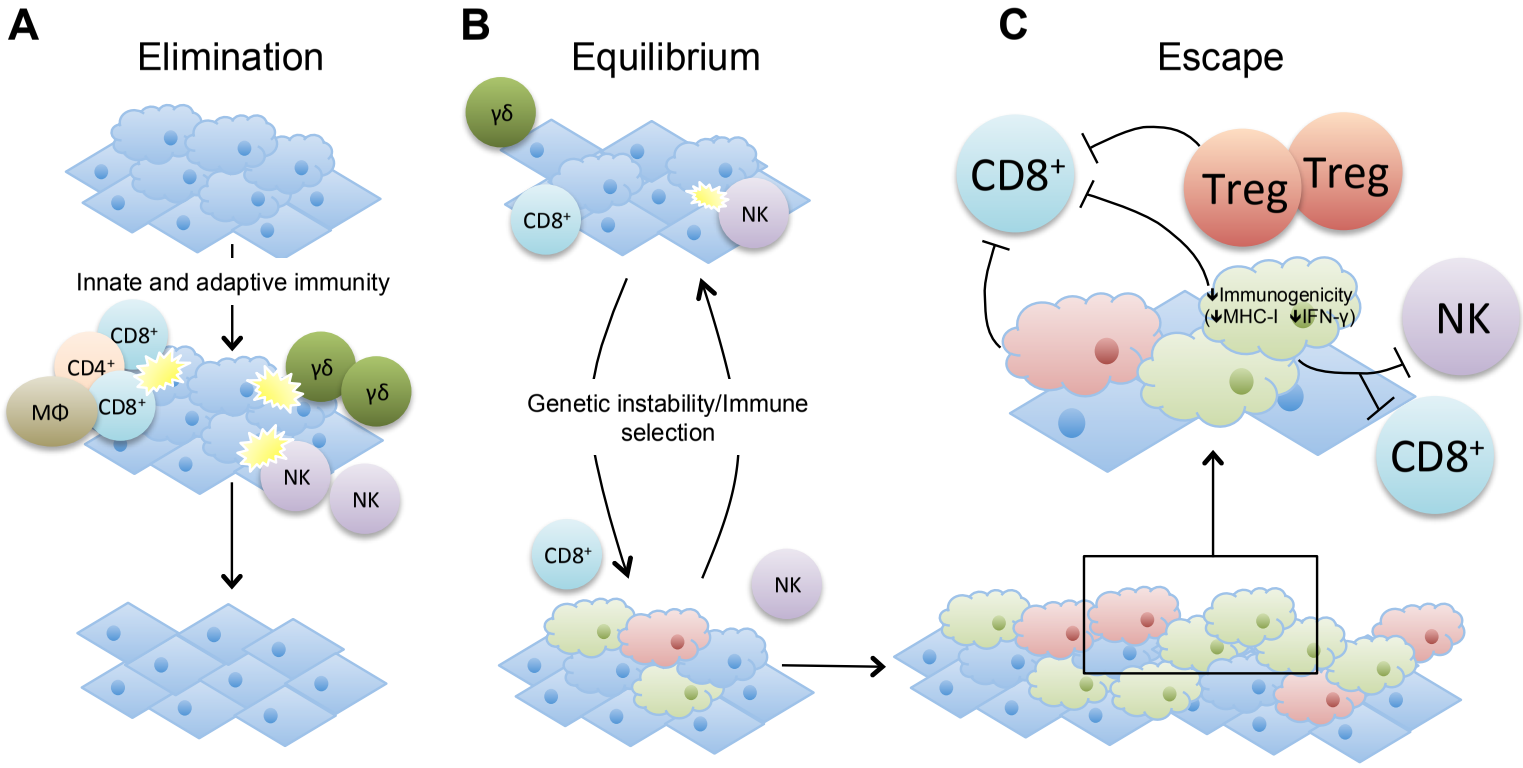

Figure 1.6. Immunosurveillance and immunoediting of cancer. The immune response against malignant cells and the mechanisms of tumour evasion can be broadly described in three stages: (A) The immune system is able to recognise and respond to transformed cells and, if successful, are able to eliminate the malignancy. (B) The immune system is able to recognise cancer cells but cannot completely eliminate them. However, the immune system is still able to perform immune functions that prevent tumour progression. (C) Equilibrium between immune cells and cancer cells can result in selective pressure that eventually leads to the evolution of cancer cell clones that are able to evade immune destruction and exert immunosuppressive measures, resulting in tumour progression.

1.3 Chronic lymphocytic leukaemia

1.3.1 Epidemiology

Chronic lymphocytic leukaemia (CLL) is the most common form of leukaemia in the UK and western world, comprising 40% of all leukaemia cases in patients aged 65 years and older (Oscier et al. 2004; Motta et al. 2009). Overall, UK incidence is thought to be approximately 3 per 100,000 people per year (Oscier et al. 2004), with 3,515 new cases of CLL reported in 2014 (CRUK 2016). There is a higher proportion of male CLL patients (approximately 2:1, male:female)(Oscier et al. 2004), but why CLL is more prominent in males is unclear. Median age at diagnosis is between 64-70 years (Redaelli et al. 2004), although 20-30% of patients are identified under 55 years (Oscier et al. 2004).

CLL is defined by the accumulation of malignant $CD5^{+}CD19^{+}$ B-cells (Damle 2002) and there is evidence that CLL cells could derive from the B1 B-cell subtype (Chiorazzi and Ferrarini 2011; Hayakawa et al. 2016; Rosén et al. 2012). However, the driving force behind this malignancy is still largely unknown. It is thought that inheritable genetic factors play a part, with approximately 17-21% of CLL patients reporting a family history of CLL or other lymphoproliferative disorders (Brown 2014).

1.3.2 Pathology

As CLL is an accumulation of malignant monoclonal B-cells, patients are immunodeficient in many aspects. 85% of patients have dramatically reduced serum Ig (hypogammaglobulinaemia), resulting in impaired humoral responses and antibody mediated immunity, and increased susceptibility to bacterial infections. Reactivation of dormant viruses are also highly common, including herpes simplex virus, cytomegalovirus (CMV) and Epstein-Bar virus (EBV) (Pourgheysari et al. 2010), suggesting that cell-mediated responses are also impaired. Therefore, infections are one of the main causes of death in CLL, causing mortality in 25-50% of CLL patients (A. D. Hamblin and T. J. Hamblin 2008).

Little is known about non-malignant B-cells in CLL, except that they are significantly reduced. Due to the low levels of Ig detected, normal B-cell activity is probably suppressed, but whether they are directly suppressed by CLL cells or indirectly by other modes of immunosuppression is uncertain (A. D. Hamblin and T. J. Hamblin 2008).

1.3.3 Diagnosis and staging

CLL can be either a relatively stable, indolent disease that does not require treatment, or a more severe form with poorer prognosis and a shorter life expectancy (Rai et al. 1975; A. D. Hamblin and T. J. Hamblin 2008). Therefore, although patients can present with symptoms, including lymphadenopathy, tiredness, weight loss, abdominal pain and persistent infections, many patients are initially asymptomatic and 70-80% are diagnosed following routine blood tests (Oscier et al. 2004). Current diagnosis is based on a lymphocyte count of $>5 \times 10^9$ B-cells/L in peripheral blood with immunophenotypic confirmation of B-cell clonality (Hallek et al. 2008).

CLL is normally classified by either Rai (Rai et al. 1975) or Binet (Binet et al. 1981) clinical staging systems for prognosis (Oscier et al. 2004; Hallek et al. 2008), with Rai being the predominant system in the USA and Binet in Europe (Redaelli et al. 2004). Rai staging focuses upon lymphocytosis (Stage 0) leading to lymphadenopathy (Stage I), splenomegaly or hepatomegaly (Stage II), anaemia (Stage III) and thrombocytopenia (Stage IV); these stages can be considered as low risk (Stages 0-I), intermediate risk (Stages II-III) and high risk (Stage IV). The Binet staging system also focuses on lymphocyte infiltration but by the number of lymphoid sites: <3 sites (Stage A, approximately 60% of patients), ≥3 lymph sites (Stage B, approximately 30% of patients) and ≥3 lymph sites plus anaemia or thrombocytopenia (Stage C, approximately 10% of patients) (Oscier et al. 2004). Median survival is >10 years for Binet stage A patients, <8 years for Binet Stage B patients and 6.5 years for Binet Stage C patients (Eichhorst et al. 2011).

1.3.4 Prognostic markers

Due to the heterogeneity of the disease, there is a clear clinical need to be able to identify whether a patient will have good or bad prognosis. In addition to Binet/Rai staging, several other prognostic markers have demonstrated clinical potential for grouping patients by prognosis.

1.3.4.1 *IGHV* mutation status

As previously described in Section 1.1.3.1, activated B-cells undergo major genetic rearrangements to produce high affinity Ig (BCR) on their cell surface. Originally, the $CD5^+$ B-cells in CLL were thought to be naïve-like. However, it became apparent that

CLL patients could by stratified by whether the CLL cells had undergone somatic hypermutation of the Immunoglobulin heavy chain variable region (*IGHV*). Approximately 30-40% of CLL patients demonstrated somatic *IGHV* rearrangement (Moreno and Montserrat 2008). Furthermore, patients with unmutated *IGHV* (≥98% homology to the closest germ line sequence) had significantly poorer median survival of 8 years versus 25 years in the mutated *IGHV* patients, in addition to poorer response to chemotherapy (Damle et al. 1999; T. J. Hamblin et al. 1999). *IGHV* mutation status is therefore considered a powerful prognostic marker in CLL; however, sequencing is still one of the more time-consuming and costly methods. Therefore, *IGHV* mutation status is still not used routinely outside of the clinical trials setting (Moreno and Montserrat 2008).

1.3.4.2 CD38

Patients with unmutated *IGHV* also have significantly higher frequencies of $CD38^+$ B-cells than their mutated counterparts (63.9% versus 7.3%) and this was suggested as a surrogate marker for *IGHV* mutation status (Damle et al. 1999). Later studies with larger patient cohorts demonstrated that CD38 is a prognostic marker of CLL in its own right and can be used in combination with *IGHV* mutation status to identify the poorer prognosis patients, i.e. patients with unmutated *IGHV* and $CD38^+$ (T. J. Hamblin et al. 2002). $CD38^+$ CLL patients (≥ 20% $CD38^+$) had an inferior prognosis, with more advanced pathology, poorer response to chemotherapy, shorter time to first treatment and shorter overall survival (Dürig et al. 2002). Ease of phenotypic testing means CD38 could pose as a beneficial marker, although the optimum value to define CD38 positivity is hard to determine as individual studies have opted for different cut off values for CD38 expression (5-30%) (Moreno and Montserrat 2008; Oscier et al. 2004). There is also longitudinal evidence to suggest that the expression of CD38 is temporal in CLL patients (T. J. Hamblin et al. 2002).

1.3.4.3 Zap-70

70-kDa zeta-associate protein (Zap-70) is a key signalling molecule in T-cells and NK cells, but is not usually expressed in B-cells (Schroers et al. 2005). However, analysis comparing differential gene expression between mutated and unmutated *IGHV* in CLL revealed that expression of Zap-70 is upregulated in the unmutated *IGHV* subpopulation. The strong association between Zap-70 and *IGHV* status and the ability to measure Zap-70 by flow cytometry suggests it as a candidate for prognosis in the

clinical setting, however, it is not easy to measure since it is an intracellular molecule and its levels are highly changeable (Schroers et al. 2005; Moreno and Montserrat 2008). Median survival in Zap-70^{+} patients was 9.3 years, versus 24.4 years survival in Zap-70^{-} patients (Orchard et al. 2004). Furthermore, Zap-70^{+}CD38^{+} patients were prognostically worse off than Zap-70^{-}CD38^{-} or discordant (Zap-70^{-}CD38^{+} or Zap-70^{+}CD38^{-}) cohorts (Schroers et al. 2005).

1.3.4.4 CD49d

CD49d is a cell surface adhesion molecule (Zucchetto et al. 2005). Initially studies demonstrated that CD49d^{high} patients (>30% CD49d expression) had shorter time to first treatment, and CD49d expression was strongly associated with CD38 expression, *IGHV* mutation status and Zap-70 expression (Zucchetto et al. 2005; Gattei et al. 2008). More recent work lends further support to the prognostic relevance of CD49d, where a pooled analysis of 2,972 CLL patients showed CD49d as the strongest phenotypic marker in regards to prognosis (Bulian et al. 2014).

1.3.4.5 Genetic aberrations

Cytogenic abnormalities have been reported in up to 90% of CLL patients (Moreno and Montserrat 2008). The most common genetic aberration is deletion on the long arm of chromosome 13 (13q-deletion), found in more than 50% of CLL patients and associated with significantly improved prognosis (Redaelli et al. 2004; Puiggros et al. 2014). Deletions have also been observed in the long arm of chromosome 11 (11q-deletions, 10-20% of patients) and short arm of chromosome 17 (17p-deletions, 1.5-7% of patients), but both are associated with significantly poorer outcome (Redaelli et al. 2004; Puiggros et al. 2014). Patients with 17p-deletions are most at risk with the shortest overall survival and shortest progression free survival. Elevated CD38 expression, Zap-70 expression, and unmutated *IGHV* has been associated with 17p-deletions, in addition to strong links with aberrations in the TP53 gene (75% of cases) that codes for p53 (Puiggros et al. 2014).

Trisomy of chromosome 12 occurs in 10-30% of patients (Redaelli et al. 2004). Often it appears as the only genetic aberration in 40-60% of Trisomy 12 cases, but can also appear alongside other abnormalities including trisomy (chromosome 18 and 19) and deletions (13q, 11q, 14q, or 17p). The prognostic potential of trisomy 12 is unclear as studies have identified trisomy 12 patients with varying prognosis: trisomy 12 patients

with poor clinical outcome also present other markers including CD38 and unmutated *IGHV* (Puiggros et al. 2014).

Telomere length has also demonstrated strong prognostic potential. A previous study demonstrated that Binet A patients had significantly longer telomeres than Binet B/C patients, and that shorter telomere length (≤6.0 kb) had significantly poorer survival (Bechter et al. 1998). Telomere length has also been suggested as an additional marker to IgHV mutational status to further classify patients with poorer prognosis (Grabowski et al. 2005). More recently, high resolution single telomere length analysis (STELA) showed that Binet A CLL patients could be stratified into subgroups with good (91% survival at 10 years) or poor prognosis (13% survival at 10 years) based on mean telomere length with telomeric fusion potential (2.26kb) (T. T. Lin et al. 2014). Furthermore, telomere length was the strongest prognostic factor when compared against Binet stage, *IGHV* mutation status, CD38, Zap-70 and cytogenetics.

1.3.5 Treatment

With the heterogeneous presentation of the disease, patients who are diagnosed as early stage (Rai 0, Binet A) and are asymptomatic are subjected to a 'wait and see' approach, with therapy induction only if the disease progresses (Hallek et al. 2008). Indications for treatment (as defined by the National Cancer Institute) include: progressive marrow failure (development or worsening of anaemia/thrombocytopenia); massive/progressive lymphadenopathy; massive/progressive splenomegaly; progressive lymphocytosis; systemic symptoms; autoimmune cytopenias (Oscier et al. 2004).

Initial first-line treatment is usually the combined chemotherapy of fludarabine and cyclophosphamide (FC), or FC and rituximab (FCR). For patients where FCR is unsuitable, treatment is chlorambucil or bendamustine in combination with CD20 antibodies (e.g. obinutuzumab or ofatumumab) (Oscier et al. 2012; NICE 2015a; NICE 2015b). Rituximab, obinutuzumab and ofatumumab are monoclonal antibodies (mAbs) that recognise and bind to the CD20 molecule on the B-cell surface, helping the host immune cells to identify and kill CLL cells via ADCC (Coiffier et al. 2008).

Patients with 17p/TP53 deletions do not respond as well to the standard FC or FCR treatment (Puiggros et al. 2014) and because of this, current guidance now

recommends pre-treatment screening for TP53 loss to allow adequate p53-independent treatment (Oscier et al. 2012).

If patients relapse >2 years following initial treatment, they are continued on the same treatment (i.e. FCR, chlorambucil or bendamustine) unless it is considered inappropriate to do so (Oscier et al. 2012). However, if patients relapse within 2 years, treatment with idelalisib is recommended, similar to high-risk patients (TP53 abnormality). Idelalisib is a small molecule inhibitor of PI3Kδ, a kinase molecule that plays a downstream role in many B-cell signalling pathways, including the BCR, CD40, CXCR4/CXCR5 and CD49d pathways (Furman et al. 2014). This drug thereby inhibits the activation, differentiation, proliferation, migration and survival of CLL cells.

Studies are still ongoing for a further small molecule inhibitor: ibrutinib, which binds to Bruton's tyrosine kinases (BTK). BTK acts downstream of BCR signalling, and BTK inhibition leads to downregulated CD20, as well as downregulation of downstream pathways including ERK 1/2, PI3K, and NF-κB, leading to loss of cell viability (Herman et al. 2014).

1.3.6 T-cell dysfunction in CLL

Although CLL is a B-cell malignancy, T-cell abnormalities have long been observed in patients with this condition (Whelan et al. 1982), and their promotion/suppression appears to contribute to the pathology of the disease. Low frequencies of CLL-reactive T-cells have been identified (Gitelson et al. 2003), however do not appear to successfully mount a response against CLL. Direct T-cell interaction with CLL cells results in defective TCR recognition and TCR dysfunction (Ramsay et al. 2008). Gene expression profiles have revealed that cell-cell contact between CLL cells and T-cells induces molecular defects in both $CD4^+$ and $CD8^+$ T-cells (Görgün et al. 2005). Similar to the malignant B-cells, CD38 expression on T-cells (≥50%) has been associated with poorer prognosis, although in this case the association was seen only in male CLL patients (Tinhofer et al. 2006).

T-cell inhibitory cytokines produced by CLL cells include TNF, IL-6, IL-10 and TGF-β (DiLillo et al. 2013; Nosari 2012; Garaud et al. 2011). CLL cells (and B-cell lines transfected with CD5 cDNA) have been shown to produce IL-10 (Garaud et al. 2011), a cytokine not only associated with immunoregulation of T-cells and DCs but also the

promotion and survival of B-cells (Garaud et al. 2011; Defrance et al. 1992). CLL secretory molecules have also been shown to demonstrate a direct effect on reducing T-cell CD40L presentation and IL-2 expression (a Th1 cytokine) and promoting polarisation to IL-4 Th2-cells (Buggins et al. 2011), the helper subset involved in B-cell help. Th-cells specific for CLL antigens that potentially help and maintain the CLL cells within the tumour microenvironment have been identified (Os et al. 2013).

Expanded numbers of both $CD4^+$ and $CD8^+$ T-cells have been observed in CLL (Pourgheysari et al. 2010). The expansion is markedly greater in the $CD8^+$ T-cell compartment of some CLL patients, resulting in a higher number of $CD8^+$ T-cells than $CD4^+$ T-cells and an inversion in the CD4:CD8 ratio (Gonzalez-Rodriguez et al. 2010). Further analysis of the $CD8^+$ T-cell expansion revealed a decrease in naïve T-cells and an expansion in the EM and further differentiated EMRA compartments (Görgün et al. 2005). Poor prognosis patients ($Zap\text{-}70^+$, $CD38^+$) have also demonstrated a similar T-cell memory skew (Göthert et al. 2013; Monserrat et al. 2013).

In particular, an extensive study from our group (Nunes et al. 2012) involved the immunophenotyping of 110 early-stage untreated patients and demonstrated an inverted CD4:CD8 ratio in 47% of patients. Patients were then stratified into normal ratio (CLL^{NR}) and inverted ratio (CLL^{IR}) cohorts based on a threshold CD4:CD8 ratio of 1.0. CLL^{IR} patients demonstrated a significant reduction in both the naïve and CM $CD8^+$ T-cell populations and a marked expansion in the EMRA subset when compared with CLL^{NR} patients and healthy donors (HDs). Furthermore, Nunes et al. (2012) observed an increase in the $CD57^+CD27^-CD28^-$ phenotype within the inverted ratio cohort, inferring an increase in a highly differentiated, replicative senescent $CD8^+$ T-cell phenotype.

1.4 Hypothesis and aims of the current study

Previous work has reported an expansion in the $CD8^+$ T-cell compartment in a subpopulation of CLL patients, resulting in an inverted CD4:CD8 ratio that is skewed to a more differentiated phenotype and linked to poorer prognosis. However, recent research has identified several novel human T-cell subsets, and demonstrated that the $CD4^+$ and $CD8^+$ compartments are phenotypically complex.

We hypothesise that the $CD8^+$ expansion observed in these inverted ratio CLL patients is an accumulation of aged T-cells displaying signs of senescence and/or exhaustion. Furthermore, the accumulation of these T-cell populations is linked to significantly poorer prognosis. Accurate determination of these T-cell populations could consequently identify a valuable prognostic marker that may help identify patients with inferior prognosis prior to disease progression. Therefore, the overall aim of this thesis is to further characterise the expanded $CD8^+$ T-cells in CLL using higher resolution techniques to provide more precise definition of T-cell phenotypes associated with poor prognosis and to gain an understanding of the role of T-cells in disease pathology.

Firstly, we will explore the phenotypic abnormalities within this inverted T-cell compartment to identify T-cell signatures with potential prognostic value. Markers were looked at both individually and in combination to identify T-cell phenotypes of interest within the inverted ratio patients; these markers include CD57, KLRG-1 and PD-1 (for immune exhaustion/senescence) as well as HLA-DR and CD38 (to indicate activation). Further, the marker expression and definition of T-cell subsets were related to clinical data of untreated patients, to determine their prognostic value.

Next, any markers of prognostic interest were then applied to the phenotypic analyses of treated CLL patients to observe whether treatment affects T-cell populations and whether the presence of prognostic phenotypes is indicative of poorer response to treatment.

The thesis also aimed to explore the mechanisms behind the expansion of $CD8^+$ T-cells in poor prognosis CLL patients. The replicative history of $CD8^+$ T-cells in CLL patients will be studied to ascertain whether the expanded $CD8^+$ population arises due to an accumulation of 'aged' $CD8^+$ T-cells that have undergone multiple rounds of proliferation, or because of continual activation and skewed differentiation from the naïve T-cell pool. To assess replicative age this study employed single telomere length analysis (STELA) to measure telomere length distributions of the $CD4^+$ and $CD8^+$ T-cells, in addition to the $CD8^+$ T-cell memory subsets.

Chapter 2
Materials and methods

2.1. Tissue culture basics

2.1.1. Media and buffers

Freezing mix

40% Roswell Park Memorial Institute (RPMI) 1640 (Sigma-Aldrich), 10% Dimethyl Sulphoxide (DMSO) (Sigma-Aldrich), 50% foetal calf serum (FCS) (Invitrogen).

FACS buffer

1% FCS was added to Phosphate Buffered Saline (PBS, Invitrogen).

MACS buffer

0.5% Bovine Serum Albumin (BSA, Sigma) and 2 mM Ethylenediaminetetraacetic acid (EDTA, Sigma) was added to 100 ml PBS. The buffer was then sterile filtered using a 0.2 µm filter (Millipore).

Red blood cell lysis buffer

1 part red blood cell lysis solution (Miltenyi Biotec) was diluted in 9 parts distilled water.

QIAamp DNA extraction buffers

Qiagen separation kits provided the following buffers: ATL, AL, AW1 and AW2. Before initial use 25 ml 100% ethanol was added to 19 ml Buffer AW1 concentrate, and 30 ml 100% ethanol was added to 13 ml Buffer AW2 concentrate.

1XTEN buffer

1XTEN buffer was made using a 1:10 dilution of 10xTEN stock (Biorad, Hoechst kit).

Tris-HCl

Working stock of 10 mM Tris-HCl was prepared by diluting 1 part 1 M Trizma® hydrochloride buffer solution (Sigma-Aldrich) with 9 parts ddH_20.

Taq/PWO (10:1) reagent

10 µl PWO DNA polymerase (Roche) was added to 100 µl Red Hot DNA polymerase (Thermoprime, Fisher).

Telorette 2 (Tel2) primer

Working stock of Tel2 primer (10 µM) was prepared by diluting 10 µl Tel2 stock with 90 µl ddH_20. Any leftover stock was stored at −20°C and used in subsequent experiments.

Teltail primer

Teltail primer (5 µM) was made by adding 5 µl Teltail stock and 95 µl ddH_20. Any leftover stock was stored at −20°C and used in subsequent experiments.

XpYpE2 (Telomere Adjacent) primer

5 µl of XpYpE2 stock was added to 95 µl ddH_2O to make a 5 µM working solution. Any leftover stock was stored at −20°C and used in subsequent experiments.

Depurination buffer (0.25 M HCl)

108 ml of hydrochloric acid was made up to 5 L with ddH_2O and mixed thoroughly.

Denaturation buffer (1.5 M NaCl/0.5 M NaOH)

438.3 g sodium chloride and 100 g sodium hydroxide was solubilised in 5 L ddH_2O.

Church buffer

0.5 M sodium phosphate buffer (pH7.2) was made using 1 M disodium dihydrogen phosphate, 1 M disodium hydrogen phosphate, 1% BSA, 1 mM EDTA and 7% SDS (Fisher Scientific).

Hybridisation wash buffer

2.5 ml SSC (sodium chloride sodium citrate) and 2.5 ml SDS (sodium dodecyl sulphate) (Fisher Scientific) was made up with ddH_2O to make 500 ml.

2.1.2. Tissue culture plastics

Pasteur pipettes and Falcon tubes (15 ml, 50 ml; Corning Incorporated), pipette tips (1000, 200, 20 and 2 µl; Star Lab), FACS tubes (BD Biosciences).

2.1.3. Cell viability and counting

Cell counts were performed using a Beckman Coulter Vi-cell®. 50μl of sample was added to 450µl of PBS (1:10 dilution) in a sample cup and placed into the Vi-cell carousel. Cell type (CLL lymphs) dilution (1:10) and sample name were entered into the Vi-cell software. Once set to run, the Vi-cell stained the sample with trypan blue, a dye that is taken up by dead cells, which allows the Vi-cell to calculate the number of viable cells per ml.

2.2. Blood donors and preparation

2.2.1. Blood donors

All blood samples were taken with informed consent and appropriate ethical approval. Professor Chris Fegan obtained CLL blood samples from patients attending clinics at the University Hospital Wales and Llandough Hospital. Samples were also obtained through collaboration with Dr Guy Pratt at Birmingham University. Control samples were also obtained from healthy, age-matched patients or healthy volunteers within the department.

2.2.2. Isolation of PBMC

Peripheral blood mononuclear cells (PBMC) were isolated via density gradient centrifugation using Ficoll-Histopaque (Histopaque-1077, Sigma). Whole blood was layered onto histopaque at a 1:1 volume ratio and centrifuged for 20 minutes at 840×g with the brake disabled. After centrifugation, PBMC formed a monolayer on top of the histopaque and were harvested using sterile Pasteur pipettes. PBMC were then transferred to a 15 ml falcon tube and resuspended in fresh PBS. Samples were further centrifuged at 470×g for 5 minutes, and supernatant poured off. If the pellet showed signs of red blood cell contamination, the pellet was suspended in 1 ml red blood cell lysis buffer, incubated for 10 minutes at room temperature and washed with PBS as above. The pellet was then resuspended in 1-15 ml of PBS (determined by pellet size) and counted using the Vi-Cell (Section 2.1.3). To allow potential use for other laboratory projects, samples were also stained for CD19 and CD38 (later also stained for CD3 and CD49d; see Table 2.1 for antibody details) and analysed on the BD Accuri Flow Cytometer with BD Accuri C6 Software.

2.3. T-cell enrichment using MACS

T-cell enrichment was performed on PBMC in preparation for FACS Aria cell sorting. Cells were transferred to a fresh 15 ml falcon tube and centrifuged at 470×g for 5 minutes to form a pellet before resuspending in 1 ml MACS buffer. 50 µl of anti-CD19 microbeads (MACS, Miltenyi) per 100 x 10^6 cells were added and then put onto a roller mixer (Bibby Stuart Scientific, SRT2) for 15 minutes at 4°C. Cells were washed again and resuspended in a 1 ml fresh MACS buffer before loading onto the MACs AutoMACS machine. This passed the cell/microbead suspension through magnetic columns, allowing anti-CD19 labelled cells to attach. Unlabelled cells passed through the columns and were aliquoted into a fresh 15 ml falcon tube as the negative fraction. The $CD19^+$ cells were then released from the columns into a positive fraction 15 ml falcon tube. The negative fraction was retained for further T-cell subset isolations via FACS sorting.

2.4. Fluorescent antibody staining and flow cytometric analysis

Flow cytometry was undertaken using BD Accuri, BD FACS Canto II and BD FACS Aria machines. During data collection Accuri C6 or BD FacsDiva software were used, and data was later analysed using Accuri C6 or FlowJo analysis (version 9) software.

2.4.1. Antibodies used

Tables 2.1-2.6 below depict the antibody panels used. To determine optimum staining, antibodies were titrated by comparing mean fluorescent intensity (MFI) of the full test volume as recommended by the manufacturer versus half of the recommended test volume. If half the test volume produced similar MFI to the full test, half test volume was used for the main experiments; if not, the full recommended test was used.

Table 2.1. Blood sample preparation panel (Accuri C6)

Antibody	Fluorochrome	Company (Ref no.)	Description
CD19	APC	Invitrogen (MHCD1905)	Mouse IgG1, Clone SJ25-C1
CD38	PE	Invitrogen (MHCD3804)	Mouse IgG1, Clone HIT2
CD49d	PerCP-Cy5.5	Biolegend (304312)	Mouse IgG1, Clone 9F10
CD3	FITC	Biolegend (300440)	Mouse IgG1, Clone UCHT1

Table 2.2. T-cell memory subsets (Accuri C6)

Antibody	Fluorochrome	Company (Ref no.)	Description
CD3	PE-Cy5.5	Invitrogen (MHCD0318)	Mouse IgG2a, Clone 7D6
CD8	APC	BD Biosciences (555369)	Mouse IgG1, Clone RPA-T8
CCR7	PE	R&D Systems (FAB197P)	Mouse IgG2a, Clone #150503
CD45RO	FITC	Biolegend (304204)	Mouse IgG2a, Clone UCHL1

Table 2.3. T-cell subsets and activation/senescence markers – Panel 1 (Accuri C6)

Antibody	Fluorochrome	Company (Ref no.)	Description
CD3	AmCyan	BD Biosciences (339186)	Mouse IgG1, Clone SK7
CD8	APC-Cy7	Biolegend (344714)	Mouse IgG1, Clone SK1
CD4*	PE	Biolegend (300508)	Mouse IgG1, Clone RPA-T4
CCR7	PE-Cy7	BD Biosciences (557648)	Rat IgG2a, Clone 3D12
CD45RO	FITC	Biolegend (304204)	Mouse IgG2a, Clone UCHL1
CD57	APC	Biolegend (322314)	Mouse IgM, Clone HCD57
HLA-DR	PerCP-Cy5.5	Biolegend (307630)	
PD-1	Brilliant Violet 421	Biolegend (329920)	Mouse IgG2a, Clone L243
***Panel 1 initially included an antibody for BCL-2 (see below): later substituted with anti-CD4.**			
BCL-2	PE	BD Biosciences (340576)	Mouse IgG1, Clone 100

Table 2.4. T-cell subsets and activation/senescence markers – Panel 2 (Accuri C6)

Antibody	Fluorochrome	Company (Ref no.)	Description
CD3	AmCyan	BD Biosciences (339186)	Mouse IgG1, Clone SK7
CD8	APC-Cy7	Biolegend (344714)	Mouse IgG1, Clone SK1
CCR7	PE-Cy7	BD Biosciences (557648)	Rat IgG2a, Clone 3D12
CD45RO	PE	Biolegend (304205)	Mouse IgG1, Clone UCHL1
CD57	APC	Biolegend (322314)	Mouse IgM, HCD57
CD38	PerCP-Cy5.5	Biolegend (303522)	Mouse IgG1, Clone HIT2
CD127	Brilliant Violet 421	BD Biosciences (562436)	Mouse IgG1, Clone hIL-7R-M21
KLRG-1	Alexa-Fluor488	Pircher, Germany	Mouse IgG2a, Clone 13F12F2

Table 2.5. T-cell memory sorting (FACS Aria)

Antibody	Fluorochrome	Company (Ref no.)	Description
CD3	AmCyan	BD Biosciences (339186)	Mouse IgG1, Clone SK7
CD4	PE	Biolegend (300508)	Mouse IgG1, Clone RPA-T4
CD8	APC-Cy7	Biolegend (344714)	Mouse IgG1, Clone SK1
CCR7	PE-Cy7	BD Biosciences (557648)	Rat IgG2a, Clone 3D12
CD45RO	FITC	Biolegend (304204)	Mouse IgG2a, Clone UCHL1

Table 2.6. T-cell subsets and activation/senescence markers – Treated Patient Panel (Accuri C6)

Antibody	Fluorochrome	Company (Ref no.)	Description
CD3	PerCP-Cy5.5	Biolegend (317336)	Mouse IgG2a, Clone OKT3
CD8	APC-Cy7	Biolegend (344714)	Mouse IgG1, Clone SK1
CD4	Alexafluor488	Biolegend (300519)	Mouse IgG1, Clone RPA-T4
CCR7	PE-Cy7	Biolegend (353226)	Mouse IgG2a, Clone G043H7
CD45RO	Brilliant Violet 510	Biolegend (304246)	Mouse IgG2a, Clone UCHL1
CD57	APC	Biolegend (322314)	Mouse IgM, Clone HCD57
HLA-DR	PE	Biolegend (307606)	Mouse IgG2a, Clone L243
PD-1	Brilliant Violet 421	Biolegend (329920)	Mouse IgG1, Clone EH12.2H7

2.4.2. Flow cytometer and compensation set-up

For immunophenotyping on the Accuri cytometer, fluorescence compensation was achieved with Accuri C6 software. Initial compensation was applied using manufacturer's recommended compensation values, which were then manually optimised for the panel using known positive and negative samples for each marker.

For the BD FACS Canto II or BD FACS Aria, fluorescence compensations were achieved automatically using the BD FacsDiva software and positive (anti-mouse Ig and, where appropriate, anti-rat Ig) and negative control CompBeads (BD). Three drops of both anti-mouse Ig beads and negative control beads were added per 700 µl of FACS buffer; 100 µl of which was transferred to fresh FACS tubes per each antibody to be compensated, plus an unstained control. Each antibody required for that panel (see respective tables in Section 2.4.1) was added to a tube containing the beads at the same volume that would be added to a cell sample and incubated for 10 minutes at room temperature (in the dark). Following incubation, the stained beads (along with one tube of unstained beads) were diluted with 900 µl of FACS buffer, ready to run through the cytometer machine.

The unstained control was run through the flow cytometer to gate on the beads using forward and side scatter, as well as to adjust voltages of the appropriate fluorescent channels to achieve negatively positioned populations within quadrant gates. Following this each single-stained compensation sample was run through the machine and the single peak of the positively stained bead population was tightly gated on a histogram. If needed, voltages were further adjusted to bring peaks into the parameters of the software graphs; if this adjustment was performed all previously run samples would be re-analysed to ensure accurate gating. Once all single-stained controls were analysed, BD FacsDiva software automatically calculated compensation for the panel. Compensation settings could then be checked by eye using a multi-stained cell sample for all relevant antibodies to ensure that all the cell populations aligned appropriately on the scatter plots.

2.4.3. Immunofluorescent staining

1 ml FACS buffer was added to 1-2 x 10^6 cells in a FACS tube and centrifuged at 470×g for 5 minutes, and then the supernatant discarded. Antibodies were then added directly to the pelleted cells before vortexing briefly and incubating for 30-45 minutes at 4°C in the dark. The samples were then washed a further time in FACS buffer and either analysed straight away or fixed in 1% paraformaldehyde (PFA) for later analysis. Cells for the FACS Canto II panels were always fixed before analysis. Cells destined for the FACS Aria were used immediately and were not fixed to allow for further downstream DNA (STELA) analyses.

For most immunophenotyping experiments, cells were stained in a single step as above. However, initial experiments using Panel 1 for the FACS Canto II (Section 2.4.1, Table 2.3) contained an antibody for the intracellular marker BCL-2. In the first instance staining was performed as above for all antibodies with the exception of anti-BCL-2. Following the second wash 50 µl of Fixation (ThermoFisher) solution was added and cells were incubated for 15 minutes at room temperature, in the dark. After a further wash, 50 µl Perm solution (ThermoFisher) was then added to the cell pellet directly followed by the anti-BCL-2 and incubated for a further 15 minutes at room temperature. Cells were then washed a final time with FACS buffer before being resuspended in 1% PFA for later analysis.

2.4.4. Fluorescent minus ones (FMOs)

Negative controls for this study included both unstained cells and fluorescent minus ones (FMOs). To achieve an FMO control, 1-2x10^6 cells were stained with antibodies as described above for standard samples, with the exception that the sample was stained with all antibodies minus the single antibody that the control is for (see an explanatory example of FMOs in Table 2.7). Samples were then incubated for 30-45 minutes at 4°C in the dark, as above, before washing and fixing with 1% PFA.

On running and analysing the samples, FMOs were used for constitutively expressed markers where there is no clear positive/negative population, e.g. CCR7, HLA-DR, CD38, PD-1. FMOs were used to help gauge where the negative population lies, taking into account any fluorescent spillover from other antibodies in the panel, thus helping to make a more accurate gating of positive populations in the fully stained samples (Figure 2.1).

Table 2.7. Example matrix for fluorescence minus one (FMO) samples

FMO	Antibody				
	CD3:AmCyan	CD4:PE	CD8:APC-Cy7	CCR7:PE-Cy7	CD45RO:FITC
CD3	–	✔	✔	✔	✔
CD4	✔	–	✔	✔	✔
CD8	✔	✔	–	✔	✔
CCR7	✔	✔	✔	–	✔
CD45RO	✔	✔	✔	✔	–

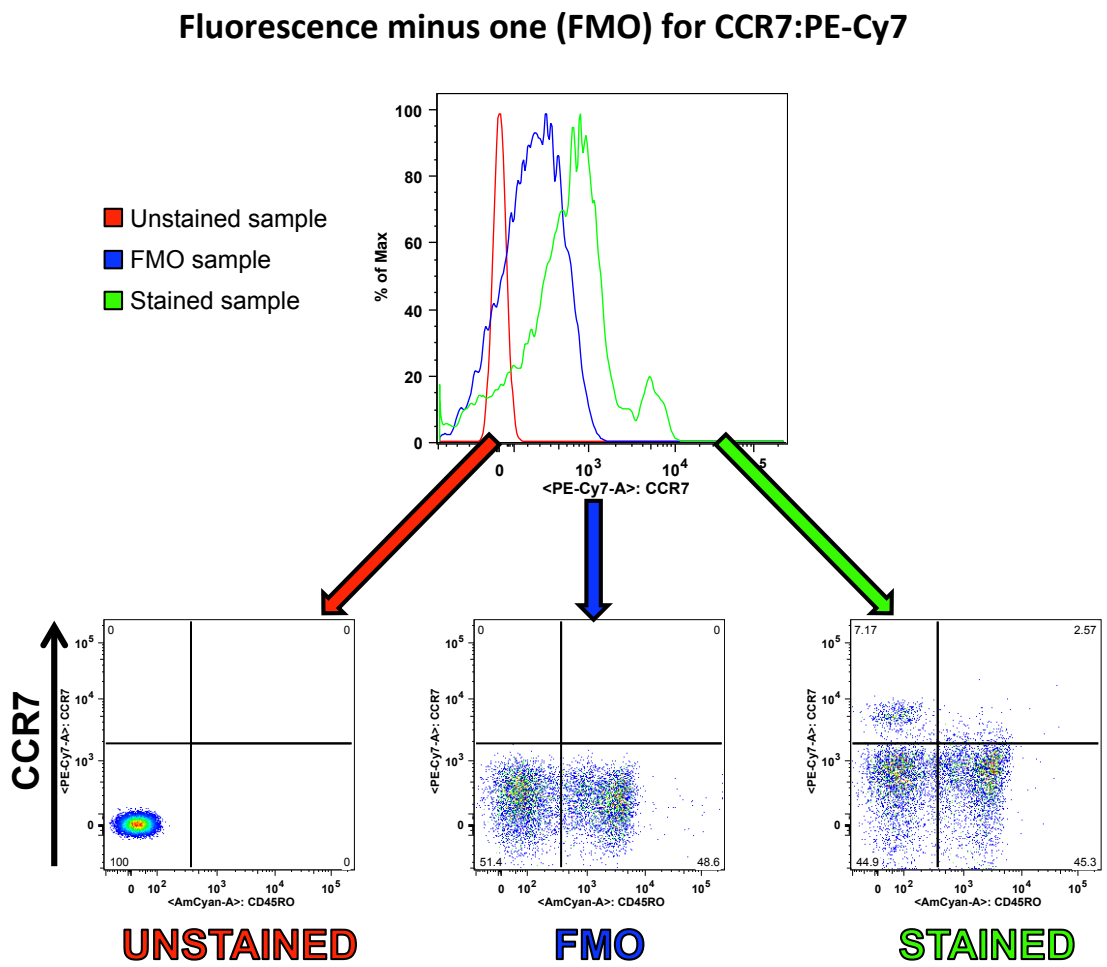

Figure 2.1. Example of fluorescence minus one (FMO) control for flow cytometric analysis – CCR7:PE-Cy7. FMO sample was stained with all antibodies, with the exception of anti-CCR7. The CCR7 negative population was gated based on the negative population of the FMO sample. This gave a more accurate gating strategy than if using an unstained control as it accounts for fluorescence spillover from other antibodies used in the staining.

2.4.5. Absolute counts

Absolute counts were performed using BD Trucount tubes, containing a freeze-dried pellet with a known quantity of fluorescent Trucount beads. To ensure volume accuracy, a reverse pipetting technique was employed.

An antibody master mix was made for the number of samples to be stained, using T-cell subset Panel 1 antibodies. 2 x 10^6 PBMC sample was transferred to a FACS tube and washed with 1 ml FACS buffer. The sample was centrifuged at 470×g for 5 minutes and supernatant poured off. The sample was then resuspended in 50 µl of FACS buffer and transferred to the Trucount tube, ejecting the sample just above the metal retainer. The appropriate volumes of antibodies were added to the Trucount tube from the antibody mastermix. The tube was then vortexed gently to mix, and incubated for 15 minutes at room temperature in the dark.

Following incubation 200 µl of FACS buffer was added and the sample was stored covered and on ice, until ready to run through the BD FACS Canto II flow cytometer. Prior to running samples on the flow cytometer, each sample was vortexed gently and PMT voltages were adjusted on the machine in order to visualise the forwards and side scatter profile of the beads (SSC-A/FSC-A).

Following data acquisition, the following calculation was performed in Excel to determine absolute counts:

$$\frac{\text{\# of events in region containing cell}}{\text{\# of events in absolute count bead region}} \times \frac{\text{\# of beads per test}}{\text{test volume}} = \text{absolute count of cell}$$

Where the number of events in the region containing the cell is the count within the gated population of interest, and the absolute count bead region is gated in the forward/side scatter graph. The number of beads per test was obtained from the Trucount packaging (number varies from lot to lot) and the test volume was the final volume of PBMC, antibodies and FACS buffer added to the Trucount tube.

2.4.6. Statistical analyses

Phenotypic data was collated in Excel, and statistics performed in GraphPad Prism. Initial column statistics were performed to analyse distribution of immunophenotyping data and determined that the majority of columns were non-parametric: therefore, use

of non-parametric tests were applied. The Mann-Whitney U test was used to analyse differences between two independent parameters (HD versus CLL) and the Kruskal-Wallis test with post-hoc Dunns was applied for comparisons between three or more variables (HD versus CLL^{NR} versus CLL^{IR}). Correlation analyses were performed using Spearman's rank correlation coefficient and Kaplan-Meier curves were used to determine survival. For associations between Inverted Ratio and clinical data, Fisher's exact test was used. Pestle (Pestle 1.7) was used to convert data text files into SPICE files, and SPICE (SPICE 5.3 software) was used to create pie chart overviews and calculate significance between pies and variables. Multivariate analyses were performed by Professor Robert Hills (Haematology Clinical Trials Unit, Cardiff University).

2.5. Single telomere length analysis (STELA) of T-cell subsets

2.5.1. Acquisition of samples

Isolated PMBC were separated via autoMACS as described in Section 2.3. The CD19-negative fraction was retained and stained with the T-cell memory sorting antibody panel (Section 2.4.1, Table 2.5) and FACS sorted using BD FACS Aria for $CD4^+$, $CD8^+$ and $CD8^+$ memory T-cells into 1.5 ml eppendorf tubes. Cells were pelleted by spinning at 3400×g for 5 minutes, and the supernatant removed. Cells were then washed twice in 1 ml PBS and all but 20 µl of supernatant removed. Samples were then stored on ice ready for DNA extraction.

2.5.2. DNA extraction

DNA extraction was performed using QIAamp DNA Micro kits (Qiagen) according to manufacturer instructions (Figure 2.2). Briefly, 80 µl of Buffer ATL was added to the 20 µl samples to make a final volume of 100 µl. Buffer AL (100 µl per sample) was aliquoted into a fresh eppendorf tube and 1 µl of carrier RNA added per 100 µl of Buffer AL. 10 µl proteinase K and 101 µl of the Buffer AL/carrier RNA mix were then added to each sample sequentially and mixed by vortexing for 15 seconds. The samples were then transferred to a heating block and incubated at 56°C for 10 minutes.

Following incubation, samples were pulse-centrifuged briefly to remove droplets from the lid before adding 50 µl 100% ethanol (stored at −20°C) and pulse-vortexing again

for 15 seconds. Samples were incubated for 3 minutes at room temperature and briefly centrifuged to remove droplets from the lid.

Cell lysate was carefully transferred to a QIAamp MinElute column (inside a 2 ml collection tube), the lid closed and sample centrifuged at 6000×g for 1 minute to allow the lysate to pass through the membrane. The collection tube and flow-through was then discarded and the MinElute column transferred to a fresh collection tube. 500 µl Buffer AW1 was added to the MinElute column and centrifuged as before, discarding the collection tube for a fresh one. The same process was then repeated with 500 µl Buffer AW2. The column was then centrifuged at full speed for 3 minutes to dry the column membrane completely, before transferring the MinElute column into a fresh 1.5 ml eppendorf tube (lid removed). An appropriate amount of Buffer AE (between 20-100 µl, depending on the number of cells in the original sample) was added to the column and incubated for 5 minutes at room temperature. Tubes were then centrifuged at full speed for one minute. To ensure complete elution of the DNA, the flow through was then transferred back into the MinElute column and incubated for a further 5 minutes, then centrifuged. The MinElute column was discarded and DNA sample was then quantified or stored at −80°C for future quantification.

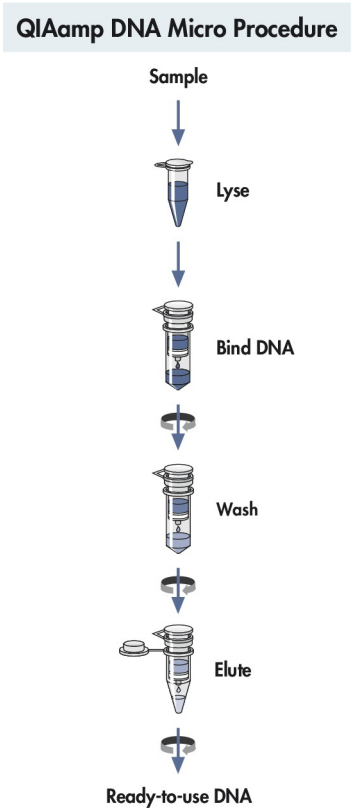

Figure 2.2. Brief overview of the QIAamp DNA Micro procedure, used to isolate DNA from T-cell populations. $CD19^-$ PBMC was cell-sorted to obtain whole $CD4^+$ T-cells, whole $CD8^+$ T-cells and $CD8^+$ memory T-cell populations. DNA was isolated from these populations using the QIAamp DNA micro kits (Qiagen) according to manufacturers instructions. Figure obtained from QIAamp® DNA micro handbook (3rd ed., 2014).

2.5.3. DNA quantification

DNA was quantified using a fluorometer and Hoechst DNA quantification kit (BioRad). The fluorometer was turned on and left to warm up for a minimum of 30 minutes prior to DNA quantification. DNA samples were kept on ice at all times and, if frozen, left on ice to thaw prior to quantification. An appropriate volume of 1XTEN was made for the number of samples, before adding Hoechst for a 1:10,000 dilution (i.e. for 100 ml 1XTEN, 10 µl Hoechst would be added). Blank and Standard controls were used for fluorometer calibration: 2 ml of 1XTEN/Hoechst was transferred to a fresh cuvette for the Blank control, and the Standard control was made by adding 10 µl calf thymus DNA (100 ng/µl) to a second cuvette with 2 ml 1XTEN/Hoechst.

To quantify the DNA, 2 µl of the DNA sample was added to a fresh cuvette with 2 ml 1XTEN/Hoechst. The cuvette was placed in the fluorometer and the relative fluorescent unit (RFU) value recorded. Each sample was measured in triplicates and the mean RFU was used to give the quantity of DNA (ng/µl).

2.5.4. STELA polymerase chain reaction (PCR)

Following quantification of DNA, PCR was performed. If the initial concentration of sample DNA was above 10 ng/µl, DNA was further diluted with tris-HCl to a concentration of 10 ng/µl in 20 µl total. Telorette 2/DNA mix (Tel2/DNA) was then prepared using 1 µl DNA (10 ng/µl), 1 µl Tel2 (10 µM) and 38 µl tris-HCl. If the original DNA concentration was <10 ng/µl the dilution step was missed and a sample volume equivalent to 10 ng DNA was added to 1 µl Tel2 and the volume of tris-HCl adjusted accordingly to give a final volume of 40 µl.

For this study 6 PCR reactions were carried out per DNA sample, but calculations were made to allow for 7 reactions to allow for error. PCR reaction mix was made in a 1.5 ml eppendorf as described in Table 2.8 for the number of samples needed (e.g. if doing PCR for 5 patient samples, with 7 reactions per sample, a PCR mastermix for 35 reactions is needed). The telomere specific primer used in this study was XpYpE2. The reagents were added to a fresh eppendorf with the exception of the Taq/PWO. 7 µl of each DNA/Tel2 was added to a fresh 0.5 ml eppendorf. Taq/PWO was transferred from a freezer (−20°C) to cold block (also stored at −20°C) and the required volume quickly added to the reaction mix. The reaction mix was then mixed briefly by gently inverting the tube and 63 µl was added to the 7 µl aliquots of DNA/Tel2 and briefly mixed again.

The final PCR mix was then transferred to PCR strips in 10 µl aliquots (6 aliquots for each strip). 10 µl mineral oil was then dropped on the surface of each PCR reaction and strips transferred to a PCR block and run through a primer-dependant PCR programme. For XpYpE2 primers the programme was 22 cycles of: 94°C, 20 seconds; >65°C, 30 seconds; >68°C, 8 minutes. On completion of the programme samples were kept at 10°C in the PCR block until ready to use, or transferred to be stored at 4°C.

Table 2.8. Reagents for PCR master mix, with 7 reactions used per DNA sample.

Reagent	1 reaction (µl)	7 reactions (µl)
H_2O	4.98	34.9
Taq 10xbuffer	1	7.0
$MgCl_2$ (25mM)	0.8	5.6
NTPs (100mM total)	0.12	0.84
Teltail (5μM)	1	7.0
Telomere specific primer XpYpE2 (5μM)	1	7.0
Taq/Pwo (10:1)*	0.1	0.7
Total volume	9.0	63.0
*Taq/Pwo to be added directly before aliquoting to DNA/Tel2		

2.5.5. Gel electrophoresis

Forty well 0.5% agarose gels were prepared in a 40 cm submarine gel tank: 2 g agarose MP (Roche) was completely dissolved in 400 ml 1xTAE by heating in a microwave. Once the agarose had cooled to hand hot temperature 40 µl ethidium bromide (10 mg/ml) solution was added and mixed in gently. The agarose was then poured into the 40 cm submarine containing a 40 well comb and left for a minimum of 30 minutes to set. Once set the gel was submerged in 1xTAE, which was left to cool for a minimum of 30 minutes via buffer circulation through a cooling incubator before sample loading.

PCR samples were prepared for loading by adding 2 µl 6x Ficoll loading dye to each reaction. DNA ladders were prepared using 0.5 µl 1 kb ladder (Stratagene), 0.5 µl 2.5 kb ladder (Bio-Rad), 1 µl 6xFicoll and 4 µl of ddH_2O per ladder lane needed. 5 µl of sample (or ladder) were then loaded per lane and the gel was run overnight with chilled buffer recirculation at 120v (approximately 60mA).

2.5.6. Southern blotting

Once removed from the tank, gels were visualised using a UV transilluminator and, using the DNA ladder as a guide, was cut above the largest fraction and below the smallest fraction. Gels were then transferred to a shallow tray and washed twice in depurination buffer (0.25 M HCl) for 6 minutes on a shaker. Following each depurination wash, the gel was briefly washed in milli-Q water. Following depurination gels were then washed for 15 minutes with denaturation buffer (1.5 M NaCl, 500 mM NaOH). Gels were then transferred to a Southern Blot system, as outlined in Figure 2.3. Briefly, Whatman paper was placed over a glass plate in a deep tray and wetted with denaturation buffer until buffer filled the tray to a depth of approximately 5 cm and the sides of the Whatman paper dipped into the buffer. A second piece of Whatman paper, cut to the size of the glass plate, was then placed on top of the first and wetted. The gel was then transferred on top of the Whatman paper and Hybond-XL GE membrane (cut to the size of the gel) placed directly on top. Clingfilm was placed around the gel to prevent the buffer short-circuiting. The gel was then covered by a third Whatman paper pre-wet with denaturation buffer (cut to the size of the gel) and paper towels. Pressure was applied by placing another (dry) glass plate with a 500ml glass bottle filled with water on top of the blot. This was then left to blot for a minimum of 4 hours, occasionally replacing the wet paper towels as needed. After blotting the membrane was removed ready for hybridisation, or dried and stored until needed.

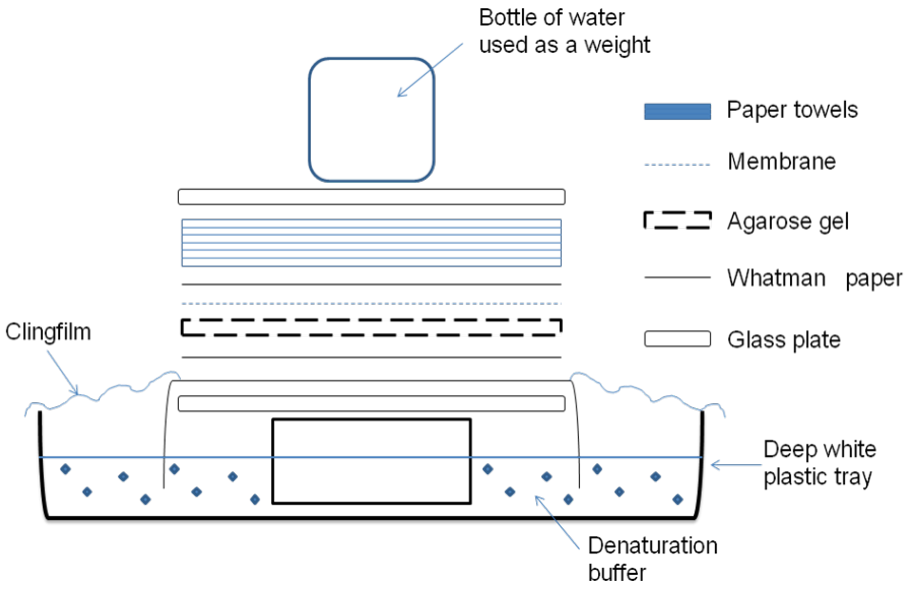

Figure 2.3. Southern blot system for STELA.

2.5.7. Radioactive labelling of STELA membranes.

1 µl of telomere probe DNA (25 ng/µl) was diluted with 44 µl TE buffer and denatured by incubating at 96°C for 5 minutes, followed by snap cooling on ice for 5 minutes. After briefly centrifuging, the DNA was then transferred to a 1.5 ml tube containing a DNA labelling bead or rediprime II labelling system (Amersham/GE Biosciences) and gently pipetted until the bead/mix had dissolved. 4 µl of ^{33}P isotope was then added and the mix was incubated for a minimum of 1 hour in a water bath set to 37°C. Once incubation was complete the tube was once again briefly centrifuged and 1 µl of pre-labelled 1 Kb/2.5 Kb ladder marker was added. The probe was then diluted with 50 µl ddH_2O (giving a total volume of 100 µl). The probe could then be used straight away or stored at 4°C until needed.

STELA southern blots were briefly washed in ddH_2O before transferring to a clean hybridisation bottle (ensuring the side with DNA was facing inwards) with 15 ml church buffer (hybridisation buffer). Bottles were then placed in the hybridisation oven and incubated at 56°C until ready to add the probe. The radioactive probe was denatured by incubating at 96°C for 5 minutes, then used immediately. Bottles were removed from the oven and 25 µl of the denatured probe was added to each bottle before being returned to the oven. Bottles were left to incubate for at least overnight.

Following sufficient incubation, the hybridisation solution was then carefully disposed of down the designated sink. The membrane then underwent three brief washes with 50 ml pre-warmed wash buffer, allowing the membrane to roll and unroll. The bottle was then returned to the oven with 50 ml wash buffer and incubated twice for 30 minutes, replacing the wash buffer between incubations. The membranes were briefly washed a further 3 times before removing the membrane and placing DNA side up on 3MM folded paper, patted dry with a piece of blue roll and placed in an oven to dry. Once completely dry, membranes were transferred to storage cassettes with a phosphoimager screen (Amersham) that had been 'blanked' using a 15 minute exposure to visible light and left for a minimum of 24 hours. The screen was then visualised by scanning with Typhoon 9410 or Typhoon 9500 biomolecular imager (GE Healthcare).

2.5.8. Statistical analysis

Gel images were analysed using ImageQuant. The telomeres visualised on the blot were identified and molecular weights calculated using Phoretix 1D software. Microsoft Excel

was used to obtain actual telomere lengths (by subtracting the STELA primer) and calculate mean, standard deviation, standard error and 95% confidence intervals. General statistical analyses of telomere lengths were performed in GraphPad Prism.

Chapter 3

Immunophenotyping of $CD8^+$ T-cells in CLL

Although a B-cell malignancy, altered immunological function has long been observed within the T-cell compartment of CLL patients (Whelan et al. 1982; Rossmann et al. 2002; Riches et al. 2013). These T-cell abnormalities may reduce any immunological response against the disease, and may thereby contribute to the CLL pathology. Recent studies exploring the CLL T-cell compartment have revealed a sub-group of patients with a preferential expansion within the $CD8^+$ T-cell subset, leading to an inverted CD4:CD8 T-cell ratio (Nunes et al. 2012; Gonzalez-Rodriguez et al. 2010). Nunes et al. (2012) demonstrated that patients showing this inverted phenotype had shorter time to first treatment and a poorer prognosis. Therefore, immunophenotypic characterisation of $CD8^+$ T-cells, particularly within the inverted ratio cohort, may help further understanding of the role of T-cells within CLL pathology.

The main aim of this chapter was to further explore the $CD8^+$ T-cell phenotypes in CLL using multi-colour flow cytometry. This study used the peripheral blood mononuclear cells (PBMC) from 99 CLL patients and 14 age-matched healthy donors. 25 of the 99 CLL patients were analysed using a 4-colour T-cell memory panel (see Chapter 2, Table 2.2) and the full phenotypic analysis was performed on the remaining 74 patients (see Chapter 2, Tables 2.3 and 2.4). The majority of CLL patients tested (63/74 [85%]) were Binet Stage A. These patients were analysed as a complete cohort, and also stratified into subgroups according to their CD4:CD8 ratio; patients with a ratio <1.0 were considered to have an inverted ratio (CLL^{IR}) whereas patients with a ratio >1.0 were assigned a normal ratio (CLL^{NR}) (Nunes et al. 2012).

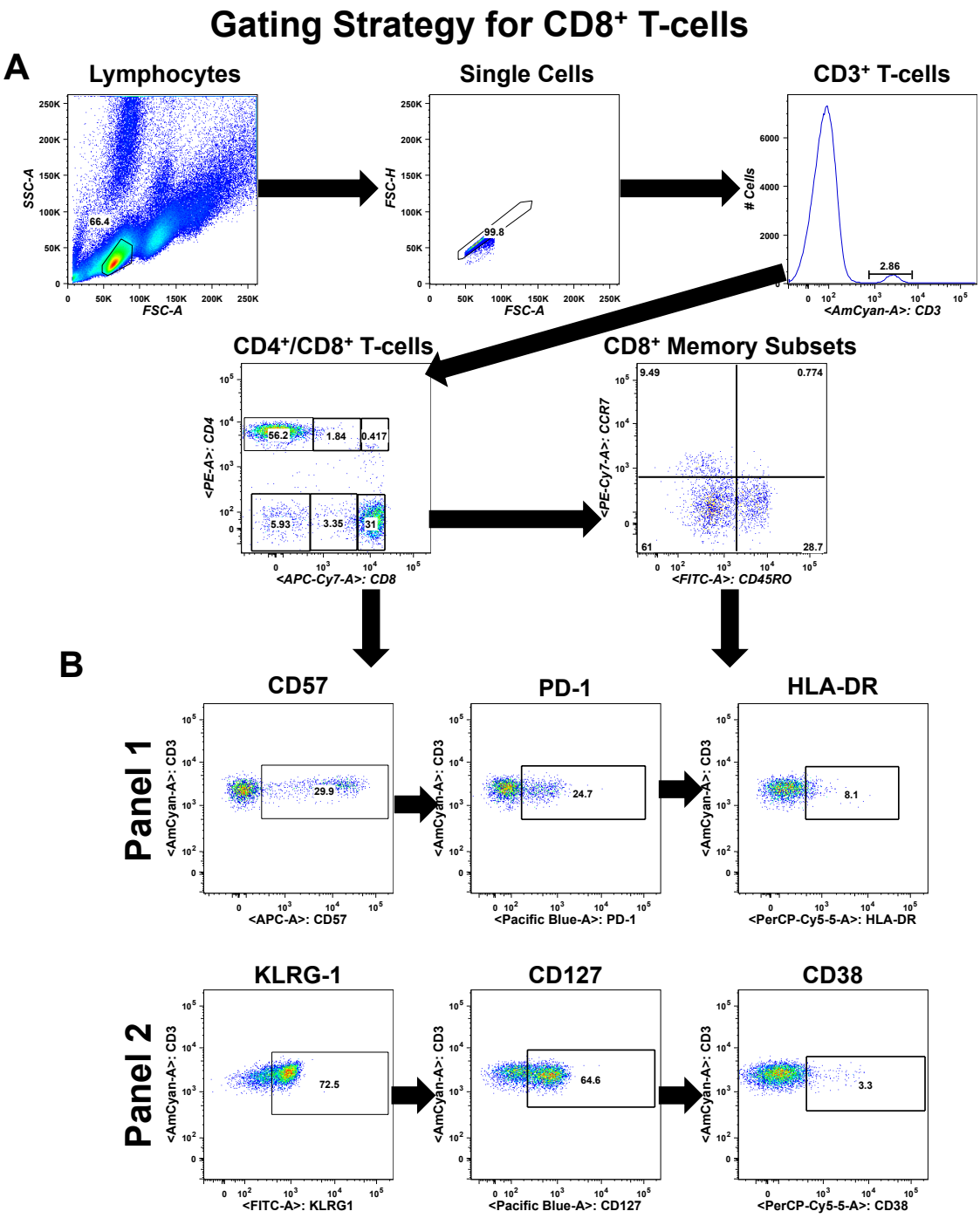

Figure 3.1. Gating strategy used for phenotypic analysis of CD8$^+$ T-cells derived from CLL patients and healthy donors. (A) Cells were labelled with an 8-colour panel of antibodies (see Chapter 2 Materials and methods, Tables 2.3 and 2.4 for complete antibody list) prior to data acquisition using flow cytometry (FACS CantoII, BD FACSDiva) and analysed with FlowJo (v.9). Lymphocytes were gated based on forward and side scatter profile; single cells were gated by forward scatter area and height. CD8$^+$ T-cells were identified by gating on CD3$^+$ and then CD8$^+$ populations. Memory T-cell subsets were defined using CCR7 and CD45RO memory markers: naïve (CCR7$^+$CD45RO$^-$), central memory (CM, CCR7$^+$CD45RO$^+$), effector memory (EM, CCR7$^-$CD45RO$^+$) and EMRA (CCR7$^-$CD45RO$^-$). (B) Gating strategy for activation and senescence/exhaustion markers within the CD8$^+$ T-cell compartments and memory subsets. The boundary of the gating was determined by using fluorescence-minus-one (FMO) controls where necessary.

3.1. Memory subsets

The T-cell compartment can be divided into functionally different subsets: naïve, Central Memory (CM), Effector Memory (EM) and EMRA (Sprent and Surh 2002; Sallusto et al. 2004; Harty and Badovinac 2008). These subsets can be phenotypically defined based on the co-expression of different cell-surface markers; in this study CCR7 and CD45RO were used (for gating strategy see Figure 3.1A).

Distinct differences in $CD8^+$ memory subset distribution were observed between the CLL cohort and the healthy donors (Figure 3.2). Specifically, the CLL cohort showed a significant 3-fold reduction within the naïve subset ($p < 0.001$) as well as a reduction in the CM compartment ($p = 0.0013$). On the other hand the EM subset was significantly increased in CLL patients ($p = 0.0087$); the EMRA subset was also increased in frequency in CLL patients but this did not reach significance. The $CD8^+$ population therefore demonstrated a marked shift towards a differentiated memory phenotype when compared with age-matched healthy donors.

To determine whether the shift towards a memory phenotype contributed to the different CD4:CD8 ratios found in CLL patients, the cohort was stratified into inverted and normal ratio subgroups (Figure 3.3). Patients with an inverted ratio (CLL^{IR}, CD4:CD8 ratio <1.0) had a more significant decrease in the naïve subset when compared with both the healthy donors and CLL patients with a normal ratio (CLL^{NR}) ($p \leq 0.001$ for both). A stepwise increasing trend ($CLL^{IR} > CLL^{NR} > HD$) was seen in both the EM and EMRA subsets, with the CLL^{IR} EM subset showing a significantly increased frequency when compared with healthy donors ($p \leq 0.01$).

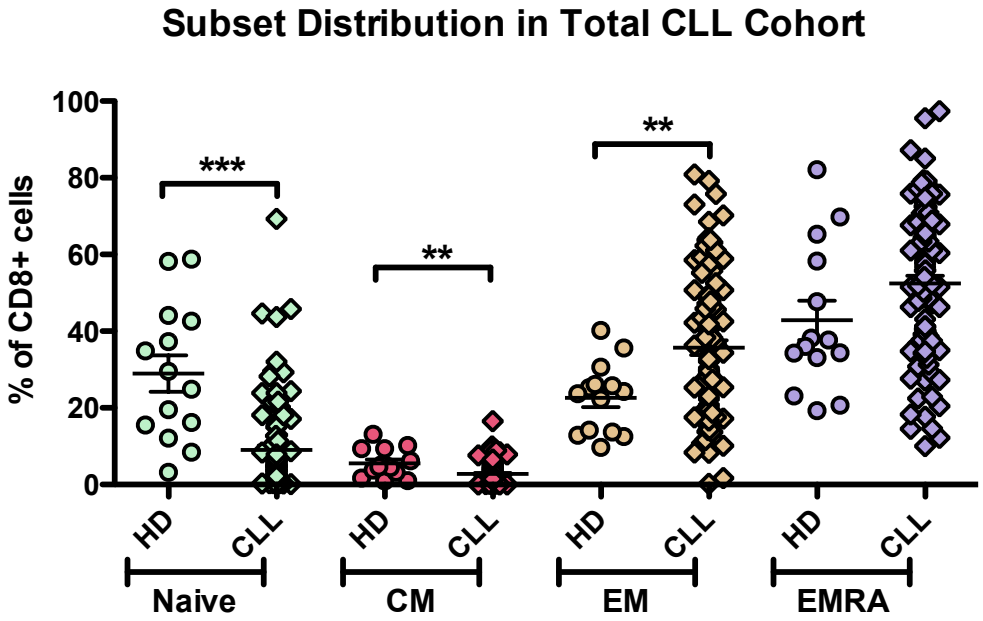

Figure 3.2. Comparison of CD8$^+$ T-cell memory subsets in CLL patients (n = 99) and age-matched healthy donors (HD, n = 14). Cells were collected using flow cytometry (FACS CantoII, BD FACSDiva) and analysed with FlowJo (v.9) using gating as described in Figure 3.1. Pairwise statistical analysis (HD vs CLL) was performed using the non-parametric Mann-Whitney test. Significant results were included on the graph (* = p ≤0.05; ** = p ≤0.01; *** = p ≤0.001).

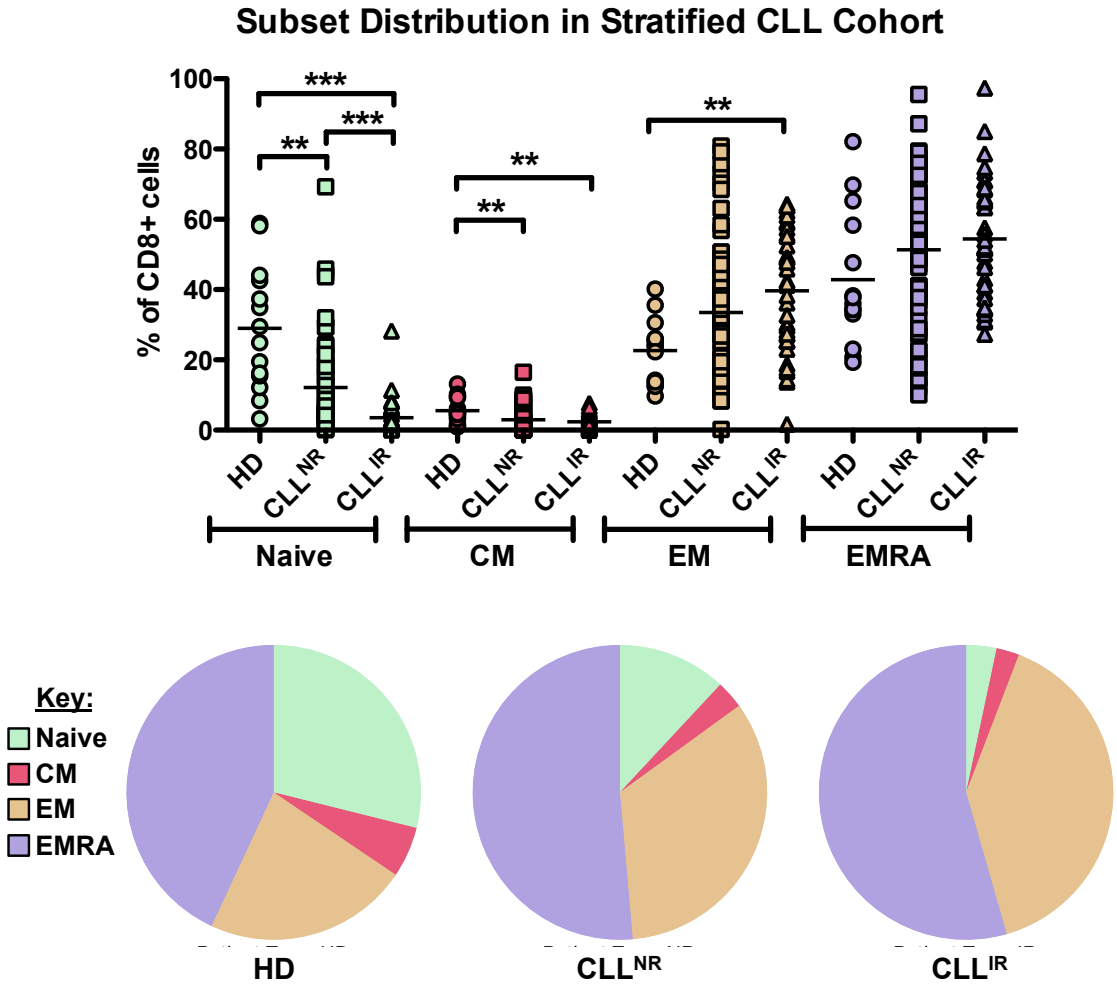

Figure 3.3. Comparison of CD8$^+$ T-cell memory subsets in healthy donors (HD, n = 14) and CLL patients with a normal (CLL^{NR}, n = 63) and inverted (CLL^{IR}, n = 36) CD4:CD8 T-cell ratio. Cells were collected using flow cytometry (FACS CantoII, BD FACSDiva) and analysed with FlowJo (v.9) using gating as described in Figure 3.1. CLL patients with a CD4:CD8 ratio <1.0 were considered inverted. Three-way ANOVA statistical analysis was performed using Kruskal-Wallis test (HD vs CLL^{NR} vs CLL^{IR}), with all pairs of data assessed using the Dunn's post-test. Significant results were included on the graph (* = p ≤0.05; ** = p ≤0.01; *** = p ≤0.001).

3.2. Phenotypic overview

Previous work has shown a preferential expansion within the $CD8^+$ population of some CLL patients that is linked with a more differentiated, potentially senescent phenotype (Nunes et al. 2012). Consequently, the phenotypic composition of the $CD8^+$ compartment was further explored in this study using additional markers for senescence (KLRG-1), activation (HLA-DR, CD38), and differentiation (CD127), across two multi-colour flow cytometry panels (for gating strategy see Figure 3.1B).

Pie charts were generated using SPICE version 5.3 (Roederer et al. 2011) to provide an expansive overview of the relationships between the different markers. This demonstrated the phenotypic complexity within the $CD8^+$ T-cell compartment of CLL patients (Figure 3.4). SPICE also performed statistical analysis to compare the differences in pies (permutation analyses, Table 3.1 and 3.2) and marker combinations (two-tailed t-tests: see Appendix I for t-test tables). Overall, there were significant phenotypic differences between the CLL patients and healthy age-matched donors (Table 3.1). The pie charts clearly show that the CLL patients possessed a greater proportion of $CD8^+$ T-cells that were positive for one or more of the phenotypic markers used in both panels; co-expressing 2 or 3 markers in particular. For example, by looking at the arcs above the Panel 1 pie charts it can be seen that there were greater numbers of $CD8^+$ T-cells co-expressing CD57 and HLA-DR in CLL patients versus healthy donors ($p = 0.0012$), as well as $CD57^+PD\text{-}1^+$ ($p = 0.0003$) and $HLA\text{-}DR^+PD\text{-}1^+$ ($p < 0.0001$). An expansion of triple-positive $CD57^+HLA\text{-}DR^+PD\text{-}1^+$ cells in CLL was also observed ($p < 0.0001$). Similarly, the Panel 2 pie charts demonstrated that CLL patients had a higher proportion of triple positive $CD57^+CD38^+CD127^+$ ($p = 0.0002$), $CD57^+KLRG\text{-}1^+CD38^+$ ($p = 0.0012$), $CD57^+CD127^+KLRG\text{-}1^+$ ($p = 0.0001$) $CD8^+$ T-cells than healthy donors. Overall, there appeared to be a greater complexity of T-cell subsets in the CLL patients as more phenotypically distinct groups of T-cells could be defined based on differential expression of the markers studied.

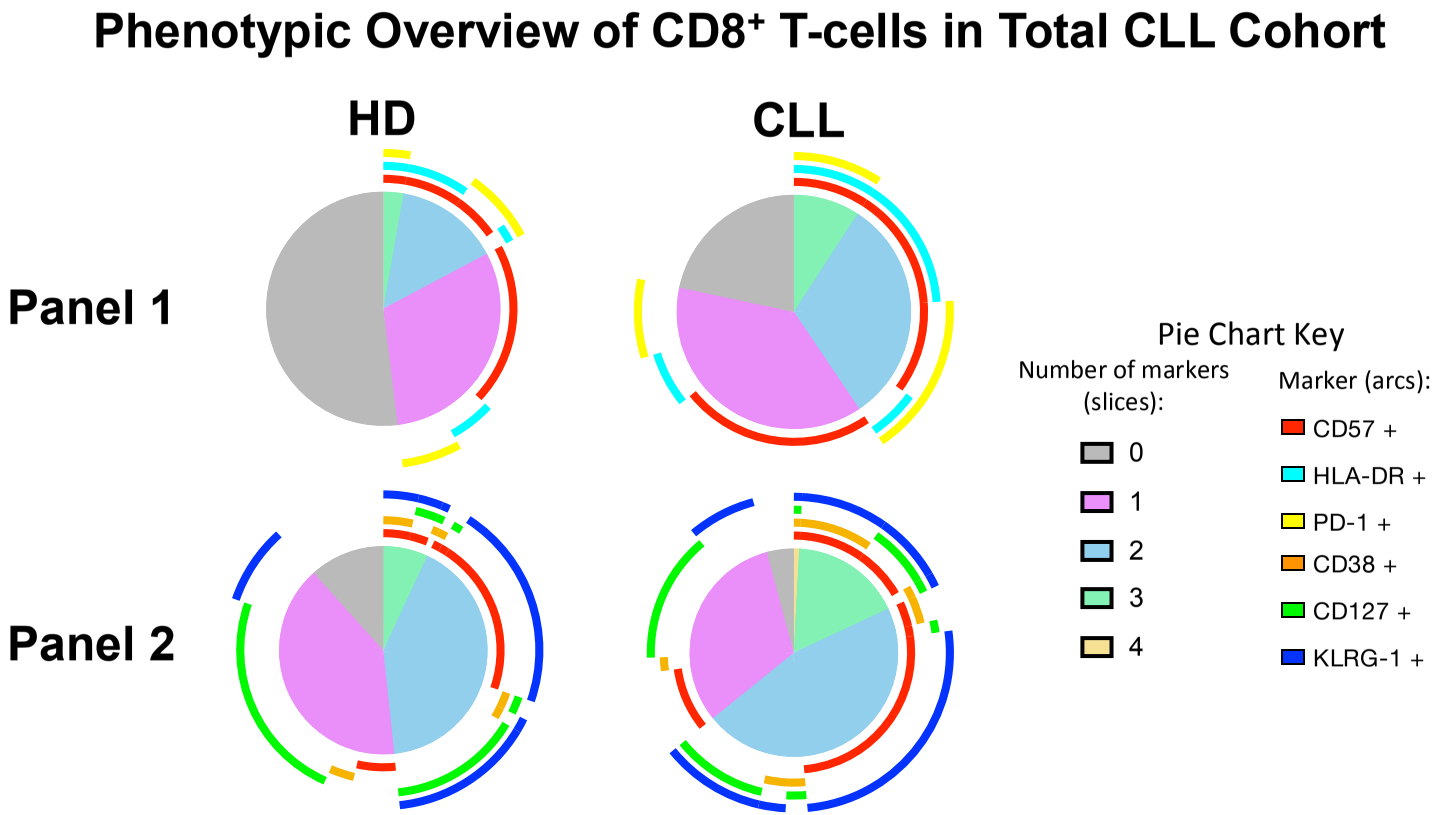

Figure 3.4. Phenotypic overview of total CD8⁺ T-cell compartment in CLL patients (n = 74) and healthy donors (n = 14). Cells were stained with various markers for senescence, exhaustion and activation and analysed using multi-colour flow cytometry (BD FACS Canto II) using gating as described in Figure 3.1. Samples were analysed with FlowJo to created Boolean combination gating for Panel 1 (CD57, HLA-DR, PD-1) and Panel 2 (CD57, CD38, CD127, KLRG-1). Pie charts and statistics were generated using SPICE (v5.3) software.

Furthermore, distinct phenotypic differences between the stratified CLL^{NR} and CLL^{IR} cohorts were also seen in both panels (Figure 3.5, Table 3.2). Compared to the healthy donors, the proportion of $CD8^+$ T-cells expressing one or more of the markers was higher in the CLL^{NR} sub-group and even higher in the CLL^{IR} sub-group. For Panel 1, $CD57^+HLA\text{-}DR^+$ expressing T-cells were increased in the CLL^{IR} cohort compared to both CLL^{NR} ($p = 0.0010$) and healthy donors ($p < 0.001$). The population of the triple positive ($CD57^+HLA\text{-}DR^+PD\text{-}1^+$) cells was also higher in CLL^{IR}, but only significant against healthy donors ($p < 0.0001$). Testing with Panel 2 revealed that $CD57^+KLRG\text{-}1^+CD38^+$ T-cells made up a higher proportion of the CLL^{IR} subgroup compared to both CLL^{NR} and healthy donors ($p = 0.0026$ and p 0.0002, respectively).

These pie charts clearly present overall phenotypic differences in the $CD8^+$ T-cells of CLL patients and healthy donors. They also show that certain phenotypes are exacerbated within the CLL^{IR} subgroup. In the following sections, the distribution of single and co-expressed markers will be compared between CLL and healthy donors in more detail.

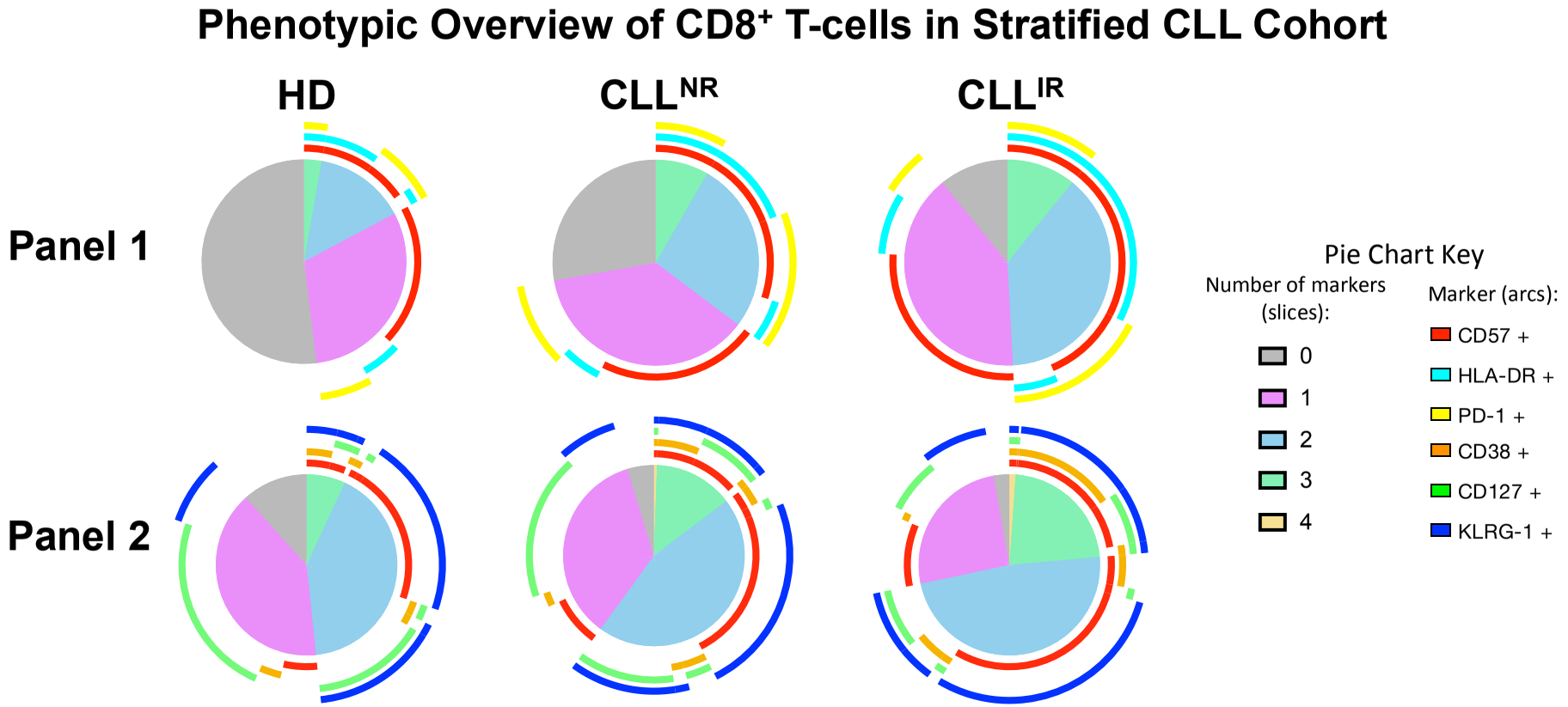

Figure 3.5. Phenotypic overview of CD8$^+$ subsets in CLL^{NR} (n = 47), CLL^{IR} (n = 27) and healthy donors (HD; n = 14). Cells were stained with various markers for senescence, exhaustion and activation and analysed using multi-colour flow cytometry (BD FACS Canto II) using gating as described in Figure 3.1. CLL patients with a CD4:CD8 ratio <1.0 were considered inverted. Samples were analysed with FlowJo to created Boolean combination gating for Panel 1 (CD57, HLA-DR, PD-1) and Panel 2 (CD57, CD38, CD127, KLRG-1). Pie charts and statistics were generated using SPICE software (v5.3).

Table 3.1 Overall $CD8^+$ phenotypic pie chart analysis (HD vs CLL)

Panel	HD vs CLL
Panel 1	<0.0001
Panel 2	0.0130

Table 3.2 Overall $CD8^+$ phenotypic pie chart analysis (HD vs CLL^{NR} vs CLL^{IR})

Panel	HD vs CLL^{NR}	HD vs CLL^{IR}	CLL^{NR} vs CLL^{IR}
Panel 1	0.0006	<0.0001	<0.0001
Panel 2	0.1342	<0.0001	0.0004

3.3. Markers associated with senescence and/or exhaustion

3.3.1. CD57 and PD-1

Previous work showed higher levels of $CD57^+$ and $PD\text{-}1^+$ cells within the $CD8^+$ T-cell compartment of CLL patients when compared with healthy donors (Nunes et al. 2012). In keeping with this, the current study also showed that CLL patients had a significantly higher frequency of $PD\text{-}1^+$ $CD8^+$ T-cells compared with healthy donors ($p = 0.0001$, Figure 3.6A). When subdividing into memory subsets, the increase in PD-1 frequency was observed in both the EM and EMRA subsets ($p = 0.0013$ and $p = 0.008$, respectively). When stratified based on ratio, the CLL^{NR} and CLL^{IR} subgroups demonstrated significantly higher PD-1 frequencies than healthy donors in both the EM ($p \leq 0.05$ and $p \leq 0.01$) and EMRA ($p \leq 0.01$ and $p \leq 0.05$) subsets (Figure 3.6B): however, no difference was seen between the CLL^{NR} and CLL^{IR} subgroups. This implies that although PD-1 is a T-cell marker of interest in CLL, its expression is not associated with the inverted ratio in this cohort.

The frequency of $CD57^+$ T-cells was also higher in the CLL cohort than healthy donors ($p = 0.0063$, Figure 3.7A). Similar to PD-1, the subsets containing the highest frequencies of $CD57^+$ T-cells were the EM and EMRA subsets, although only the EMRA subset was significantly increased compared to healthy donors (Figure 3.7A, $p = 0.0281$). CLL^{IR} patients had significantly higher CD57 frequency within the whole $CD8^+$ T-cell compartment versus both CLL^{NR} and healthy donors ($p \leq 0.05$ and $p \leq 0.001$, Figure 3.7B). Interestingly, $CD8^+CD57^+$ did not differ in the EMRA subset of CLL^{NR} and CLL^{IR} patients, but the EM population of CLL^{IR} patients demonstrated a dramatic increase in this phenotype that was on average 2-fold higher than both the CLL^{NR} subgroup and healthy donors ($p \leq 0.001$ and $p \leq 0.05$, respectively). This suggests that it is the EM population, not the EMRA population, which predominantly contributes to the increase in $CD8^+CD57^+$ T-cells in CLL^{IR} patients.

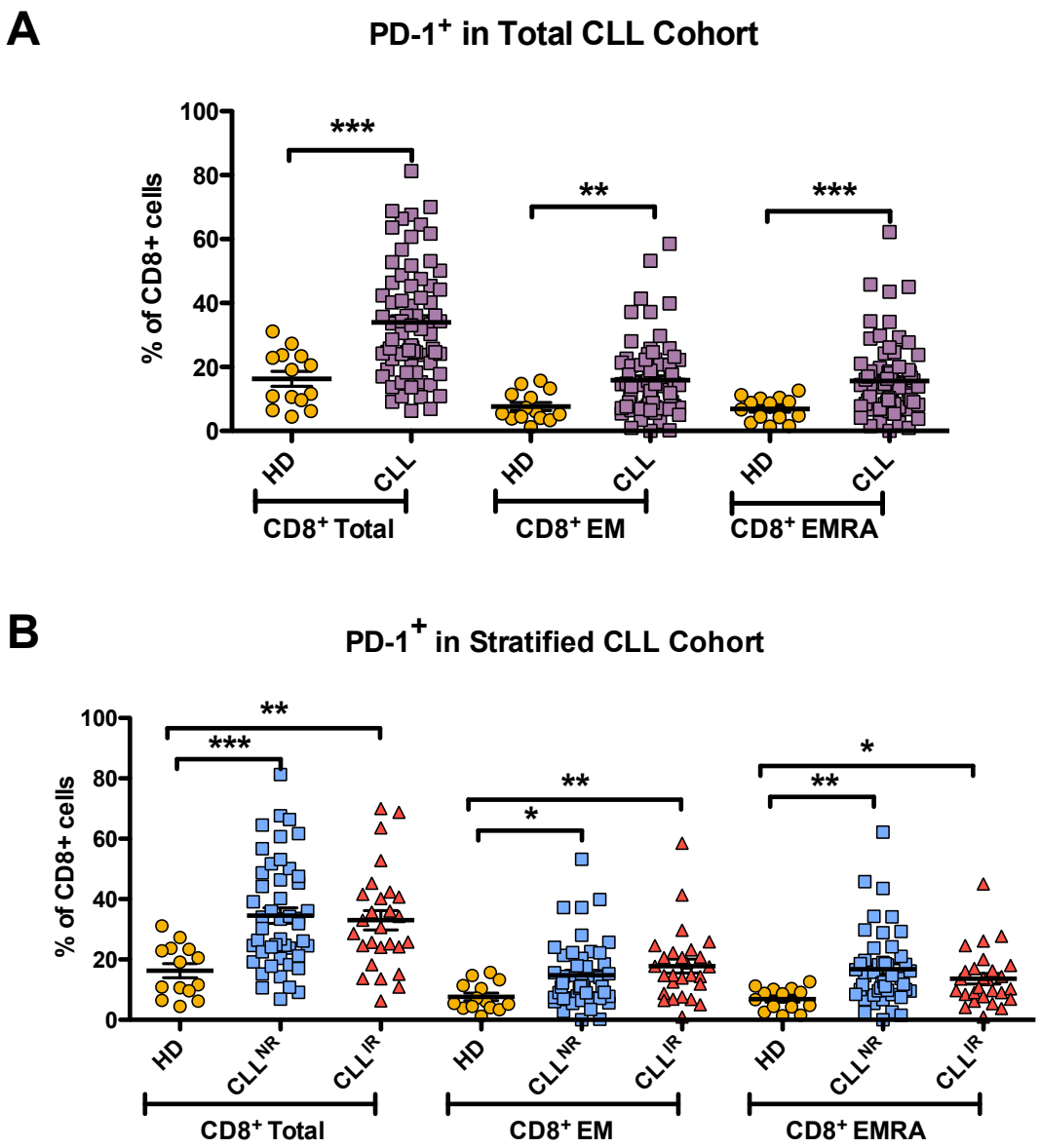

Figure 3.6. PD-1 frequency in CD8$^+$ T-cell memory subsets of CLL patients and healthy donors. Cells were collected using flow cytometry (FACS CantoII, BD FACSDiva) and analysed with FlowJo (v.9) using gating as described in Figure 3.1. (A) CD8$^+$PD-1$^+$ T-cells in the whole CD8$^+$ T-cell compartment, CD8$^+$ EM and CD8$^+$ EMRA memory subsets of CLL patients (n = 74) and healthy donors (n = 14). Pairwise statistical analysis (HD vs CLL) was performed using the non-parametric Mann-Whitney test. Patients were stratified based on CD4:CD8 ratio: a ratio <1.0 was considered inverted (CLL^{IR}). Patients with a ratio ≥1.0 were considered normal ratio patients (CLL^{NR}). (B) Frequency of CD8$^+$PD-1$^+$ T-cells in the whole CD8$^+$ T-cell compartment, CD8$^+$ EM and CD8$^+$ EMRA memory subsets of CLL^{NR} (n = 47), CLL^{IR} (n = 27) and healthy donors (n = 14). Three-way ANOVA statistical analysis was performed using Kruskal-Wallis test (HD vs CLL^{NR} vs CLL^{IR}), with all pairs of data assessed using the Dunn's post-test. Significant results were included on the graph (* = p ≤0.05; ** = p ≤0.01; *** = p ≤0.001).

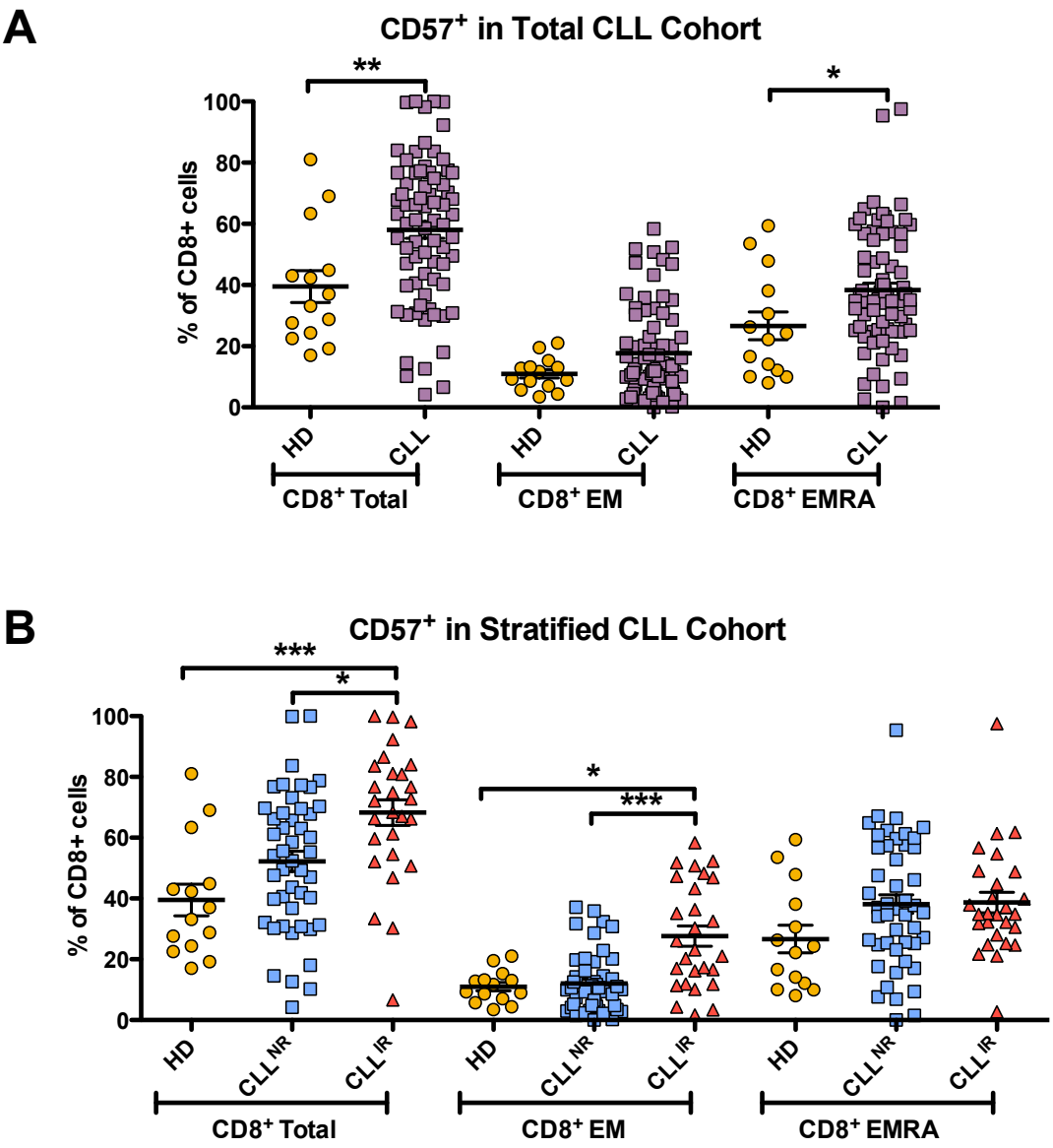

Figure 3.7. CD57 frequency in CD8$^+$ T-cell memory subsets of CLL patients and healthy donors. Cells were collected using flow cytometry (FACS CantoII, BD FACSDiva) and analysed with FlowJo (v.9 using gating as described in Figure 3.1. (A) CD8$^+$CD57$^+$ T-cells in the whole CD8$^+$ T-cell compartment, CD8$^+$ EM and CD8$^+$ EMRA memory subsets of CLL patients (n = 74) and healthy donors (n = 14). Pairwise statistical analysis (HD vs CLL) was performed using the non-parametric Mann-Whitney test. Patients were stratified based on CD4:CD8 ratio: a ratio <1.0 was considered inverted (CLL^{IR}). Patients with a ratio ≥1.0 were considered normal ratio patients (CLL^{NR}). (B) Frequency of CD8$^+$CD57$^+$ T-cells in the whole CD8$^+$ T-cell compartment, CD8$^+$ EM and CD8$^+$ EMRA memory subsets of CLL^{NR} (n = 47), CLL^{IR} (n = 27) and healthy donors (n = 14). Three-way ANOVA statistical analysis was performed using Kruskal-Wallis test (HD vs CLL^{NR} vs CLL^{IR}), with all pairs of data assessed using the Dunn's post-test. Significant results were included on the graph (* = p ≤0.05; ** = p ≤0.01; *** = p ≤0.001).

In addition to looking at the PD-1 and CD57 independently, the relationship between CD57 and PD-1 was further explored by investigating co-expression of the two molecules on the same cell. As seen in Figure 3.8A, CLL patients had significantly higher $CD57^{+}PD\text{-}1^{+}$ co-expression in the whole $CD8^{+}$ T-cell compartment when compared with age-matched healthy donors ($p = 0.0012$). When divided into memory subsets, significantly higher $CD57^{+}PD\text{-}1^{+}$ frequency was observed in both the $CD8^{+}$ EM and EMRA subsets ($p = 0.0077$ and $p = 0.0026$, respectively). No significant change was seen in $CD57^{+}PD\text{-}1^{+}$ frequency in the overall $CD8^{+}$ compartment or the EM/EMRA subsets of CLL^{IR} and CLL^{NR} patients (Figure 3.8B). CD57 co-expression with PD-1 is therefore not a factor associated with inverted ratio in this CLL cohort.

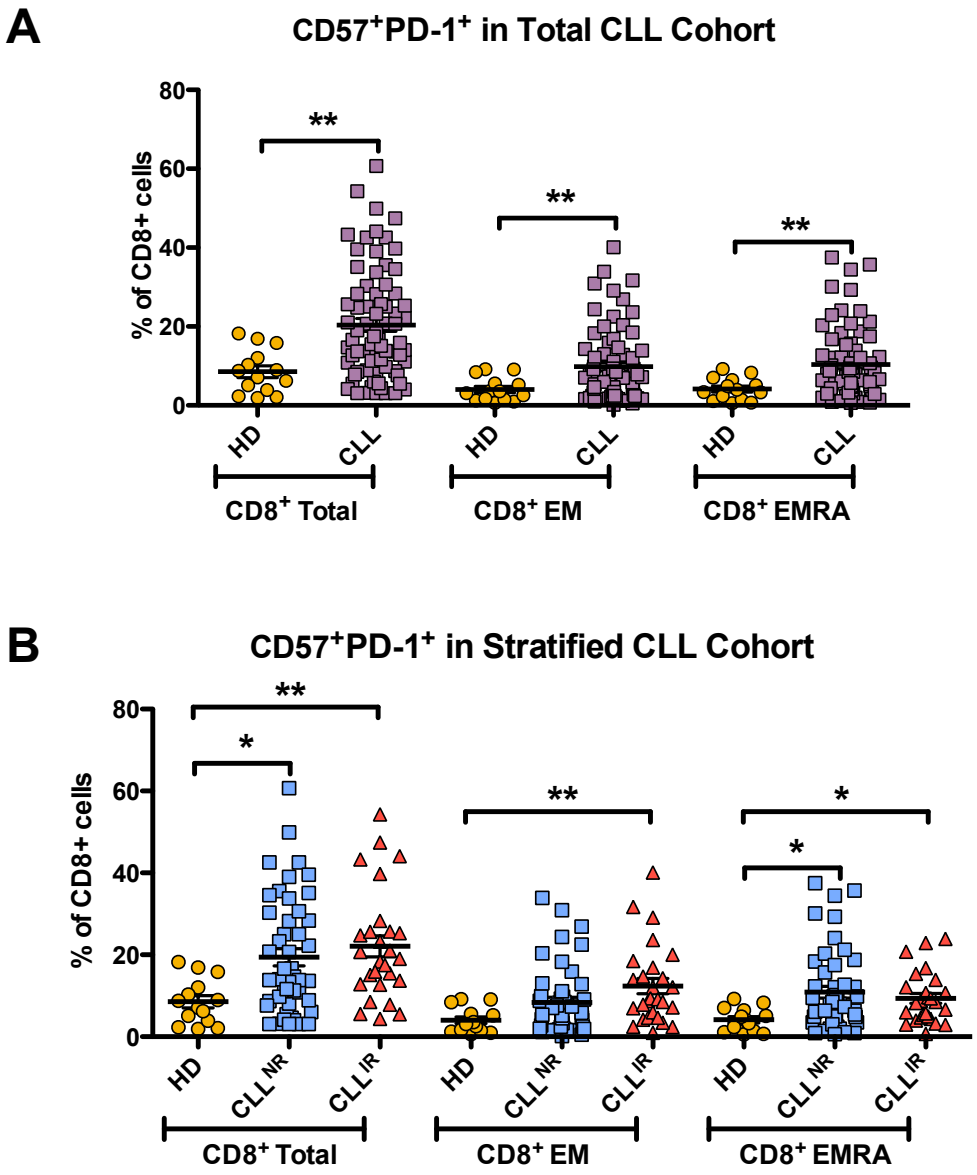

Figure 3.8. CD57 and PD-1 co-expression in CD8$^+$ T-cell memory subsets of CLL patients and healthy donors. Cells were collected using flow cytometry (FACS CantoII, BD FACSDiva) and analysed with FlowJo (v.9) using gating as described in Figure 3.1. (A) CD8$^+$CD57$^+$PD-1$^+$ T-cells in the whole CD8$^+$ T-cell compartment, CD8$^+$ EM and CD8$^+$ EMRA memory subsets of CLL patients (n = 74) and healthy donors (n = 14). Pairwise statistical analysis (HD vs CLL) was performed using the non-parametric Mann-Whitney test. Patients were stratified based on CD4:CD8 ratio: a ratio <1.0 was considered inverted (CLL^{IR}). Patients with a ratio ≥1.0 were considered normal ratio patients (CLL^{NR}). (B) Frequency of CD8$^+$CD57$^+$PD-1$^+$ T-cells in the whole CD8$^+$ T-cell compartment, CD8$^+$ EM and CD8$^+$ EMRA memory subsets of CLL^{NR} (n = 47), CLL^{IR} (n = 27) and healthy donors (n = 14). Three-way ANOVA statistical analysis was performed using Kruskal-Wallis test (HD vs CLL^{NR} vs CLL^{IR}), with all pairs of data assessed using the Dunn's post-test. Significant results were included on the graph (* = p ≤0.05; ** = p ≤0.01; *** = p ≤0.001).

3.3.2. CD57 and KLRG-1

KLRG-1 is a marker associated with poor proliferative capacity in a more highly differentiated memory T-cell type (Göthert et al. 2013; Ibegbu et al. 2005). The CLL cohort showed a trend of increase in KLRG-1 frequency within the $CD8^+$ compartment and the more differentiated memory subsets (Figure 3.9A), but only the EM subset showed a significant increase ($p = 0.0096$). Subdividing by T-cell ratio showed that the CLL^{IR} $CD8^+$ compartment had significantly higher expression of KLRG-1 than both the CLL^{NR} patients and healthy donors ($p \leq 0.05$ for both, Figure 3.9B). Sub-dividing further into memory subsets demonstrated that the increased expression of KLRG-1 was within the EM subset of CLL^{IR} group when compared to healthy donors ($p \leq 0.05$) but not CLL^{NR} patients: again the EMRA subset showed an increasing trend, but this was not significant ($p = 0.1252$).

KLRG-1 and CD57 have been associated together as markers of senescence (Ibegbu et al. 2005). Therefore this study tested whether the co-expression of the two markers associated with CLL disease (Figure 3.10A). $CD57^+KLRG\text{-}1^+$ cells were present at a significantly higher frequency within the total CLL $CD8^+$ T-cell compartment than the healthy donors ($p = 0.0065$). This phenotype was also significantly increased within the $CD8^+$ EM subset ($p = 0.0104$), and the EMRA subsets showed a similar increasing trend, though it did not reach statistical significance ($p = 0.0646$).

Stratification of the CLL cohort into the CLL^{IR} and CLL^{NR} subgroups showed the same patterns of increase as seen in KLRG-1 frequency alone; increased frequency of $CD57^+KLRG\text{-}1^+$ was exaggerated in the total $CD8^+$ T-cells of the CLL^{IR} cohort compared to CLL^{NR} group ($p \leq 0.05$) and healthy donors ($p \leq 0.001$; Figure 3.10B). The stepwise pattern of increased frequency between HD, CLL^{NR} and CLL^{IR} was also reflected within the $CD8^+$ EM and EMRA T-cells. However, a significant difference was only seen within the EM subset ($p \leq 0.05$) when compared to healthy donors.

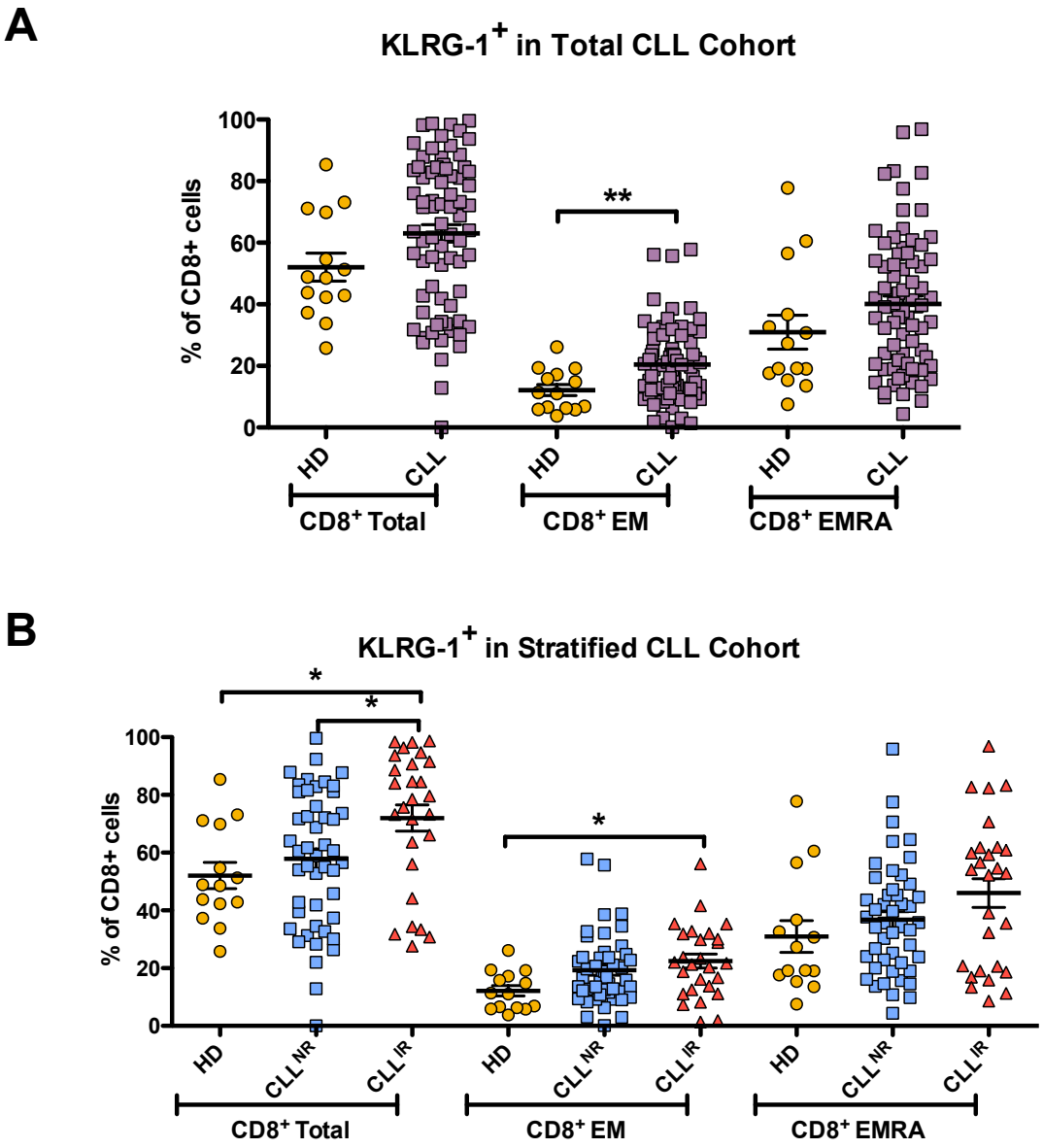

Figure 3.9. KLRG-1 frequency in CD8$^+$ T-cell memory subsets of CLL patients and healthy donors. Cells were collected using flow cytometry (FACS CantoII, BD FACSDiva) and analysed with FlowJo (v.9) using gating as described in Figure 3.1. (A) CD8$^+$KLRG-1$^+$ T-cells in the whole CD8$^+$ T-cell compartment, CD8$^+$ EM and CD8$^+$ EMRA memory subsets of CLL patients (n = 74) and healthy donors (n = 14). Pairwise statistical analysis (HD vs CLL) was performed using the non-parametric Mann-Whitney test. Patients were stratified based on CD4:CD8 ratio: a ratio <1.0 was considered inverted (CLL^{IR}). Patients with a ratio ≥1.0 were considered normal ratio patients (CLL^{NR}). (B) Frequency of CD8$^+$KLRG-1$^+$ T-cells in the whole CD8$^+$ T-cell compartment, CD8$^+$ EM and CD8$^+$ EMRA memory subsets of CLL^{NR} (n = 47), CLL^{IR} (n = 27) and healthy donors (n = 14). Three-way ANOVA statistical analysis was performed using Kruskal-Wallis test (HD vs CLL^{NR} vs CLL^{IR}), with all pairs of data assessed using the Dunn's post-test. Significant results were included on the graph (* = p ≤0.05; ** = p ≤0.01; *** = p ≤0.001).

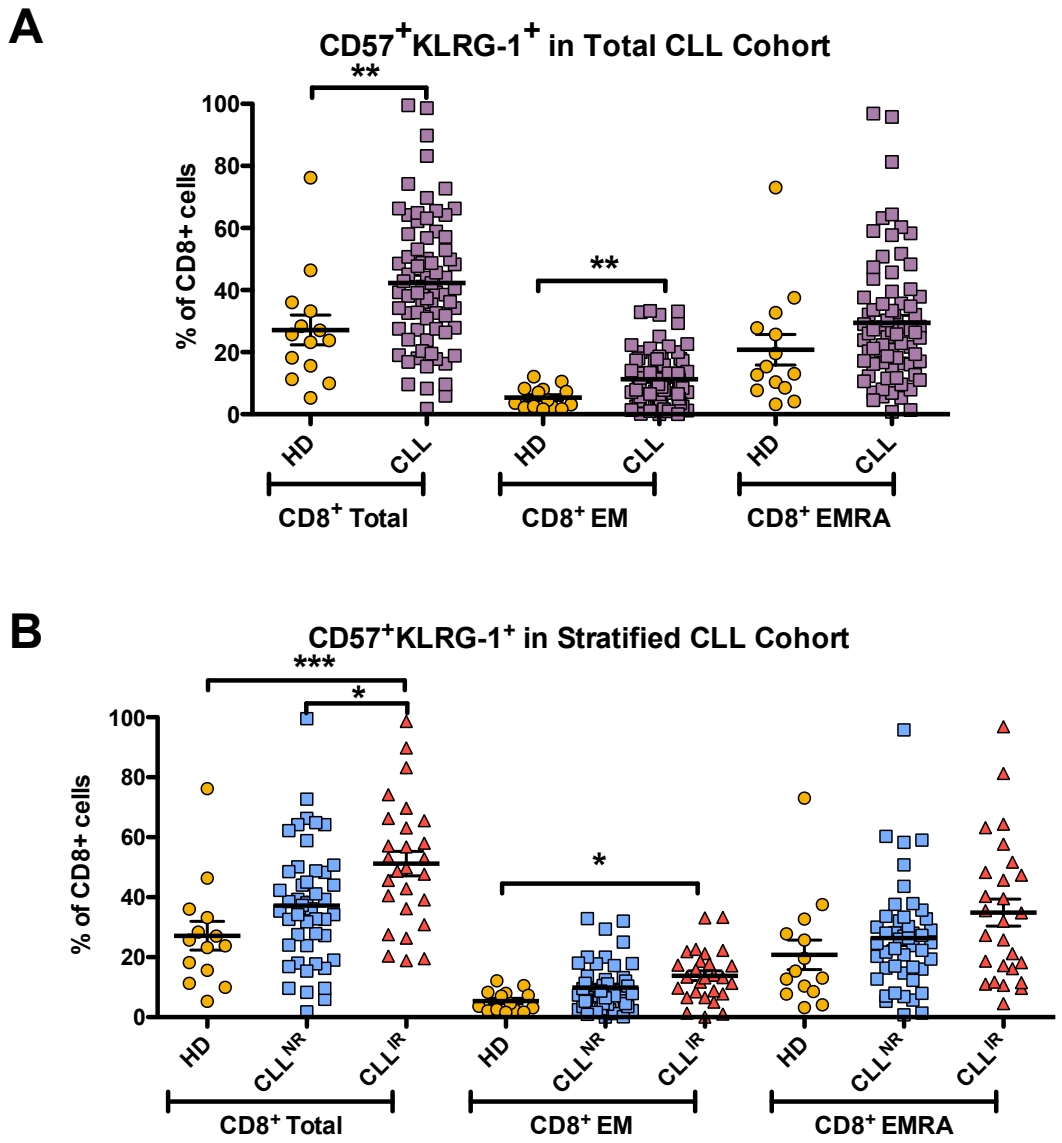

Figure 3.10. CD57 and KLRG-1 co-expression in CD8$^+$ T-cell memory subsets of CLL patients and healthy donors. Cells were collected using flow cytometry (FACS CantoII, BD FACSDiva) and analysed with FlowJo (v.9) using gating as described in Figure 3.1. (A) CD8$^+$CD57$^+$KLRG-1$^+$ T-cells in the whole CD8$^+$ T-cell compartment, CD8$^+$ EM and CD8$^+$ EMRA memory subsets of CLL patients (n = 74) and healthy donors (n = 14). Pairwise statistical analysis (HD vs CLL) was performed using the non-parametric Mann-Whitney test. Patients were stratified based on CD4:CD8 ratio: a ratio <1.0 was considered inverted (CLL^{IR}). Patients with a ratio ≥1.0 were considered normal ratio patients (CLL^{NR}). (B) Frequency of CD8$^+$CD57$^+$KLRG-1$^+$ T-cells in the whole CD8$^+$ T-cell compartment, CD8$^+$ EM and CD8$^+$ EMRA memory subsets of CLL^{NR} (n = 47), CLL^{IR} (n = 27) and healthy donors (n = 14). Three-way ANOVA statistical analysis was performed using Kruskal-Wallis test (HD vs CLL^{NR} vs CLL^{IR}), with all pairs of data assessed using the Dunn's post-test. Significant results were included on the graph (* = p ≤0.05; ** = p ≤0.01; *** = p ≤0.001)

Although patterns of increased KLRG-1$^+$ and CD57$^+$KLRG-1$^+$ were seen in the CLL cohort, and in some cases the increases were exacerbated within the CLL^{IR} subgroup, they did not always reach significance. For example, in the case of the CD8$^+$ EM subset significance was observed between the inverted group and healthy donors, but not in inverted versus normal ratio. Therefore, although a facet of ratio inversion may include the accumulation of these 'phenotypically senescent' cells, it is not a defining feature of the inverted ratio.

3.3.3. CD127

IL-7 is a key cytokine for lymphocyte growth and differentiation, including the proliferation required to maintain T-cell memory populations (A. Ma et al. 2006). The IL-7 receptor (IL-7R) would therefore be a good potential marker for non-senescent cells that are still able to undergo activation and divide. This study looked at the expression of IL7Rα (CD127), a molecule that forms part of the IL-7R. Reduced IL7Rα expression has previously been associated with a more differentiated phenotype (Golden-Mason et al. 2006). As a whole, the presentation of this marker in the CLL cohort showed significance in only the naïve subset: a 2-fold reduction in CD127 frequency was seen in CLL versus healthy donors ($p = 0.0008$; Figure 3.11A).

As shown in Figure 3.11B, CLL^{IR} patients a significant reduction in the frequency of CD127$^+$ CD8$^+$ T-cells compared to CLL^{NR} patients and healthy donors ($p \leq 0.01$ and $p \leq 0.05$ respectively). This was primarily reflected in the 3-fold decrease in the CD8$^+$CD127$^+$ naïve population, ($p \leq 0.001$ for both), and appeared to reflect the 3-fold reduction of the CLL^{IR} naïve population as a whole (Section 3.1, Figure 3.3). The frequency of CD127$^+$ T-cells was also lower in the CD8$^+$ EM and EMRA subsets of CLL^{IR} patients compared to the CLL^{NR} subgroup ($p \leq 0.05$ for both).

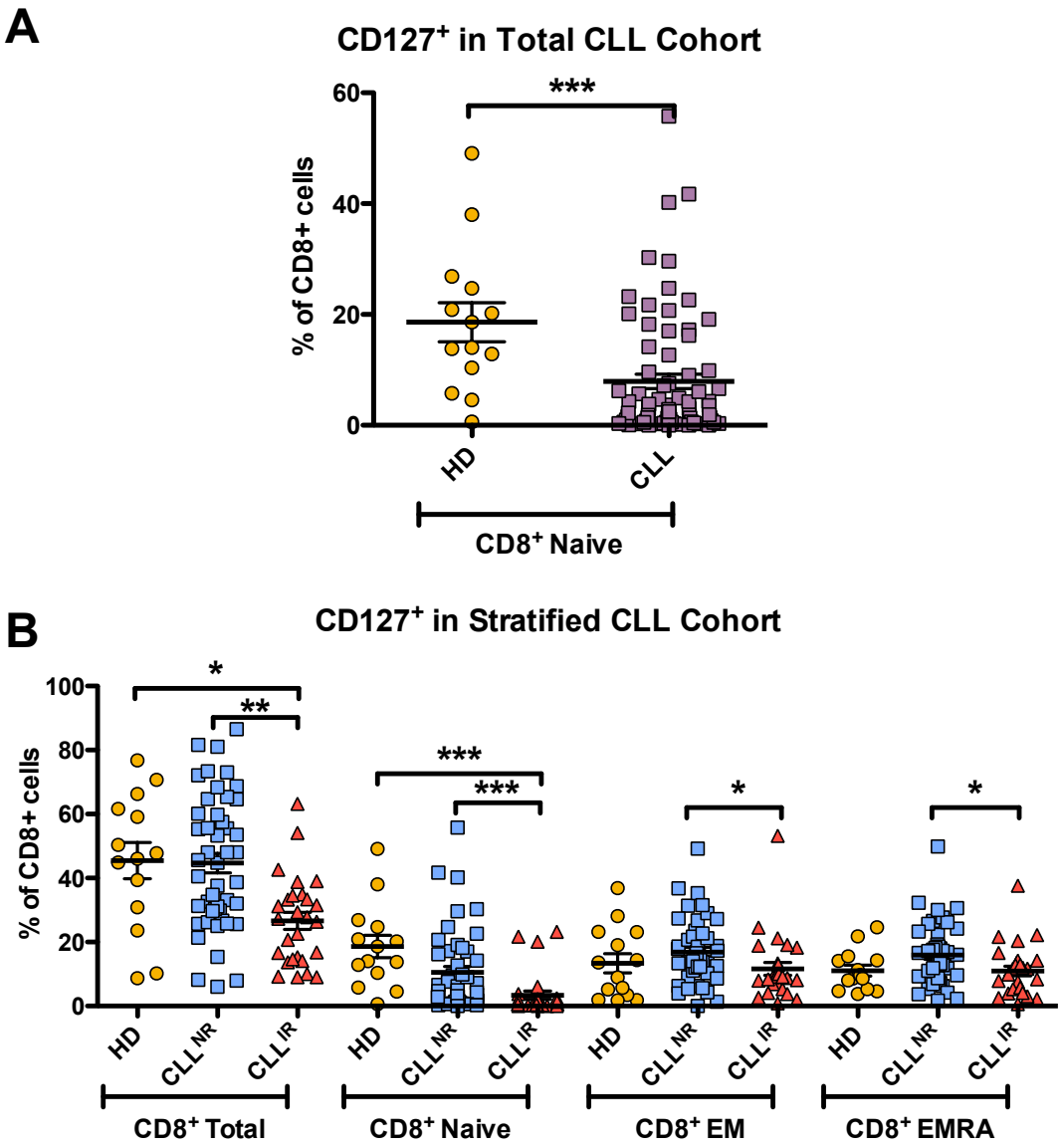

Figure 3.11. CD127 in CD8$^+$ T-cell memory subsets of CLL patients and healthy donors. Cells were collected using flow cytometry (FACS CantoII, BD FACSDiva) and analysed with FlowJo (v.9) using gating as described in Figure 3.1. (A) CD8$^+$CD127$^+$ naïve T-cells of CLL patients (n = 74) and healthy donors (n = 14). Pairwise statistical analysis (HD vs CLL) was performed using the non-parametric Mann-Whitney test. Patients were stratified based on CD4:CD8 ratio: a ratio <1.0 was considered inverted (CLL^{IR}). Patients with a ratio ≥1.0 were considered normal ratio patients (CLL^{NR}). (B) Frequency of CD8$^+$CD127$^+$ T-cells in the whole CD8$^+$ T-cell compartment, CD8$^+$ Naïve, CD8$^+$ EM and CD8$^+$ EMRA memory subsets of CLL^{NR} (n = 47), CLL^{IR} (n = 27) and healthy donors (n = 14). Three-way ANOVA statistical analysis was performed using Kruskal-Wallis test (HD vs CLL^{NR} vs CLL^{IR}), with all pairs of data assessed using the Dunn's post-test. Significant results were included on the graph (* = p ≤0.05; ** = p ≤0.01; *** = p ≤0.001).

3.3.4. CD127 and KLRG-1

Differential expression of CD127 and KLRG-1 has been shown to be relevant in identifying antigen-specific populations (Bengsch et al. 2007; Ibegbu et al. 2005). It has previously been postulated that virus-specific $CD8^+$ T-cells in resolved infections are predominantly $CD127^+KLRG\text{-}1^-$, whereas $CD127^-KLRG\text{-}1^+$ T-cells are associated with chronic viral persistence (Bengsch et al. 2007). This study also investigated these phenotypes to see whether $CD8^+$ T-cells of CLL patients presented a phenotype representative of chronic or acute antigenic stimulation.

Overall $CD127^+KLRG\text{-}1^-$ T-cells were significantly reduced within the $CD8^+$ compartment of the CLL cohort ($p = 0.0191$), but no significant difference was seen in the frequency of $CD127^-KLRG\text{-}1^+$ T-cells ($p = 0.0532$; Figure 3.12). The majority of changes within the CD127/KLRG-1 phenotypes were seen when the CLL cohort was stratified based on T-cell CD4:CD8 ratio (Figure 3.13). The CLL^{IR} subgroup showed a significant reduction in $CD8^+CD127^+KLRG\text{-}1^-$ T-cells compared with both CLL^{NR} and healthy donors ($p \leq 0.001$ for both), and a marked increase in the $CD127^-KLRG\text{-}1^+$ phenotype when compared with CLL^{NR} and healthy donors ($p \leq 0.01$ in both cases; Figure 3.13A). The CLL^{IR} $CD8^+$ EM subset showed a similar pattern (Figure 3.13B): $CD127^+KLRG\text{-}1^-$ frequency was significantly higher in the CLL^{IR} subgroup than the CLL^{NR} subgroup ($p \leq 0.01$), and $CD127^-KLRG\text{-}1^+$ frequency was significantly reduced when compared to the healthy donors ($p \leq 0.01$). $CD8^+$ EMRAs also followed this pattern with a significant decrease in the $CD127^+KLRG\text{-}1^-$ phenotype compared to both the CLL^{NR} and healthy donors ($p \leq 0.05$ and $p \leq 0.01$, respectively; Figure 3.13C). It is worth noting that the same relationships were observed between CD57 and CD127 co-expression (supplementary Appendix II).

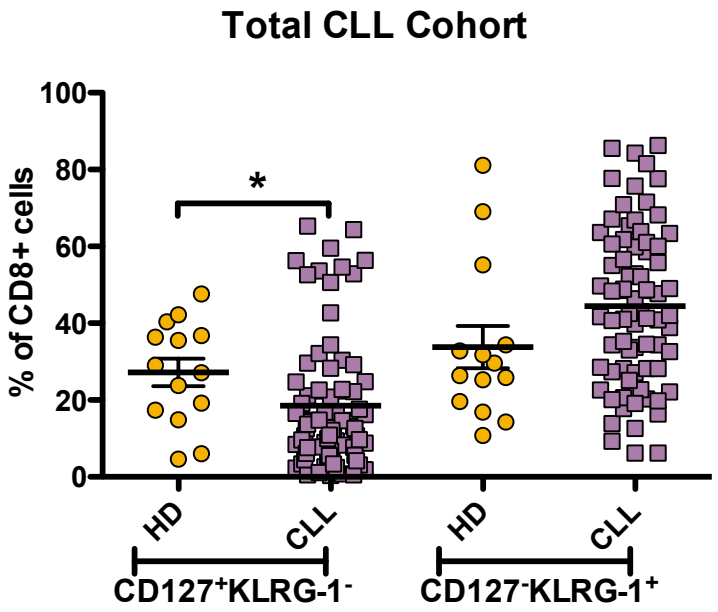

Figure 3.12. Co-expression of CD127 and KLRG-1 in CD8$^+$ T-cells of total CLL cohort (n = 74) and healthy donors (HD; n = 14). Cells were collected using flow cytometry (FACS CantoII, BD FACSDiva) and analysed with FlowJo (v.9) using gating as described in Figure 3.1. Frequency of CD127$^+$KLRG-1$^-$ and CD127$^-$KLRG-1$^+$ T-cells in the whole CD8$^+$ T-cell compartment are shown. Pairwise statistical analysis (HD vs CLL) was performed using the non-parametric Mann-Whitney test. Significant results were included on the graph (* = p ≤0.05; ** = p ≤0.01; *** = p ≤0.001).

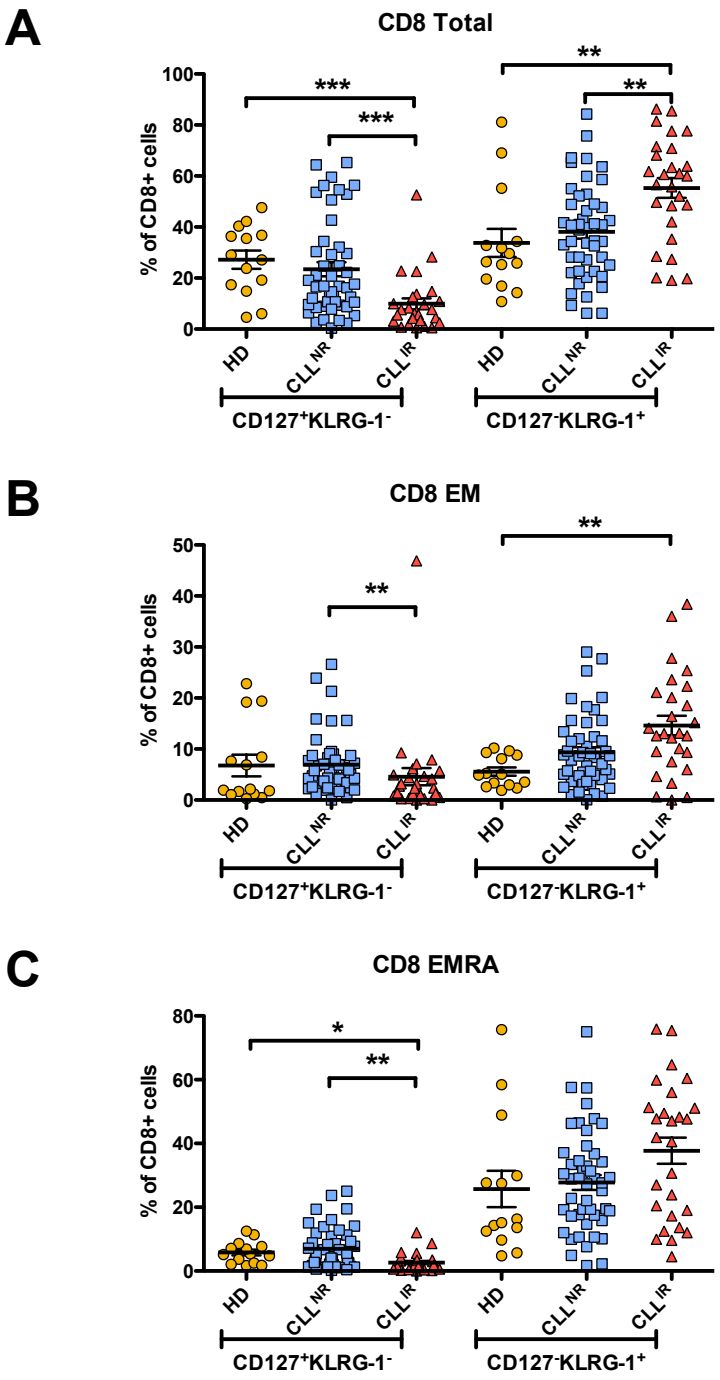

Figure 3.13. Co-expression of CD127 and KLRG-1 in CD8$^+$ T-cell memory subsets of CLL^{NR} (n = 47), CLL^{IR} (n = 27) and healthy donors (HD; n = 14). Cells were collected using flow cytometry (FACS CantoII, BD FACSDiva) and analysed with FlowJo (v.9) using gating as described in Figure 3.1. Patients were stratified based on CD4:CD8 ratio: a ratio <1.0 was considered inverted. Patients with a ratio ≥1.0 were considered normal ratio patients. CD127$^+$KLRG-1$^-$ and CD127$^-$KLRG-1$^+$ frequency of (A) the whole CD8$^+$ T-cell compartment, (B) CD8$^+$ EM, and (C) CD8$^+$ EMRA memory subsets. Three-way ANOVA statistical analysis was performed using Kruskal-Wallis test (HD vs CLL^{NR} vs CLL^{IR}), with all pairs of data assessed using the Dunn's post-test. Significant results were included on the graph (* = p ≤0.05; ** = p ≤0.01; *** = p ≤0.001).

To further define these phenotypic subsets of T-cells, CD57, a marker associated with differentiation and senescence (Focosi et al. 2010; Nunes et al. 2012; Brenchley et al. 2003), was studied in conjunction with KLRG-1 and CD127 (Figure 3.14A). The CLL cohort showed an increase in $CD8^+$ T-cells with a $CD57^+KLRG\text{-}1^+CD127^-$ phenotype ($p = 0.0269$) and reduction in $CD57^-KLRG\text{-}1^-CD127^+$ phenotype ($p = 0.0115$). Greater significance was seen when patients were stratified based on CD4:CD8 ratio (Figure 3.14B): the increase in $CD57^+KLRG\text{-}1^+CD127^-$ phenotype was exacerbated in the CLL^{IR} $CD8^+$ compartment compared to both CLL^{NR} and healthy donors ($p \leq 0.01$ for both). Furthermore, a significant reduction in the percentage of cells expressing the $CD57^-KLRG\text{-}1^-CD127^+$ phenotype was also observed ($p \leq 0.001$ for both). The CLL^{IR} $CD8^+$ EM subset also demonstrated an increase in $CD57^+KLRG\text{-}1^+CD127^-$ and a reduction in $CD57^-KLRG\text{-}1^-CD127^+$. The CLL^{IR} EMRA population only showed a significant reduction in the $CD57^-KLRG\text{-}1^-CD127^+$ (supplementary data, see Appendix II).

Overall there appeared to be an increase in T-cell phenotypes consistent with senescence associated with persistent infection or chronic antigenic stimulation. This was particularly enhanced in the CLL^{IR} patient subgroup, suggesting a preferential accumulation of chronically stimulated $CD8^+$ T-cells.

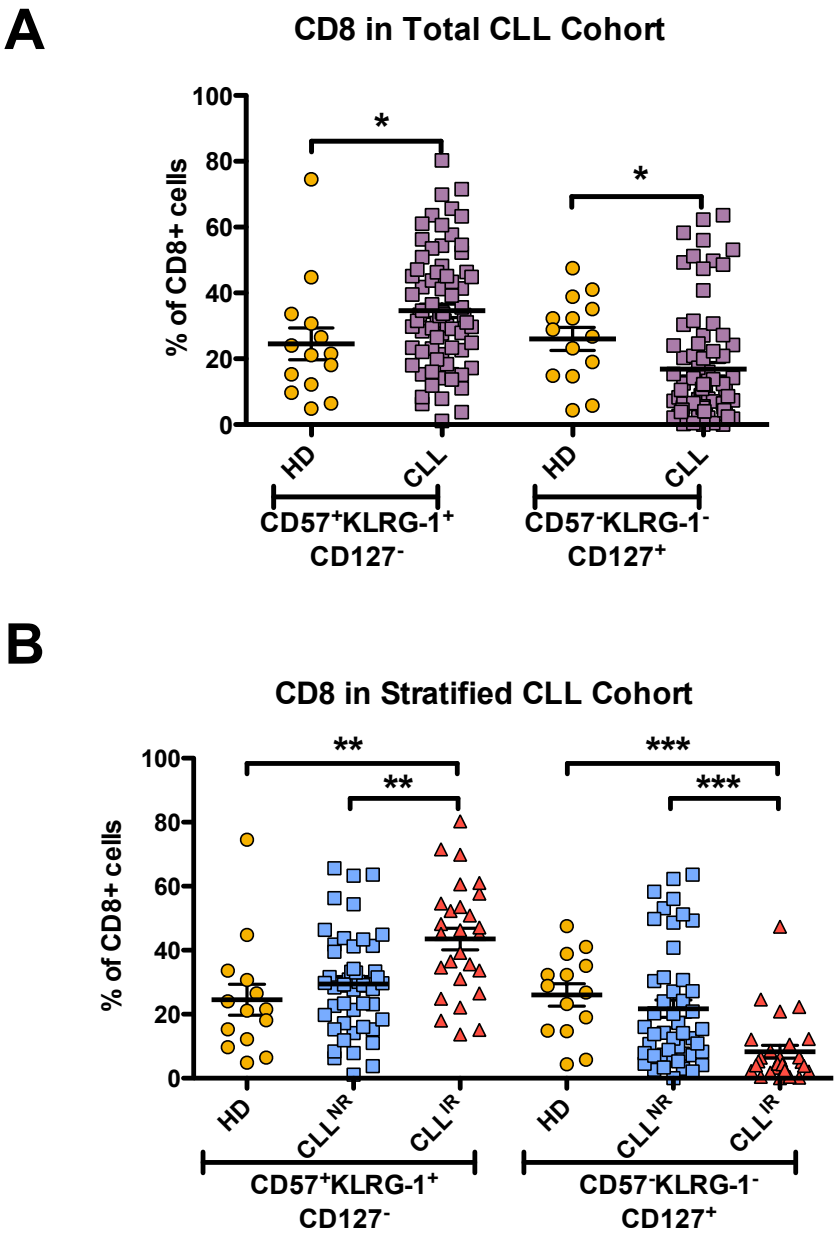

Figure 3.14. CD57, KLRG-1, and CD127 co-expression in CD8$^+$ T-cells of CLL patients and healthy donors. Cells were collected using flow cytometry (FACS CantoII, BD FACSDiva) and analysed with FlowJo (v.9) using gating as described in Figure 3.1. (A) CD8$^+$CD57$^+$KLRG-1$^+$CD127$^-$ T-cells in the whole CD8$^+$ T-cell compartment of CLL patients (n = 74) and healthy donors (n = 14). Pairwise statistical analysis (HD vs CLL) was performed using the non-parametric Mann-Whitney test. Patients were stratified based on CD4:CD8 ratio: a ratio <1.0 was considered inverted (CLL^{IR}). Patients with a ratio ≥1.0 were considered normal ratio patients (CLL^{NR}). (B) Frequency of CD8$^+$CD57$^+$KLRG-1$^+$CD127$^-$ T-cells in the whole CD8$^+$ T-cell compartment of CLL^{NR} (n = 47), CLL^{IR} (n = 27) and healthy donors (n = 14). Three-way ANOVA statistical analysis was performed using Kruskal-Wallis test (HD vs CLL^{NR} vs CLL^{IR}), with all pairs of data assessed using the Dunn's post-test. Significant results were included on the graph (* = p ≤0.05; ** = p ≤0.01; *** = p ≤0.001).

3.3.5. BCL-2

The anti-apoptotic protein BCL-2 plays an important role in T-cell survival and is thought to play a role in the regulation of T-cell memory (Dunkle et al. 2013). Initial phenotypic analyses included BCL-2 to assess whether the $CD8^+$ memory T-cell expansion present in CLL^{IR} was attributable to an accumulation of surviving long-lived $BCL\text{-}2^+$ memory cells. However, preliminary results revealed a significantly lower percentage of $CD8^+BCL\text{-}2^+$ in CLL patients compared to the healthy donors ($p = 0.0048$). The subset that most reflected this decrease was the naïve compartment ($p = 0.0089$); no significant change was observed in the $CD8^+$ EM or EMRA subsets. When stratified by T-cell ratio, the $CD8^+$ compartment as a whole showed little difference between the CLL^{NR} and CLL^{IR} patients. A trend towards decrease in the number of $BCL\text{-}2^+$ T-cells was observed in the $CD8^+$ naïve subset ($HD > CLL^{NR} > CLL^{IR}$): a mean 4-fold reduction was seen between the CLL^{NR} and CLL^{IR} patients (n.s.), and a significant 9-fold reduction was observed between healthy donors and CLL^{IR} patients ($p \leq 0.01$). The decrease in BCL-2 aligns with the decrease seen in the naïve $CD8^+$ T-cell frequency (Section 3.1, Figure 3.2 and 3.3) and the reduction in CD127 expression (Section 3.3.3, Figure 3.11). Previous work has shown that BCL-2 is regulated by IL-7/IL-7R (Niu and Qin 2013), so it is not surprising that they follow similar patterns of presentation here. Overall, with regards to the memory compartments, no change in EM/EMRA subsets suggests that there is not an increase in long-lived memory T-cells primed for survival.

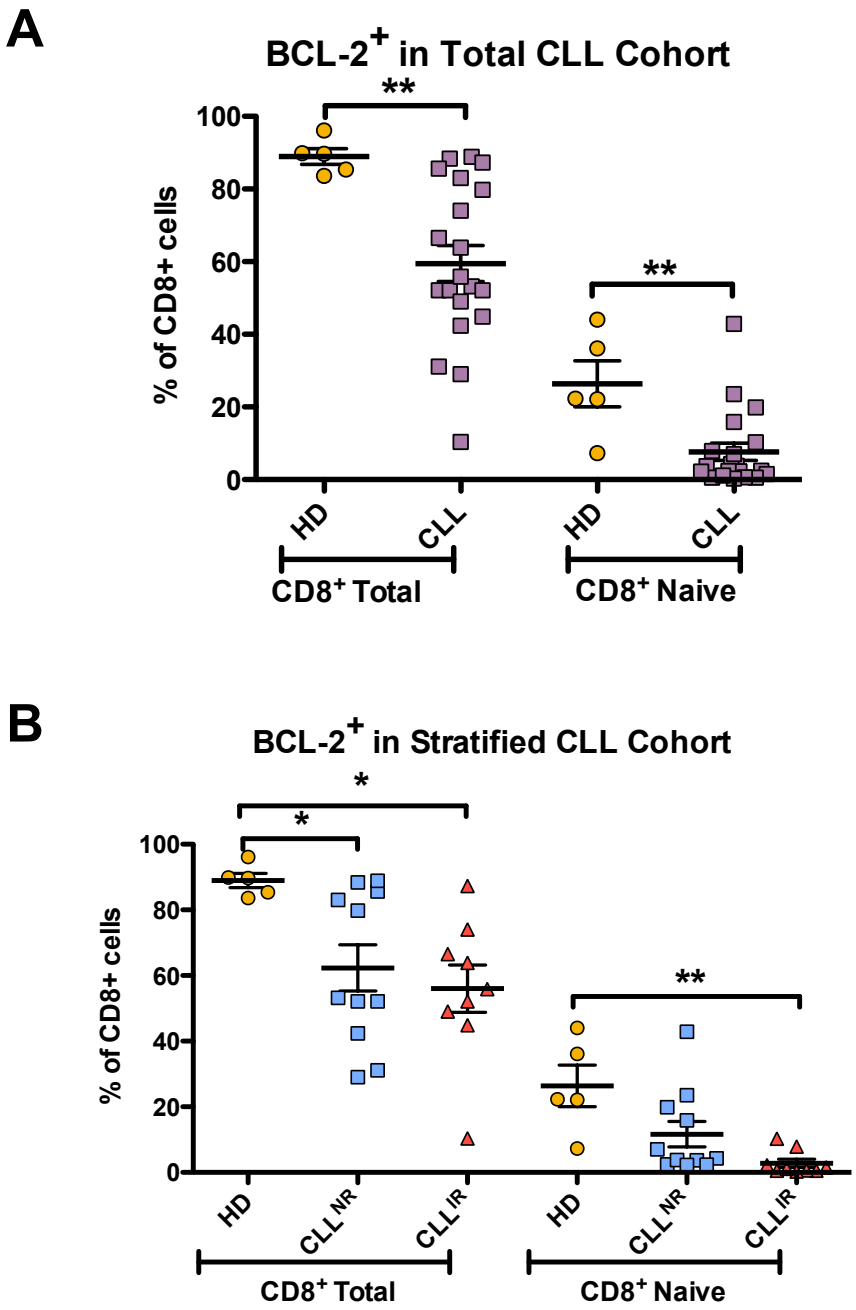

Figure 3.15. BCL-2 frequency in CD8$^+$ T-cell memory subsets of CLL patients and healthy donors (HD). Cells were collected using flow cytometry (FACS CantoII, BD FACSDiva) and analysed with FlowJo (v.9) using gating as described in Figure 3.1. (A) CD8$^+$BCL-2$^+$ T-cells in whole CD8$^+$ T-cell compartment and CD8$^+$ naïve subset of CLL patients (n = 20) and healthy donors (n = 5). Pairwise statistical analysis (HD vs CLL) was performed using the non-parametric Mann-Whitney test. Patients were stratified based on CD4:CD8 ratio: a ratio <1.0 was considered inverted (CLL^{IR}). Patients with a ratio ≥1.0 were considered normal ratio patients (CLL^{NR}). (B) Frequency of CD8$^+$BCL-2$^+$ T-cells in whole CD8$^+$ T-cell compartment and CD8$^+$ naive subset of CLL^{NR} (n = 11), CLL^{IR} (n = 9) and healthy donors (n = 5). Three-way ANOVA statistical analysis was performed using Kruskal-Wallis test (HD vs CLL^{NR} vs CLL^{IR}), with all pairs of data assessed using the Dunn's post-test. Significant results were included on the graph (* = p ≤0.05; ** = p ≤0.01; *** = p ≤0.001).

3.4. Markers associated with activation

3.4.1. HLA-DR and CD38

Increases in senescent and exhausted T-cell phenotypes within CLL have been reported in the literature (Göthert et al. 2013; Riches et al. 2013; Nunes et al. 2012), but an increase in absolute numbers of activated HLA-DR$^+$ T-cells have also been reported (Tötterman et al. 1989). T-cells displaying an activated phenotype have been described in other cancers; a tumour-reactive "early effector" CD8$^+$ T-cell subset expressing activation markers HLA-DR and CD38 has been reported in metastatic melanoma (Anichini et al. 2010). Furthermore, expression of CD38 on T-cells has been proposed as a potential prognostic marker in CLL (Tinhofer et al. 2006). Therefore, this study included HLA-DR (Panel 1) and CD38 (Panel 2) within the phenotypic analysis to identify the presence of any potentially activated subgroups of CD8$^+$ T-cells within CLL, and specifically the CLL^{IR} subgroup.

CD8$^+$HLA-DR$^+$ T-cells were significantly higher in frequency within the CLL cohort than the healthy donors ($p = 0.0123$), an increase that was reflected within both the CD8$^+$ EM and CD8$^+$ EMRA T-cells ($p = 0.0257$ and $p = 0.0277$, respectively; Figure 3.16A). Stratification by ratio revealed that HLA-DR expressing CD8$^+$ T-cells were higher in CLL^{IR} patients than either CLL^{NR} patients or healthy donors ($p \leq 0.05$ and $p \leq 0.01$, respectively; Figure 3.16B). This was shown predominantly within the CD8$^+$ EM subset ($p \leq 0.001$ against both CLL^{NR} and healthy donors). The CD8$^+$ EMRA subset of the CLL cohort demonstrated a significantly higher frequency of HLA-DR expressing T-cells than the EMRA subset in the healthy donors ($p \leq 0.05$). However, there was no difference in the frequency of HLA-DR$^+$ T-cells between the EMRA subsets of the CLL^{IR} vs CLL^{NR} patients. These results suggest an activated subgroup of T-cells in CLL, more specifically the CLL^{IR} patients.

The maximum frequency of CD38 expressing T-cells was higher in the CLL patients (~80%) compared to healthy donors (~40%), and there was a trend towards higher frequencies in the CLL cohort, although this was not significant. When looking at the CD8$^+$ memory subsets, the frequency of CD38$^+$ T-cells was on average 3-fold higher in the EM subset ($p = 0.0014$) and 2-fold higher in EMRA subset ($p = 0.0453$) of CLL patients (Figure 3.17A). Stratified into CD4:CD8 ratio subgroups, CLL^{IR} patients had a significantly higher frequency of CD8$^+$CD38$^+$ T-cells than CLL^{NR} patients and healthy

donors ($p \leq 0.05$ for both, Figure 3.17B). Similar to the results seen with HLA-DR, the memory subset where this pattern was the most pronounced was the CLL^{IR} EM subset ($p \leq 0.01$ versus CLL^{NR}, $p \leq 0.001$ versus healthy donors). These results, along with the increase in HLA-DR^+ T-cells described earlier in the section, support the presence of an activated subgroup of $CD8^+$ memory T-cells within the CLL^{IR} cohort.

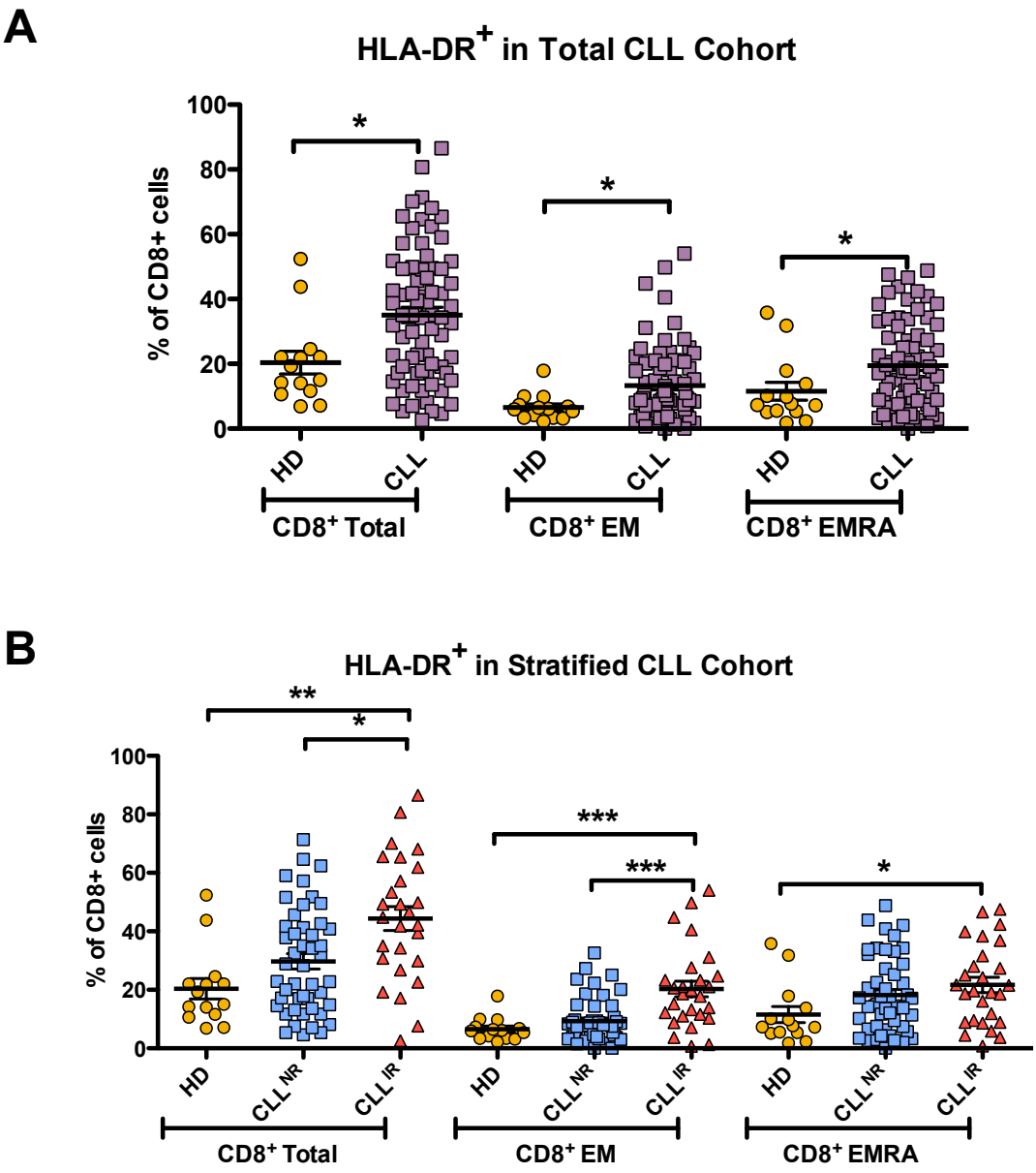

Figure 3.16. HLA-DR frequency in CD8$^+$ T-cell memory subsets of CLL patients and healthy donors (HD). Cells were collected using flow cytometry (FACS CantoII, BD FACSDiva) and analysed with FlowJo (v.9) using gating as described in Figure 3.1. (A) CD8$^+$HLA-DR$^+$ T-cells in the whole CD8$^+$ T-cell compartment, CD8$^+$ EM and CD8$^+$ EMRA memory subsets of CLL patients (n = 74) and healthy donors (n = 14). Pairwise statistical analysis (HD vs CLL) was performed using the non-parametric Mann-Whitney test. Patients were stratified based on CD4:CD8 ratio: a ratio <1.0 was considered inverted (CLL^{IR}). Patients with a ratio ≥1.0 were considered normal ratio patients (CLL^{NR}). (B) Frequency of CD8$^+$HLA-DR$^+$ T-cells in the whole CD8$^+$ T-cell compartment, CD8$^+$ EM and CD8$^+$ EMRA memory subsets of CLL^{NR} (n = 47), CLL^{IR} (n = 27) and healthy donors (n = 14). Three-way ANOVA statistical analysis was performed using Kruskal-Wallis test (HD vs CLL^{NR} vs CLL^{IR}), with all pairs of data assessed using the Dunn's post-test. Significant results were included on the graph (* = p ≤0.05; ** = p ≤0.01; *** = p ≤0.001).

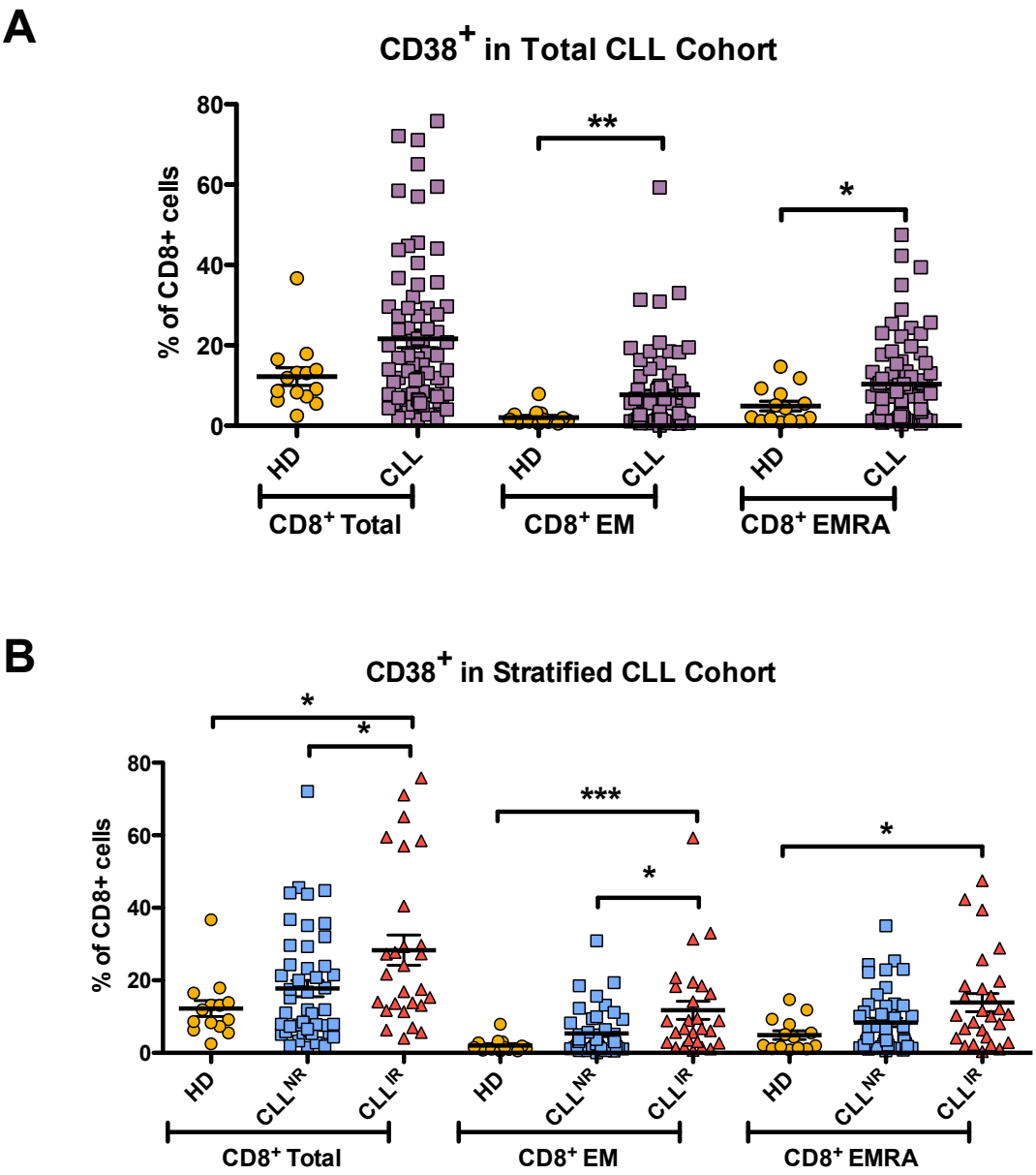

Figure 3.17. CD38 frequency in CD8$^+$ T-cell memory subsets of CLL patients and healthy donors (HD). Cells were collected using flow cytometry (FACS CantoII, BD FACSDiva) and analysed with FlowJo (v.9) using gating as described in Figure 3.1. (A) CD8$^+$CD38$^+$ T-cells in the whole CD8$^+$ T-cell compartment, CD8$^+$ EM and CD8$^+$ EMRA memory subsets of CLL patients (n = 74) and healthy donors (n = 14). Pairwise statistical analysis (HD vs CLL) was performed using the non-parametric Mann-Whitney test. Patients were stratified based on CD4:CD8 ratio: a ratio <1.0 was considered inverted (CLL^{IR}). Patients with a ratio ≥1.0 were considered normal ratio patients (CLL^{NR}). (B) Frequency of CD8$^+$CD38$^+$ T-cells in the whole CD8$^+$ T-cell compartment, CD8$^+$ EM and CD8$^+$ EMRA memory subsets of CLL^{NR} (n = 47), CLL^{IR} (n = 27) and healthy donors (n = 14). Three-way ANOVA statistical analysis was performed using Kruskal-Wallis test (HD vs CLL^{NR} vs CLL^{IR}), with all pairs of data assessed using the Dunn's post-test. Significant results were included on the graph (* = p ≤0.05; ** = p ≤0.01; *** = p ≤0.001).

3.4.2. PD-1, CD57 and HLA-DR

There is controversy around both PD-1 and CD57 in their usage as markers for senescence or exhaustion. PD-1 is often described as a marker for exhaustion due to its inhibitory role in T-cell activation and co-expression with other senescence/exhaustion markers (Bengsch et al. 2010; Brusa et al. 2013). However, PD-1 is initially up-regulated during T-cell activation and the early stages of differentiation, and is then down-regulated during the later stages of differentiation (Sauce et al. 2007). Furthermore, PD-1 can be co-expressed with activation markers CD38 and HLA-DR (Sauce et al. 2007). CD57 is often used as a marker for replicative senescence, but studies have demonstrated that $CD8^+CD57^+$ T-cells are capable of rapid proliferation and cytokine secretion (Chong et al. 2008). This study therefore looked at whether the expression of PD-1 and CD57 were associated with markers of activation. As PD-1 and CD57 were included together on antibody Panel 1, relationships were investigated with HLA-DR.

This study observed that $PD\text{-}1^+HLA\text{-}DR^+$ frequency was increased 3-fold in the CLL cohort versus healthy donors (Figure 3.18), both in the whole $CD8^+$ T-cell compartment ($p = 0.0001$) and the EM and EMRA subsets ($p = 0.0004$ and $p = 0.0005$, respectively). No significant difference was seen between the CLL^{NR} and CLL^{IR} subgroups, and therefore PD-1 co-expression with HLA-DR was considered of phenotypic interest within CLL, but not the CD4:CD8 ratio. Unfortunately, this study was unable to look at the co-expression of PD-1 and CD38 due to the antibodies being included on different flow cytometry panels (Panel 1 and Panel 2).

CD57 and HLA-DR co-expression on $CD8^+$ T-cells was significantly higher in the CLL patients versus their healthy counterparts ($p = 0.0012$, Figure 3.19A). $CD57^+HLA\text{-}DR^+$ frequency was increased in the $CD8^+$ EM ($p = 0.0144$) and the highly differentiated $CD8^+$ EMRA memory cells ($p = 0.0027$). The increased $CD57^+HLA\text{-}DR^+$ phenotype observed in the whole CLL cohort was more marked within the CLL^{IR} subgroup (Figure 3.19B): CLL^{IR} had significantly higher levels of $CD57^+HLA\text{-}DR^+$ cells within the $CD8^+$ T-cell compartment than either the CLL^{NR} or healthy donors ($p \leq 0.01$ and $p \leq 0.001$, respectively). This seemed to be predominantly due to an increase of this phenotype within the EM compartment ($p \leq 0.001$ versus both CLL^{NR} and healthy donors). The EMRA population of CLL^{IR} patients demonstrated higher $CD57^+HLA\text{-}DR^+$ frequency compared to the healthy donors ($p \leq 0.01$) but not CLL^{NR} patients.

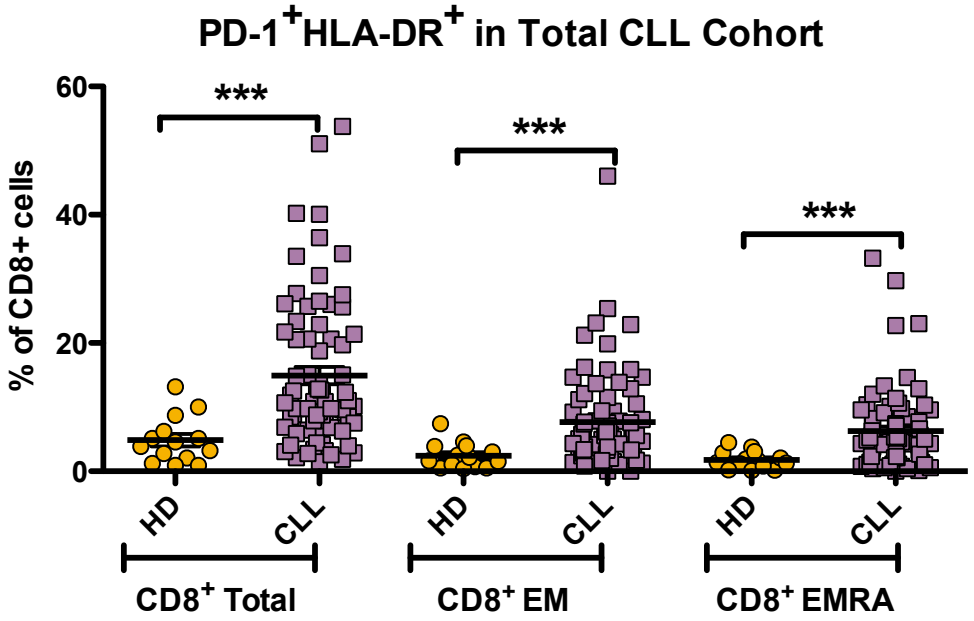

Figure 3.18. PD-1 and HLA-DR co-expression in $CD8^+$ T-cell memory subsets of CLL patients and healthy donors. Cells were collected using flow cytometry (FACS CantoII, BD FACSDiva) and analysed with FlowJo (v.9) using gating as described in Figure 3.1. $CD8^+PD\text{-}1^+HLA\text{-}DR^+$ T-cells in the whole $CD8^+$ T-cell compartment, $CD8^+$ EM and $CD8^+$ EMRA memory subsets of CLL patients (n = 74) and healthy donors (n = 14). Pairwise statistical analysis (HD vs CLL) was performed using the non-parametric Mann-Whitney test. Significant results were included on the graph (* = $p \leq 0.05$; ** = $p \leq 0.01$; *** = $p \leq 0.001$).

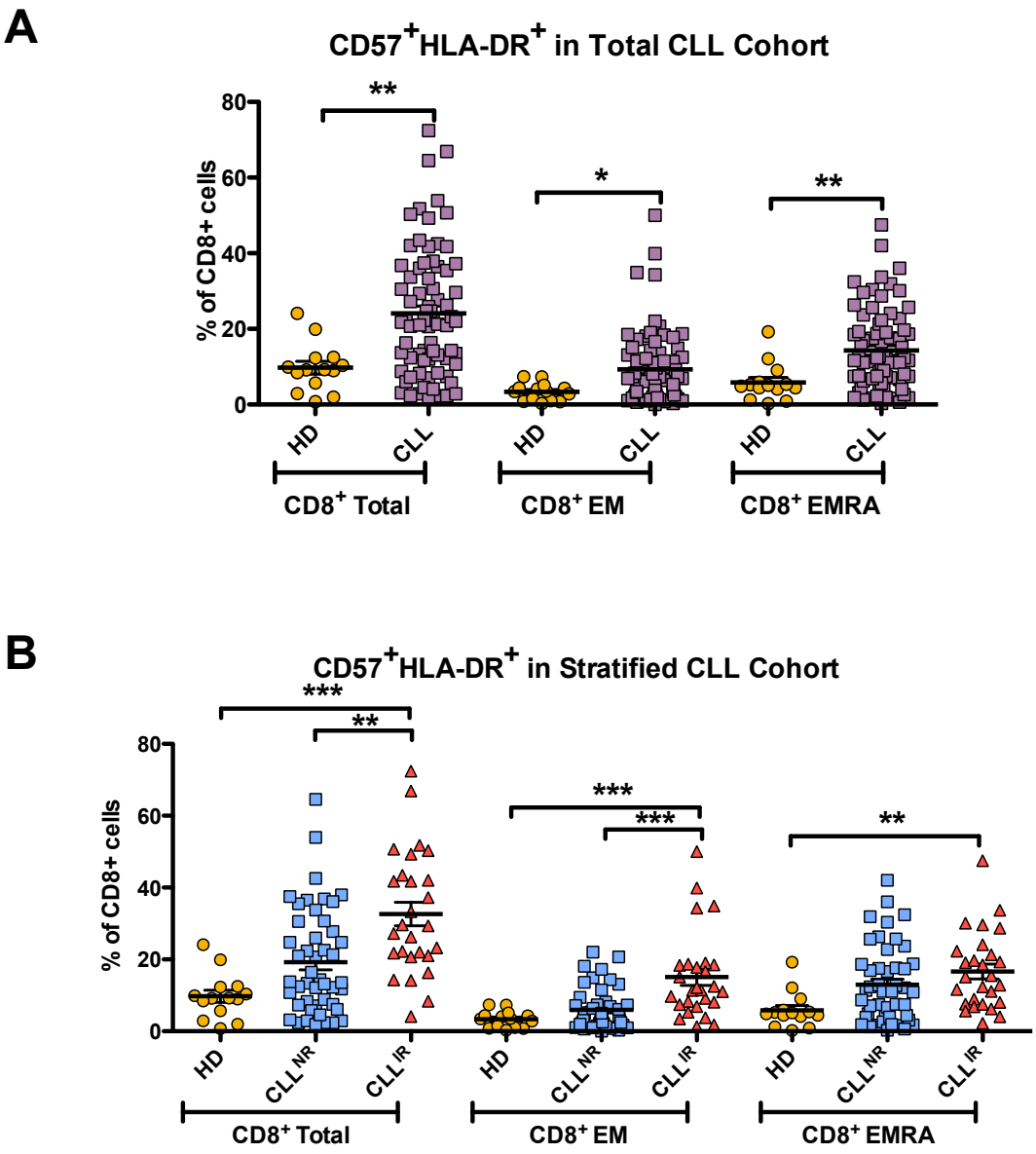

Figure 3.19. CD57 and HLA-DR co-expression in CD8$^+$ T-cell memory subsets of CLL patients and healthy donors. Cells were collected using flow cytometry (FACS CantoII, BD FACSDiva) and analysed with FlowJo (v.9) using gating as described in Figure 3.1. (A) CD8$^+$CD57$^+$HLA-DR$^+$ T-cells in the whole CD8$^+$ T-cell compartment, CD8$^+$ EM and CD8$^+$ EMRA memory subsets of CLL patients (n = 74) and healthy donors (n = 14). Pairwise statistical analysis (HD vs CLL) was performed using the non-parametric Mann-Whitney test. Patients were stratified based on CD4:CD8 ratio: a ratio <1.0 was considered inverted (CLL^{IR}). Patients with a ratio ≥1.0 were considered normal ratio patients (CLL^{NR}). (B) Frequency of CD8$^+$CD57$^+$HLA-DR$^+$ T-cells in the whole CD8$^+$ T-cell compartment, CD8$^+$ EM and CD8$^+$ EMRA memory subsets of CLL^{NR} (n = 47), CLL^{IR} (n = 27) and healthy donors (n = 14). Three-way ANOVA statistical analysis was performed using Kruskal-Wallis test (HD vs CLL^{NR} vs CLL^{IR}), with all pairs of data assessed using the Dunn's post-test. Significant results were included on the graph (* = p ≤0.05; ** = p ≤0.01; *** = p ≤0.001).

As both PD-1$^+$HLA-DR$^+$ and CD57$^+$HLA-DR$^+$ frequencies were higher in the CLL cohort than healthy donors, the presence of triple positive cells (CD57$^+$HLA-DR$^+$PD-1$^+$; Figure 3.20) was investigated. Overall, the CLL cohort showed an increased frequency of CD57$^+$HLA-DR$^+$PD-1$^+$ in the CD8$^+$ T-cell compartment when compared to healthy donors ($p = 0.0004$, Figure 3.20A). The triple positive phenotype was also increased in the CD8$^+$ EM subset of CLL patients ($p = 0.0016$) and the EMRA subset ($p = 0.0070$). The CD8$^+$ EMRA subset also showed higher levels of CD57$^+$HLA-DR$^+$PD-1$^-$ ($p = 0.0338$).

When stratified into CLL^{NR} and CLL^{IR} subgroups, there was no difference in CD57$^+$HLA-DR$^+$PD-1$^+$ frequency based on ratio but the CD8$^+$ EM subset did demonstrate a higher frequency of the CD57$^+$HLA-DR$^+$PD-1$^+$ phenotype versus CLL^{NR} and healthy donors ($p \leq 0.05$ and $p \leq 0.001$, respectively; Figure 3.20B). However, stronger significance was seen in CD57$^+$HLA-DR$^+$ T-cells lacking PD-1 (CD57$^+$HLA-DR$^+$PD-1$^-$; Figure 3.20C). Compared to CLL^{NR} patients and healthy donors, CLL^{IR} patients showed significantly higher CD57$^+$HLA-DR$^+$PD-1$^-$ frequency in both the CD8$^+$ compartment as a whole ($p \leq 0.01$ and $p \leq 0.001$), as well as the CD8$^+$ EM subset ($p \leq 0.001$ and $p \leq 0.01$). This, along with the absence of any significant difference in the frequency of CD8$^+$PD-1$^+$ T-cells between CLL^{IR} and CLL^{NR} (Section 3.3.1, Figure 3.6B) demonstrates that although PD-1 expression is not an independent marker of CLL^{IR}, co-expression of PD-1 with other markers may further define populations that are significantly different between patient cohorts. However, CD57$^+$HLA-DR$^+$ co-expression, without PD-1, is a stronger characteristic within the CLL^{IR} subgroup.

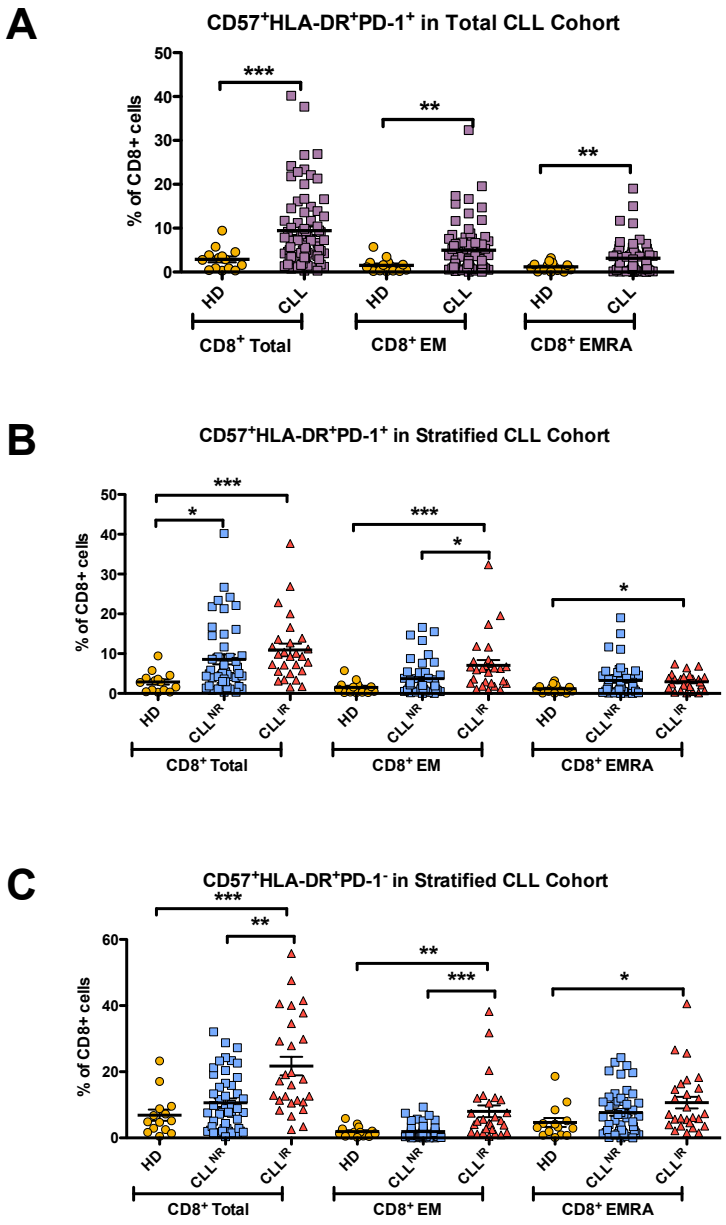

Figure 3.20. CD57, HLA-DR and PD-1 co-expression in $CD8^+$ T-cell memory subsets of CLL patients and healthy donors. Cells were collected using flow cytometry (FACS CantoII, BD FACSDiva) and analysed with FlowJo (v.9) using gating as described in Figure 3.1. (A) $CD8^+CD57^+HLA\text{-}DR^+PD\text{-}1^+$ T-cells in the whole $CD8^+$ T-cell compartment, $CD8^+$ EM and $CD8^+$ EMRA memory subsets of CLL patients (n = 74) and healthy donors (n = 14). Pairwise statistical analysis (HD vs CLL) was performed using the non-parametric Mann-Whitney test. Patients were stratified based on CD4:CD8 ratio: a ratio <1.0 was considered inverted (CLL^{IR}). Patients with a ratio ≥1.0 were considered normal ratio patients (CLL^{NR}). (B) Frequency of $CD8^+CD57^+HLA\text{-}DR^+PD\text{-}1^+$ T-cells in the whole $CD8^+$ T-cell compartment, $CD8^+$ EM and $CD8^+$ EMRA memory subsets of CLL^{NR} (n = 47), CLL^{IR} (n = 27) and healthy donors (n = 14). (C) Frequency of $CD8^+CD57^+HLA\text{-}DR^+PD\text{-}1^-$ T-cells in the whole $CD8^+$ T-cell compartment, $CD8^+$ EM and $CD8^+$ EMRA memory subsets of CLL^{NR}, CLL^{IR} and healthy donors. Three-way ANOVA statistical analysis was performed using Kruskal-Wallis test (HD vs CLL^{NR} vs CLL^{IR}), with all pairs of data assessed using the Dunn's post-test. Significant results were included on the graph (* = p ≤0.05; ** = p ≤0.01; *** = p ≤0.001).

3.4.3. CD57, KLRG-1 and CD38

As described in the previous section, senescence markers can be co-expressed with activation markers. This study explored associations between senescence markers CD57 and KLRG-1 with the activation marker CD38 (Panel 2). Co-expression of CD57 and CD38 was significantly higher in the total CLL $CD8^+$ T-cell compartment when compared with healthy donors ($p = 0.0057$). This was also observed in the $CD8^+$ EM and EMRA memory subsets when compared with healthy donors ($p = 0.0031$ and $p = 0.0441$, respectively; Figure 3.21A). The higher $CD57^+CD38^+$ frequency was exacerbated in CLL^{IR} $CD8^+$ T-cells compared to both the CLL^{NR} subgroup and healthy donors ($p \leq 0.01$ and $p \leq 0.001$; Figure 3.21B). Again, a similar pattern was observed when the CD8 T-cells were sub-divided on the basis of EM ($p \leq 0.01$ versus CLL^{NR} and $p \leq 0.001$ versus HD) and EMRA cells ($p \leq 0.05$ versus both CLL^{NR} and HD).

KLRG-1^+CD38^+ frequency showed the same increasing trends as $CD57^+CD38^+$ frequency, particularly with regards to the inverted ratio patients (see Appendix III). Furthermore, expression of CD57 and KLRG-1 together with CD38 was more prevalent in the $CD8^+$ T-cells of the CLL patients than the healthy donors ($p = 0.0169$; Figure 3.22A). When patients were stratified based on CD4:CD8 ratio, the CLL^{IR} patients had higher frequencies of $CD57^+$KLRG-1^+CD38^+ T-cells than either the CLL^{NR} cohort or healthy donors ($p \leq 0.001$ for both; Figure 3.22B). However, the most prevalent CD57/KLRG-1/CD38 combination was the $CD57^+$KLRG-1^+CD38^- population in both CLL patients and healthy donors (see Appendix III). This suggests that the majority of T-cells with a highly senescent/differentiated phenotype ($CD8^+CD57^+KLRG1^+$) are not activated. However, there is a smaller subgroup of these T-cells that appear to be activated and are enriched in CLL^{IR} patients.

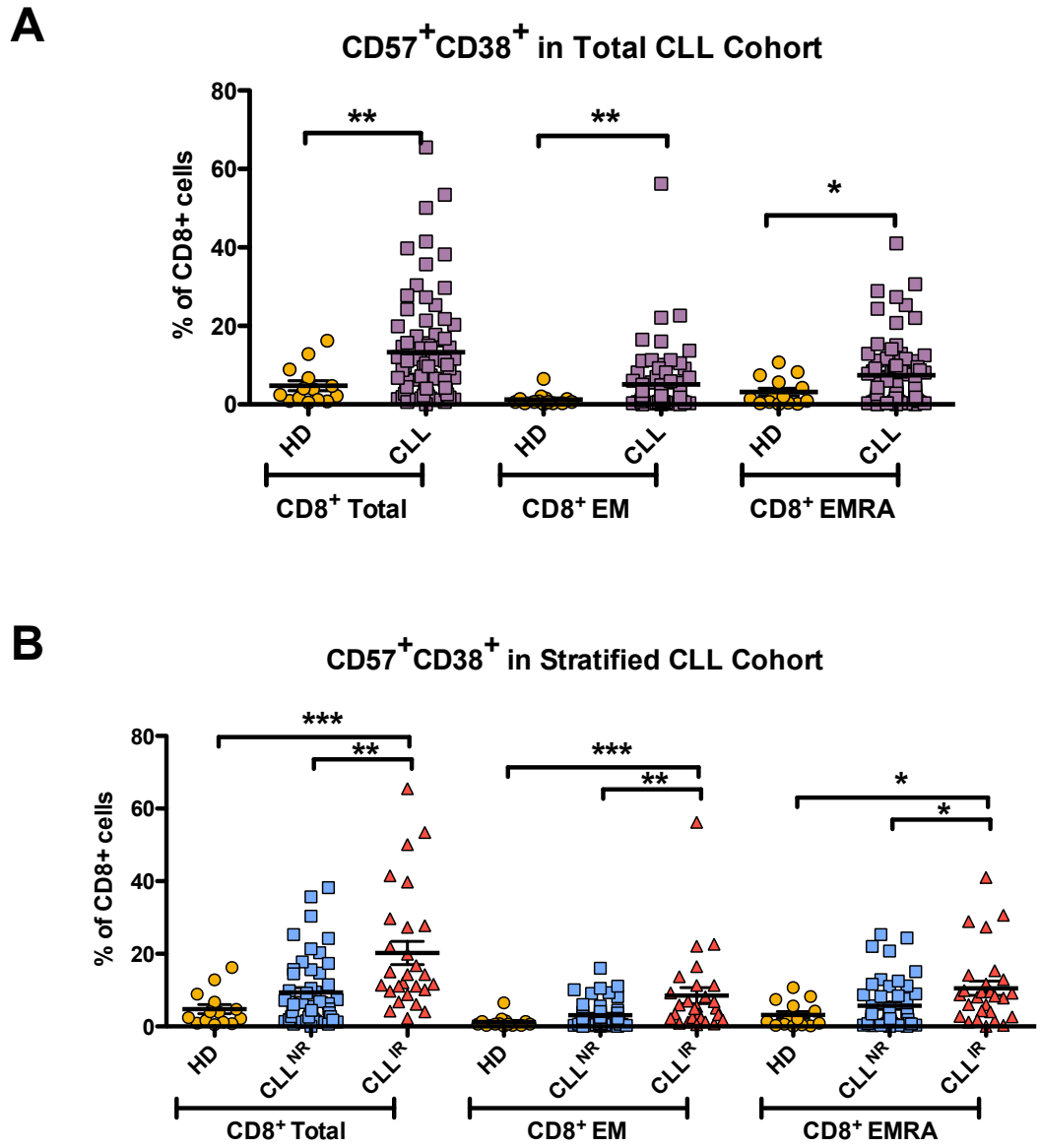

Figure 3.21. CD57 and CD38 co-expression in CD8$^+$ T-cell memory subsets of CLL patients and healthy donors. Cells were collected using flow cytometry (FACS CantoII, BD FACSDiva) and analysed with FlowJo (v.9) using gating as described in Figure 3.1. (A) CD8$^+$CD57$^+$CD38$^+$ T-cells in the whole CD8$^+$ T-cell compartment, CD8$^+$ EM and CD8$^+$ EMRA memory subsets of CLL patients (n = 74) and healthy donors (n = 14). Pairwise statistical analysis (HD vs CLL) was performed using the non-parametric Mann-Whitney test. Patients were stratified based on CD4:CD8 ratio: a ratio <1.0 was considered inverted (CLL^{IR}). Patients with a ratio ≥1.0 were considered normal ratio patients (CLL^{NR}). (B) Frequency of CD8$^+$CD57$^+$CD38$^+$ T-cells in the whole CD8$^+$ T-cell compartment, CD8$^+$ EM and CD8$^+$ EMRA memory subsets of CLL^{NR} (n = 47), CLL^{IR} (n = 27) and healthy donors (n = 14). Three-way ANOVA statistical analysis was performed using Kruskal-Wallis test (HD vs CLL^{NR} vs CLL^{IR}), with all pairs of data assessed using the Dunn's post-test. Significant results were included on the graph (* = p ≤0.05; ** = p ≤0.01; *** = p ≤0.001).

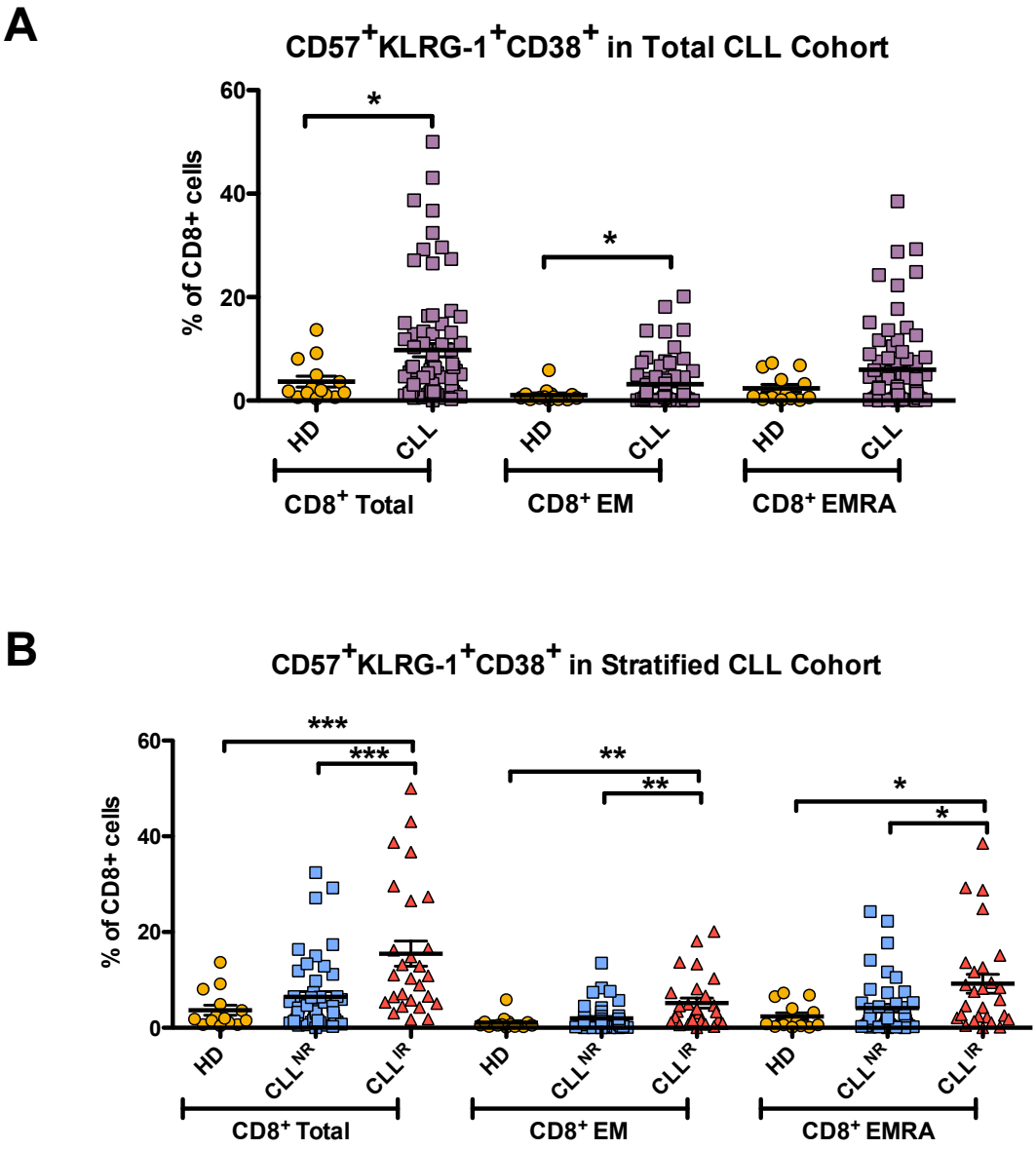

Figure 3.22. CD57, KLRG-1 and CD38 co-expression in CD8$^+$ T-cell memory subsets of CLL patients and healthy donors. Cells were collected using flow cytometry (FACS CantoII, BD FACSDiva) and analysed with FlowJo (v.9) using gating as described in Figure 3.1. (A) CD8$^+$CD57$^+$KLRG-1$^+$CD38$^+$ T-cells in the whole CD8$^+$ T-cell compartment, CD8$^+$ EM and CD8$^+$ EMRA memory subsets of CLL patients (n = 74) and healthy donors (n = 14). Pairwise statistical analysis (HD vs CLL) was performed using the non-parametric Mann-Whitney test. Patients were stratified based on CD4:CD8 ratio: a ratio <1.0 was considered inverted (CLL^{IR}). Patients with a ratio ≥1.0 were considered normal ratio patients (CLL^{NR}). (B) Frequency of CD8$^+$CD57$^+$KLRG-1$^+$CD38$^+$ T-cells in the whole CD8$^+$ T-cell compartment, CD8$^+$ EM and CD8$^+$ EMRA memory subsets of CLL^{NR} (n = 47), CLL^{IR} (n = 27) and healthy donors (n = 14). Three-way ANOVA statistical analysis was performed using Kruskal-Wallis test (HD vs CLL^{NR} vs CLL^{IR}), with all pairs of data assessed using the Dunn's post-test. Significant results were included on the graph (* = p ≤0.05; ** = p ≤0.01; *** = p ≤0.001).

3.5. Inverted ratio and cytomegalovirus (CMV) infection

Cytomegalovirus (CMV) is a common persistent viral infection in the elderly population (Vasto et al. 2007; Pita-Lopez et al. 2009). Previous work has shown that both the $CD4^+$ and $CD8^+$ T-cell compartments in CMV-positive patients are skewed towards more differentiated memory subsets (Pourgheysari et al. 2010; Khan et al. 2002). This is thought to be due to expansions in chronically stimulated CMV-specific T-cells that are defined as senescent, although there is evidence that CMV-specific T-cells from CLL patients can act in a functional capacity (Raa et al. 2014). Therefore, to assess whether CMV was a contributing factor in this study, patient serum from a cohort of CLL patients was collected and serotyped by Public Health Wales Microbiology Lab, UHW, Cardiff.

The CMV serostatus was assessed in 63 of the CLL patients used in this study: of those tested, over 68% were CMV^+ (43 patients). Patients were stratified based on CD4:CD8 T-cell ratio and CMV seropositivity. In line with previous work by our group (Nunes et al. 2012), there were no significant differences between groups (Fisher's exact test, $p = 0.0922$; Figure 3.23) suggesting that CLL CD4:CD8 T-cell ratio is not driven by CMV. Furthermore, SPICE software analysis was used to compare the distribution of memory T-cell subsets among CLL patients based on CMV serostatus using pie charts (Figure 3.34). This showed that the distribution of $CD8^+$ memory subsets were significantly different in CMV^+ and CMV^- CLL patients ($p = 0.0192$), and this was due to a proportionally larger EMRA subset in CMV^+ patients (Figure 3.24). Overall these results lend support to CMV infection not being a contributing factor to inversion of the CD4:CD8 ratio or phenotypic abnormalities associated with CLL (Nunes et al. 2012).

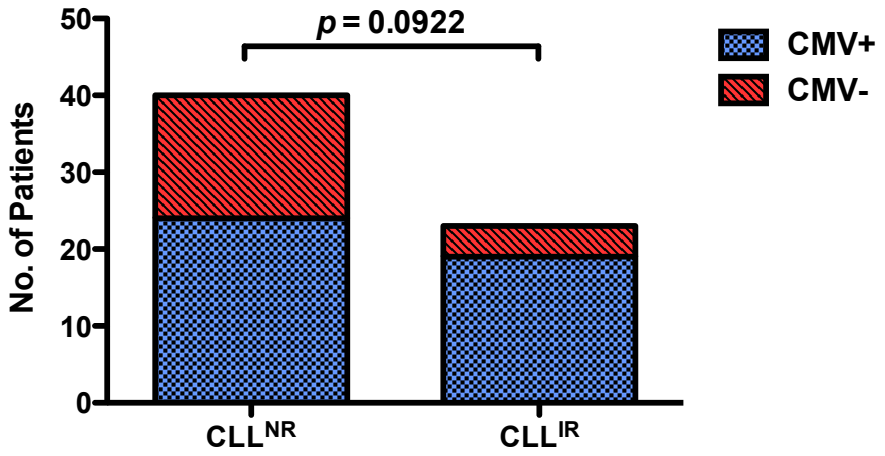

Figure 3.23. CMV serostatus in CLL patients. Plasma samples from CLL patients were serotyped for cytomegalovirus. To observe the relationship between CMV and CD4:CD8 ratio, patients were stratified into four groups based ratio (CLL^{NR} and CLL^{IR}) and CMV seropositivity: CLL^{NR} CMV^{+} (n = 24), CLL^{NR} CMV^{-} (n = 16), CLL^{IR} CMV^{+} (n = 19) and CLL^{IR} CMV^{-} (n = 4). Fisher's exact test was used for analysis.

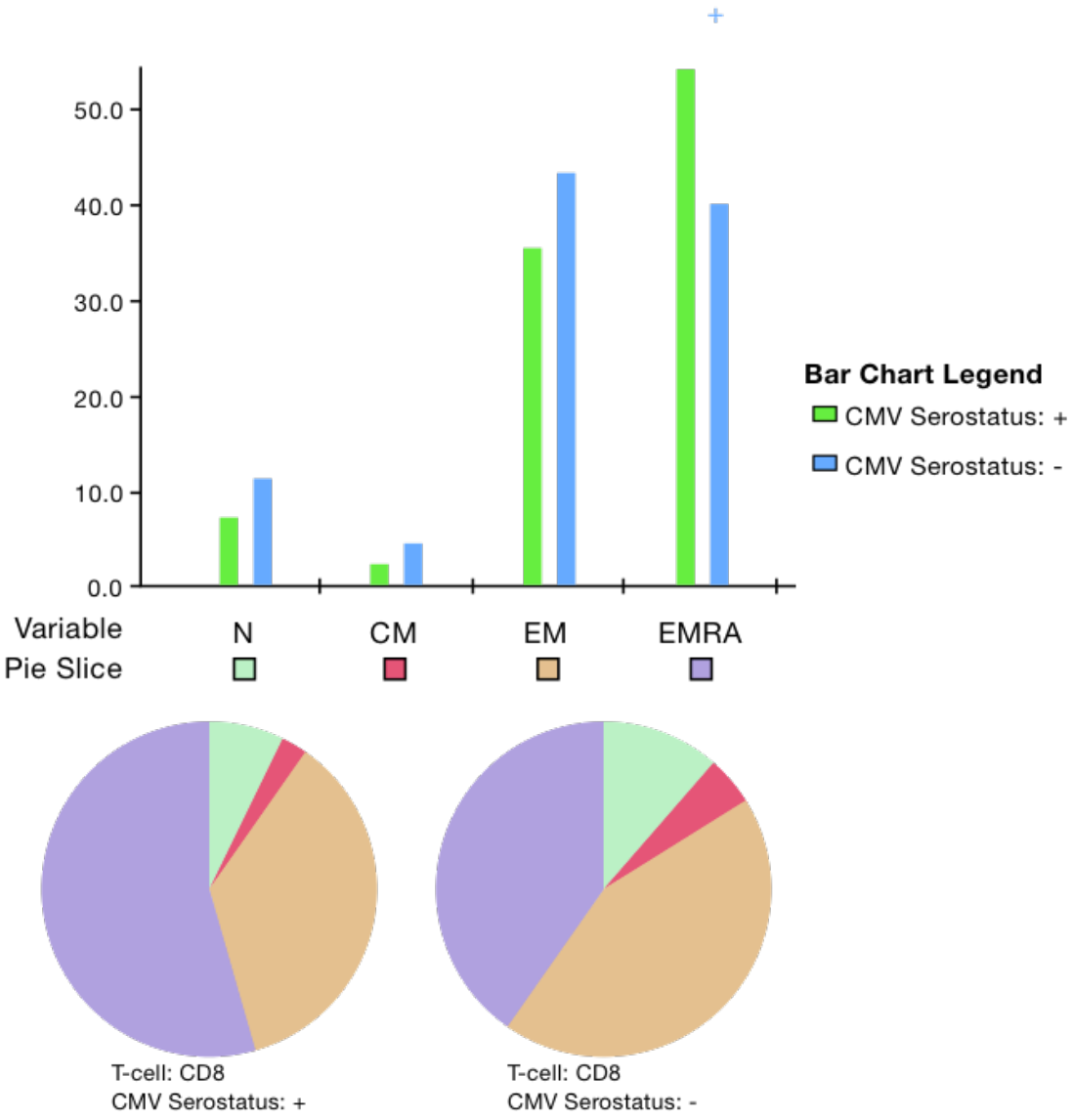

Figure 3.24. Distribution of CD8$^+$ memory subsets in CMV seropositive (n = 43) and CMV seronegative (n = 20) CLL patients. Cells were collected using flow cytometry (FACS CantoII, BD FACSDiva) and analysed with FlowJo (v.9) using gating as described in Figure 3.1. Plasma samples from CLL patients were serotyped for cytomegalovirus. Flow cytometry data and CMV information were analysed using SPICE software (v5.3).

3.6. Assessment of CD4:CD8 ratio with prognosis

3.6.1. Established prognostic markers

There are many documented tumour associated markers in CLL that relate to disease prognosis. Where available, the ratio data acquired in this study was collated with previously recorded prognostic characteristics, including: Binet stage, lymphocyte doubling time (LDT), $CD38^+$ status (of CLL B-cells), and immunoglobulin heavy-chain variable region (*IGHV*) mutational status. Patients were stratified based on CD4:CD8 ratio and the relevant characteristic (see Figure 3.25). Performance of Fisher's exact tests revealed that there was no association between the established prognostic markers and CD4:CD8 ratio.

3.6.2. Univariate analysis

To reaffirm the prognostic value of the inverted ratio reported in previous studies (Nunes et al. 2012), Kaplan-Meier curves for progression-free survival (PFS) were produced. The CLL cohort was subdivided by CD4:CD8 ratio as before i.e. patients with a CD4:CD8 ratio <1.0 were considered inverted and patients with a ratio ≥ 1.0 were considered normal. A ratio of 1.00 was initially considered the best cut-off for this study for two reasons. First, it represents the true point of numerical inversion, where there are more $CD8^+$ T-cells than $CD4^+$ T-cells. Second, previous work within the group analysed a CLL cohort with a median ratio of 1.00 (Nunes et al. 2012).

Figure 3.26A shows the Kaplan-Meier curve comparing the PFS for these 'traditional' CLL^{NR} and CLL^{IR} subgroups. CLL^{IR} patients have a significantly worse prognosis ($HR = 5.539$, $p = 0.0002$). Kaplan-Meier curves with CLL patients divide based on the ratio median are also shown (Figure 3.26B). The prognostic effect was decreased when patients were stratified by the median ($HR = 3.200$, $p = 0.0056$). This lends further support for 1.0 as the best limit to subdivide based on ratio; therefore, using 1.0 as the cut-off ratio was continued in this study.

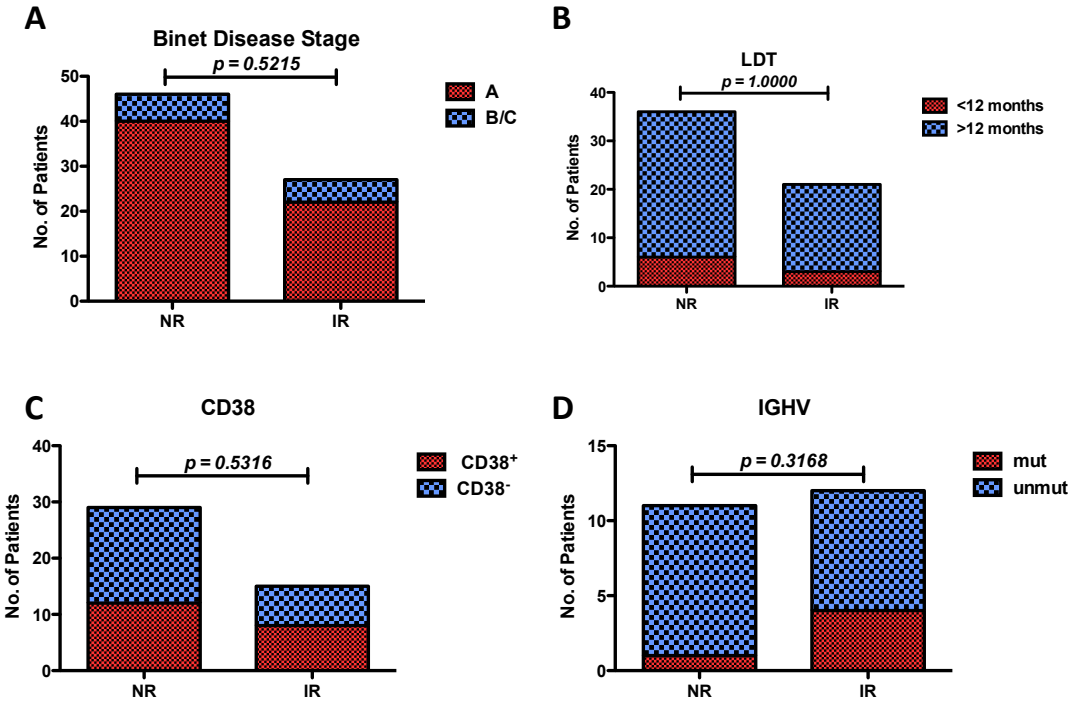

Figure 3.25. Prognostic markers in CLL^{NR} and CLL^{IR} patients. (A) Binet disease stage in CLL patients with normal (n = 46) and inverted ratio (n = 27). (B) Lymphocyte doubling time in CLL patients with normal (n = 36) and inverted (n = 21) ratio. (C) CD38^{+} status in CLL patients with normal (n = 29) and inverted (n = 15) ratio. (D) *IGHV* mutational status in CLL patients with normal (n = 11) and inverted ratio (n = 12). Analysis performed using Fisher's exact test.

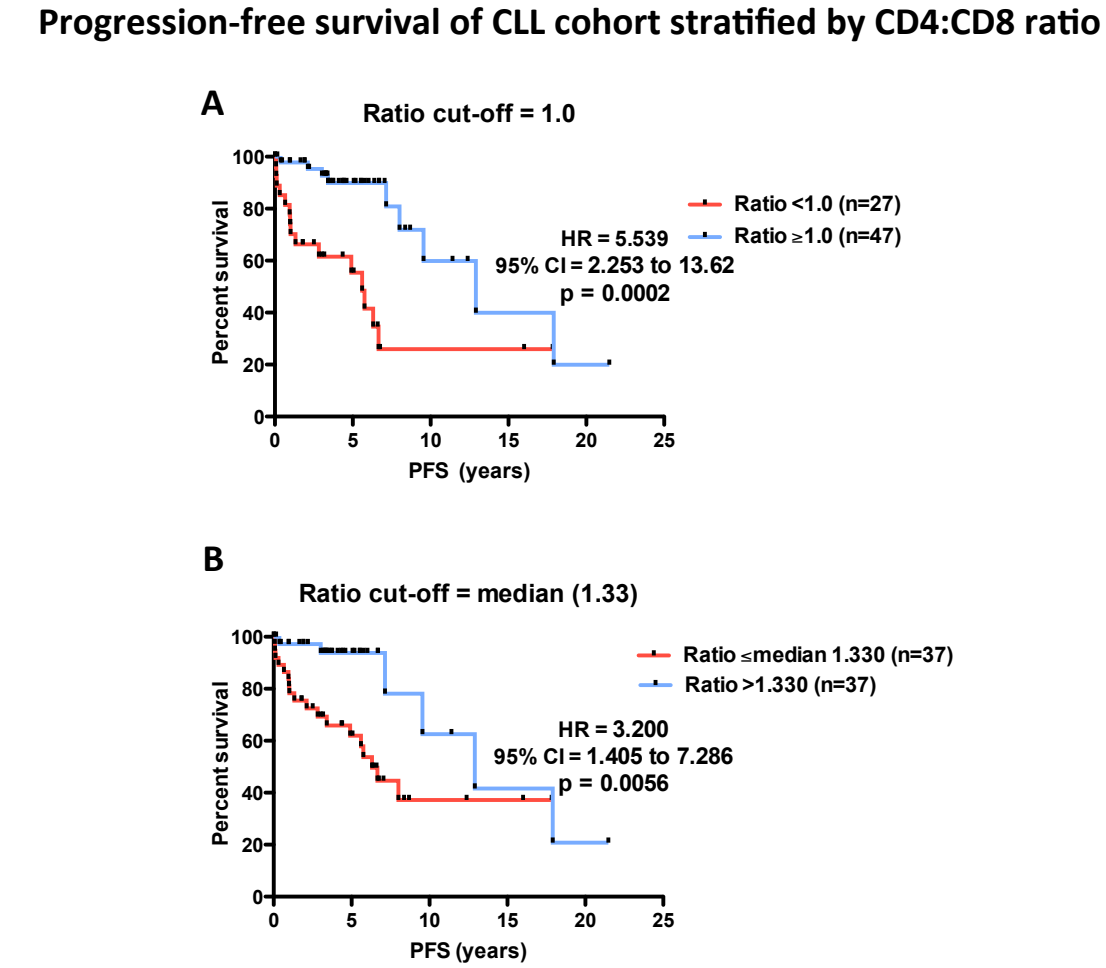

Figure 3.26. Prognosis of CLL patients stratified by CD4:CD8 ratio. Cells were collected using flow cytometry (FACS CantoII, BD FACSDiva) and analysed with FlowJo (v.9) using gating as described in Figure 3.1. Multivariate recursive partitioning was performed to establish significant 'cut-off' ratio values within the study group. Kaplan-Meier curves for progression-free survival of CLL patients stratified by a ratio of (A) the 'traditional' 1.0, and (B) the median ratio 1.33 are shown. Univariate analyses (Kaplan-Meier curves and survival statistics) were performed using GraphPad Prism.

3.7. Multivariate analysis

Multivariate analyses were performed by Professor Robert Hills (Haematology Clinical Trials Unit, Cardiff University). Due to the large number of variables generated in this phenotypic study, separate data sets were built to include either the single frequency and Boolean combination data from either Panel 1 or Panel 2: these data sets contained 70 and 128 variables respectively. Initial cox-proportional hazard regression with forward selection was performed on each data set to establish which variables had the greatest effect on PFS within each panel. The results of these analyses were then used to compile the variables of importance from both Panels into a single data set for a further multivariate analysis to determine the variables that had greatest effect across the two panels. A total of 128 variables were considered in the final analysis. In addition to the cox-proportional hazard regression, correlation analyses were performed comparing CD4:CD8 ratio against all phenotypic variables. Complete analyses for the final multivariate set is provided in Appendix IV, including simple variable statistics, correlation statistics and hazard modelling. For the purposes of completeness, phenotypic data for the $CD4^+$ T-cell compartment was also included in the analyses.

3.7.1. Correlations with CD4:CD8 ratio

Correlation analyses were performed for each variable versus the CD4:CD8 ratio. Table 3.3 summarises the variables that demonstrated the strongest correlation with ratio (where $r > 0.5$ or > -0.5, $p \leq 0.05$; see Appendix IV for complete correlation analysis). As expected, frequency of total $CD4^+$ and total $CD8^+$ strongly correlated with ratio ($r = 0.870$ and $r = -0.850$, $p < 0.0001$, respectively). Both the $CD4^+$ and $CD8^+$ naïve memory populations positively correlated with ratio ($r = 0.575$ and $r = 0.712$, respectively; $p < 0.0001$ for both). The variables that had the strongest negative relationships with ratio were $CD4^+$ populations: these included EM $CD57^+HLA\text{-}DR^+$ ($r = -0.634$, $p < 0.0001$), $CD57^+PD\text{-}1^+$ ($r = -0.616$, $p = < 0.0001$), $CD57^+HLA\text{-}DR^+$ ($r = -0.612$, $p < 0.0001$), and $CD57^+PD\text{-}1^+$ ($r = -0.605$, $p < 0.001$). The $CD8^+$ phenotypes that demonstrated the strongest correlations were $CD38^+CD57^+KLRG\text{-}1^+$ ($r = -0.519$, $p < 0.0001$) and $CD57^+$ ($r = -0.510$, $p < 0.0001$). These results confirm the phenotypic analysis that demonstrated that both $CD8^+CD57^+$ and $CD8^+CD38^+CD57^+KLRG\text{-}1^+$ frequency were both significantly higher in the CLL^{IR} subgroup of patients (Section 3.3.1 an 3.4.3, respectively). Taken together these results suggest that these two $CD8^+$ phenotypes appear to be most linked with decreasing CD4:CD8 ratio.

Table 3.3 Ratio correlations against T-cell phenotypes in CLL.

Variable	r	p-value
Positive Correlation[1]		
$CD4^+$	0.87022	<0.0001
$CD8^+$ Naïve	0.71172	<0.0001
$CD4^+$ Naïve	0.57513	<0.0001
Negative Correlation[2]		
$CD8^+$	−0.85023	<0.0001
$CD4^+EM^+CD57^+HLA\text{-}DR^+$	−0.634	<0.0001
$CD4^+CD57^+PD\text{-}1^+$	−0.61579	<0.0001
$CD4^+CD57^+HLA\text{-}DR^+$	−0.61185	<0.0001
$CD4^+CD57^+PD\text{-}1^+$	−0.60481	<0.0001
$CD4^+EM^+CD57^+HLA\text{-}DR^+PD\text{-}1^+$	−0.6013	<0.0001
$CD4^+CD57^+HLA\text{-}DR^+PD\text{-}1^+$	−0.5868	<0.0001
$CD4^+EM^+CD57^+$	−0.57537	<0.0001
$CD4^+HLA\text{-}DR^+PD\text{-}1^+$	−0.5718	<0.0001
$CD4^+HLA\text{-}DR^+PD\text{-}1^+$	−0.55478	<0.0001
$CD4^+EM^+HLA\text{-}DR^+$	−0.54785	<0.0001
$CD4^+HLA\text{-}DR^+$	−0.54439	<0.0001
$CD4^+CD57^+$	−0.52054	<0.0001
$CD8^+CD38^+CD57^+KLRG\text{-}1^+$	−0.51862	<0.0001
$CD8^+CD57^+$	−0.51858	<0.0001
$CD4^+CD38^+CD57^+$	−0.51012	<0.0001

[1] A positive correlation indicates that the phenotypic marker(s) are associated with an increase in the CD4:CD8 ratio.
[2] A negative correlation indicates that the phenotypic marker(s) are associated with a decrease in the CD4:CD8 ratio.

3.7.2. Cox-proportional hazards regression

A cox-proportional hazard regression model with forward selection was used to determine which phenotypic factors had the strongest effect on CLL patient prognosis (progression-free survival: PFS). The aim of this chapter was to investigate the $CD8^+$ T-cell population in CLL: interestingly, the most powerful variable given by the multivariate analysis was $CD4^+HLA\text{-}DR^+PD\text{-}1^+$ (Table 3.4), which initiated subsequent phenotypic exploration of the $CD4^+$ compartment in the next chapter (Chapter 4).

There were three $CD8^+$ variables that demonstrated a significant effect (at the 0.05 level entry; Table 3.4): $CD8^+$, $CD8^+CD57^+HLA\text{-}DR^+$ and $CD8^+$ EMRA $CD57^+HLA\text{-}DR^+PD\text{-}1^+$. These variables were then subjected to univariate analysis. For each phenotype, patients were initially stratified based on the median value (frequency of $CD8^+$ T-cells); however, the median cut-off did not always provide a significant difference in prognosis between the two patient subgroups (see Appendix IV). Therefore, using the median frequency was not the best cut-off point on which to divide the patient population into better/poorer prognosis subgroups. To address this, further multivariate analyses were implemented to perform recursive partitioning (using a regression model with forward selection) and identify the optimum frequency thresholds that had the greatest effect on PFS for each phenotype. Ratio was also included to assess whether the 1.0 boundary identified by previous work was the optimum cut-off for this study. The analyses gave an output for each variable showing the frequencies that had the strongest effect (at 0.05 level entry). For each variable, survival analyses (Kaplan-Meier curves and hazard ratios) were produced to identify which cut-offs identified the optimum frequency for prognostic assessment (Table 3.4). Here the most prognostically relevant results are summarised. Comprehensive results tables and Kaplan-Meier curves are shown in Appendix IV.

Table 3.4 Summary of Cox-proportional hazard regression model with forward selection.

Variable	Number in	Chi-square	p
$CD4^+HLA\text{-}DR^+PD\text{-}1^+$	1	23.4347	<0.0001
$CD8^+$	2	5.5428	0.0186
$CD8^+CD57^+HLA\text{-}DR^+$	3	4.7188	0.0298
$CD8^+EMRA^+CD57^+HLA\text{-}DR^+PD\text{-}1^+$	4	5.2623	0.0218

Section 3.6.2. showed that the 'traditional' ratio cut-off of 1.0 based on prior research by (Nunes et al. 2012) held more prognostic value than using the median ratio of this study's patient cohort. In this analysis, recursive partitioning identified the CD4:CD8 ratios of 0.95, 0.99 and 1.01 as having a great effect on PFS (Figure 3.27A-C), supporting the use of 1.0 as a reasonable cut-off point for patient stratification. In addition, the greatest effect on prognosis was observed with a ratio of 0.52 or lower (Figure 3.27D). This further supports that decreasing ratio leads to an exacerbated prognosis, and suggests that a cut-off ratio around 0.5 could be used to identify a high-risk inverted ratio group.

The frequency of $CD8^+$ T-cells was also a factor that had a significant effect on prognosis, which might be expected given the link between inverted CD4:CD8 ratios and inferior prognosis. Both 31% and the median 33.2% $CD8^+$ T-cells were identified as prognostic thresholds via recursive partitioning (Figure 3.28A-B). Higher frequencies revealed even poorer prognosis for patients with 56.9-58.5% $CD8^+$ T-cells and above, with 56.9% given as the strongest cut-off within the multivariate analyses (Figure 3.28C-D).

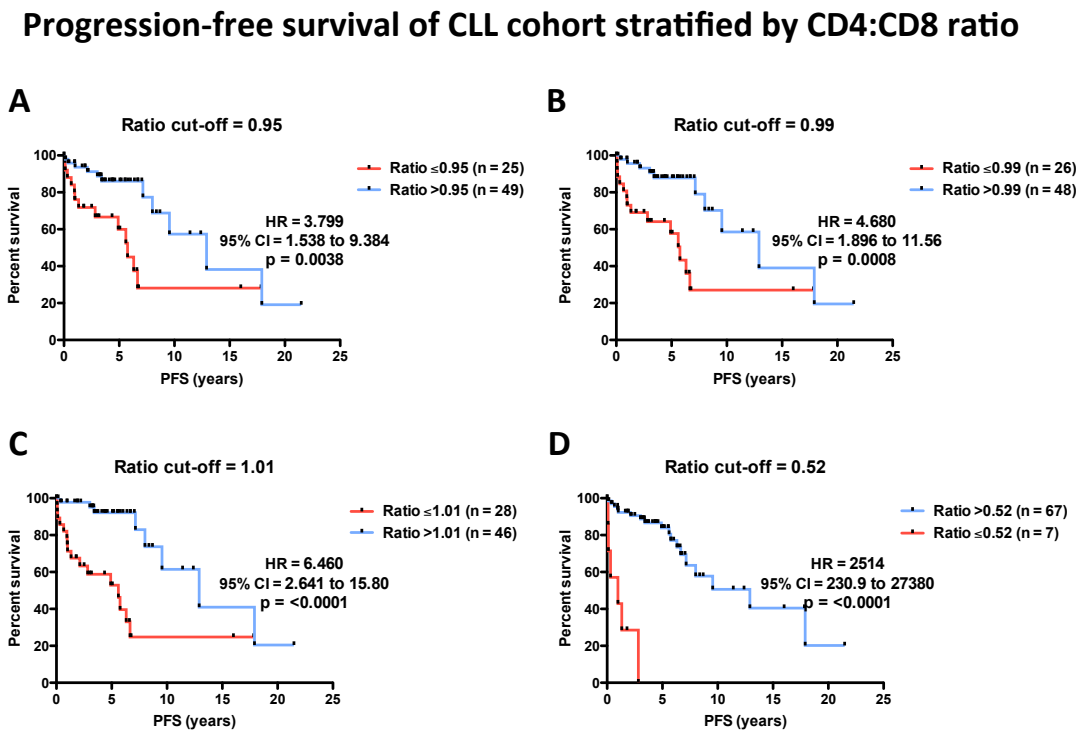

Figure 3.27. Prognosis of CLL patients stratified by CD4:CD8 ratio. Cells were collected using flow cytometry (FACS CantoII, BD FACSDiva) and analysed with FlowJo (v.9) using gating as described in Figure 3.1. Multivariate recursive partitioning was performed to establish significant 'cut-off' ratio values within the study group. Kaplan-Meier curves for progression-free survival of CLL patients stratified by a ratio of (A) 0.95 (B) 0.99 (C) 1.01 and (D) 0.52 are shown. These were the most prognostically relevant thresholds based on the combined multivariate and univariate analyses. Multivariate analyses were performed by Dr. Robert Hills (Haematology Clinical Trials Unit, Cardiff University). Univariate analyses (Kaplan-Meier curves and survival statistics) were performed using GraphPad Prism.

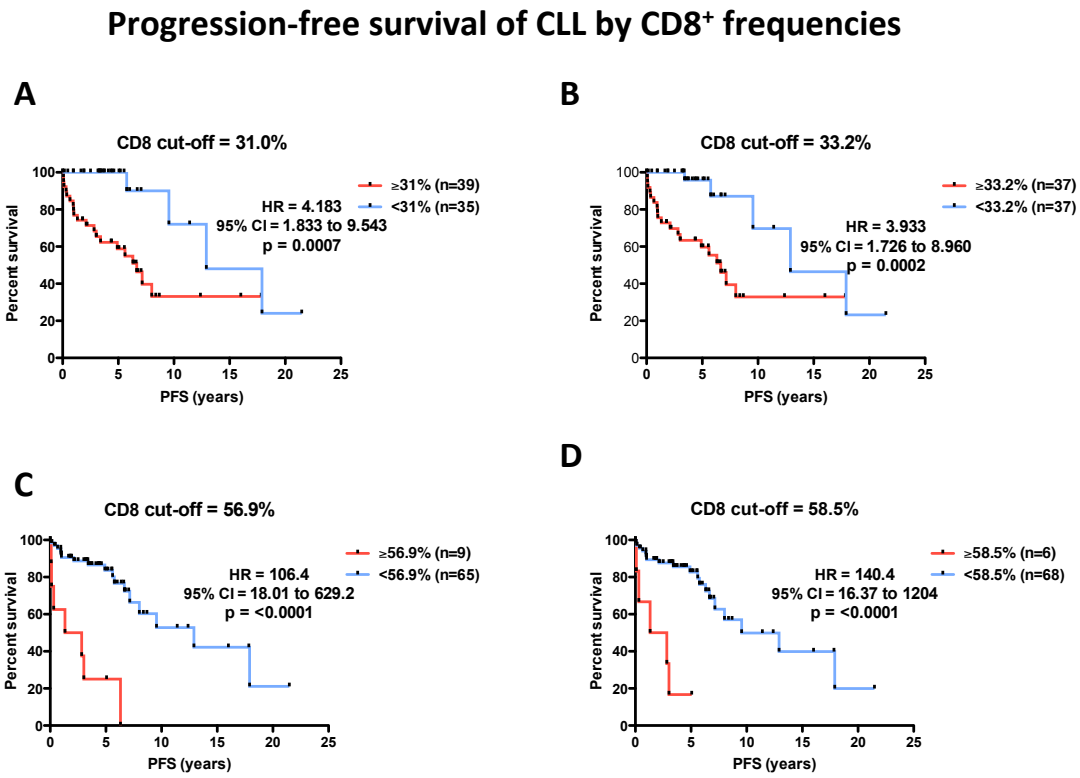

Figure 3.28. Prognosis of CLL patients stratified based on CD8$^+$ frequencies. Cells were collected using flow cytometry (FACS CantoII, BD FACSDiva) and analysed with FlowJo (v.9) using gating as described in Figure 3.1. Lymphocytes were gated based on forward and side scatter profile; forward scatter area and height were used for exclusion of doublet cells. CD8$^+$ T-cells were identified by gating first on CD3$^+$ then CD8$^+$ cells. Multivariate recursive partitioning was performed to establish significant 'cut-off' ratio values within the study group. Kaplan-Meier curves for progression-free survival of CLL patients stratified by a CD8$^+$ frequency of (A) 31%, (B) 33.2% (the median), (C) 56.9% and (D) 58.5% are shown. These were the most prognostically relevant thresholds based on the combined multivariate and univariate analyses. Multivariate analyses were performed by Dr. Robert Hills (Haematology Clinical Trials Unit, Cardiff University). Univariate analyses (Kaplan-Meier curves and survival statistics) were performed using GraphPad Prism.

The frequency of the $CD8^+CD57^+HLA\text{-}DR^+$ phenotype was also shown to have a significant impact on PFS. Recursive partitioning followed by univariate analyses revealed that the ideal prognostic cut-off for this cohort was between 24.7-26.2% (Figure 3.29A-B). Patients with a $CD8^+CD57^+HLA\text{-}DR^+$ frequency above this threshold had significantly poorer prognosis. The phenotypic analysis undertaken earlier in this chapter demonstrated that CLL patients had higher frequencies of $CD8^+CD57^+HLA\text{-}DR^+$, and this was further accentuated in the CLL^{IR} subgroup (Section 3.4.2, Figure 3.19). As CLL^{IR} patients also have poorer prognosis, it is not surprising that some inverted ratio patients also have high $CD8^+CD57^+HLA\text{-}DR^+$. However, a strong correlation was not observed between these two variables ($r = -0.455$), implying that although there is some relationship between the two, they are not directly linked.

The final $CD8^+$ variable to demonstrate a significant effect on prognosis within the CLL cohort was the frequency of $CD57^+HLA\text{-}DR^+PD\text{-}1^+$ within the $CD8^+$ EMRA memory subset. The potential cut-offs suggested by recursive portioning were 6.45-6.86% (Figure 3.29C and D); the seven patients who had this frequency or higher (ranging from 6.45 to 19%) had significantly poorer prognosis compared to the remainder of the cohort. This phenotype was significantly higher in CLL patients versus healthy donors in Section 3.4.2 (Figure 3.20), but not exacerbated in CLL^{IR} patients, indicating that any phenotypic effect of increased $CD57^+HLA\text{-}DR^+PD\text{-}1^+$ in the $CD8^+$ EMRA compartment was independent of CD4:CD8 ratio.

Forward selection was also performed to include additional phenotypes that could have potential as contributing factors to prognosis (See Table 4 in Appendix IV for the complete multivariate results). This included the CD4:CD8 ratio, supporting the concept that ratio does contribute to prognosis, but to a lesser effect than the phenotypes described above (Table 3.4). $CD4^+CD57^+PD\text{-}1^+$ and $CD8^+$ EMRA $CD57^+HLA\text{-}DR^+$ were also shown to contribute to prognosis in a co-dependent manner.

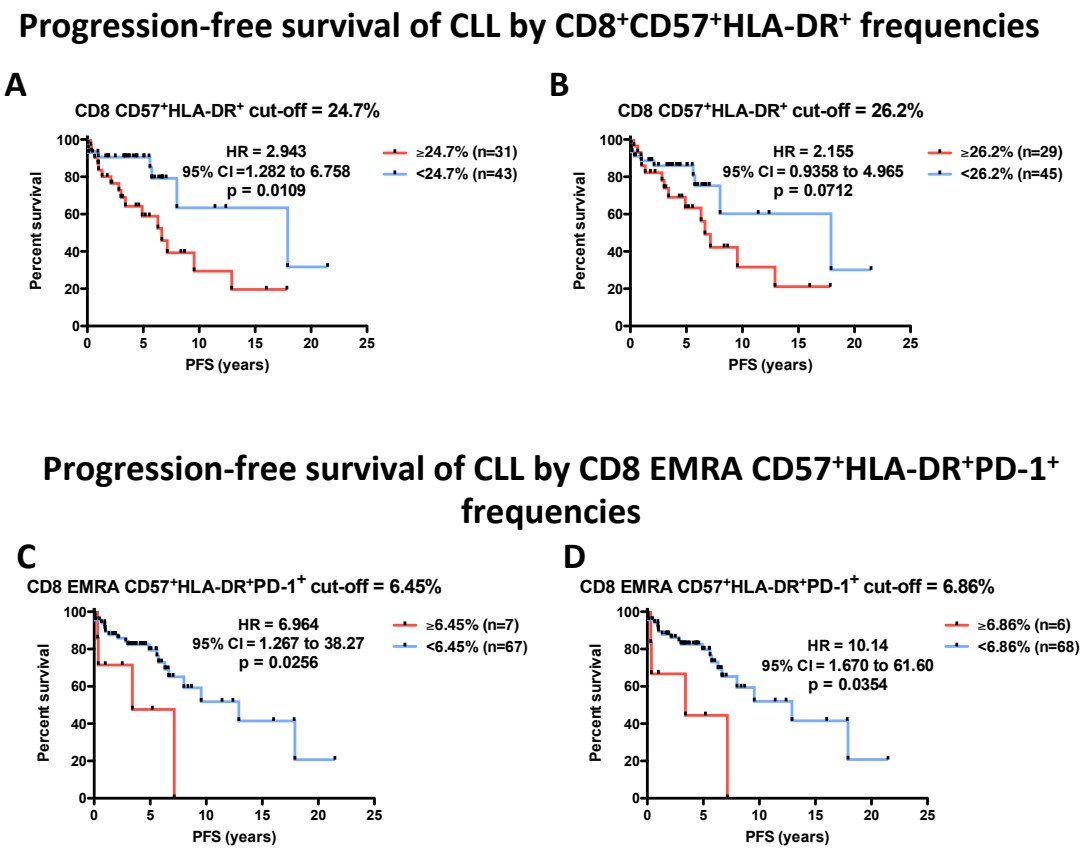

Figure 3.29. Prognosis of CLL patients stratified based on $CD8^+$ phenotype frequencies. Cells were collected using flow cytometry (FACS CantoII, BD FACSDiva) and analysed with FlowJo (v.9) using gating as described in Figure 3.1. Multivariate recursive partitioning was performed to establish significant 'cut-off' ratio values within the study group. Kaplan-Meier curves for progression-free survival of CLL patients stratified by: $CD8^+CD57^+HLA\text{-}DR^+$ frequency of (A) 24.7% and (B) 26%; and by $CD8^+$ EMRA $CD57^+HLA\text{-}DR^+PD\text{-}1^+$ frequency of (C) 6.45% and (D) 6.86%. These were the most prognostically relevant thresholds based on the combined multivariate and univariate analyses. Multivariate analyses were performed by Dr. Robert Hills (Haematology Clinical Trials Unit, Cardiff University). Univariate analyses (Kaplan-Meier curves and survival statistics) were performed using GraphPad Prism.

Overall, results from the multivariate analysis further outline the complexity of the T-cell compartment in CLL and the impact it can have on prognosis. CD4:CD8 ratio was shown to be a contributing factor in prognosis confirming earlier work with a different patient cohort. However, ratio was shown to have a contributing effect alongside many other variables (Table 4, Appendix IV). The higher resolution analysis in this study revealed additional phenotypes that had a much stronger, significant effect on PFS.

3.8. Absolute counts

This study revealed several changes in phenotype frequency between healthy donors, the total CLL patient cohort and stratified CLL^{NR} and CLL^{IR} subgroups. However, this does not determine if the shift in frequency is due to an expansion of the T-cell subpopulation presenting the phenotype of interest or a reduction in the numbers of other T-cell sub-populations. To address these two possibilities, absolute counts were performed on 19 CLL patients, 8 of which had an inverted CD4:CD8 ratio.

Absolute numbers of $CD8^+$ T-cells were significantly higher in CLL^{IR} versus CLL^{NR} patients, implying that the inversion was caused by an expansion within the $CD8^+$ T-cell population ($p = 0.0073$; Figure 3.30A). In addition, the absolute counts of the $CD8^+$ EM and EMRA memory subsets were significantly higher in CLL^{IR} patients ($p = 0.0015$ and $p = 0.0093$, respectively), whereas there was no change in the number of $CD8^+$ naïve subset (Figure 3.30B-D). This would suggest that the skewing in $CD8^+$ T-cell memory distribution observed in Section 3.1 (Figure 3.3) is due to an increase within the more differentiated memory subsets rather than a reduction in the naïve population. Together, these results suggest that the CD4:CD8 inversion is due to a preferential expansion of $CD8^+$ EM/EMRA T-cells, which is in line with previously published work (Nunes et al. 2012).

This study also observed an absolute increase in $CD8^+$ T-cells expressing CD57 ($p = 0.0093$), HLA-DR ($p = 0.0118$) or PD-1 ($p = 0.0118$) in the CLL^{IR} subgroup (Figure 3.31A). Therefore, the increase in frequency for these markers observed in CLL^{IR} patients described in Sections 3.3.1 and 3.4.1 was due to an expansion of the cells expressing each marker (Figures 3.6, 3.7 and 3.16, respectively). The absolute count analyses were then applied to phenotypes combining multiple markers that had been shown to have the greatest prognostic potential by multivariate analyses (Section

3.7.2.). The $CD8^+$ T-cell phenotypes that showed a significant effect on PFS were $CD8^+CD57^+HLA\text{-}DR^+$ and $CD8^+$ EMRA cells presenting $CD57^+HLA\text{-}DR^+PD\text{-}1^+$. Earlier phenotypic analyses showed that the overall frequency of $CD8^+CD57^+HLA\text{-}DR^+$ was significantly greater in CLL^{IR} patients than CLL^{NR} patients. This was also reflected in the absolute number of $CD8^+CD57^+HLA\text{-}DR^+$ cells, which were significantly higher in CLL^{IR} patients versus CLL^{NR} ($p = 0.0149$; Figure 3.31B), demonstrating that the higher frequency of this phenotype within the $CD8^+$ T-cell compartment was due to an expansion of said phenotype. The absolute count analysis also demonstrated an expansion of $CD57^+HLA\text{-}DR^+PD\text{-}1^+$ in the $CD8^+$ EMRA T-cell CLL^{IR} population (Figure 3.31C). Interestingly, this pattern was not reflected in the prior phenotypic analysis based on frequency. This apparent discrepancy could be explained by the fact that although the $CD57^+HLA\text{-}DR^+PD\text{-}1^+$ population is expanding within CLL^{IR} patients, other $CD8^+$ phenotypes in the inverted ratio patients may also have expanded in a similar fashion. Therefore, changes in the absolute number of these other phenotypes could lead to the lack of difference observed in the frequency of the triple positive phenotype between the patient subgroups.

To summarise, the absolute counts support previous work that the CD4:CD8 inverted ratio was due to an expansion within the $CD8^+$ T-cell compartment, specifically within the EM/EMRA memory subsets. Importantly, this analysis also demonstrated expansion of prognostically relevant T-cell phenotypes defined in the current study, such as $CD8^+CD57^+HLA\text{-}DR^+$ and $CD8^+CD57^+HLA\text{-}DR^+PD\text{-}1^+$. It is not clear what is driving the expansion of these particular subsets.

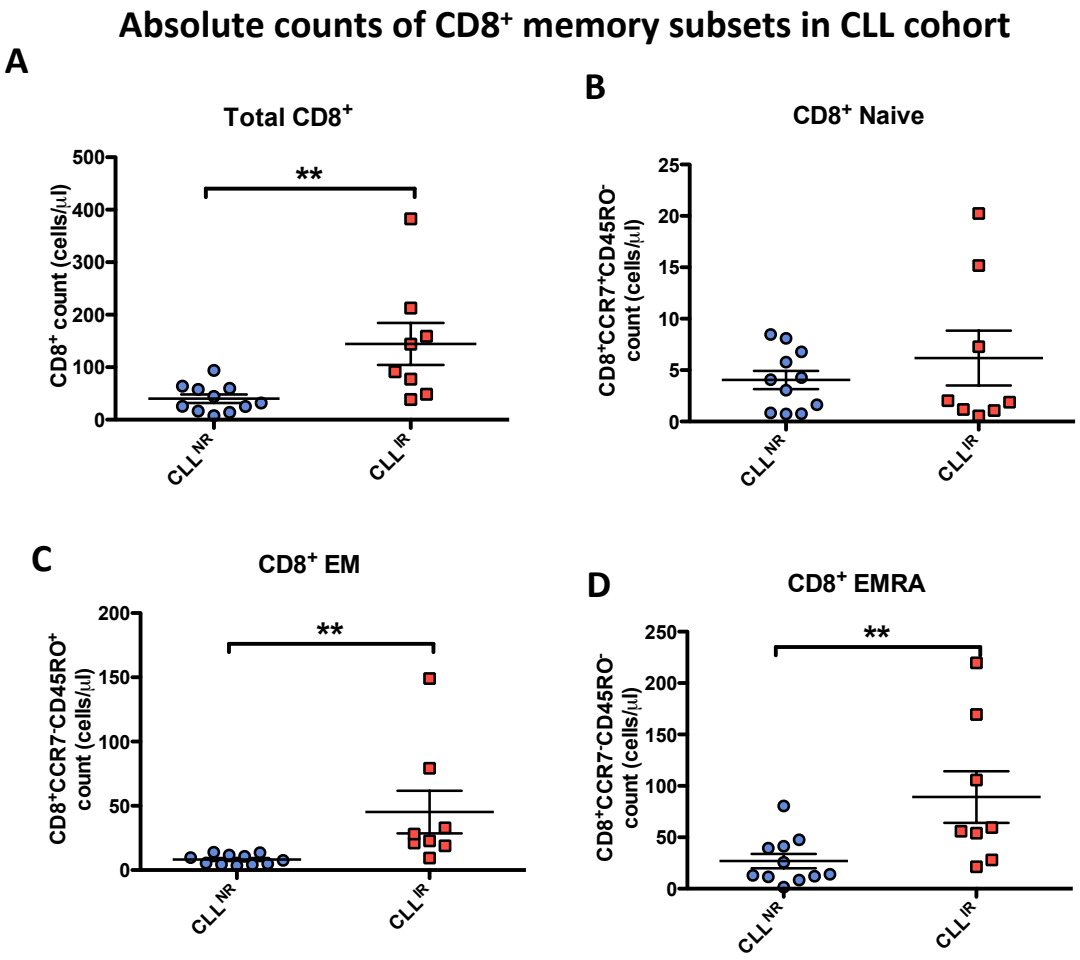

Figure 3.30. Absolute counts of CD8$^+$ T-cells in CLL^{NR} (n = 11) and CLL^{IR} (n = 8) patients. Cells and BD Trucount beads were collected using flow cytometry (FACS CantoII, BD FACSDiva) and analysed with FlowJo (v.9) using gating as described in Figure 3.1. Patients were stratified based on CD4:CD8 ratio: a ratio <1.0 was considered inverted (CLL^{IR}). Patients with a ratio ≥1.0 were considered normal ratio patients (CLL^{NR}). Memory subsets were defined using CCR7 and CD45RO memory markers: naïve (CCR7$^+$CD45RO$^-$), central memory (CM, CCR7$^+$CD45RO$^+$), effector memory (EM, CCR7$^-$CD45RO$^+$) and EMRA (CCR7$^-$CD45RO$^-$). Absolute counts for (A) overall CD8$^+$, (B) CD8$^+$ naïve, (C) CD8$^+$ EM and (D) CD8$^+$ EMRA between CLL^{NR} and CLL^{IR} patients are shown. Pairwise statistical analysis (CLL^{NR} vs CLL^{IR}) was performed using the non-parametric Mann-Whitney test. Significant results were included on the graph (* = p ≤0.05; ** = p ≤0.01; *** = p ≤0.001).

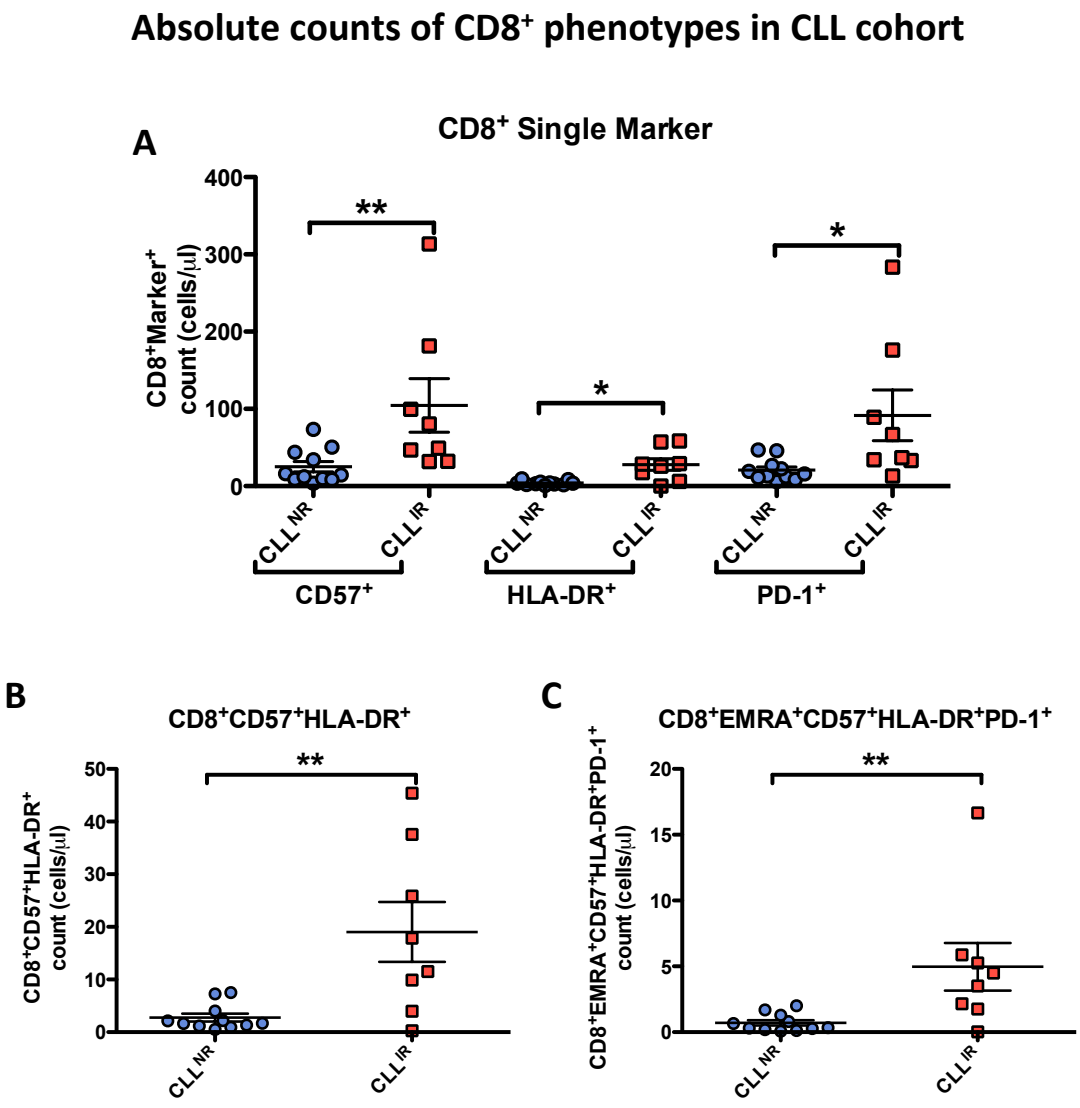

Figure 3.31. Absolute counts of CD8$^+$ T-cell phenotypes in CLL^{NR} (n = 11) and CLL^{IR} (n = 8) patients. Cells and BD Trucount beads were collected using flow cytometry (FACS CantoII, BD FACSDiva) and analysed with FlowJo (v.9) using gating as described in Figure 3.1. Patients were stratified based on CD4:CD8 ratio: a ratio <1.0 was considered inverted (CLL^{IR}). Patients with a ratio ≥1.0 were considered normal ratio patients (CLL^{NR}). Memory subsets were defined using CCR7 and CD45RO memory markers: naïve (CCR7$^+$CD45RO$^-$), central memory (CM, CCR7$^+$CD45RO$^+$), effector memory (EM, CCR7$^-$CD45RO$^+$) and EMRA (CCR7$^-$CD45RO$^-$). Absolute counts for: (A) CD57$^+$, HLA-DR$^+$ or PD-1$^+$ cells in the CD8$^+$ compartment; (B) CD8$^+$CD57$^+$HLA-DR$^+$ T-cells, and (C) CD57$^+$HLA-DR$^+$PD-1$^+$ cells in the CD8$^+$ EMRA subset. Pairwise statistical analysis (CLL^{NR} vs CLL^{IR}) was performed using the non-parametric Mann-Whitney test. Significant results were included on the graph (* = p ≤0.05; ** = p ≤0.01; *** = p ≤0.001).

3.9. Discussion

The aim of this study was to further explore the phenotypic composition of the $CD8^+$ T-cell compartment of CLL patients. More specifically, it set out to investigate potential phenotypic differences between CLL patients with an inverted CD4:CD8 ratio (CLL^{IR}) and CLL patients presenting with a 'normal' T-cell ratio (CLL^{NR}). Associations between T-cell ratio, disease pathology and prognosis have been reported previously, in both HIV infection and CLL (Buggert et al. 2014; Gonzalez-Rodriguez et al. 2010). CLL^{IR} has been linked to poorer prognosis and shorter time to first treatment, compared with their 'normal' ratio counterparts. Therefore, further analysis within the CLL^{IR} subgroup may reveal more powerful prognostic markers. Previous work had shown that CD4:CD8 T-cell ratio inversion in CLL patients was due to a significant expansion within the $CD8^+$ T-cells (Nunes et al. 2012), therefore the $CD8^+$ T-cell compartment was the focus of this study.

For this study, the CD4:CD8 stratification point was based on the previous work within our group (Nunes et al. 2012) that demonstrated a ratio of 1.0 was the optimum prognostic cut-off point. Later multivariate and univariate analyses during this study also supported that a cut-off point of around 1.0 was prognostically relevant: splitting the cohort based on the patients with a ratio closest to 1.0 (0.99 and 1.01) yielded the strongest prognostic difference in CLL patients. Interestingly, stratifying patients above and below a CD4:CD8 ratio of 0.52 revealed that a more extreme inversion of the CD4:CD8 ratio that identified patients with an even worse prognosis. This result should be taken with caution as there were wide confidence intervals, probably due to the low patient numbers within the subgroup with a ratio of 0.52 and below (n = 7). However, it does lend support to the relevance of the CD4:CD8 ratio in identifying CLL patients with poorer prognosis and imply that the skewing in the CD4:CD8 ratio has functional consequences on the T-cell pool that adversely impact upon disease pathology. Certainly further studies in a larger cohort appear to be warranted.

Primary analysis of the T-cell memory subset distributions showed significant differences between healthy donors and both the total and stratified CLL cohorts. A reduction in naïve and increase in the EM T-cell frequency was observed in both the $CD8^+$ and $CD4^+$ T-cell compartments of CLL; this shift was more dramatic within the CLL^{IR} cohort. Adding to this, absolute counts of $CD8^+$ T-cells in CLL^{IR} patients, revealed an increase in the numbers of more differentiated $CD8^+$ EM/EMRA cells but no

significant change in the numbers of naïve cells. This study, therefore supports previous evidence of a move to more differentiated $CD8^+$ memory phenotypes in CLL^{IR} patients (Nunes et al. 2012), and also expands on this to show that the skewing is due to an increase in the number of $CD8^+$ EM and $CD8^+$ EMRA T-cells.

Similar shifts towards a more differentiated memory phenotype have been associated with chronic antigenic stimulation, particularly persistent viral infections (Champagne et al. 2001; Wherry and Ahmed 2004). This response has also been observed in tumour immunology (Klebanoff et al. 2006). The move toward a more differentiated memory phenotype in this study supports the presence of persistent antigenic stimulation. EMRA T-cells are thought to be 'terminally' differentiated whereas EM T-cells are thought to be more responsive to antigenic/cytokine stimulation (Geginat 2003). As this study primarily observed larger increases in the EM subset in the CLL^{IR} cohort, it is possible that the expansion of CD8 T-cells in CLL may reflect the accumulation of T-cells responding to antigenic stimulation.

The shift to more differentiated memory subsets was further analysed by observing changes in markers previously associated with highly differentiated and senescent cells. CD57 is a marker associated with T-cell senescence, and its expression is elevated on more differentiated, functionally incompetent memory cells (Focosi et al. 2010; Strioga et al. 2011). This study saw a marked increase in $CD8^+CD57^+$ T-cells in the CLL cohort compared to healthy donors. When stratified by ratio, higher CD57 was more associated with the CLL^{IR} group $CD8^+$ T-cells: the absolute counts infer this increased frequency is due to an absolute increase in the number of $CD8^+CD57^+$ T-cells themselves. This ratio-associated increase in $CD57^+$ frequency was seen in the $CD8^+$ EM population but not the $CD8^+$ EMRAs.

High frequencies of $CD57^+$ T-cells have been observed in CLL patients in previous studies, originating within the $CD8^+$ EM and EMRA subsets (Nunes et al. 2012). The current study aimed to provide a more detailed, clinically relevant phenotype for these T-cells. One novel finding was the demonstration of an increase in $CD8^+CD57^+$ EM cells and not EMRA cells within the CLL^{IR} subgroup. Based on the previous studies an increase in $CD8^+CD57^+$ EMRA cells would be predicted, particularly as this subset is considered the more 'terminally differentiated'. However, in this study, there was an

expansion of $CD8^+CD57^+$ EM cells in CLL^{IR} patients, suggesting that this subset is associated with the development of the inverted ratio.

Although the overall skewing observed in this study supports the previous work within our group (Nunes et al. 2012), there were some differences between the two studies. The previous report observed significantly higher $CD8^+$ EMRA frequency within the CLL^{IR} subgroup; this study did see a trend towards increasing frequency of $CD8^+$ EMRAs between the CLL cohort and the healthy donors, and a stepwise trend from healthy donors to CLL^{NR} to CLL^{IR}, but the differences did not reach significance. Nunes et al. (2012) also demonstrated an increase in $CD8^+PD\text{-}1^+$ within the CLL^{IR} cohort. Here an increase in $CD8^+PD\text{-}1^+$ T-cells was observed in the CLL cohort as a whole when compared to healthy donors, but no difference was seen between the CLL^{NR} and CLL^{IR} patients. Similar PD-1 results to this study were also observed in a parallel study carried out in our laboratory (Reiss Reid, PhD Thesis 2015). These differences may be due to inherent variation between the patients included in each study that led to differences in the clinical characteristics of the study group, such as age, gender and *IGHV* status. For example, the mean age of each cohort differed greatly between studies; the mean age of patients enrolled into this study was 63.3 years, whereas the previous study had a mean age of 73.5 years. As age is known to be related to T-cell memory and phenotype shifts (Koch et al. 2008), it is conceivable that some differences would be observed between the cohorts.

Contrary to the phenotyping results, preliminary absolute counts demonstrated higher numbers of $PD\text{-}1^+$ cells within the $CD8^+$ T-cell compartment of the CLL^{IR} patients. This may not be reflected in an increased frequency due to parallel increases in $PD\text{-}1^-$ cells within the expanded $CD8^+$ compartment of the CLL^{IR} subgroup. Taken together with the phenotyping frequencies, these results support PD-1 as a marker that distinguishes CLL patients from healthy donors, but not as a marker involved in the $CD8^+$ T-cell expansion observed within the CLL^{IR} subgroup. This is further corroborated when analysing the co-expression of CD57 and PD-1. The frequency of $CD8^+CD57^+PD\text{-}1^+$ T-cells was higher in the CLL cohort than the healthy donors, but no difference was seen between ratio subgroups within CLL patients (CLL^{IR} vs CLL^{NR}).

KLRG-1 was also included in this study to ascertain the senescence status of the $CD8^+$ compartment. KLRG-1 has been shown to be expressed by more differentiated $CD8^+$

T-cells that possess poor proliferative capacity (Göthert et al. 2013; Ibegbu et al. 2005). A study of German CLL patients reported higher levels of KLRG-1 in the $CD8^+$ compartment that was replicated in the naïve and EM memory subsets (Göthert et al. 2013). The $CD8^+KLRG\text{-}1^+$ frequency of the total CLL cohort analysed in this study did not significantly differ from healthy donors, but elevated $KLRG\text{-}1^+$ T-cell frequencies were observed in the EM subset. When stratified into the ratio subgroups, the CLL^{IR} patients demonstrated an elevated $CD8^+KLRG\text{-}1^+$ T-cell frequency compared to CLL^{NR} and HD patients. EM $CD8^+KLRG\text{-}1^+$ was higher in CLL^{IR} patients versus healthy donors, but not CLL^{NR} patients. $CD57^+KLRG\text{-}1^+$ frequency was also elevated in the CLL cohort's $CD8^+$ compartment and EM subset in the CLL cohort as a whole. As with single KLRG-1 presentation, this was exacerbated in the CLL^{IR} total $CD8^+$ T-cells, but the CLL^{IR} EM population did not differ from the CLL^{NR} patients. Therefore, although KLRG-1 appears to be more prevalent within the CLL^{IR} subgroup, it is not a phenotype rising from the EM subset.

CD127 expression as part of a senescent profile was also investigated. CD127, or IL-7Rα, is a component of a T-cell surface ligand for the cytokine interleukin-7 (IL-7), and is usually found in higher levels on naïve T-cells and central memory (CM) T-cells (A. Ma et al. 2006). Lower CD127 expression on T-cells has been associated with a more differentiated state and reduced capacity to respond and divide (Golden-Mason et al. 2006; Bengsch et al. 2010). The frequency of $CD8^+CD127^+$ T-cells was markedly reduced in the CLL^{IR} cohort compared to both the CLL^{NR} and healthy donors. This appeared to be connected to the lower proportion of naïve T-cells – as naïve cells have high $CD127^+$, lower naïve frequency within the $CD8^+$ T-cell compartment would logically mean a decline in the frequency of $CD127^+$ cells. This is supported by a retrospective correlation analysis of the phenotyping data that demonstrates significant correlation between $CD8^+$ naïve and $CD8^+CD127^+$ frequencies ($r = 0.5360$, $p < 0.0001$; Appendix V).

Reduced CD127 frequency was also observed within the EM and EMRA subset of the $CD8^+$ compartment of CLL^{IR} patients. CD127 is usually used in tandem with KLRG-1 to help further differentiate between different subsets of antigen-experienced cells: $CD127^+KLRG\text{-}1^-$ memory T-cells are found following resolution of acute viral infections, whereas $CD127^-KLRG\text{-}1^+$ memory cells are present in chronic infection. This study observed reduced frequency of the $CD127^+KLRG\text{-}1^-$ phenotype and higher

$CD127^{-}KLRG\text{-}1^{+}$ in the $CD8^{+}$ T-cells of CLL patients, which was exacerbated with the inverted ratio. This supports the increased presence of a senescent $CD127^{-}KLRG\text{-}1^{+}$ phenotype associated with chronic antigenic stimulation. Inverse expression of CD127 with CD57 has been described in a similar capacity (Ibegbu et al. 2005; Bengsch et al. 2007); in this study cohort $CD127^{-}CD57^{+}$ and $CD127^{+}CD57^{-}$ frequencies followed the same patterns as CD127 with KLRG-1 (Appendix II), adding further weight to the presence of a chronically stimulated, senescent $CD8^{+}$ population in CLL that is exaggerated in CLL^{IR} patients. An increase in the $CD57^{+}KLRG\text{-}1^{+}CD127^{-}$ phenotype also supports this shift.

It is clear from this study that there is an increasing shift to a more differentiated phenotype presenting markers for exhaustion and senescence in the CLL cohort compared to healthy donors. This is exaggerated further in the CLL^{IR} subgroup. For the most part the increase is driven from both the EM and EMRA subsets. However, in some cases significant increases in phenotypes were only observed in the whole $CD8^{+}$ compartment with non-significant increases in the EM or EMRA subset, suggesting that neither the EM nor EMRA subsets were individually responsible for the phenotypic changes. Another observation is that when stratifying by ratio, the CLL^{IR} subgroup data appears to be more heterogeneous than the CLL^{NR} data: the CLL^{IR} subgroup includes some patients who possess phenotypic frequencies similar to those in the CLL^{NR} group, but other CLL^{IR} patients display much higher frequencies. Perhaps this represents varying stages of T-cell senescence among inverted patients, and further stratification of CLL^{IR} 'high-expressing' patients in a larger cohort may reveal more specific patient subgroups with potential clinical relevance.

This study included HLA-DR and CD38 as markers for T-cell activation to more precisely define the T-cell subsets driving the $CD8^{+}$ T-cell expansion in CLL. Overall, the CLL cohort had significantly higher frequencies of $CD8^{+}HLA\text{-}DR^{+}$ T-cells compared to healthy donors. This difference was exaggerated in the CLL^{IR} subgroup: this was reflected predominantly in the EM subset, but also the EMRA subset. CD38 showed a similar pattern in the CLL^{IR} $CD8^{+}$ compartment: a higher frequency was seen both in the whole $CD8^{+}$ fraction, and the $CD8^{+}$ EM subset. Although an increase in T-cells with markers associated with senescence/exhaustion has previously been observed in CLL patients (Nunes et al. 2012; Göthert et al. 2013), this increase in activation markers suggest that a significant proportion of expanded T-cells in CLL are activated rather

than senescent/exhausted. Furthermore, the increase in absolute number of $CD8^+$ T-cells with HLA-DR imply that the higher frequency of activated cells is due to higher number of these cells in CLL^{IR} patients than the CLL^{NR} patients.

Although CD57 expression is associated with a senescent T-cell phenotype, some evidence shows that under certain conditions $CD57^+$ T-cells are able to respond to stimuli, extensively proliferate and produce cytokines (Chong et al. 2008). Therefore $CD57^+$ T-cells may not be truly senescent, but instead represent highly differentiated cells that require certain conditions to respond. This study looked at the presentation of senescent markers CD57 and KLRG-1 with activation markers HLA-DR and CD38. The phenotypes $CD57^+HLA\text{-}DR^+$, $CD57^+CD38^+$ and $KLRG\text{-}1^+CD38^+$ were markedly higher in the $CD8^+$ T-cell compartment of CLL^{IR} patients. This pattern of expression was reflected in both the EM and EMRA subsets. This demonstrates that there is a subgroup of $CD8^+$ T-cells that, although are highly differentiated, are also activated and potentially responsive to stimulus. Furthermore, as demonstrated in the increased number of $CD8^+CD57^+HLA\text{-}DR^+$ T-cells in CLL^{IR} patients (Figure 3.41B), these cells are more prevalent in this patient subgroup. This could be due to an accumulation of these cells under chronic stimulation. Due to the constraints of the Panels, the relationship between KLRG-1 and HLA-DR could not be explored. However, the results obtained suggest activation and proliferation of highly differentiated $CD8^+$ T-cells in CLL^{IR} patients. It is not clear what antigenic stimulus (if any) is driving the expansion of these T-cells.

PD-1 is usually referred to as a marker for exhaustion, but is upregulated during activation: previous studies have demonstrated higher expression of PD-1 during T-cell activation than on resting cells, and co-expression with activation markers HLA-DR and CD38 – the same markers used in this study (Sauce et al. 2007). $CD8^+PD\text{-}1^+HLA\text{-}DR^+$ T-cells were higher in CLL patients, but frequency of this phenotype was not associated with inverted CD4:CD8 ratio. This adds further evidence that PD-1 is not a CLL^{IR} related marker, and activated $PD\text{-}1^+$ $CD8^+$ T-cells are not the dominant population among the expanded T-cells in the CLL^{IR} patients.

Multivariate analyses were included in this study to identify which $CD8^+$ T-cell phenotypes were considered the most important in terms of prognosis. CD4:CD8 ratio did not appear to have a strong effect on prognosis, although it did have a contributing

effect alongside some other T-cell phenotypes (Table 4, Appendix IV). Furthermore, $CD8^+$ frequency had a significant association with prognosis, implying that the $CD8^+$ expansion did have prognostic weight. The two $CD8^+$ phenotypes that did appear to have an independent effect on the prognosis of CLL patients were $CD57^+HLA\text{-}DR^+$ and EMRA $CD57^+HLA\text{-}DR^+PD\text{-}1^+$. Recursive partitioning helped to subdivide the whole CLL cohort by the most prognostically relevant frequencies of these phenotypes: overall, patients with higher frequencies of $CD8^+$ T-cells with these markers had poorer prognosis. It is worth noting that there were potential cut-offs at even higher frequencies: these subgroups of 'high-expressing' patients had a much poorer prognosis. This further supports that the higher the frequency of these phenotypes, the poorer prognosis the patient may have, although low patient numbers and wide confidence intervals mean that these results should be taken with caution.

Both of these phenotypes are characteristic of highly differentiated, but activated, T-cells. It is possible that the accumulation of these T-cells are potentially either contributing to, or are a result of, the CLL pathology. Furthermore this may be driven by antigenic stimulation from the CLL cells themselves. Both of these phenotypes were shown to be higher in absolute numbers within the CLL^{IR} subgroup, which further supports the expansion and accumulation of these phenotypes from stimuli driven proliferation. The multivariate analyses demonstrated there are some $CD8^+$ phenotypes identified from this study that have improved prognostic value over T-cell ratio; it may be that ratio is prognostically valuable due to the phenotypes that are driving the inversion.

In the majority of cases, CLL diagnosis is in elderly patients. The CLL cohort used in this study had an average age of 63.3 years at diagnosis. The elderly have been shown to have a compromised immunophenotypic profile compared to their younger counterparts, including an age-associated decrease in the naïve $CD8^+$ T-cell frequency and increase in $CD8^+$ EMRA T-cell frequency (Koch et al. 2008). This study used age-matched healthy donors to ensure that differences in T-cell phenotypes observed between CLL patients and healthy donors were not age-related. The memory T-cell phenotype skewing observed in this study was more predominantly within the EM T-cell subset rather than the further differentiated EMRA subset, providing further evidence that the observed phenotypic changes were related to disease rather than age.

In addition to age, secondary diseases and infections are also known to affect the T-cell compartment. Cytomegalovirus (CMV) is a common herpes virus that the majority of people encounter during their lifetime; infection is usually asymptomatic in the immunocompetent. However, once infected, CMV persists in a latent form for the rest of an individual's lifetime. This can lead to skewing of the T-cell compartment due to the presence of chronically stimulated CMV-specific T-cells (Vasto et al. 2007).

Due to its prevalence and persistence, a majority of elderly patients are CMV-positive, and exhibit CMV driven phenotypic changes in their T-cells (Vasto et al. 2007; Pita-Lopez et al. 2009). Accumulation of highly differentiated but responsive CMV-specific T-cells in CLL has been shown previously (Raa et al. 2014). The current study observed no association between CMV and the CD4:CD8 T-cell ratio of CLL patients. Furthermore, stratifying patients based on CMV seropositivity showed a skewing towards a $CD8^+$ EMRA phenotype. This is in line with the CMV driven phenotypic skewing recorded in previous work. This is different from the memory phenotype effect observed in the CLL^{IR} patients of this study, which is more biased towards the EM memory subset. Therefore, findings observed here within the CLL^{IR} cohort are independent of a CMV driven T-cell response. This confirms the previous study from our laboratory that demonstrated that the inverted CD4:CD8 ratio in CLL is independent of CMV (Nunes et al. 2012).

The number of available CMV^- patients restricted the analysis of CMV further in this study: a total 4 CLL^{IR} patients were CMV^- and only 1 of those patients was subjected to the complete phenotypic analysis (3 were analysed for memory subsets only). This prevented a more in depth exploration of CMV seropositivity and potential correlations with marker expression. As previously mentioned, the majority of elderly patients have encountered CMV, so this will limit any study of CMV^- individuals in a CLL cohort. However, the high prevalence of CMV^+ patients in both CLL^{NR} and CLL^{IR} subgroups would in itself suggest that results observed in CLL^{IR} patients is not CMV driven. Regardless, future studies with larger numbers of CLL patients are required in order to obtain sufficient numbers of CMV^- patients and eliminate CMV as a confounding factor when comparing the CLL subgroups.

This study clearly demonstrates that application of multiple markers in tandem is more beneficial than looking at a single marker independently. The phenotypic complexity of

T-cells within CLL was missed in earlier studies, and this has an impact on interpretation of the role of T-cells in disease, e.g. that $CD8^+PD\text{-}1^+$ T-cells may not necessarily be "exhausted" in CLL as they often co-express activation markers, such as HLA-DR. One limitation of this study, however, was in the segregation of markers on two different phenotypic panels. This was a constraint of the FACS Canto II machine because only 8 parameters could be measured in a single sample. This prevented some comparisons between markers that could have been relevant, such as PD-1 with CD38, as they were not on the same panel. Future work could include compiling markers onto one larger phenotyping panel, using a flow cytometer that can analyse more parameters, such as the FACS Aria (11-16 parameters). This could also include further markers that allow for a more precise definition of T-cell subsets, including additional memory defining markers to further accurately identify the EM and EMRA populations, as well as additional senescence/activation markers. Another potential direction would be to rationalise the markers into a more streamlined, relevant flow cytometry panel including the markers deemed more prognostically relevant. This is further explored in Chapter 6, where a panel was developed based on the results of this chapter to analyse treated patients.

Although $CD8^+$ T-cells were the primary focus of the study, $CD4^+$ T-cell data was also collected and analysed in the multivariate analyses. $CD4^+PD\text{-}1^+HLA\text{-}DR^+$ was revealed to be the phenotype that had the strongest independent effect on PFS in this study, stronger than any $CD8^+$ phenotype. Therefore, phenotypic evaluation of the $CD4^+$ T-cells would be important in furthering our understanding of T-cells in CLL patients, and this is the focus of the next chapter.

To conclude, this study has observed a skewing towards a more differentiated memory phenotype in CLL patients with an inverted CD4:CD8 ratio. As may be expected with an increase in differentiated memory, the CLL^{IR} patients also possessed a larger percentage of $CD8^+$ T-cells that displayed phenotypes associated with senescence. However, elevated levels of activation phenotypes are also observed, including co-expression with the senescence markers, implying that a small proportion of the differentiated cells have a mixed phenotype. Preliminary absolute counts suggest that these elevated levels of these phenotypes are due to an increase in absolute number. Therefore, there appears to be an increase in senescent, but activated T-cell phenotypes that could be an accumulation of chronically stimulated $CD8^+$ T-cells, perhaps driven by the CLL tumour

antigens. That these phenotypes are exacerbated in CLL^{IR} patients, who have been proven to have poorer prognosis than their normal ratio counterparts, implies that accumulation of these cells could be linked to the CLL disease and prognosis, either as a factor driving the poorer prognosis and exacerbated disease, or as a resulting effect of other factors that are driving the prognostic disease. There are some phenotypes in this study that have been shown to have greater prognostic power than ratio; as these phenotypes are shown in greater frequency in the CLL^{IR} subgroup, it could be that the ratio and phenotypes are linked, but it is the phenotype that is more relevant in CLL pathology.

In any case, the CD4:CD8 ratio does appear to be a prognostic factor that can identify patients who are more 'at risk', but this study has uncovered more relevant $CD8^+$ T-cell phenotypes with greater prognostic potential and therefore more clinical relevance. These new phenotypic markers now need to be validated in a prospective fashion in larger cohorts of CLL patients.

Chapter 4

Immunophenotyping of $CD4^+$ T-cells in CLL

The original aim of this thesis was to explore the $CD8^+$ T-cell compartment of CLL patients in order to further understand their potential role in disease. This was based on previous descriptions of a subgroup of patients with inferior prognosis who had a preferentially expanded $CD8^+$ T-cell compartment resulting in an inverted CD4:CD8 ratio (CLL^{IR}). Phenotypic exploration of these $CD8^+$ T-cells in Chapter 3 demonstrated great phenotypic complexity, with distinct differences between CLL^{NR} and CLL^{IR} patients.

When multivariate analyses were performed to elucidate whether distinct $CD8^+$ T-cell phenotypes were linked to poorer prognosis in the CLL cohort, the $CD4^+$ phenotype HLA-$DR^+PD\text{-}1^+$ was also shown to be prognostically relevant. In fact, this phenotype had a greater effect on progression-free survival (PFS) than the $CD8^+$ phenotypes identified in the analysis (Chapter 3, Table 3.4).

Like their $CD8^+$ counterparts, $CD4^+$ T-cell abnormalities have also been reported previously in CLL (Görgün et al. 2005; Tinhofer et al. 2009; Monserrat et al. 2013). In addition to this, $CD4^+$ helper T-cells have been shown to activate and maintain CLL cells both *in vitro* and *in vivo* (Os et al. 2013). It was therefore apparent that phenotypic exploration of $CD4^+$ T-cells in CLL patients could reveal $CD4^+$ subpopulations with potential relevance to CLL disease. Although we previously showed that preferential expansion of $CD8^+$ T-cells was the major contributor to the CLL^{IR} phenotype, a detailed analysis of the $CD4^+$ subset could reveal phenotypes that are more prominent within the inverted ratio patients that could potentially exacerbate the disease.

Therefore, this Chapter set out to characterise the $CD4^+$ T-cells of CLL patients, with specific reference to the CLL^{NR} and CLL^{IR} subgroups. Focus was given to phenotypic markers that were identified in the previous chapter.

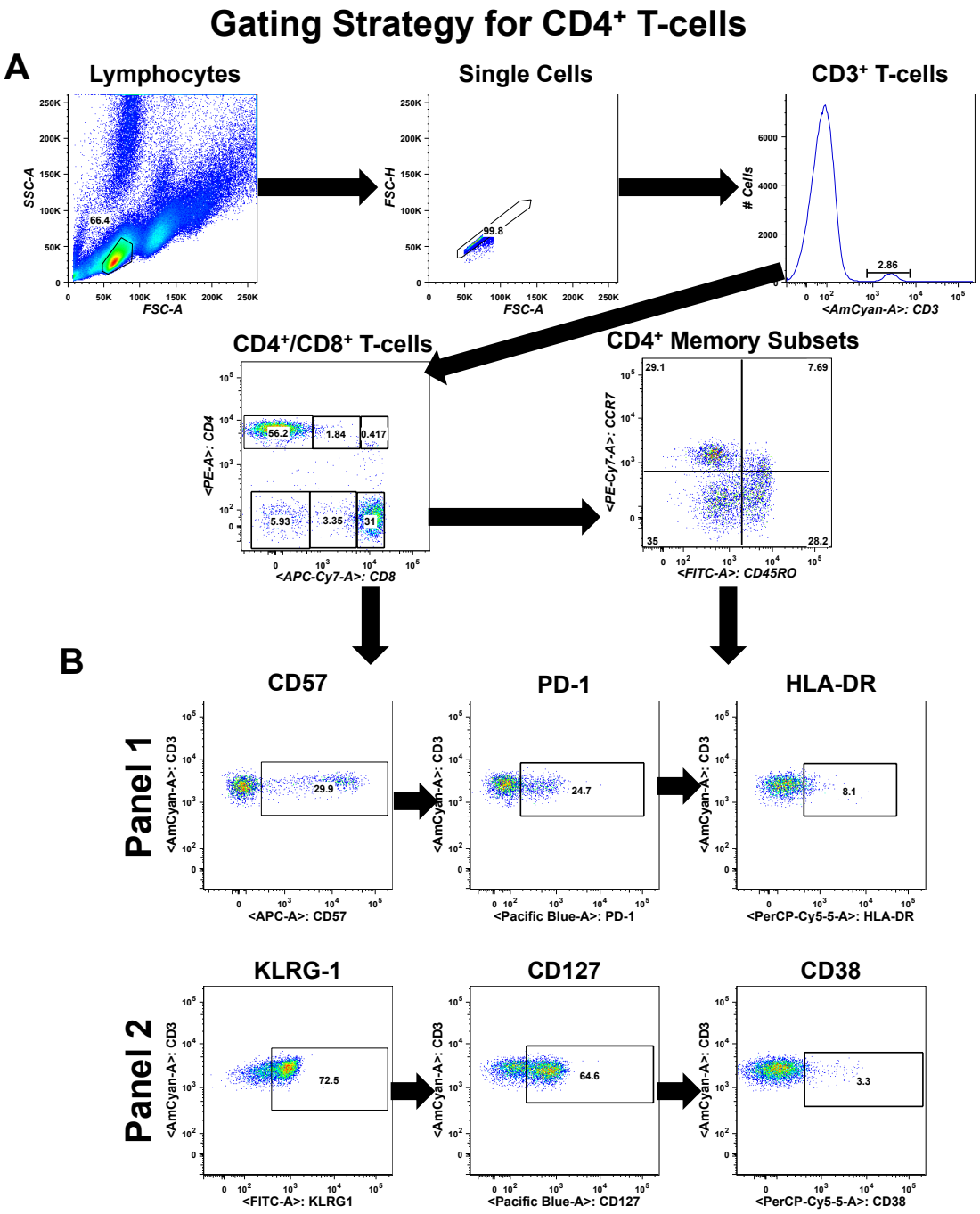

Figure 4.1. Representative gating strategy used for phenotypic analysis of CD4$^+$ T-cells. (A) Gating strategy for CD4$^+$ T-cells and their respective memory subsets. Cells were collected using flow cytometry (FACS CantoII, BD FACSDiva) and analysed using FlowJo (v.9). Lymphocytes were gated based on forward and side scatter profile; single cells were gated by forward scatter area and height. CD4$^+$ T-cells were identified by gating on CD3$^+$ and then CD8$^-$ or CD4$^+$ populations. Memory subsets were defined using CCR7 and CD45RO memory markers: naïve (CCR7$^+$CD45RO$^-$), central memory (CM, CCR7$^+$CD45RO$^+$), effector memory (EM, CCR7$^-$CD45RO$^+$) and EMRA (CCR7$^-$CD45RO$^-$). (B) Gating strategy for activation and senescence/exhaustion markers within the CD4$^+$ T-cell compartments and memory subsets. Gating of positive populations was confirmed with fluorescence-minus-one (FMO) controls where necessary.

4.1. Gating for $CD4^+$ T-cells: use of $CD8^-$

The gating strategy applied to the $CD4^+$ analysis was similar to that applied to $CD8^+$ T-cells (Figure 4.1). During the initial phases of analysis, restrictions on the numbers of markers in the antibody panels meant that it was not possible to include an antibody for CD4. Instead, primary analysis was performed on an Accuri C6 4-colour flow cytometer, and initial 8-colour analyses on the BD FACS Canto II included an additional marker, BCL-2 (see Chapter 2 for further Panel information). Subsequently, a CD4 antibody was substituted into one of the two FACS Canto II panels to positively identify this subset of T-cells.

To assess whether gated $CD8^-$ T-cells from previous panels could be used in lieu of a defined $CD4^+$ population, SPICE analysis was performed to compare memory subset distribution between the $CD8^-$ (when a CD4 antibody was not included) and $CD4^+$ T-cell compartments (Figure 4.2, Table 4.1). No statistical difference was seen between the average memory subset distributions between these subsets for CLL patients as a whole ($p = 0.39$) or when subdivided in CLL^{NR} and CLL^{IR} subgroups ($p = 0.67$ and $p = 0.66$, respectively), suggesting that the $CD8^-$ gate in the earlier analyses was analogous to the $CD4^+$ T-cell population. Therefore, the $CD8^-$ data was amalgamated with the $CD4^+$ data and included in the phenotypic analysis.

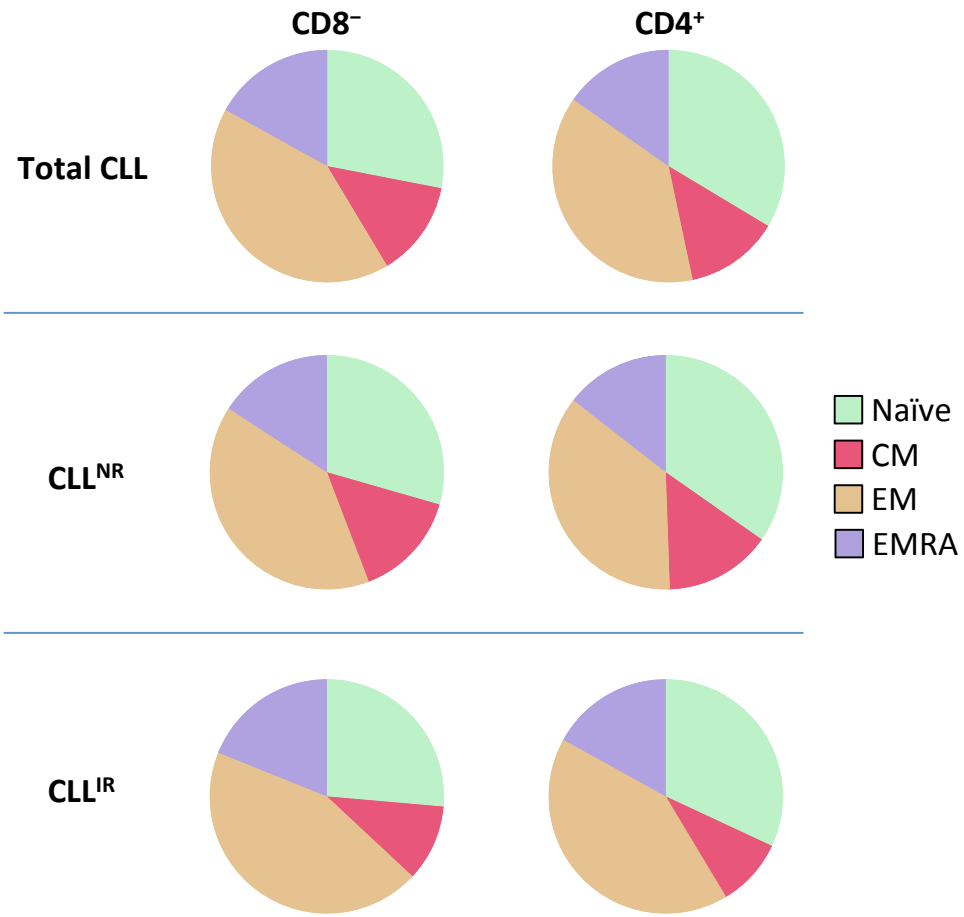

Figure 4.2. Subset comparison of CD4⁺ and CD8⁻ memory subsets in CLL. Cells were collected using flow cytometry (FACS CantoII, BD FACSDiva) and analysed with FlowJo (v.9) using gating as described in Figure 4.1. Pie charts and accompanying statistics comparing $CD8^-$ (n = 61) and $CD4^+$ (n = 95) memory subsets were generated using SPICE software (v5.3).

Table 4.1. Pie chart analysis of memory subsets in CLL patients ($CD8^-$ vs $CD4^+$)

Patient Group	$CD8^-$ vs $CD4^+$
Total CLL	0.3939
CLL^{NR}	0.6718
CLL^{IR}	0.6620

4.2. $CD4^+$ memory subsets in CLL

Skewing to a more differentiated memory T-cell phenotype has already been demonstrated within the $CD8^+$ compartment of CLL^{IR} patients in the previous chapter (Chapter 3). The same analysis was performed on the $CD4^+$ compartment to see if $CD4^+$ memory cells of CLL patients were also abnormal when compared to age-matched healthy donors.

As Figure 4.3 demonstrates, $CD4^+$ naïve T-cells were significantly reduced in the CLL cohort compared to healthy donors ($p = 0.0034$), as were the CM subset ($p = 0.0082$). Inversely, The $CD4^+$ EM compartment was larger in CLL patients compared to healthy donors, with an approximately 2-fold increase in frequency from 22.03% to 40.22% ($p = 0.0009$). Therefore, it would seem that like the $CD8^+$ compartment, $CD4^+$ T-cells also demonstrate a more differentiated memory EM phenotype in CLL patients when compared with healthy age-matched controls.

This was exacerbated when patients were stratified according to CD4:CD8 ratio (Figure 4.4): CLL^{IR} patients had a significantly reduced naïve compartment ($p \leq 0.001$ versus both CLL^{NR} and HD) and increased EM compartment ($p \leq 0.01$ versus CLL^{NR} and $p \leq 0.001$ versus HD). As was the case for $CD8^+$ T-cells, $CD4^+$ T-cells demonstrated a significant skewing to a more differentiated EM phenotype within the memory subsets in the CLL^{IR} subgroup. In contrast, the $CD4^+$ EMRA population showed no significant increase; a trend that was evident in the $CD8^+$ T-cell compartment (Chapter 3, Figure 3.2). However, the $CD4^+$ EMRA population represented a relatively low proportion of the $CD4^+$ compartment compared to the EMRA compartment of the $CD8^+$ (16.6% versus 52.5%, $p < 0.0001$). Furthermore, it is interesting to note that although $CD4^+$ T-cells showed a reduction in naïve T-cells, a greater proportion of the $CD4^+$ compartment is naïve when compared with $CD8^+$ T-cells.

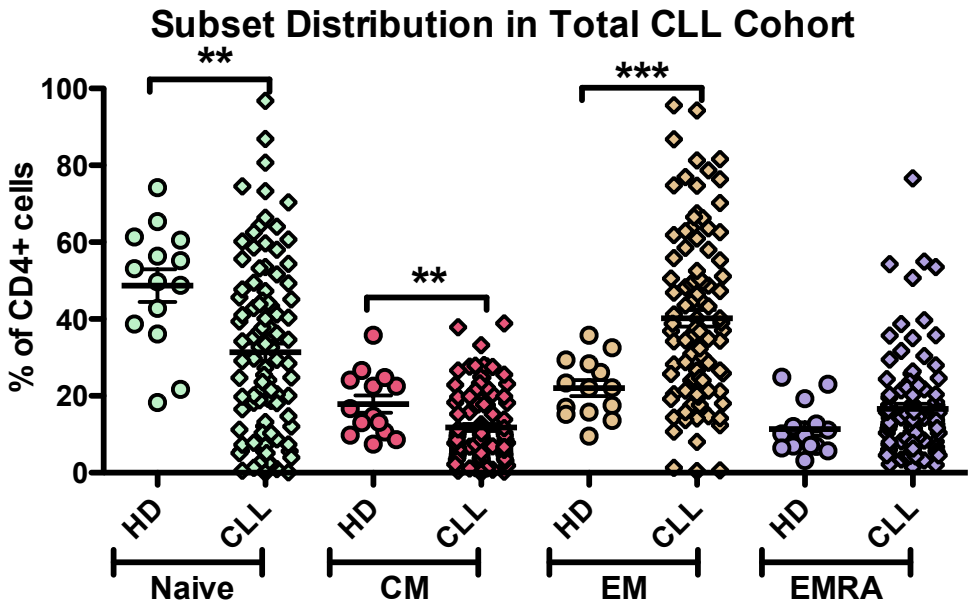

Figure 4.3. $CD4^+$ T-cell memory subsets in age-matched healthy donors (HD, n = 14) and CLL patients (n = 99). Cells were collected using flow cytometry (FACS CantoII, BD FACSDiva) and analysed with FlowJo (v.9) using gating as described in Figure 4.1. Lymphocytes were gated based on forward and side scatter profile; forward scatter area and height were used for exclusion of doublet cells. $CD4^+$ T-cells were identified by gating on $CD3^+$ and then $CD8^-$or $CD4^+$ populations. Memory subsets were defined using CCR7 and CD45RO memory markers: naïve ($CCR7^+CD45RO^-$), central memory (CM, $CCR7^+CD45RO^+$), effector memory (EM, $CCR7^-CD45RO^+$) and EMRA ($CCR7^-CD45RO^-$). Pairwise statistical analysis (HD vs CLL) was performed using the non-parametric Mann-Whitney test. Significant results were included on the graph (* = $p \leq 0.05$; ** = $p \leq 0.01$; *** = $p \leq 0.001$).

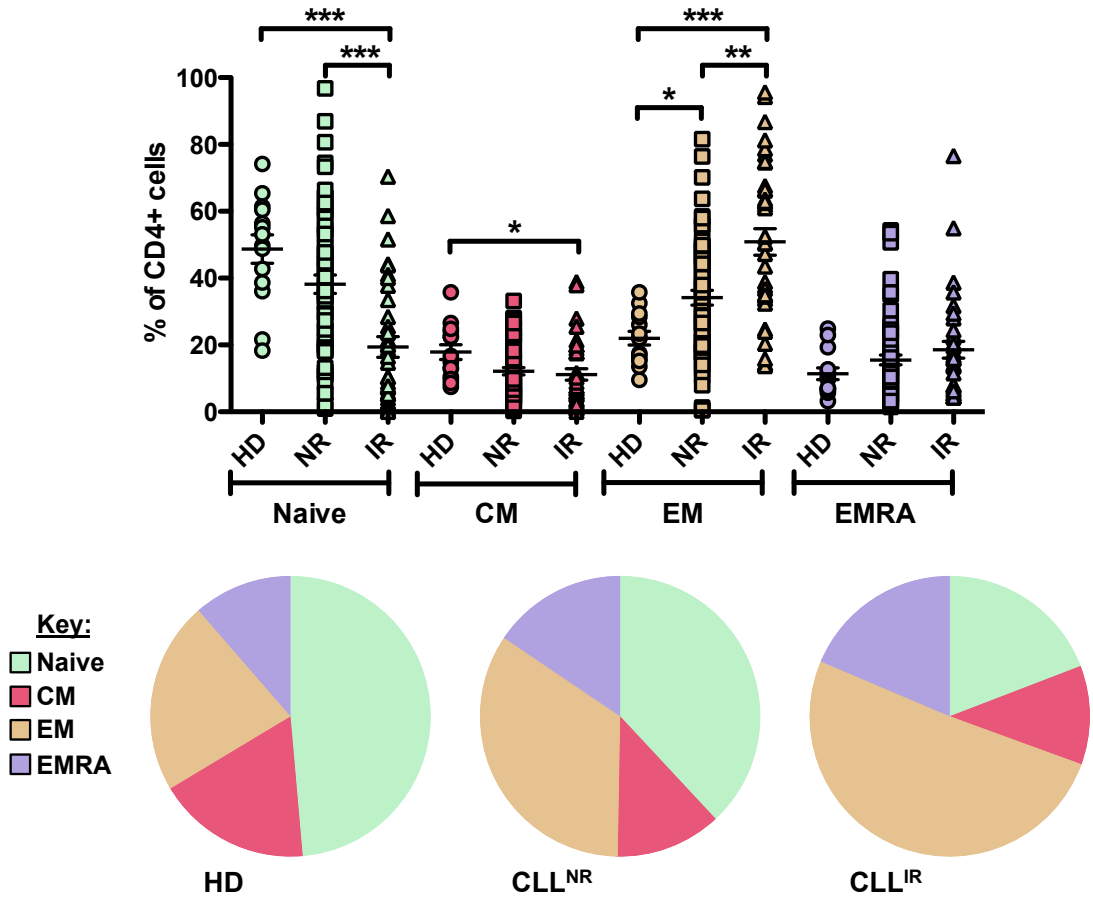

Figure 4.4. $CD4^+$ T-cell memory subsets in age-matched healthy donors (HD, n = 14) and CLL patients with a normal (CLL^{NR}, n = 63) and inverted (CLL^{IR}, n = 36) CD4:CD8 T-cell ratio. Cells were collected using flow cytometry (FACS CantoII, BD FACSDiva) and analysed with FlowJo (v.9) using gating as described in Figure 4.1. CLL patients with a CD4:CD8 ratio <1.0 were considered inverted. Three-way ANOVA statistical analysis was performed using Kruskal-Wallis test (HD vs CLL^{NR} vs CLL^{IR}), with all pairs of data assessed using the Dunn's post-test. Significant results were included on the graph (* = p ≤0.05; ** = p ≤0.01; *** = p ≤0.001).

4.3. Phenotypic overview

A graphical overview of the different phenotypes and statistical comparisons for the whole $CD4^+$ compartment was generated using SPICE version 5.3 (Figure 4.5, Table 4.2; see Appendix VI for complete statistics). As with the $CD8^+$ compartment, the $CD4^+$ subset manifested phenotypic complexity with many sub-populations of T-cells defined based on the expression of multiple markers. Statistical comparison of the pie charts showed significant phenotypic differences between the $CD4^+$ profile of CLL patients when compared with age-matched healthy donors in Panel 1, but not Panel 2 (Table 4.2). An increase in $CD4^+$ T-cells expressing one or more of the Panel 1 markers was clearly apparent, particularly the increase in PD-1^+ ($p < 0.0001$) and PD-1^+HLA-DR^+ ($p < 0.0001$) cells. Triple positive cells ($CD57^+$HLA-DR^+PD-1^+) also constituted a greater proportion of the $CD4^+$ compartment in CLL patients compared to age-matched healthy donors ($p < 0.0001$).

Overall phenotypic changes were also observed in the CLL^{IR} cohort compared to CLL^{NR} patients and healthy donors (Figure 4.6, Table 4.3). Panel 1 showed the most significant differences, particularly with the increase in $CD4^+$ T-cells co-expressing two or three markers at once. For example, CLL^{IR} had a higher proportion of PD-1^+HLA-DR^+ ($p < 0.0001$) and $CD57^+$HLA-DR^+ ($p = 0.0012$) expressing cells in the $CD4^+$ compartment compared to CLL^{NR}, as well as an increase in triple positive cells ($CD57^+$PD-1^+HLA-DR^+, $p < 0.0001$). In Panel 2, the CLL^{IR} $CD4^+$ compartment showed reduced $CD127^+CD38^+$ expressing cells ($p = 0.0085$), but an increase in $CD57^+$KLRG-1^+CD38^+ cells ($p = 0.0187$). Unlike Panel 1, there were no overall differences in panel 2 markers between the CLL^{NR} subgroup and age-matched healthy donors (Table 4.3).

This phenotypic overview shows the complexity of sub-populations within the $CD4^+$ T-cell compartment, and lends further support to the idea that both $CD4^+$ and $CD8^+$ T-cells experience preferential phenotypic changes within CLL and the CLL^{IR} patients.

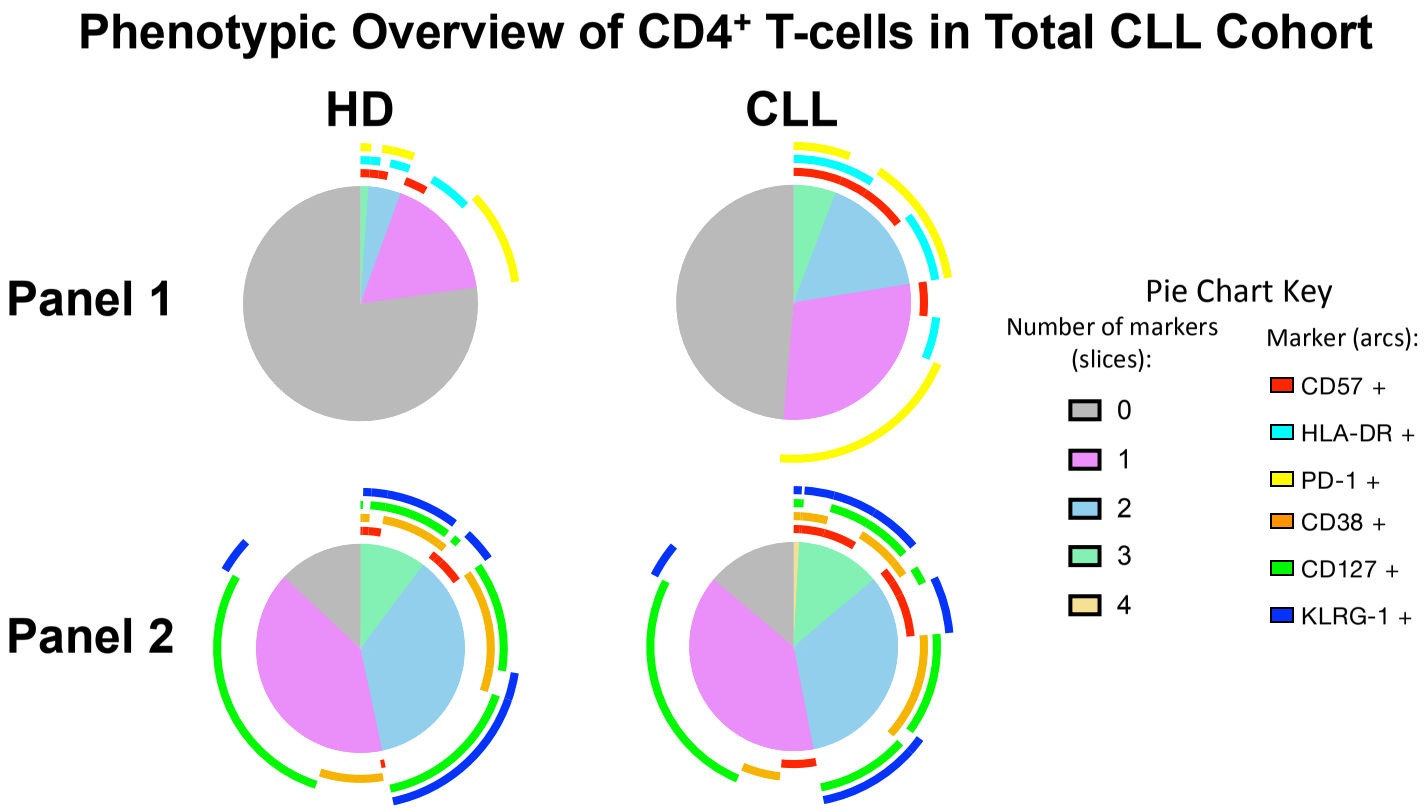

Figure 4.5. Phenotypic overview of total CD4⁺ T-cell compartment in CLL patients (n = 74) and age-matched healthy donors (n = 14). Cells were stained with various markers for senescence, exhaustion and activation, and analysed using multi-colour flow cytometry (BD FACS Canto II) using gating as described in Figure 4.1. Samples were analysed using FlowJo to created Boolean combination gating for Panel 1 (CD57, HLA-DR, PD-1) and Panel 2 (CD57, CD38, CD127, KLRG-1). Pie charts and statistics were generated using SPICE software.

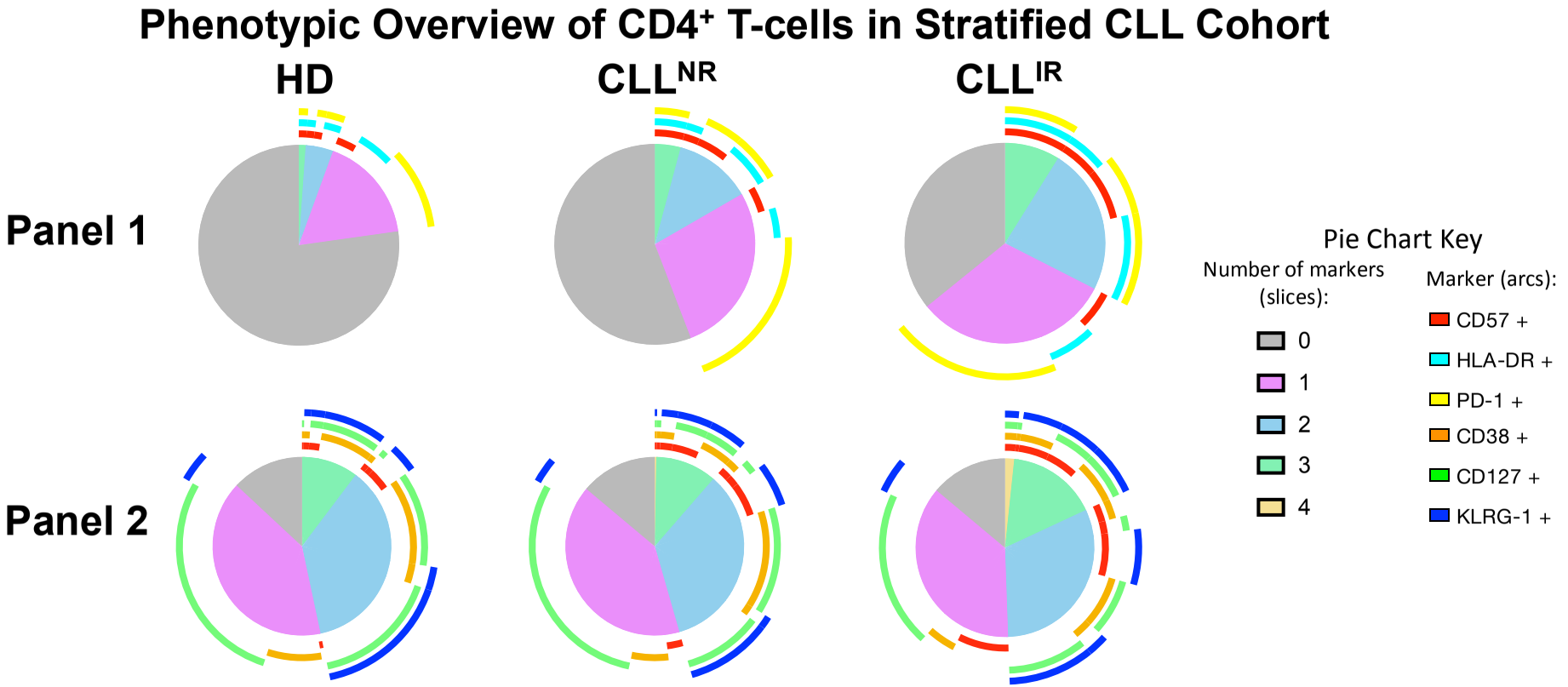

Figure 4.6. Phenotypic overview of CD4⁺ Subsets in CLL^{NR} (n=47), CLL^{IR} (n = 27) and age-matched healthy donors (n = 14). Cells were stained with various markers for senescence/exhaustion and activation and analysed using multi-colour flow cytometry (BD FACS Canto II) using gating as described in Figure 4.1. CLL patients with a CD4:CD8 ratio <1.0 were considered inverted. Samples were analysed using FlowJo to created Boolean combination gating for Panel 1 (CD57, HLA-DR, PD-1) and Panel 2 (CD57, CD38, CD127, KLRG-1). Pie charts and statistics were generated using SPICE software.

Table 4.2. Overall $CD4^+$ phenotypic pie chart analysis (age-matched HD vs CLL)

Panel	HD vs CLL
Panel 1	<0.0001
Panel 2	0.2110

Table 4.3. Overall $CD4^+$ phenotypic pie chart analysis (age-matched HD vs CLL^{NR} vs CLL^{IR})

Panel	HD vs CLL^{NR}	HD vs CLL^{IR}	CLL^{NR} vs CLL^{IR}
Panel 1	0.0005	<0.0001	0.0009
Panel 2	0.3492	0.0044	0.0044

4.4. Markers associated with senescence and/or exhaustion

4.4.1. PD-1 and CD57

It was clear that phenotypic changes also occurred within the $CD4^+$ T-cell population of the CLL patients, and like the $CD8^+$ T-cells there was an observed skewing to the EM memory subset. To determine whether CLL patients were driven to a more exhausted, or highly differentiated, $CD4^+$ phenotype, frequencies of PD-1^+ and $CD57^+$ T-cells were assessed.

Within the $CD4^+$ compartment, there was evidence of significantly higher PD-1 frequencies in CLL patients when compared with age-matched healthy donors ($p < 0.0001$; Figure 4.7A). This increase in PD-1-expressing cells appeared to originate predominantly from the $CD4^+$ EM T-cells ($p < 0.0001$), but was also increased in the EMRA subset ($p = 0.0101$).

Interestingly, when stratified by CD4: CD8 ratio, the CLL patients in the CLL^{IR} subgroup showed significantly higher levels of $CD4^+$PD-1^+ EM T-cells than the CLL^{NR} subgroup and age-matched healthy donors ($p \leq 0.05$ and $p \leq 0.001$, respectively; Figure 4.7B). These findings contrasted with the proportions of $CD8^+$PD-1^+ expressing T-cells observed in the previous chapter, where the percentage of PD-1^+ T-cells were not significantly different between CLL^{NR} and CLL^{IR} patients.

In line with previous results (Nunes et al. 2012), a higher $CD4^+CD57^+$ T-cell frequency was observed in CLL patients compared to the healthy donors ($p = 0.0088$; Figure 4.8A). On subdividing into memory subsets, this higher frequency appeared to be attributable to the EM subset ($p = 0.0049$). This significant increase was reflected in both the EM and EMRA memory subsets of CLL patients versus healthy donors ($p < 0.0001$ and 0.0127, respectively), although a greater proportion originated from the EM subset. The pattern of $CD4^+CD57^+$ expression was exacerbated in the CLL^{IR} subgroup (Figure 4.8B), where higher frequencies of $CD4^+CD57^+$ T-cells were seen compared to both CLL^{NR} patients and healthy donors, and again this seemed to be attributable to higher frequencies in the $CD4^+$ EM memory subset ($p \leq 0.001$ for both).

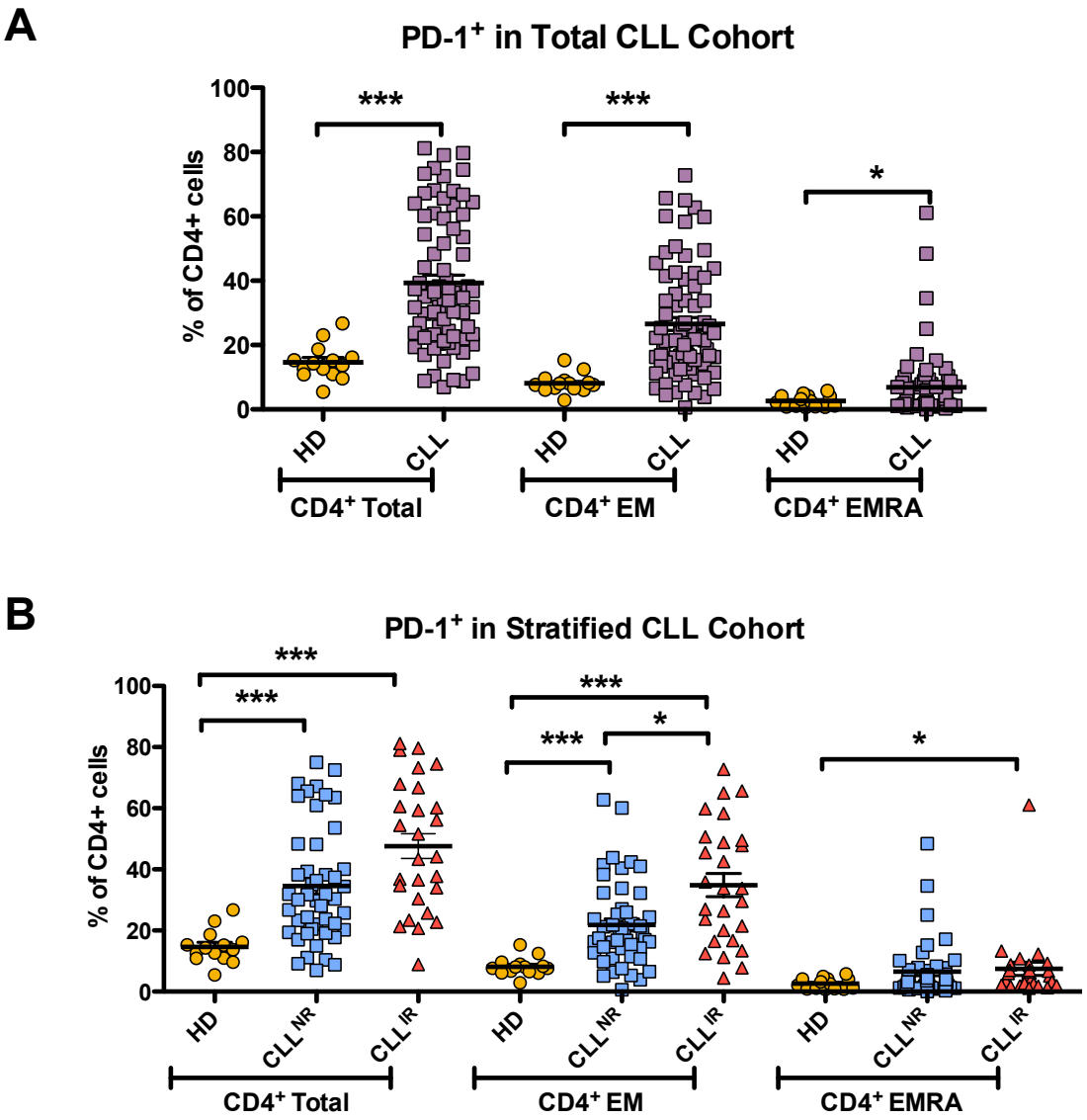

Figure 4.7. PD-1 frequency in CD4$^+$ T-cell memory subsets of CLL patients and age-matched healthy donors. Cells were collected using flow cytometry (FACS CantoII, BD FACSDiva) and analysed with FlowJo (v.9) using gating as described in Figure 4.1. (A) CD4$^+$PD-1$^+$ T-cells in the whole CD4$^+$ T-cell compartment, CD4$^+$ EM and CD4$^+$ EMRA memory subsets of CLL patients (n = 74) and healthy donors (n = 14). Pairwise statistical analysis (HD vs CLL) was performed using the non-parametric Mann-Whitney test. Patients were stratified based on CD4:CD8 ratio: a ratio <1.0 was considered inverted (CLL^{IR}). Patients with a ratio ≥1.0 were considered normal ratio patients (CLL^{NR}). (B) Frequency of CD4$^+$PD-1$^+$ T-cells in the whole CD4$^+$ T-cell compartment, CD4$^+$ EM and CD8$^+$ EMRA memory subsets of CLL^{NR} (n = 47), CLL^{IR} (n = 27) and healthy donors (n = 14). Three-way ANOVA statistical analysis was performed using Kruskal-Wallis test (HD vs CLL^{NR} vs CLL^{IR}), with all pairs of data assessed using the Dunn's post-test. Significant results were included on the graph (* = p ≤0.05; ** = p ≤0.01; *** = p ≤0.001).

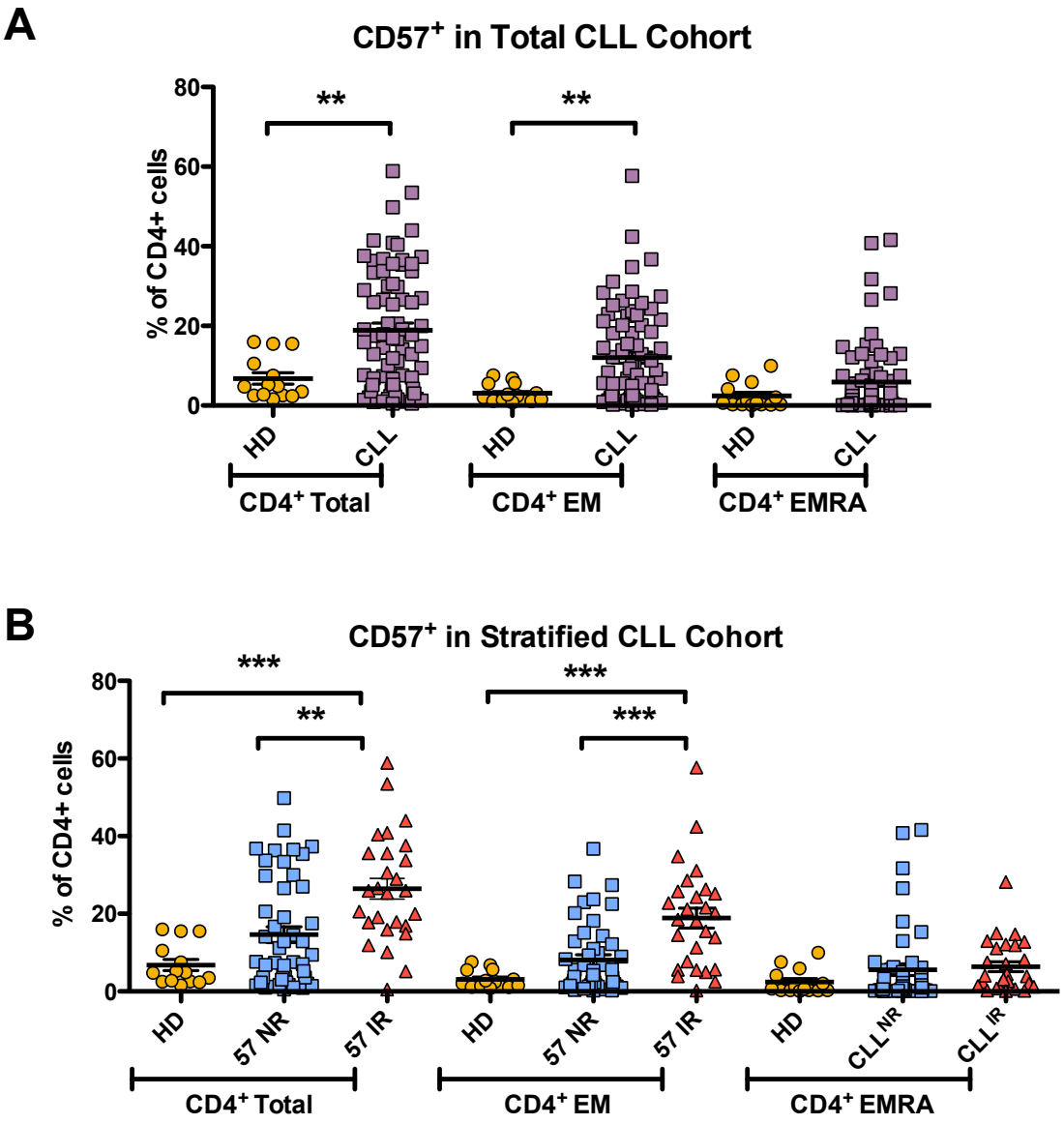

Figure 4.8. CD57 frequency in CD4$^+$ T-cell memory subsets of CLL patients and age-matched healthy donors. Cells were collected using flow cytometry (FACS CantoII, BD FACSDiva) and analysed with FlowJo (v.9) using gating as described in Figure 4.1. (A) CD4$^+$CD57$^+$ T-cells in the whole CD4$^+$ T-cell compartment, CD4$^+$ EM and CD4$^+$ EMRA memory subsets of CLL patients (n = 74) and healthy donors (n = 14). Pairwise statistical analysis (HD vs CLL) was performed using the non-parametric Mann-Whitney test. Patients were stratified based on CD4:CD8 ratio: a ratio <1.0 was considered inverted (CLL^{IR}). Patients with a ratio ≥1.0 were considered normal ratio patients (CLL^{NR}). (B) Frequency of CD4$^+$CD57$^+$ T-cells in the whole CD4$^+$ T-cell compartment, CD4$^+$ EM and CD8$^+$ EMRA memory subsets of CLL^{NR} (n = 47), CLL^{IR} (n = 27) and healthy donors (n = 14). Three-way ANOVA statistical analysis was performed using Kruskal-Wallis test (HD vs CLL^{NR} vs CLL^{IR}), with all pairs of data assessed using the Dunn's post-test. Significant results were included on the graph (* = p ≤0.05; ** = p ≤0.01; *** = p ≤0.001).

Taking these markers together, the average $CD57^+PD\text{-}1^+$ T-cell frequency was more than 5-fold higher in the $CD4^+$ T-cells of the CLL cohort than the healthy age-matched donors (11.56% versus 2.28% respectively; $p < 0.0001$; Figure 4.9A). Again, this was exacerbated in the CLL^{IR} subgroup which demonstrated significantly higher $CD4^+CD57^+PD\text{-}1^+$ T-cells than both the CLL^{NR} subgroup and the healthy donors ($p \leq 0.001$ for both; Figure 4.9B), with average $CD57^+PD\text{-}1^+$ frequency of CLL^{IR} patients more than 7-fold higher than healthy donors.

Increased frequency of the CD57 and PD-1 markers, both individually and co-expressed, further support a skew to a more differentiated subset in the $CD4^+$ T-cells, which was more marked in the CLL^{IR} subgroup. Interestingly, the increase in $PD\text{-}1^+$ and $CD57^+PD\text{-}1^+$ frequencies within the $CD4^+$ compartment of CLL^{IR} patients differed from the results seen with $CD8^+$, where PD-1 expression was not associated with an inverted CD4:CD8 ratio (Chapter 3, Section 3.3.1, Figure 3.8).

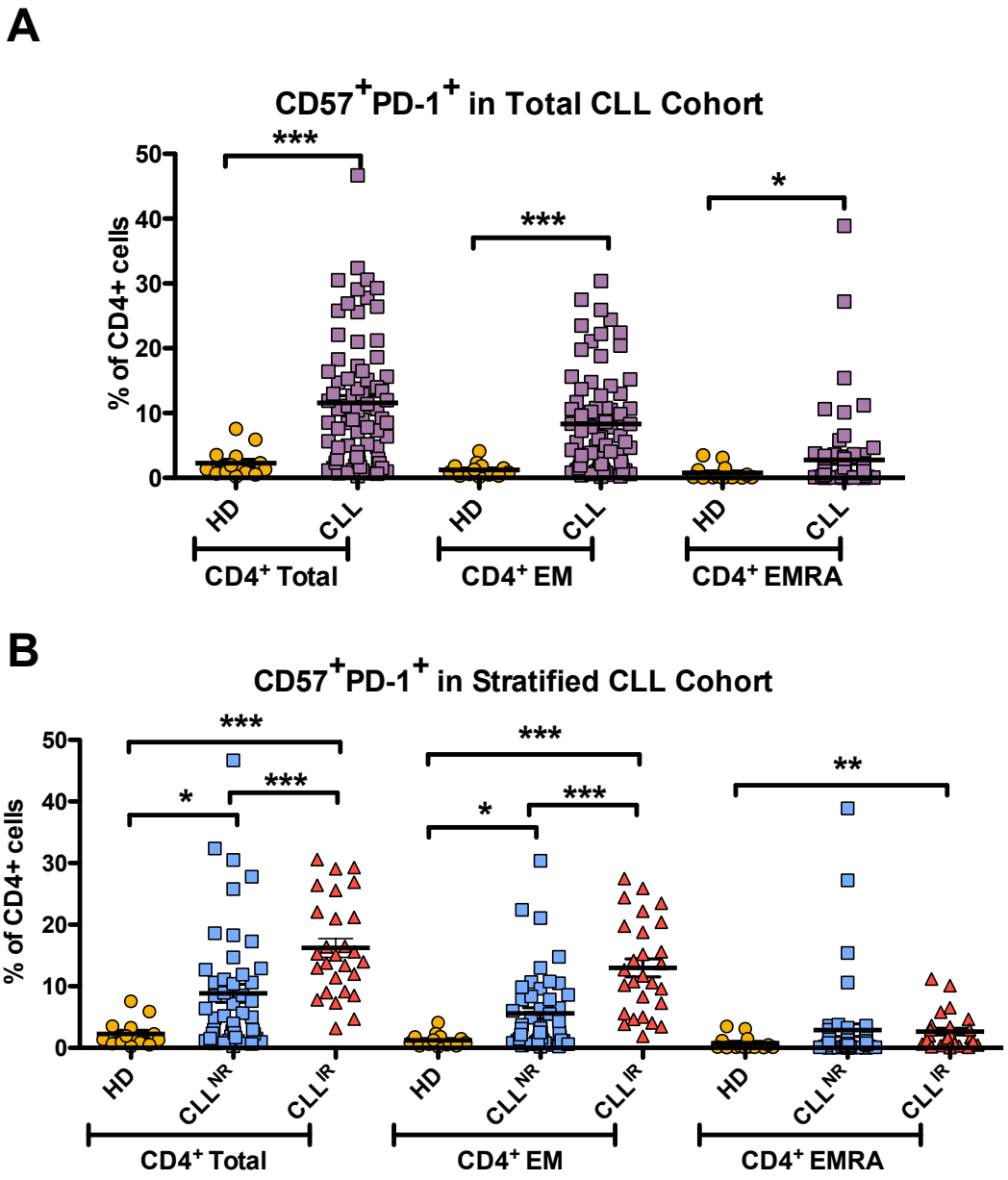

Figure 4.9. CD57 and PD-1 co-expression in CD4$^+$ T-cells of CLL patients and age-matched healthy donors. Cells were collected using flow cytometry (FACS CantoII, BD FACSDiva) and analysed with FlowJo (v.9) using gating as described in Figure 4.1. (A) CD4$^+$CD57$^+$PD-1$^+$ T-cells in the whole CD4$^+$ T-cell compartment, CD4$^+$ EM and CD4$^+$ EMRA memory subsets of CLL patients (n = 74) and healthy donors (n = 14). Pairwise statistical analysis (HD vs CLL) was performed using the non-parametric Mann-Whitney test. Patients were stratified based on CD4:CD8 ratio: a ratio <1.0 was considered inverted (CLL^{IR}). Patients with a ratio ≥1.0 were considered normal ratio patients (CLL^{NR}). (B) Frequency of CD4$^+$CD57$^+$PD-1$^+$ T-cells in the whole CD4$^+$ T-cell compartment, CD4$^+$ EM and CD8$^+$ EMRA memory subsets of CLL^{NR} (n = 47), CLL^{IR} (n = 27) and healthy donors (n = 14). Three-way ANOVA statistical analysis was performed using Kruskal-Wallis test (HD vs CLL^{NR} vs CLL^{IR}), with all pairs of data assessed using the Dunn's post-test. Significant results were included on the graph (* = p ≤0.05; ** = p ≤0.01; *** = p ≤0.001).

4.4.2. Naïve phenotypes (CD127 and CD38)

As described in Section 4.2, the $CD4^+$ naïve population was significantly reduced in CLL patients, particularly in the CLL^{IR} subgroup. This was also seen in $CD8^+$ T-cell compartment in Chapter 3, and aligned with a reduction of $CD127^+$ naïve cells. We therefore explored whether any of the activation or senescence phenotypic markers included in this study were associated with the reduction in $CD4^+$ naïve cells.

Like the $CD8^+$ compartment, $CD127^+$ frequencies were significantly lower in the $CD4^+$ T-cell compartment of CLL patients compared to their healthy age-matched counterparts ($p = 0.0061$; Figure 4.10A). The activation marker $CD38^+$ was also markedly reduced in the $CD4^+$ naïve compartment of CLL patients ($p = 0.0011$). The reduction of $CD127^+$ and $CD38^+$ was more severe in CLL^{IR} patients when compared to both CLL^{NR} and healthy donors ($p \leq 0.01$ and $p \leq 0.001$, respectively; Figure 4.10B). The CLL^{IR} cohort also demonstrated an extended decrease in naïve $CD4^+CD38^+$ T-cells compared to both CLL^{NR} and healthy donors ($p \leq 0.05$ and $p \leq 0.001$, respectively).

As both CD127 and CD38 followed the same pattern of reduction in the $CD4^+$ naïve population of CLL patients, further analysis was performed to explore the co-expression of both markers within the $CD4^+$ naïve subset of CLL patients. The frequency of $CD4^+CD38^+CD127^+$ naïve T-cells was markedly reduced in the CLL cohort when compared to healthy donors ($p = 0.0059$; Figure 4.11A), and this was exacerbated in the CLL^{IR} subgroup of patients, which demonstrated lower frequencies than both the CLL^{NR} and healthy donor groups ($p \leq 0.01$ and $p \leq 0.001$, respectively; Figure 4.11B). Furthermore, subsequent correlation analysis of CD38 against CD127 revealed that there was a strong linear correlation between the two markers ($r = 0.8461$, $p < 0.0001$; Figure 4.11C). Taken together this lends support to the notion that the naïve $CD127^+CD38^+$ phenotype is depleted within the $CD4^+$ compartment of CLL patients, and this is particularly evident in those with an inverted CD4:CD8 ratio.

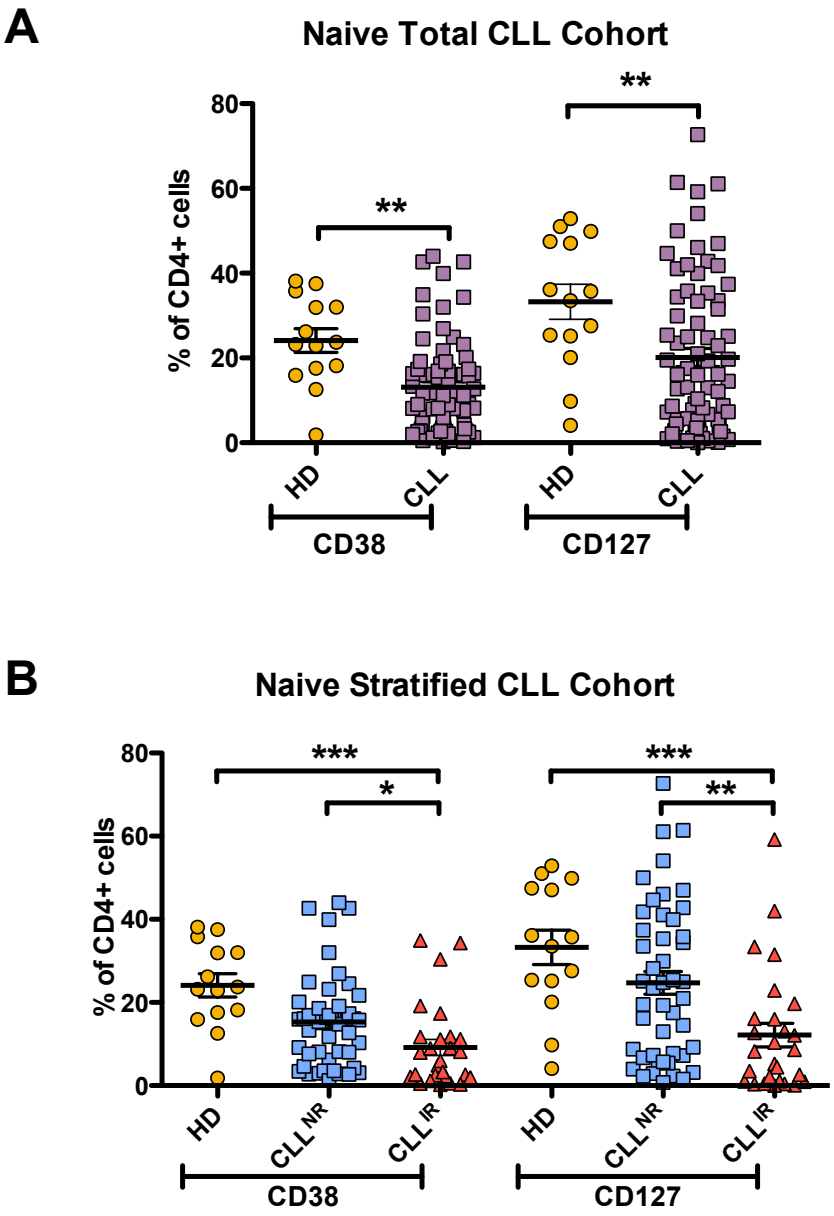

Figure 4.10. CD38 and CD127 frequency in CD4$^+$ naïve T-cells of CLL patients and age-matched healthy donors. Cells were collected using flow cytometry (FACS CantoII, BD FACSDiva) and analysed with FlowJo (v.9) using gating as described in Figure 4.1. (A) CD4$^+$CD38$^+$ and CD4$^+$CD127$^+$ T-cells in the CD4$^+$ naïve memory subset of CLL patients (n = 74) and healthy donors (n = 14). Pairwise statistical analysis (HD vs CLL) was performed using the non-parametric Mann-Whitney test. Patients were stratified based on CD4:CD8 ratio: a ratio <1.0 was considered inverted (CLL^{IR}). Patients with a ratio ≥1.0 were considered normal ratio patients (CLL^{NR}). (B) Frequency of CD4$^+$CD38$^+$ and CD4$^+$CD127$^+$ T-cells in the CD4$^+$ naïve memory subset of CLL^{NR} (n = 47), CLL^{IR} (n = 27) and healthy donors (n = 14). Three-way ANOVA statistical analysis was performed using Kruskal-Wallis test (HD vs CLL^{NR} vs CLL^{IR}), with all pairs of data assessed using the Dunn's post-test. Significant results were included on the graph (* = p ≤0.05; ** = p ≤0.01; *** = p ≤0.001).

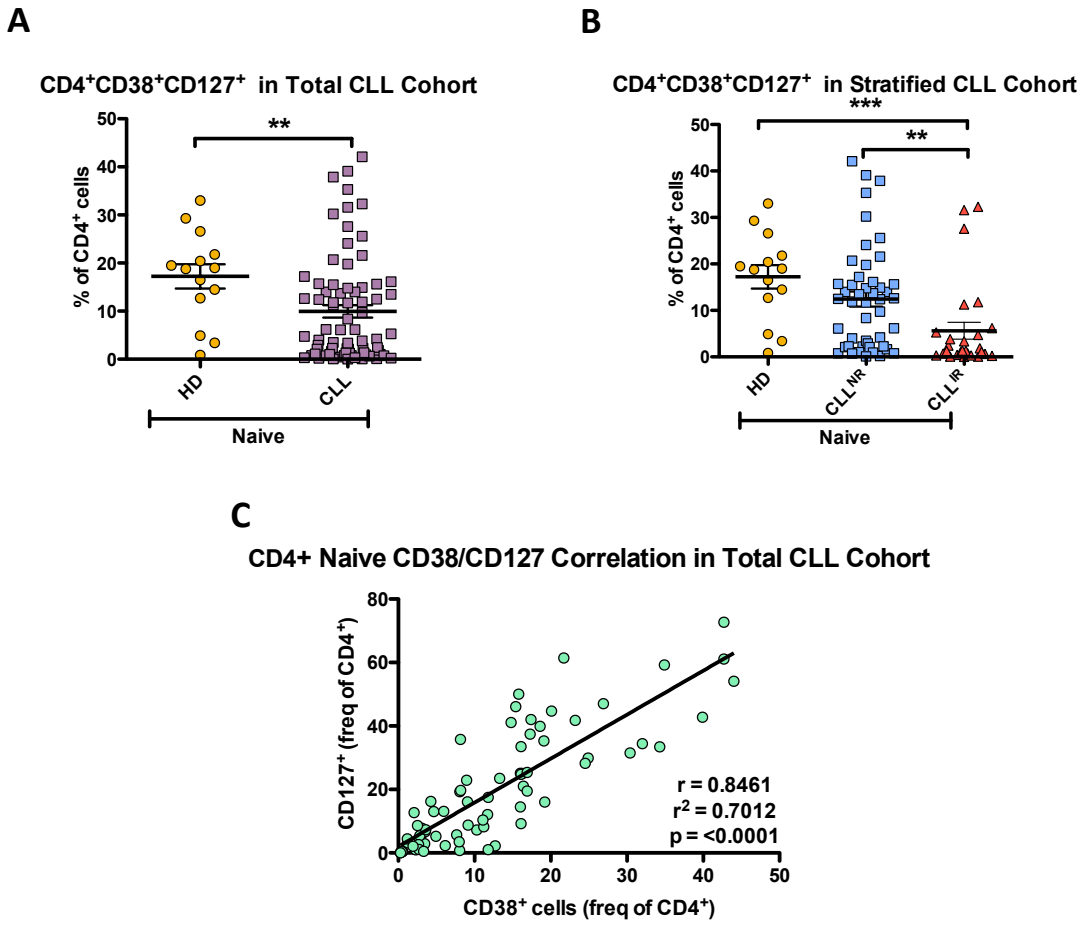

Figure 4.11. CD38 and CD127 co-expression in CD4$^+$ T-cells of CLL patients and age-matched healthy donors. Cells were collected using flow cytometry (FACS CantoII, BD FACSDiva) and analysed with FlowJo (v.9) using gating as described in Figure 4.1. (A) CD4$^+$CD38$^+$CD127$^+$ T-cells in the CD4$^+$ naïve memory compartment of CLL patients (n = 74) and healthy donors (n = 14). Pairwise statistical analysis (HD vs CLL) was performed using the non-parametric Mann-Whitney test. Patients were stratified based on CD4:CD8 ratio: a ratio <1.0 was considered inverted (CLL^{IR}). Patients with a ratio ≥1.0 were considered normal ratio patients (CLL^{NR}). (B) Frequency of CD4$^+$CD38$^+$CD127$^+$ T-cells in the CD4$^+$ naïve memory compartment of CLL^{NR} (n = 47), CLL^{IR} (n = 27) and healthy donors (n = 14). Three-way ANOVA statistical analysis was performed using Kruskal-Wallis test (HD vs CLL^{NR} vs CLL^{IR}), with all pairs of data assessed using the Dunn's post-test. (C) Correlation analysis of CD38 versus CD127 in the CD4$^+$ naive memory compartment of CLL patients. Pearson correlation analysis was performed to quantify the degree of correlation between the two parameters. Significant results were included on the graph (* = p ≤0.05; ** = p ≤0.01; *** = p ≤0.001).

4.5. Markers associated with activation

4.5.1. HLA-DR and CD38

Alongside an increase to more differentiated phenotypes in CLL patients, Chapter 3 also showed an increase in $CD8^+$ T-cells expressing markers associated with T-cell activation (HLA-DR and CD38). This was heightened in the CLL^{IR} patients and implied that there was an expansion of activated T-cells within the $CD8^+$ compartment. It is worthy of note that CD38 expression on T-cells has been previously identified as a potential prognostic marker in CLL (Tinhofer et al. 2006). As a skewing to a more differentiated phenotype was also seen in the $CD4^+$ T-cell population, the expression of HLA-DR and CD38 were also explored within this compartment.

When looking at the CLL cohort as a whole, there was no significant difference in the frequency of $CD4^+HLA\text{-}DR^+$ T-cells when compared to age-matched healthy donors. However, there was a significant difference between CLL patients and healthy donors in the $CD4^+$EM subset ($p = 0.0232$, Figure 4.12A). Stratification of the cohort showed that the CLL^{IR} subgroup had significantly higher $CD4^+HLA\text{-}DR^+$ T-cell frequencies compared to the CLL^{NR} and healthy donors in the whole $CD4^+$ compartment (Figure 4.12B, $p \leq 0.01$ for both); again, this appeared to be driven by an increased frequency within the $CD4^+$ EM T-cells ($p \leq 0.01$ versus both CLL^{NR} and CLL^{IR}).

In the $CD4^+$ T-cell compartment as a whole, the frequency of $CD38^+$ T-cells did not differ between CLL patients and healthy donors. However, the percentage of $CD4^+CD38^+$ T-cells was significantly higher within the $CD4^+$ EM subset ($p = 0.0029$, Figure 4.13A). No difference was seen between CLL^{NR} and CLL^{IR} $CD4^+CD38^+$ frequencies in either the whole population, or the EM subset (Figure 4.13B). It was reported in the previous section that $CD4^+$ naïve memory T-cells had a reduced frequency of naïve $CD38^+$ cells (Section 4.4.2): this may have negated the rise in $CD38^+$ EM frequency, resulting in the lack of frequency change in the entire $CD4^+$ T-cell population as a whole.

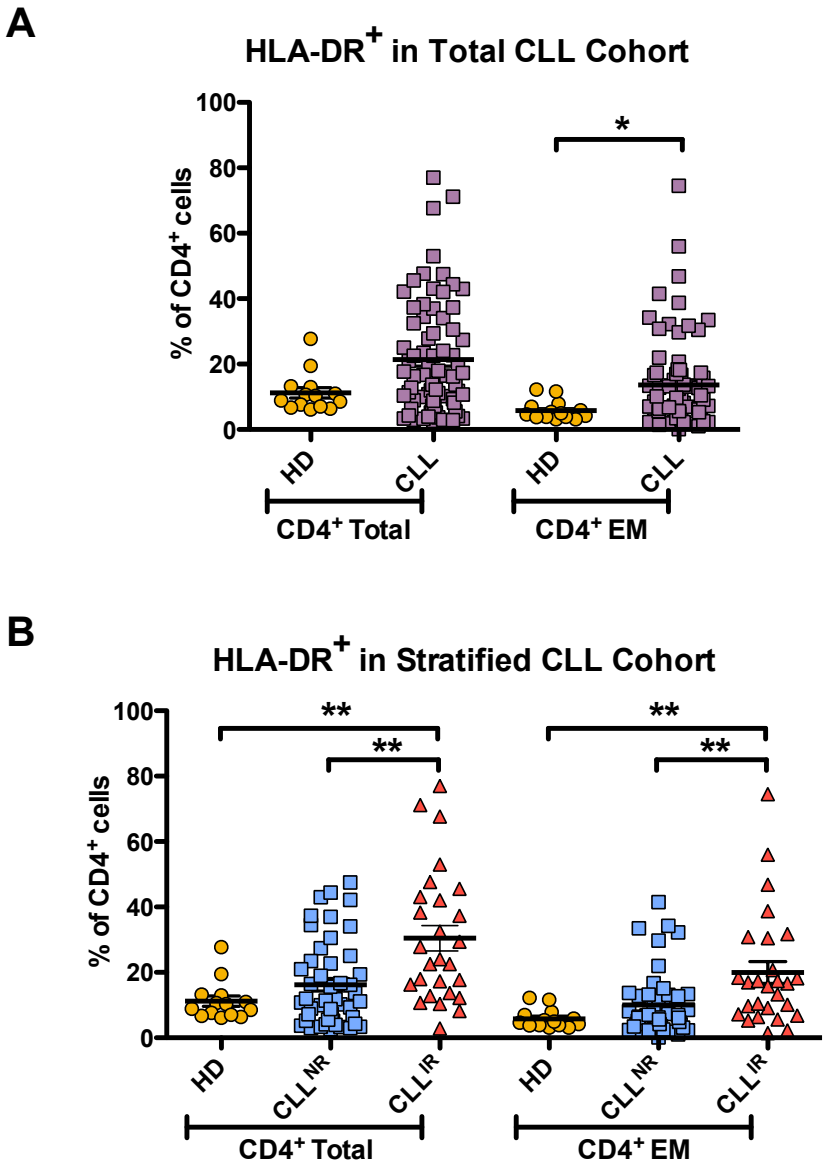

Figure 4.12. HLA-DR frequency in CD4$^+$ T-cell memory subsets of CLL patients and age-matched healthy donors. Cells were collected using flow cytometry (FACS CantoII, BD FACSDiva) and analysed with FlowJo (v.9) using gating as described in Figure 4.1. (A) CD4$^+$HLA-DR$^+$ T-cells in the whole CD4$^+$ T-cell compartment and CD4$^+$ EM memory subset of CLL patients (n = 74) and healthy donors (n = 14). Pairwise statistical analysis (HD vs CLL) was performed using the non-parametric Mann-Whitney test. Patients were stratified based on CD4:CD8 ratio: a ratio <1.0 was considered inverted (CLL^{IR}). Patients with a ratio ≥1.0 were considered normal ratio patients (CLL^{NR}). (B) Frequency of CD4$^+$HLA-DR$^+$ T-cells in the whole CD4$^+$ T-cell compartment, CD4$^+$ EM and CD8$^+$ EMRA memory subsets of CLL^{NR} (n = 47), CLL^{IR} (n = 27) and healthy donors (n = 14). Three-way ANOVA statistical analysis was performed using Kruskal-Wallis test (HD vs CLL^{NR} vs CLL^{IR}), with all pairs of data assessed using the Dunn's post-test. Significant results were included on the graph (* = p ≤0.05; ** = p ≤0.01; *** = p ≤0.001).

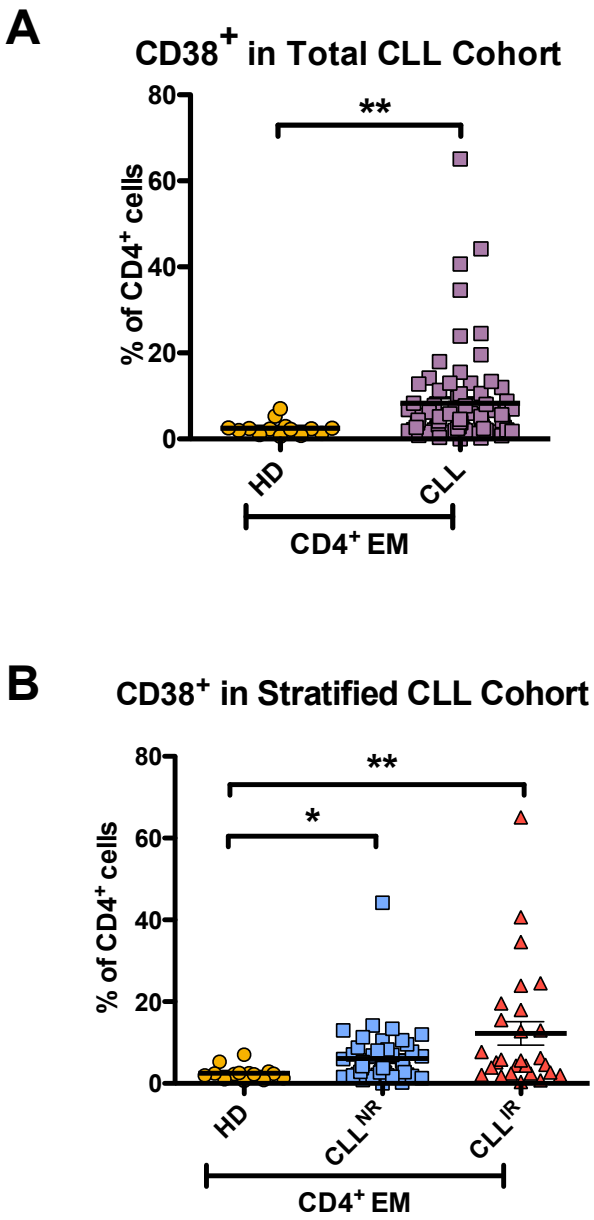

Figure 4.13. CD38 frequency in CD4⁺ EM T-cells of CLL patients and age-matched healthy donors. Cells were collected using flow cytometry (FACS CantoII, BD FACSDiva) and analysed with FlowJo (v.9) using gating as described in Figure 4.1. (A) $CD4^+CD38^+$ T-cells in the $CD4^+$ EM memory subset of CLL patients (n = 74) and healthy donors (n = 14). Pairwise statistical analysis (HD vs CLL) was performed using the non-parametric Mann-Whitney test. Patients were stratified based on CD4:CD8 ratio: a ratio <1.0 was considered inverted (CLL^{IR}). Patients with a ratio ≥1.0 were considered normal ratio patients (CLL^{NR}). (B) Frequency of $CD4^+CD38^+$ T-cells in the $CD4^+$ EM memory subset of CLL^{NR} (n = 47), CLL^{IR} (n = 27) and healthy donors (n = 14). Three-way ANOVA statistical analysis was performed using Kruskal-Wallis test (HD vs CLL^{NR} vs CLL^{IR}), with all pairs of data assessed using the Dunn's post-test. Significant results were included on the graph (* = p ≤0.05; ** = p ≤0.01; *** = p ≤0.001).

In summary, this section demonstrates that in addition to a skewed memory phenotype, CLL patients demonstrated higher proportions of activated $CD4^+$ T-cells that largely originate from the EM subset. Interestingly, elevated levels of activated $CD4^+$ T-cells were shown in the CLL^{IR} patients, but this exacerbation was only seen with the $CD4^+HLA\text{-}DR^+$ phenotype, again driven by the $CD4^+$ EM subset (Figure 4.12B). Overall, there was an increased frequency of more differentiated, potentially activated ($HLA\text{-}DR^+$) T-cells linked with inversion of the CD4:CD8 ratio.

4.5.2. CD57, PD-1 and HLA-DR

As discussed in the previous chapter, although markers such as PD-1 and CD57 are considered exhaustion/senescent markers, there remains some controversy in using them in isolation as an identifier of exhausted or senescent cells, as they can be found on T-cells that are able to respond to certain stimuli, such as CD3 with IL-2 and AB serum (Chong et al. 2008). In support of this, we identified subsets of phenotypes in the $CD8^+$ compartment that co-expressed PD-1 and/or CD57 with activation markers ($PD\text{-}1^+HLA\text{-}DR^+$, $CD57^+HLA\text{-}DR^+$, $CD57^+CD38^+$ and $CD57^+PD\text{-}1^+HLA\text{-}DR^+$) that were markedly increased in CLL patients. Furthermore, CLL^{IR} patients had a more marked increase in $CD8^+$ T-cells that co-presented CD57 with either HLA-DR or PD-1. With the previous section demonstrating increased single frequencies of these markers, further phenotypic analysis was applied to identify any patterns of co-expression of senescent/exhaustion markers with activation markers on $CD4^+$ T-cells of CLL patients.

The CLL cohort displayed an increased frequency of $CD57^+HLA\text{-}DR^+$ T-cells compared to healthy donors in the $CD4^+$ total compartment ($p = 0.0020$), as well as the $CD4^+$ EM and EMRA memory subsets ($p = 0.0013$ and $p = 0.0363$, respectively; Figure 4.14A). $CD4^+CD57^+HLA\text{-}DR^+$ frequencies were amplified in the CLL^{IR} subgroup compared to both CLL^{NR} and age-matched healthy donors (Figure 4.14B): again, this was seen in the total $CD4^+$compartment ($p \leq 0.001$ for both), $CD4^+$ EM ($p \leq 0.001$ for both) and $CD4^+$ EMRA memory subsets ($p \leq 0.05$ versus CLL^{NR}; $p \leq 0.01$ versus HD). It is worth noting that a large proportion of this phenotype appeared to originate from the EM subset rather than the EMRA subset.

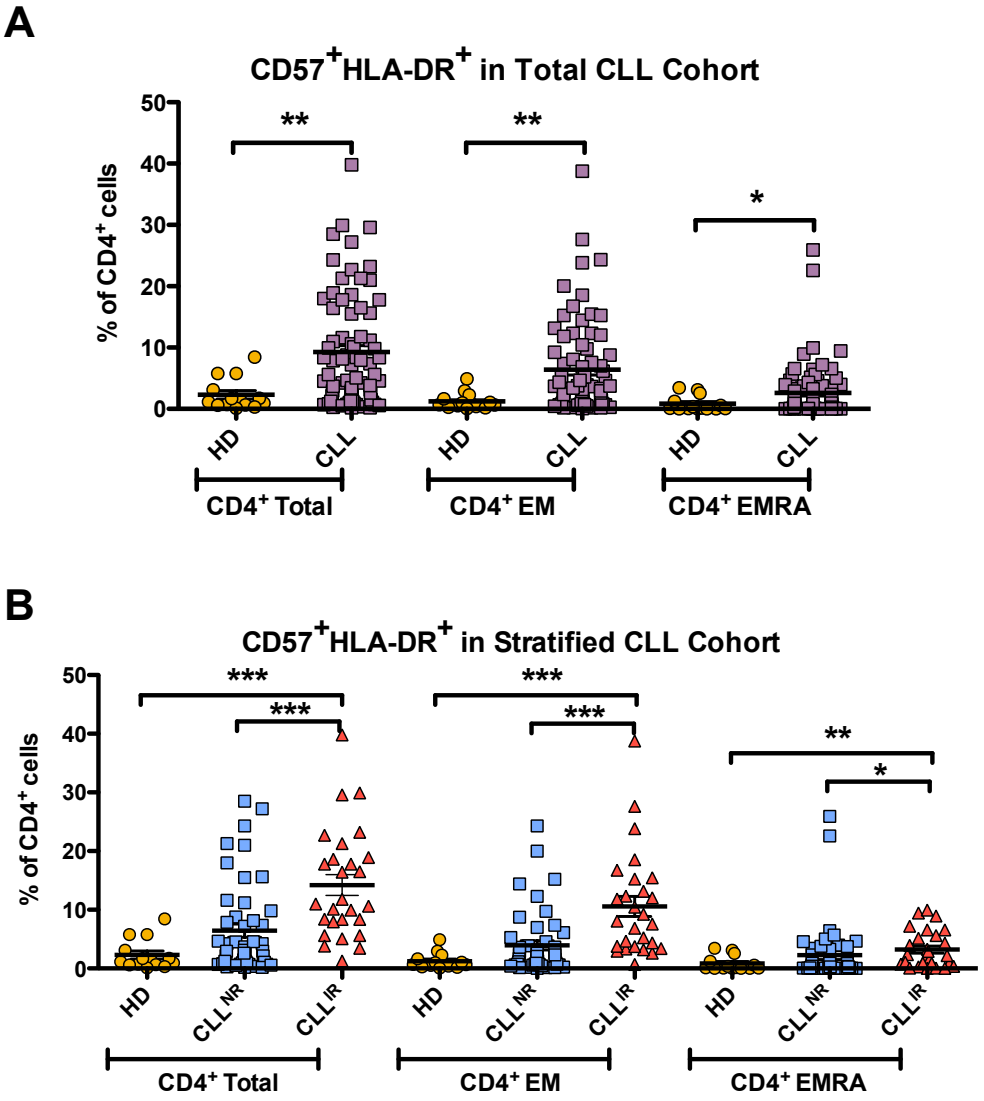

Figure 4.14. CD57 and HLA-DR co-expression in CD4$^+$ T-cells of CLL patients and age-matched healthy donors. Cells were collected using flow cytometry (FACS CantoII, BD FACSDiva) and analysed with FlowJo (v.9) using gating as described in Figure 4.1. (A) CD4$^+$CD57$^+$HLA-DR$^+$ T-cells in the whole CD4$^+$ T-cell compartment, CD4$^+$ EM and CD4$^+$ EMRA memory subsets of CLL patients (n = 74) and healthy donors (n = 14). Pairwise statistical analysis (HD vs CLL) was performed using the non-parametric Mann-Whitney test. Patients were stratified based on CD4:CD8 ratio: a ratio <1.0 was considered inverted (CLL^{IR}). Patients with a ratio ≥1.0 were considered normal ratio patients (CLL^{NR}). (B) Frequency of CD4$^+$CD57$^+$HLA-DR$^+$ T-cells in the whole CD4$^+$ T-cell compartment, CD4$^+$ EM and CD8$^+$ EMRA memory subsets of CLL^{NR} (n = 47), CLL^{IR} (n = 27) and healthy donors (n = 14). Three-way ANOVA statistical analysis was performed using Kruskal-Wallis test (HD vs CLL^{NR} vs CLL^{IR}), with all pairs of data assessed using the Dunn's post-test. Significant results were included on the graph (* = p ≤0.05; ** = p ≤0.01; *** = p ≤0.001).

Multivariate analyses of the CLL cohort performed in Chapter 3 (Section 3.7) showed that the phenotype from this study that had the strongest association with prognosis was $CD4^+HLA\text{-}DR^+PD\text{-}1^+$ (further discussed in Section 4.6.1). Comparison between healthy donors and CLL patients revealed that CLL patients had a significantly higher proportion of $HLA\text{-}DR^+PD\text{-}1^+$ cells in the $CD4^+$ T-cell compartment (Figure 4.15A, $p = 0.0008$). The CLL $CD4^+$ EM ($p < 0.0001$) and EMRA ($p = 0.0073$) subsets mirrored this increased frequency of $HLA\text{-}DR^+PD\text{-}1^+$, with the largest percentage of this phenotype found in the EM subset.

When the CLL patients were stratified according to CD4:CD8 ratio in Figure 4.15B, CLL^{IR} patients demonstrated a significantly higher frequency than both and CLL^{NR} and healthy donor patients ($p \leq 0.01$ and $p \leq 0.001$, respectively). Again, this appeared to be predominantly driven by the EM subset rather than the EMRA subset, as the $CD4^+$ EM T-cells of CLL^{IR} patients had significantly higher frequency of $HLA\text{-}DR^+PD\text{-}1^+$ versus CLL^{NR} and healthy donors ($p \leq 0.001$ for both).

It is clear, therefore, that although higher frequencies of T-cells expressing PD-1 were associated with the T-cell memory subset, a large proportion of these T-cells co-expressed activation markers.

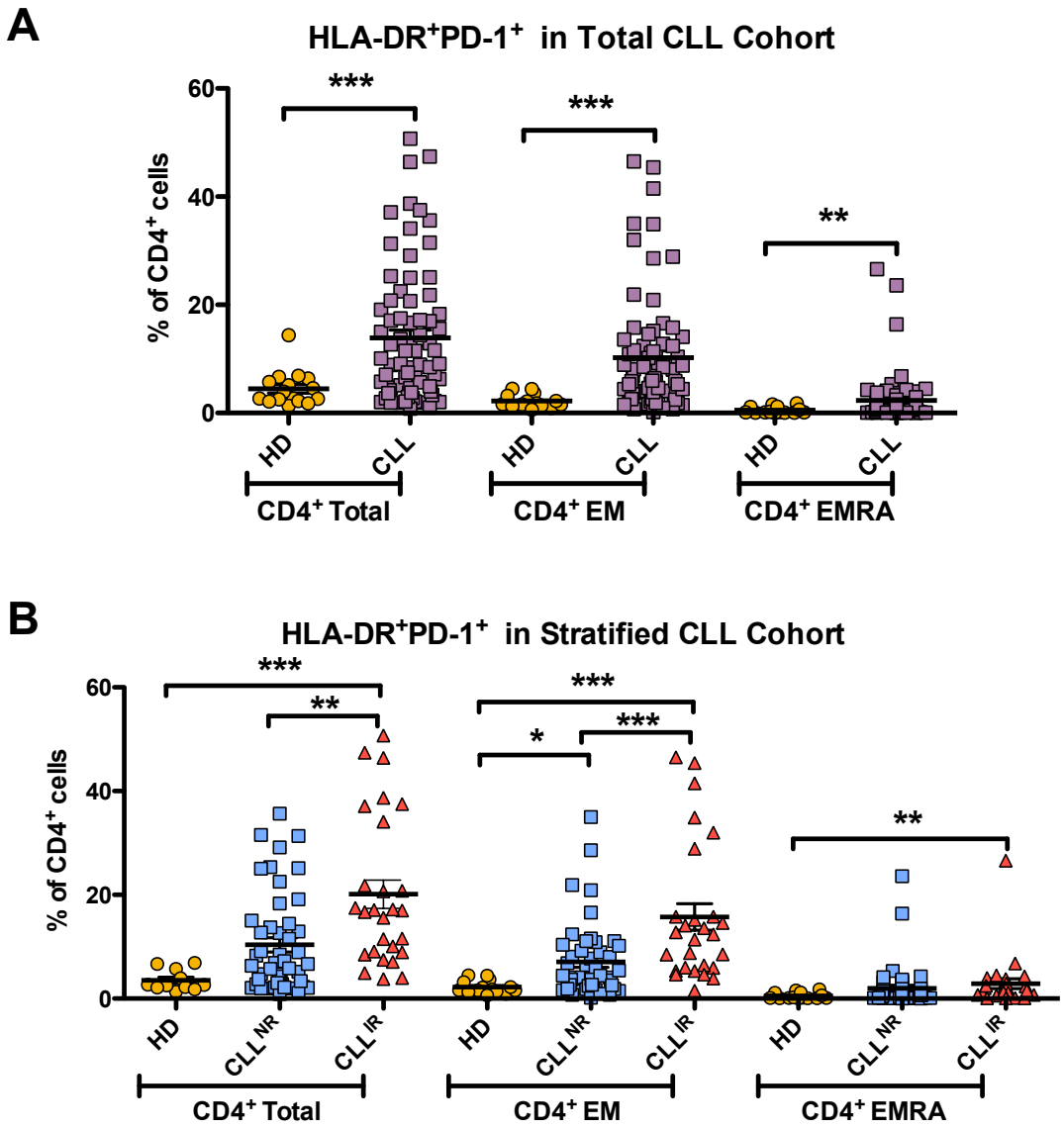

Figure 4.15. HLA-DR and PD-1 co-expression in CD4$^+$ T-cells of CLL patients and age-matched healthy donors. Cells were collected using flow cytometry (FACS CantoII, BD FACSDiva) and analysed with FlowJo (v.9) using gating as described in Figure 4.1. (A) CD4$^+$HLA-DR$^+$PD-1$^+$ T-cells in the whole CD4$^+$ T-cell compartment, CD4$^+$ EM and CD4$^+$ EMRA memory subsets of CLL patients (n = 74) and healthy donors (n = 14). Pairwise statistical analysis (HD vs CLL) was performed using the non-parametric Mann-Whitney test. Patients were stratified based on CD4:CD8 ratio: a ratio <1.0 was considered inverted (CLL^{IR}). Patients with a ratio ≥1.0 were considered normal ratio patients (CLL^{NR}). (B) Frequency of CD4$^+$HLA-DR$^+$PD-1$^+$ T-cells in whole CD4$^+$ T-cell compartment, CD4$^+$ EM and CD8$^+$ EMRA memory subsets of CLL^{NR} (n = 47), CLL^{IR} (n = 27) and healthy donors (n = 14). Three-way ANOVA statistical analysis was performed using Kruskal-Wallis test (HD vs CLL^{NR} vs CLL^{IR}), with all pairs of data assessed using the Dunn's post-test. Significant results were included on the graph (* = p ≤0.05; ** = p ≤0.01; *** = p ≤0.001).

4.6. $CD4^+$ T-cell phenotypes and cytomegalovirus (CMV) infection

Cytomegalovirus (CMV) is a common persistent viral infection in the elderly population (Görgün et al. 2005; Vasto et al. 2007; Tinhofer et al. 2009; Pita-Lopez et al. 2009; Monserrat et al. 2013). Previous work has shown that both the $CD4^+$ and $CD8^+$ T-cell compartments in CMV^+ patients are skewed towards the more differentiated memory subsets (Os et al. 2013; Pourgheysari et al. 2010; Khan et al. 2002). However, no association has been shown between CMV infection and clinical prognosis in CLL (Parry et al. 2016). The skewed phenotypes in CMV^+ patients are thought to be due to expansions in chronically stimulated CMV-specific T-cells that are defined as senescent, although there is evidence that CMV-specific T-cells in CLL patients can act in a functional capacity (Raa et al. 2014). To assess whether CMV was a contributing factor for the unusual phenotypes that were observed in the $CD4^+$ compartment, patient serum for a cohort of CLL patients was collected and serotyped by the Public Health Wales Microbiology Laboratory, UHW, Cardiff.

The CMV serostatus was assessed in 63 of the CLL patients used in this study; of those tested, 43/63 (68%) were CMV seropositive. The previous chapter demonstrated that the CD4:CD8 ratio and the skewing to $CD8^+$ EM T-cells in CLL were not driven by CMV infection (Chapter 3, Section 3.5).

SPICE software analysis was used to compare the distribution of memory $CD4^+$ T-cell subsets among CLL patients based on CMV serostatus using pie charts (Figure 4.16). No significant $CD4^+$ subset changes were observed between CMV^+ and CMV^- CLL patients ($p = 0.1667$). As with the $CD8^+$ CMV results, this suggests that the phenotypic abnormalities observed among the $CD4^+$ memory T-cells are driven by CLL pathology rather than chronic CMV stimulation.

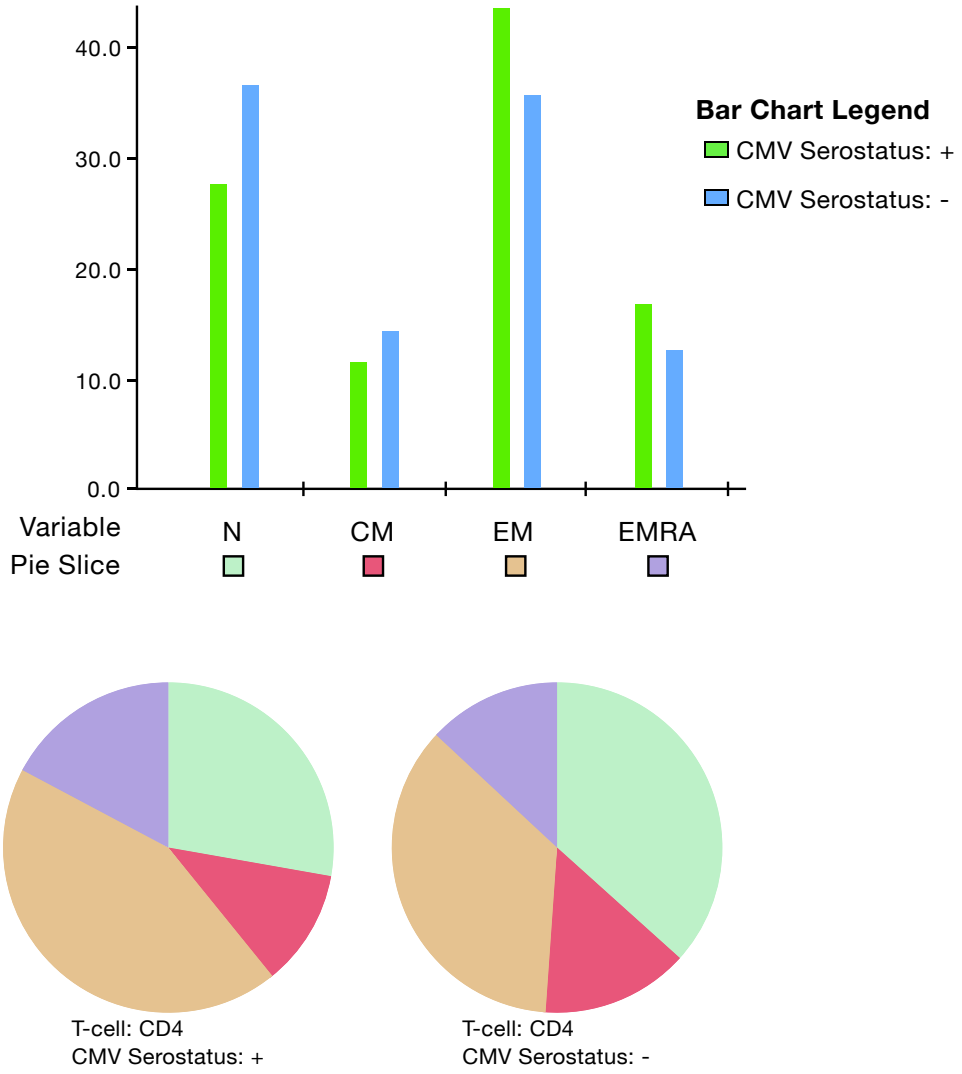

Figure 4.16. CMV serostatus in CLL patients. Cells were collected using flow cytometry (FACS CantoII, BD FACSDiva) and analysed with FlowJo (v.9) using gating as described in Figure 4.1. Plasma samples from CLL patients were serotyped for antibodies against CMV. Distribution of $CD4^+$ memory subsets in CMV seropositive (n = 43) and CMV seronegative (n = 20) CLL patients. Flow cytometry data and CMV information were analysed and t-tests performed using SPICE software (v5.3).

4.7. Prognostic significance of CD4$^+$ T-cell phenotypes

To investigate whether the phenotypes in this study were associated with prognostic significance in CLL, multivariate analyses were performed on both the CD4$^+$ and CD8$^+$ compartments (full details of the multivariate process is outlined in Chapter 3, Section 3.7). Interestingly, the cox proportional hazards regression model (with forward selection) revealed that the phenotype with the greatest effect on progression-free survival (PFS) in this study was CD4$^+$HLA-DR$^+$PD-1$^+$. Full multivariate results, including simple statistics and correlation analyses with CD4:CD8 ratio, are included in Appendix IV.

Additional multivariate analyses consisting of recursive partitioning followed by univariate analysis (Kaplan-Meier curves) were applied to identify the optimum CD4$^+$HLA-DR$^+$PD-1$^+$ frequency cut-offs by which patients could be stratified into poor or good prognostic subgroups. The most prognostically relevant thresholds are included here; for the complete multivariate and univariate outputs see Appendix IV.

The analysis revealed that patients with more than 14.4%-16.7% of CD4$^+$HLA-DR$^+$PD-1$^+$ cells had significantly poorer prognosis, as measured by PFS (Figure 4.17A-B). The multivariate analyses also demonstrated that a 31.5% CD4$^+$HLA-DR$^+$PD-1$^+$ threshold had an even greater prognostic effect (Figure 4.17C), potentially identifying a high-risk group with an exacerbated phenotype. A low cut-off value of 4.95% was also shown by the multivariate analysis to have an effect on prognosis. Interestingly, when univariate analysis was applied to this threshold, patients with a CD4$^+$HLA-DR$^+$PD-1$^+$ population of ≤4.95% (21/74 patients [28.4%]) never experienced disease progression during the follow-up period (Figure 4.17D).

Overall it appears that an initial cut-off of around 15% CD4$^+$HLA-DR$^+$PD-1$^+$ T-cells identified patients at risk of poorer prognosis (based on the recursive partitioning cut-off frequencies of 14.4% and 16.7%), whilst frequencies of 31.5% and above identified a high-risk population. Conversely, CLL patients with less than 5% of CD4$^+$HLA-DR$^+$PD-1$^+$ cells (based on the 4.95% cut-off) demonstrated no risk of disease progression. Taken together these analyses support the concept that increasing frequency of CD4$^+$HLA-DR$^+$PD-1$^+$ T-cells is linked to inferior prognosis. Section 4.5.2 observed that on average CLL^{IR} patients had higher proportions of this phenotype, further supporting the concept that the CD4:CD8 ratio is linked to prognosis. However,

in this study, higher resolution phenotyping has identified a T-cell signature with an even stronger association with disease progression.

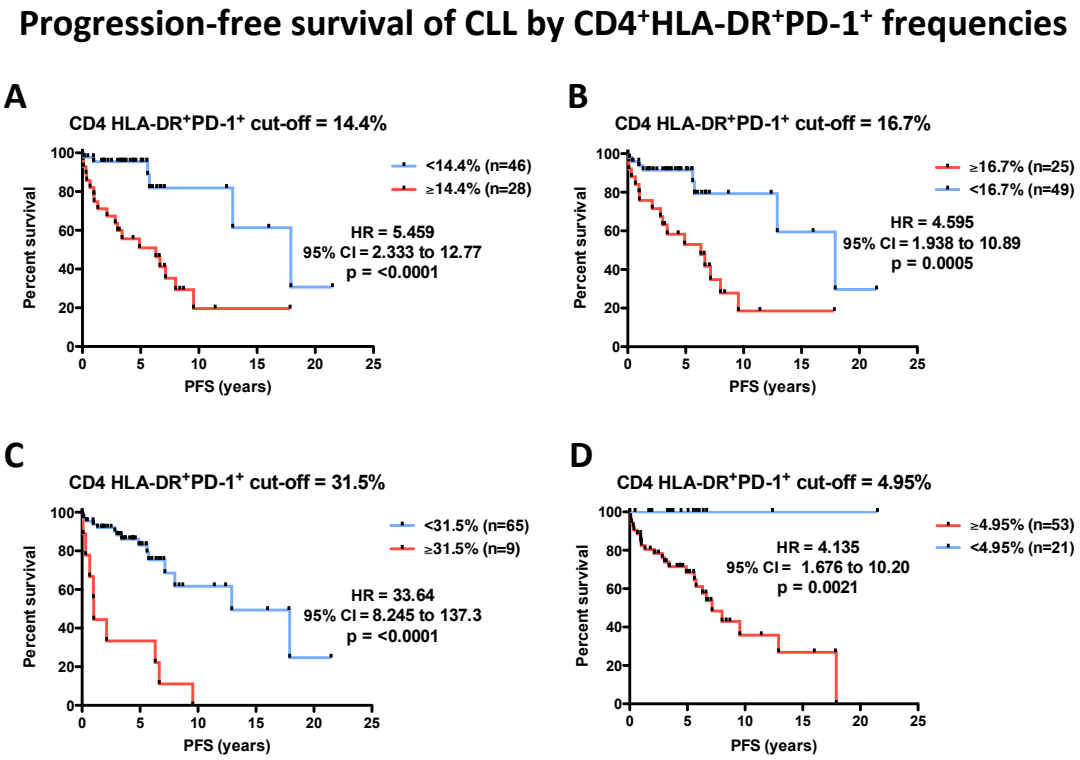

Figure 4.17. Prognosis of CLL patients stratified based on $CD4^+HLA\text{-}DR^+PD\text{-}1^+$ frequencies. Cells were collected using flow cytometry (FACS CantoII, BD FACSDiva) and analysed with FlowJo (v.9) using gating as described in Figure 4.1. Multivariate recursive partitioning was performed to establish significant 'cut-off' ratio values within the study group. Kaplan-Meier curves for progression-free survival of CLL patients stratified by a $CD4^+HLA\text{-}DR^+PD\text{-}1^+$ frequency of (A) 14.4% (B) 16.7% (C) 31.5% and (D) 4.95% are shown. Multivariate analyses were performed by Professor Robert Hills (Haematology Clinical Trials Unit, Cardiff University). Univariate analyses (Kaplan-Meier curves and survival statistics) were performed using GraphPad Prism 5.0.

4.8. Absolute counts

As rationalised in Chapter 3 (Section 3.8), preliminary absolute counts were obtained for 19 CLL patients to establish whether the changes in frequency of particular $CD4^+$ subpopulations in CLL^{IR} vs CLL^{NR} patients reflected increases or decreases in absolute number.

No change in the numbers of $CD4^+$ T-cells was observed between the CLL^{NR} and CLL^{IR} patients (Figure 4.18A). This, combined with the expansion of $CD8^+$ T-cell numbers described in Chapter 3, adds further evidence that the CD4:CD8 ratio is inverted due to an expansion in $CD8^+$ T-cell numbers, rather than a reduction in the number of $CD4^+$ T-cells. Similarly, no significant changes in absolute numbers of $CD4^+$ cells were seen in the naïve, EM and EMRA populations (Figure 4.18B-D): however, there was a trend of reduced naïve and expanded EM T-cell numbers within the inverted ratio patients. This may suggest that the skewing towards a more differentiated phenotype within the $CD4^+$ compartment could be due to a combined reduction in the number of naïve T-cells and an increase in the number of EM T-cells.

Significantly higher frequencies of $CD4^+CD57^+$, $CD4^+$HLA-DR^+ and $CD4^+$PD-1^+ T-cells were detected in the CLL^{IR} patients versus CLL^{NR} patients in the phenotypic analysis. Although trends in increased numbers of these phenotypes were observed in the $CD4^+$ compartment of CLL^{IR} patients, none reached significance (Figure 4.19A). $CD4^+$HLA-DR^+PD-1^+ was the phenotype shown to have greatest prognostic potential within this study and occurred at significantly higher frequency in CLL^{IR} subgroup compared to CLL^{NR} subgroup. By contrast, analysis of absolute cell counts did not reveal a significant difference in the numbers of $CD4^+$HLA-DR^+PD-1^+ T-cells between CLL^{NR} and CLL^{IR} patients. However, there was more heterogeneity in the counts for the CLL^{IR} subgroup, with 4/8 patients having counts above the average for CLL^{NR} (Figure 4.19B).

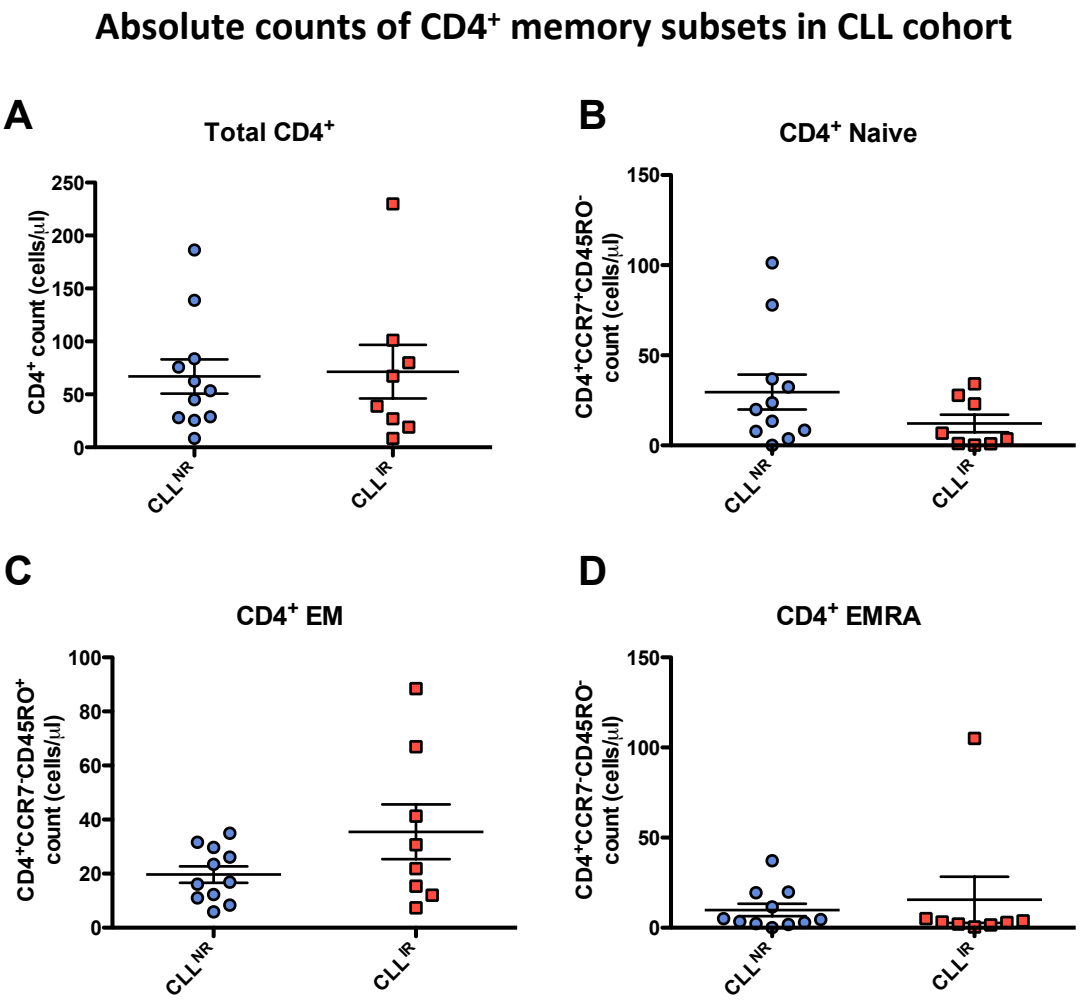

Figure 4.18. Absolute counts of CD4$^+$ T-cells in CLL^{NR} (n = 11) and CLL^{IR} (n = 8) patients. Cells and BD Trucount beads were collected using flow cytometry (FACS CantoII, BD FACSDiva) and analysed with FlowJo (v.9) using gating as described in Figure 4.1. Patients were stratified based on CD4:CD8 ratio: a ratio <1.0 was considered inverted (CLL^{IR}). Patients with a ratio ≥1.0 were considered normal ratio patients (CLL^{NR}). Absolute counts for (A) overall CD4$^+$, (B) CD4$^+$ naïve, (C) CD4$^+$ EM and (D) CD4$^+$EMRA between CLL^{NR} and CLL^{IR} patients are shown. Pairwise statistical analysis (HD vs CLL) was performed using the non-parametric Mann-Whitney test. Significant results were included on the graph (* = p ≤0.05; ** = p ≤0.01; *** = p ≤0.001).

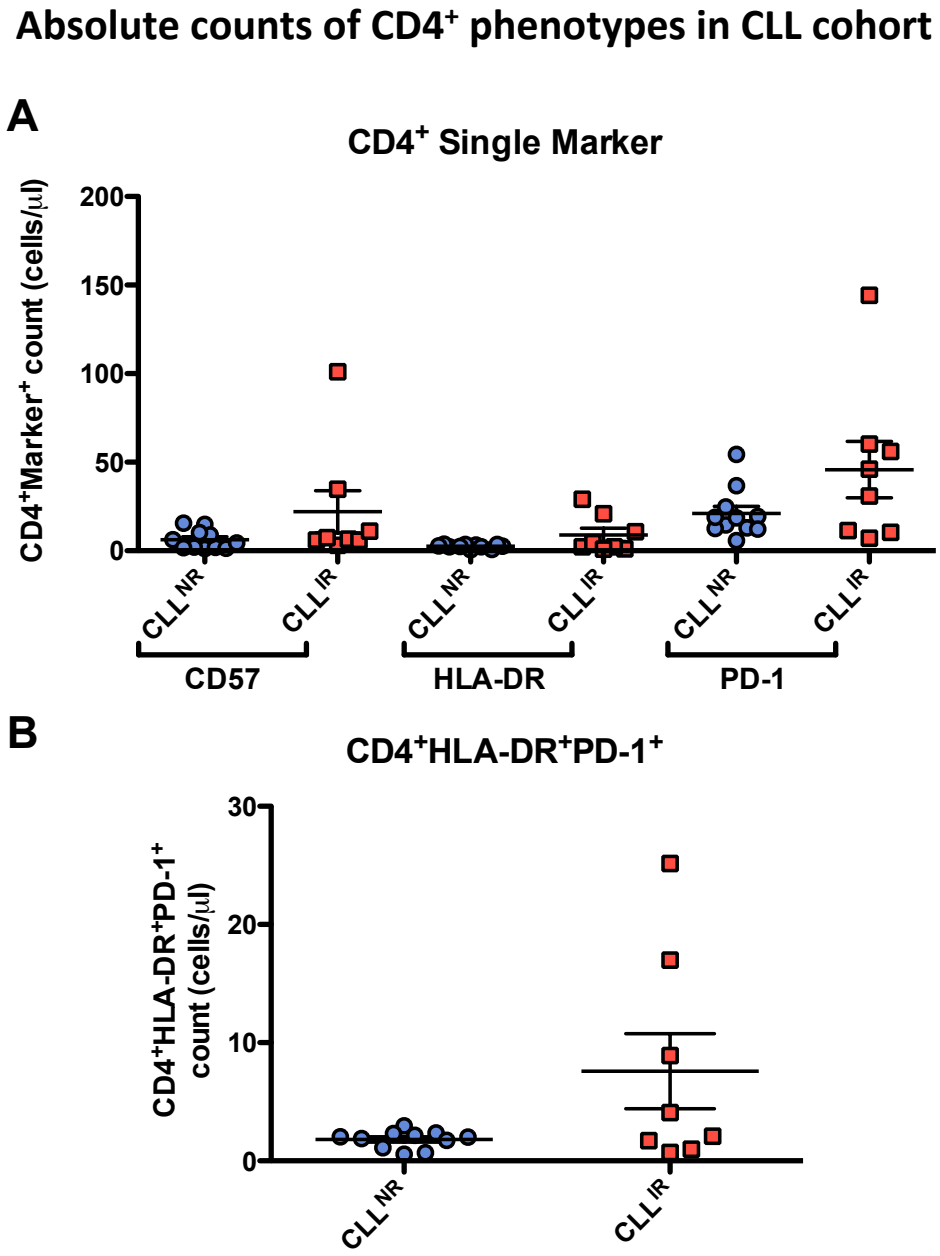

Figure 4.19. Absolute counts of CD4$^+$ T-cell phenotypes in CLL^{NR} (n = 11) and CLL^{IR} (n = 8) patients. Cells and BD Trucount beads were collected using flow cytometry (FACS CantoII, BD FACSDiva) and analysed with FlowJo (v.9) using gating as described in Figure 4.1. Patients were stratified based on CD4:CD8 ratio: a ratio <1.0 was considered inverted (CLL^{IR}). Patients with a ratio ≥1.0 were considered normal ratio patients (CLL^{NR}). Absolute counts for: (A) CD57$^+$, HLA-DR$^+$ or PD-1$^+$ cells in the CD4$^+$ compartment; (B) CD4$^+$HLA-DR$^+$PD-1$^+$ T-cells in the CD4$^+$ compartment. Pairwise statistical analysis (HD vs CLL) was performed using the non-parametric Mann-Whitney test. Significant results were included on the graph (* = p ≤0.05; ** = p ≤0.01; *** = p ≤0.001).

4.9. Relationship between $CD4^+$ and $CD8^+$ phenotypes

It is clear from the phenotypic analysis of the $CD4^+$ compartment that there are some similarities in the phenotypes present at higher frequencies in the CLL $CD4^+$ and $CD8^+$ compartments. The $CD8^+$ phenotype with the strongest prognostic relevance described in Chapter 3 (determined by multivariate analyses) was a senescent/activated phenotype $CD8^+CD57^+HLA\text{-}DR^+$, which was present at higher frequencies in the CLL^{IR} subgroup. $CD57^+HLA\text{-}DR^+$ T-cell frequencies were also increased in the $CD4^+$ T-cell compartment of CLL patients, and were exacerbated in the CLL^{IR} subgroup. Correlation analyses were used to compare $CD57^+HLA\text{-}DR^+$ frequencies in the $CD8^+$ and $CD4^+$ compartments and determine any potential relationship. As shown in Figure 4.20A, there was a significant positive relationship between $CD8^+CD57^+HLA\text{-}DR^+$ and $CD4^+CD57^+HLA\text{-}DR^+$ ($r = 0.7211$, $p < 0.0001$).

As $CD4^+HLA\text{-}DR^+PD\text{-}1^+$ was deemed the most prognostically relevant phenotype from the $CD4^+$ T-cell compartment, correlation analysis was performed to compare any association with the prognostic $CD8^+$ phenotype $CD8^+CD57^+HLA\text{-}DR^+$. There was a strong, positive relationship between $CD8^+CD57^+HLA\text{-}DR^+$ and $CD4^+HLA\text{-}DR^+PD\text{-}1^+$ ($r = 0.7684$, $p < 0.0001$; Figure 4.20B). The significant association of these phenotypes between the $CD4^+$ and $CD8^+$ compartments, together with their increased frequency in CLL^{IR} patients, suggests a connection between certain $CD4^+$ T-cell phenotypes with the expansion of the $CD8^+$ T-cell compartment and the inversion of the CD4:CD8 ratio.

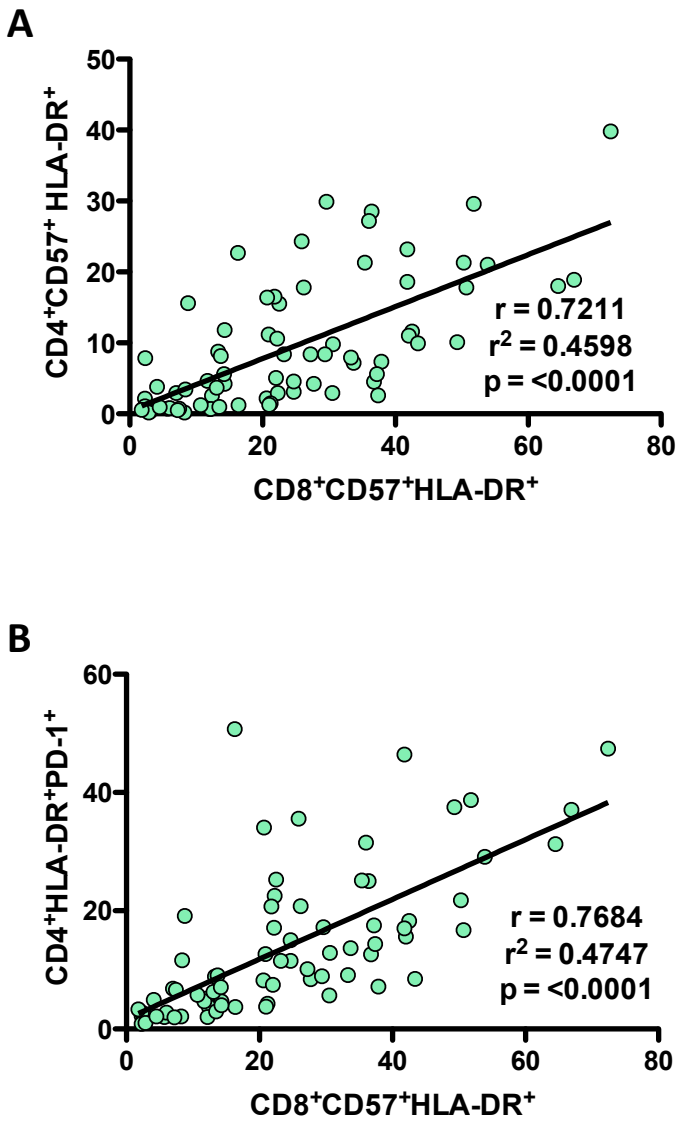

Figure 4.20. Correlation between CD4 phenotypes and $CD8^+CD57^+HLA\text{-}DR^+$ in CLL patients (n = 74). Cells were collected using flow cytometry (FACS CantoII, BD FACSDiva) and analysed with FlowJo (v.9) using gating as described in Figure 4.1. Correlation of (A) $CD8^+CD57^+HLA\text{-}DR^+$ versus $CD4^+CD57^+HLA\text{-}DR^+$, and (B) $CD8^+CD57^+HLA\text{-}DR^+$ versus $CD4^+HLA\text{-}DR^+PD\text{-}1^+$. Linear regression and Spearman's correlation coefficient were performed using GraphPad Prism 5.0.

4.10. Discussion

The aim of this chapter was to further explore the phenotypic composition of the $CD4^+$ T-cell compartment of CLL patients. This included analysing phenotypic differences between CLL patients with an inverted CD4:CD8 ratio (CLL^{IR}) and CLL patients presenting a 'normal' T-cell ratio (CLL^{NR}). The original focus of this thesis was the $CD8^+$ T-cell compartment, based on a previous study demonstrating inferior clinical prognosis in patients with expanded $CD8^+$ T cell populations. However, multivariate analyses revealed that a $CD4^+$ phenotype had a greater effect on prognosis in CLL patients. Previous studies have demonstrated an increase in absolute numbers and phenotypic alterations within the $CD4^+$ T-cell compartment in CLL (Görgün et al. 2005; Monserrat et al. 2013; Os et al. 2013). Taken together, this suggested that phenotypic analysis of $CD4^+$ T-cells in the current study was warranted.

In line with previous work (Nunes et al. 2012), preliminary counts revealed that the number of $CD4^+$ T-cells were not significantly different between the CLL^{IR} and CLL^{NR} patients, supporting that the inversion of ratio is due to a preferential expansion within the $CD8^+$ T-cell compartment. However, it is clear from the phenotypic overview that although the numeric size of the $CD4^+$ compartment did not change between CLL^{NR} and CLL^{IR} patients, there are significant phenotypic differences between the two subgroups and age-matched health donors. Therefore, this study identified differences within the $CD4^+$ T-cell compartment that are CLL-specific and not due to immunological aging, including further phenotypic aberrations in the CLL^{IR} subgroup.

$CD4^+$ T-cell memory subset distribution in CLL patients was skewed to a more differentiated phenotype, and showed significant differences between healthy donors and both the total and stratified CLL cohorts. A reduction in naïve and increase in the EM subsets was observed in both the $CD8^+$ and $CD4^+$ T-cell compartments of CLL; this shift was more dramatic within the CLL^{IR} cohort. This showed that, as previously observed with $CD8^+$ T-cells, $CD4^+$ T-cell memory within the CLL^{IR} group skewed towards a more differentiated effector memory phenotype compared to CLL^{NR} patients and healthy donors. This also supports the previous work of Nunes et. al (2012) who reported a similar shift in memory subset compositions. There is a known age-associated skewing to more differentiated memory in $CD4^+$, but this is normally characterised by a reduction in naïve and age-related increase in $CD4^+$ EMRA T-cells (Koch et al. 2008). The skewing observed in this study differs in that it is the EM compartment that sees the

relative increase. Age related effects were controlled for by using age-matched healthy donors.

Unlike $CD8^+$ T-cells, little to no inflation of CMV-specific $CD4^+$ T-cells has been observed within the $CD4^+$ T-cell pool (Kim et al. 2015; Klenerman and Oxenius 2016); however, CMV-specific $CD4^+$ T-cells do appear to accumulate with age and display a highly differentiated memory phenotype (Pourgheysari et al. 2007). Previous work has shown increased proportions of CMV-specific $CD4^+$ T-cells in CLL compared to controls (11% versus 4.7%), with higher frequencies observed with advanced disease (Pourgheysari et al. 2010). Also, the CMV^+ CLL patients had higher $CD4^+CD57^+$ T-cells compared to the CMV^+ healthy donors (Pourgheysari et al. 2010): however, as this was observed in the $CD4^+$ population as a whole, and not the CMV-specific $CD4^+$ population, it cannot be explicitly asserted that this is CMV driven. This study saw no association between CMV and CD4:CD8 ratio (see previous Chapter), and no significant difference in the distribution of $CD4^+$ memory T-cell subsets between CMV seropositive and CMV seronegative patients. Again similar to the $CD8^+$ results in the previous Chapter, the $CD4^+$ memory subset composition in this study skewed heavily to the EM population, rather than an EMRA skew that one would expect if the memory distribution was CMV-driven. This implies that the $CD4^+$ memory skewing (and the phenotypes that accumulate within the CLL^{IR} subgroup) is not caused by CMV persistence. This includes $CD4^+$HLA-DR^+PD-1^+, as the accumulation of this prognostic phenotype appears to originate within the EM compartment. Unfortunately, the number of CMV^- patients in this cohort was limited, and direct analysis of any association between CMV seropositivity and the $CD4^+$HLA-DR^+PD-1^+ could not be performed. Future work with a larger cohort of CMV^- individuals would help confirm that CMV seropositivity is not a confounding factor.

$CD4^+$ memory subset skewing has been associated with other prognostic factors of CLL. Patients stratified by *IGHV* mutational status revealed that CLL patients with unmutated *IGHV* (inferior prognosis group), had a reduction in $CD4^+$ naïve T-cells and a significant increase in CM/EM T-cells (Tinhofer et al. 2009). In another study, Zap-70^+ CLL patients also demonstrated this skewing from naïve to EM $CD4^+$ T-cells compared to the Zap-70^- CLL patients (Monserrat et al. 2013). It is clear therefore that the distribution of subsets within the $CD4^+$ memory compartment is associated with prognosis.

Further supporting the shift to more differentiated $CD4^+$ T-cells was the increase in the single CD57 and PD-1 frequencies within the CD4 compartment of CLL patients, as well as the increase in double positive $CD57^+PD\text{-}1^+$ cells. These phenotypes appeared to be predominantly derived from the $CD4^+$ EM compartment and were further enriched in the CLL^{IR} patients. This implies that there was an increased proportion of differentiated $CD4^+$ T-cells in the patients with preferentially expanded $CD8^+$ T-cell populations. These results were again in line with previous work from our research group that demonstrated higher $CD4^+CD57^+CD27^-CD28^-$ EM cells in CLL patients, particularly CLL^{IR} patients (Nunes et al. 2012). However, it is worth noting that in the previous study the average frequency of $CD57^+CD27^-CD28^-$ EM in CLL^{IR} patients was much lower (approximately 5% for the total CLL cohort and 7% for CLL^{IR} subgroup). The mean $CD57^+$ EM frequencies observed in this study were 12.1% for total CLL cohort and 18.9% for CLL^{IR} subgroup. It is possible that this disparity in $CD57^+$ expression is due to differences in the patient cohorts studied. Alternatively, it may be due to the different phenotypes defined in each study. It is possible that there are CD57 sub-phenotypes beyond the conventional replicative senescent phenotype: $CD57^+CD27^-CD28^-$. Future work using expanded flow cytometry panels to include CD27 and CD28 would help confirm this hypothesis.

As naïve T-cells are known to express CD127 (A. Ma et al. 2006; Mahnke et al. 2013), it would be expected that the reduction in the naïve subset would be synonymous with a reduction of $CD4^+CD127^+$ T-cells. This proved to be the case in this study and was associated with inverted ratio. Interestingly, this study also identified a novel reduction in naïve $CD4^+CD38^+$ frequency, particularly in the CLL^{IR} subgroup. Moreover, we investigated whether presentation of these markers were linked and found that there was indeed a strong positive correlation between CD38 and CD127 within the naïve compartment of CLL patients, and $CD4^+CD38^+CD127^+$ naïve T-cells were also greatly reduced compared to healthy donors, more so in CLL^{IR} patients. Due to the inclusion of age-matched controls, this reduction appears to be independent of age. Additionally, previous work has shown that in older patients the reduction in naïve cells is accompanied by higher proportions of senescent naïve $CD4^+CD57^+$ and activated naïve $CD4^+HLA\text{-}DR^+CD38^+$ phenotypes (Ferrando-Martínez et al. 2011). Due to antibody panel constraints CD38 and HLA-DR were on separate phenotyping panels, so co-expression could not be investigated, however, no change in $CD4^+$ naive $HLA\text{-}DR^+$ frequency was observed. Post-hoc correlation analysis showed that there was no

relationship between CD38 and HLA-DR frequencies within the $CD4^+$ naïve compartment (Appendix VII). Although the multivariate analyses did not demonstrate a significant prognostic effect of these phenotypes in the naïve compartment, overall $CD4^+CD127^+$ and $CD4^+CD38^+CD127^+$ were shown to be contributing co-variables associated with PFS (Appendix IV). This suggests that the reduction in naïve $CD4^+CD38^+CD127^+$ may be linked to CLL pathology. An additional factor to take into account is whether the naïve population represents a Treg population, as resting Tregs can present a similar $CCR7^+CD45RO^-$ phenotype (Rosenblum et al. 2015). Furthermore, no significant difference in absolute numbers of naïve $CD4^+$ T-cells between CLL^{NR} and CLL^{IR} patients could suggest that the reduced $CD127^+$ population is actually due to a shift towards $CD127^-$ within the $CD4^+$ naïve subset, a phenotype associated with Tregs (Banham 2006; Seddiki et al. 2006). However, it may be that the preliminary counts in this study were not powered enough to identify significant trends; expanded absolute count studies would address this. The inclusion of additional markers that characterise Treg cells such as CD25 and FoxP3 and would also help determine whether populations within the $CCR7^+CD45RO^-$ are truly naïve.

Following exploration of senescence/exhaustion markers, we then investigated activation in CLL $CD4^+$ T-cells using CD38 and HLA-DR as markers for activation. HLA-DR was shown to be the activation marker with most relevance in the CLL cohort, particularly in the CLL^{IR} patients: these patients had significantly higher frequencies that appeared to be driven from the EM subset. Furthermore, this study observed an increased co-expression of $CD57^+HLA\text{-}DR^+$, confirming the presence of a differentiated T cell phenotype that might be activated in response to unknown stimuli.

The increase in $PD\text{-}1^+$ within the $CD4^+$ compartment of CLL^{IR} patients is an interesting contrast to the $CD8^+$ compartment (Chapter 3), where higher frequencies of $CD8^+PD\text{-}1^+$ and $CD8^+CD57^+PD\text{-}1^+$ were only observed in the CLL cohort as a whole, with no difference between CLL^{NR} and CLL^{IR} patients. Lack of exacerbated $CD8^+PD\text{-}1^+$ in CLL^{IR} patients would suggest that the $CD8^+PD\text{-}1^+$ subset is not associated with the expanded $CD8^+$ T-cells. However, there is an increased frequency of $PD\text{-}1^+$ T-cells in the $CD4^+$ compartment of CLL patients that is associated with the inverted ratio.

Interestingly, further exploration of PD-1 with the activation marker HLA-DR revealed that there was a significantly higher proportion of $CD4^+$ T-cells co-expressing these

markers, particularly in CLL^{IR} patients. No significant effect was observed in absolute counts, but there did appear to be a trend in higher $CD4^+HLA\text{-}DR^+PD\text{-}1^+$ cell numbers in CLL^{IR} patients. As the absolute counts were preliminary and only included a small cohort of patients, an expanded analysis using a larger cohort such as that used in the phenotyping study (74 patients) would be better powered to identify changes in the phenotype cell numbers. Additionally, absolute counts of age-matched healthy donors will help distinguish CLL-specific changes.

The multivariate analyses performed on this CLL cohort determined that overall, $CD4^+HLA\text{-}DR^+PD\text{-}1^+$ had the strongest effect on prognosis. Survival analyses showed that patients with more than 14.4% $CD4^+HLAD\text{-}DR^+PD\text{-}1^+$ cells demonstrated much poorer prognosis. Furthermore, the patients in this cohort possessing the lowest $CD4^+HLA\text{-}DR^+PD\text{-}1^+$ (around 5% or less) had no reduction in survival, further demonstrating that increased presence of this phenotype related to poorer prognosis in CLL. Supporting this, the age-matched healthy donors analysed in this study had an average of 3.4% $CD4^+HLA\text{-}DR^+PD\text{-}1^+$ (ranging between 0.9-6.9%). Higher numbers of $CD4^+PD\text{-}1^+$ T-cells have previously been linked to poorer prognosis in newly diagnosed CLL patients (Rusak et al. 2015); the $CD4^+HLA\text{-}DR^+PD\text{-}1^+$ phenotype identified in this study could be further characterisation of a prognostic phenotype within the $CD4^+PD\text{-}1^+$ population. $CD4^+PD\text{-}1^+$ in HIV patients in early (<6 months after infection) versus delayed (≥2 years after infection) treatment revealed that PD-1 levels increased in patients who delayed therapy, and PD-1 levels decreased to similar levels in both subgroups following one year of anti-retroviral treatment. Adding to this, $CD4^+PD\text{-}1^+$ was significantly associated with $CD4^+CD38^+HLA\text{-}DR^+$ activation (Cockerham et al. 2014). That this phenotype was also higher in CLL^{IR} patients demonstrated that there is possibly some relationship between these $CD4^+$ phenotypes and the changes in the $CD8^+$ compartment relating to CD4:CD8 ratio. Previous studies in HIV identified significant correlation between CD4:CD8 ratio and an 'early differentiated' $CD4^+$ EM population that expressed various markers, including HLA-DR and PD-1 (Buggert et al. 2014).

It has been previously documented that PD-1 is upregulated on activated T-cells and performs negative feedback to the cell after engagement with it's ligand PD-L1 (Chikuma 2016). Increased PD-1 with activation markers has been linked to chronic stimulation in HIV (Cockerham et al. 2014). A subset of $CD4^+PD\text{-}1^{high}$ T-cells has been

identified in follicular lymphoma (Yang et al. 2015). These $CD4^+$ T-cells were mainly located in the lymph node tumour microenvironment, with a follicular helper T-cell phenotype, and supported B-cell growth. It is possible that there is a similar situation in CLL where $CD4^+$ T-cells may be responding to chronic antigenic stimulation within the tumour microenvironment and supporting the B-CLL cells, thereby helping to drive the disease. Previous work demonstrating CLL-specific Th cells that can be activated by CLL cells, and in turn directly interact with the CLL cells to drive CLL cell activation and proliferation, supports this (Os et al. 2013). PD-1 ligand (PD-1L) has been found in higher frequencies on both B- and T-cells of CLL patients, and $CD4^+PD\text{-}1^+$ cells have been found in close proximity to B-CLL cells within the lymph node (Brusa et al. 2013). Furthermore, in addition to T-B interactions between the $CD4^+$ T-cells and CLL cells, $CD4^+$ T-cell:$CD8^+$ T-cell interaction may mean that CLL-specific $CD4^+$ T-cells could also be promoting the $CD8^+$ T-cell expansion, and vice versa. This is supported by the positive relationship identified between $CD4^+$ and $CD8^+$ T-cells with an 'activated senescent' phenotype $CD57^+HLA\text{-}DR^+$, as well as $CD4^+HLA\text{-}DR^+PD\text{-}1^+$ with $CD8^+CD57^+HLA\text{-}DR^+$, both of which have a link to CLL prognosis. Functional analyses to directly establish the proliferative capacity and responsiveness of $CD4^+HLA\text{-}DR^+PD\text{-}1^+$ T-cells from CLL patients, with and without autologous B-CLL cells and $CD8^+$ T-cells, would gain further insight into the interlinking relationship between these immune cells. Furthermore, it could be suggested that the $CD8^+$ expansion is being suppressed, preventing a successful response against tumour cells. This immunosuppression could be directly from the CLL cells themselves, or possibly from Tregs, which are present in higher frequencies in CLL patients compared to healthy donors and are associated with other poor prognostic markers (Aref et al. 2014).

As discussed in the previous chapter, the ability to look at the distribution of multiple markers in tandem was somewhat limited in this study, due to BD FACS Canto II restrictions that meant a maximum of 8 parameters could be applied. This could be viewed as being simplistic as several recent studies have demonstrated that the complex nature of T-cell memory subsets, with many new functionally and phenotypically distinct T-cell subsets being defined. Furthermore, $CD4^+$ T-cells can be divided into various subtypes with different immunological functions, such as Tfh cells and Tregs. Future analyses performed on flow cytometers with capacity to analyse a greater number of parameters (up to 36 markers) (Bendall et al. 2012) would allow tandem analysis of multiple T-cell activation/senescence markers, more precise definition of

naïve/effector/memory subsets, and also the inclusion of markers that further classify $CD4^+$ T-cell types.

As with the $CD8^+$ T-cell compartment in Chapter 3, the $CD4^+$ compartment demonstrates a dramatic shift to more differentiated phenotypes in CLL^{IR}. Initially this could be assumed to be a shift towards senescence/exhaustion; however, with a synonymous increase and co-expression with HLA-DR implies that this is potentially a shift towards a differentiated, activated phenotype mainly originating from the EM compartment. Of particular relevance is the identification of the prognostically relevant phenotype in $CD4^+HLA\text{-}DR^+PD\text{-}1^+$, which has potential applications within the clinical setting to identify CLL patients who are more at risk of progressive disease or disease relapse. This phenotype needs to be further explored in additional CLL cohorts with patients of varying disease stage and treatment. The potential of $CD4^+HLA\text{-}DR^+PD\text{-}1^+$ in treated patients is explored more in the following chapter.

Chapter 5

Phenotypic analysis of treated CLL patients

Abnormal T-cell profiles have been found to be of prognostic relevance in a range of diseases, including chronic viral diseases such as HIV and CMV (Buggert et al. 2014; Trautmann et al. 2006; Champagne et al. 2001; Pawelec and Gouttefangeas 2013), and cancers (L. Zhang et al. 2003; Sato et al. 2005; Woo et al. 2002; Nunes et al. 2012). Due to the heterogeneous nature of CLL, where patients can present with asymptomatic disease or progressive aggressive disease, being able to identify patients who are more at risk of disease progression may be useful for targeting patients who need more observation and earlier treatment. The usual method of treatment for newly diagnosed CLL patients is the 'watch and wait' approach, whereby treatment is only initiated upon disease progression (Zenz et al. 2010; Oscier et al. 2012). The ability to identify indolent patients from those with progressive disease could not only optimise treatment approaches, but also prevent the uncertainty faced by patients during the 'watch and wait' phase. Furthermore, it is possible that these prognostic factors could help predict responses to standard treatment, and identify patients who are more at risk of relapse.

Previous studies have characterised an array of T-cell abnormalities within CLL that are associated with inferior prognosis, including: lymphocyte count and inversion of the CD4:CD8 ratio (Gonzalez-Rodriguez et al. 2010; Nunes et al. 2012); T-cell CD38 status (Tinhofer et al. 2006); increased expression of markers for senescence and immunosuppression, such as CD57 (Serrano et al. 1997), PD-1 (Tinhofer et al. 2006; Gonzalez-Rodriguez et al. 2010; Nunes et al. 2012; Serrano et al. 1997; Novák et al. 2015). In addition to confirming the prognostic relevance of the CD4:CD8 ratio, this thesis highlights additional T-cell phenotypes that were strongly associated with inferior clinical prognosis in CLL, namely $CD4^+HLA\text{-}DR^+PD\text{-}1^+$ and $CD8^+CD57^+HLA\text{-}DR^+$ (See Chapters 3 and 4).

The aim of this chapter was to analyse a new cohort of CLL patients who had undergone treatment, to investigate the impact of treatment on the CD4:CD8 ratio and on more complex T-cell phenotypes. These were compared to untreated CLL patients in a cross-sectional analysis. An 8-colour flow cytometry panel was designed to focus on markers that were shown to have the most prognostic relevance in the preceding chapters

(Chapters 3 and 4: CD57, HLA-DR and PD-1 – see Chapter 2 for antibody panel). Where possible, longitudinal phenotypic assessment of individual patients was used to assess whether there were changes over time.

5.1. Immunophenotyping of untreated versus treated patients

The cohort analysed in this experiment included 19 treated and 23 untreated CLL patients. To give a more robust statistical analysis, phenotyping data from this 'treated' cohort was merged with the larger CLL cohort that was used in the phenotyping study from the earlier chapters (Chapters 3 and 4). If a patient was analysed more than once, any repeated analyses were removed, unless the patient's treated status had changed between sample collections (i.e. the patient was untreated at the first analysis, but had received treatment prior to the second analysis). This gave final patient numbers of 33 treated and 68 untreated patients.

5.1.1. CD4:CD8 ratio in treated CLL

CLL patients with an inverted CD4:CD8 ratio (CD4:CD8 ratio <1.0) have previously been shown to have poorer prognosis (Buggert et al. 2014; Nunes et al. 2012; Trautmann et al. 2006; Champagne et al. 2001; Pawelec and Gouttefangeas 2013). This finding was confirmed by the present study, which also used recursive partition analysis to show that the prognostic effect of CD4:CD8 ratio was most powerful with a cut-off value of 1.0. This suggests the hypothesis that inversion of the CD4:CD8 ratio in CLL patients leads to a more aggressive disease. Given that treated patients have, by definition, a more aggressive form of the disease (L. Zhang et al. 2003; Hallek et al. 2008; Sato et al. 2005; Woo et al. 2002; Nunes et al. 2012), it might be predicted that these patients would also have a lower CD4:CD8 ratio.

To test this, CLL patients were stratified into untreated and treated cohorts and phenotyped to determine the number of events within the $CD4^+$ and $CD8^+$ T-cells gates. From this the CD4:CD8 ratio was calculated. As seen in Figure 5.1A, the treated CLL group had a significantly lower CD4:CD8 ratio when compared to the untreated group ($p = 0.0002$), with untreated patients having a mean ratio of 2.8 (95% CI 1.97-3.63) and treated patients with a mean ratio of 1.1 (95% CI 0.77-1.40). In keeping with these findings, when stratified by normal (CD4:CD8 ratio ≥1.0; CLL^{NR}) and inverted ratio (CD4:CD8 ratio <1.0; CLL^{IR}), there was an increased proportion of treated patients displaying a CD4:CD8 inversion, 60.6% (20/33) in the treated subgroup versus 27.9%

(19/68) in the untreated subgroup. The frequency of inverted CD4:CD8 ratio in the treated and untreated populations was significantly different ($p = 0.0022$; Figure 5.1B).

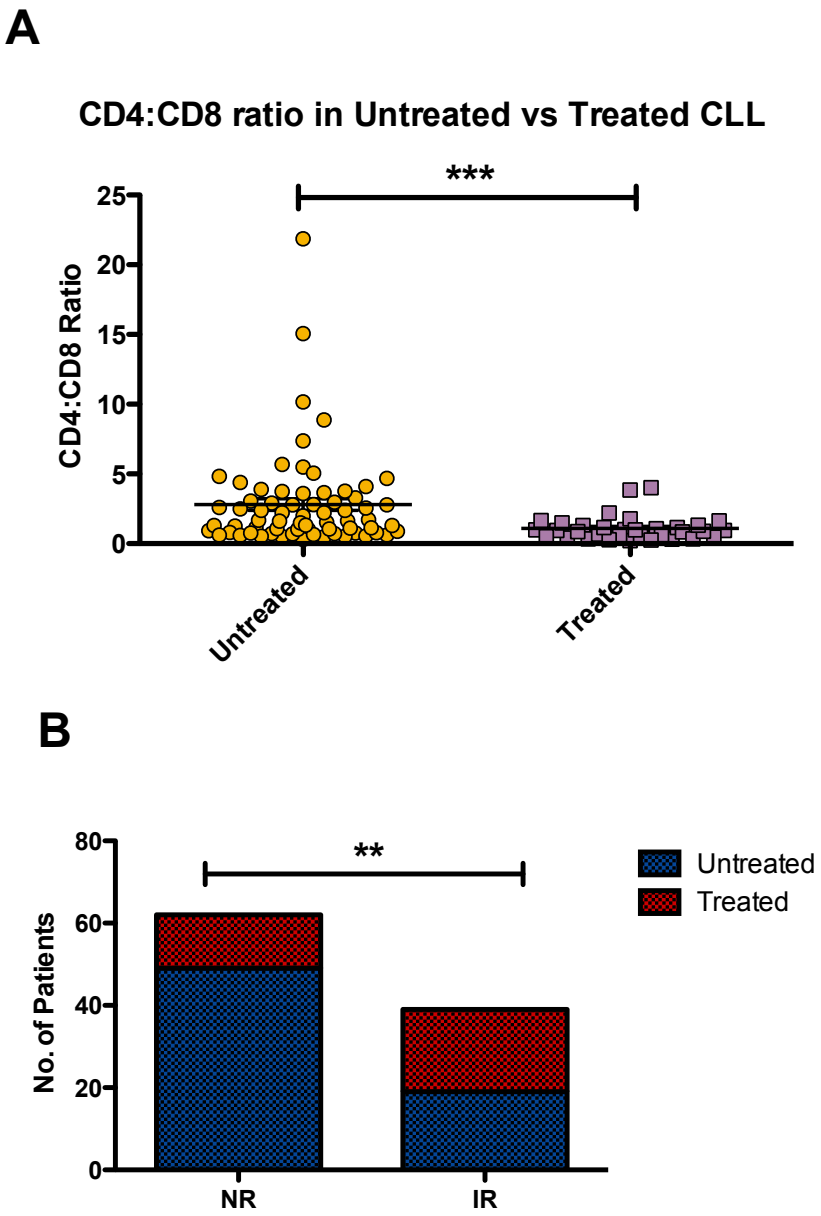

Figure 5.1. CD4:CD8 T-cell ratio in untreated (n = 68) and treated (n = 33) patients. CLL samples were collected using flow cytometry (FACS CantoII, BD FACSDiva) and analysed using FlowJo (v. 9). Lymphocytes were gated based on forward and side scatter profile; forward scatter area and height were used for exclusion of doublet cells. T-cells populations were identified by gating first on $CD3^+$ then either $CD4^+$ or $CD8^+$ cells. The number of events in $CD4^+$ and $CD8^+$ gates were used to calculate CD4:CD8 ratio. (A) CD4:CD8 ratio of CLL patients divided into untreated and treated subgroups. Mann-Whitney test was used to determine significance. (B) Patients were stratified further based on a normal (≥1.0, NR) and inverted (<1.0, IR) CD4:CD8 ratio to produce four subgroups: untreated NR (n = 49), treated NR (n = 13), untreated IR (n = 19) and treated IR (n = 20). Fisher's exact test was used for analysis (* = $p \leq 0.05$, ** = $p \leq 0.01$, *** = $p \leq 0.001$).

5.1.2. $CD8^+$ memory T-cell phenotypes in treated CLL

Work presented in the previous chapters showed a skewing of memory T-cell subsets in both the $CD8^+$ and $CD4^+$ T-cell compartments relative to age-matched controls. For the $CD8^+$ T-cell compartment, there was a reduction in the percentage of naïve T-cells ($p < 0.0001$) and an increase in the percentage of EM T-cells ($p = 0.0087$). The $CD8^+$ T-cells were also analysed for the phenotypic markers that were identified in Chapter 3 as having prognostic potential.

Initially, immunophenotyping of the $CD8^+$ T-cells was performed to analyse the distribution of T-cell memory subsets (Figure 5.2). When patients were divided based on treatment status, the treated subgroup had significantly reduced $CD8^+$ naïve T-cell frequencies when compared to the untreated group ($p < 0.0001$) alongside an expanded proportion of $CD8^+$ EM T-cells ($p = 0.0115$). These results mirror those seen when comparing the untreated CLL patients with age-matched healthy donors (Chapter 3), suggesting that treated patients exaggerate this skewed phenotype. However, no significant change in the $CD8^+$ EMRA subset was observed ($p = 0.2280$), implying that treatment does not increase the proportion of highly differentiated EMRA T-cells that are associated with T-cell exhaustion and senescence.

CD57, HLA-DR and PD-1 were identified in earlier chapters as T-cell markers that contribute to the prognosis of CLL patients (in Boolean combinations). Interestingly, CD57 and PD-1 single marker frequencies within the $CD8^+$ compartment did not differ between untreated and treated patients (Figure 5.3A). The activation marker HLA-DR, however, was more prevalent on $CD8^+$ T-cells within the treated subgroup ($p = 0.0003$), implying an increased proportion of activated $CD8^+$ T-cells in CLL patients who have undergone treatment.

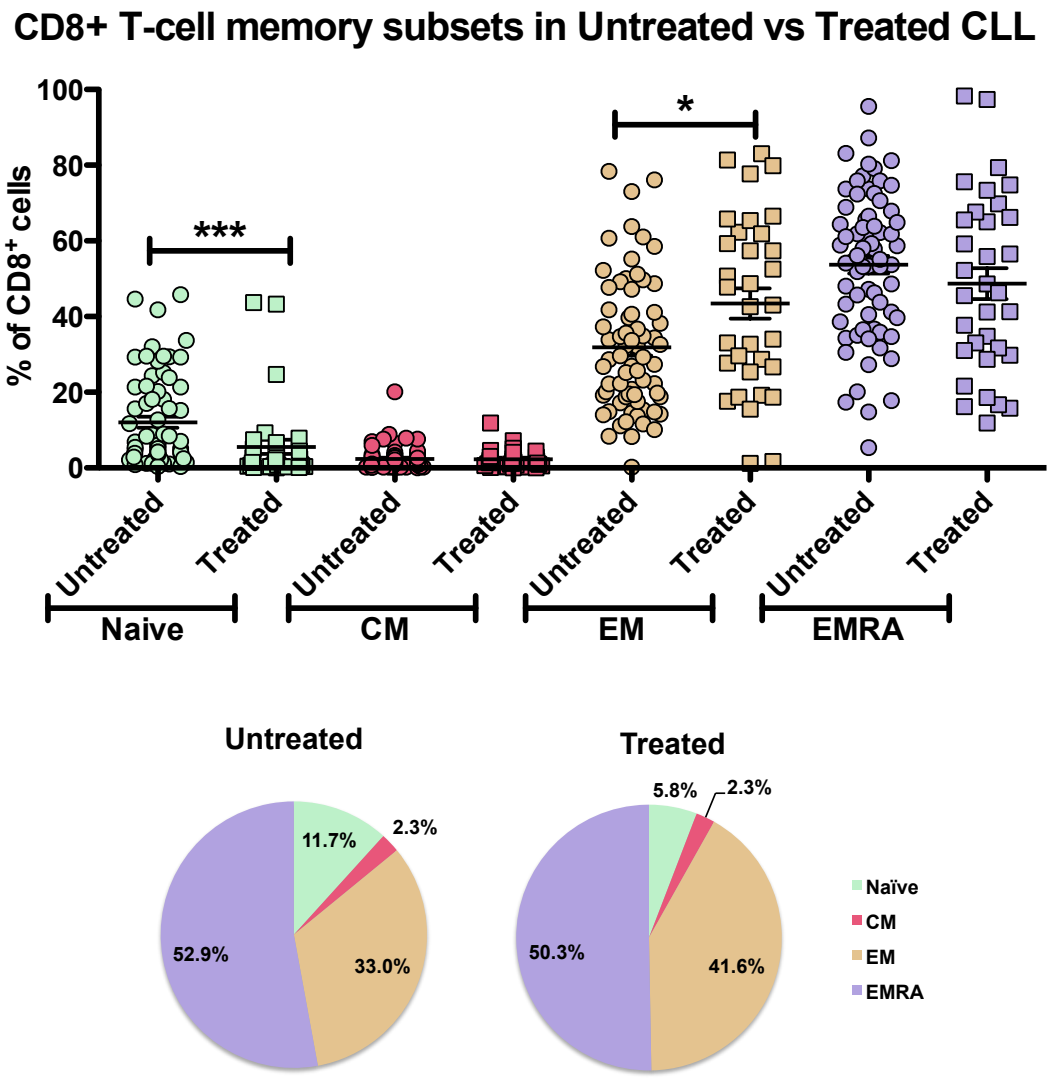

Figure 5.2. CD8⁺ T-cell memory subsets in untreated (n = 68) and treated (n = 33) CLL patients. Cells were collected using flow cytometry (FACS CantoII, BD FACSDiva) and analysed using FlowJo (v.9). Lymphocytes were gated based on forward and side scatter profile; forward scatter area and height were used for exclusion of doublet cells. $CD8^+$ T-cells were identified by gating on $CD3^+$ and then $CD8^+$ cells. Memory subsets were defined using CCR7 and CD45RO memory markers: naïve ($CCR7^+CD45RO^-$), Central Memory (CM, $CCR7^+CD45RO^+$), Effector Memory (EM, $CCR7^-CD45RO^+$) and EMRA ($CCR7^-CD45RO^-$). Pairwise statistical analysis (HD vs CLL) was performed using the non-parametric Mann-Whitney test. Significant results were included on the graph (* = $p \leq 0.05$; ** = $p \leq 0.01$; *** = $p \leq 0.001$).

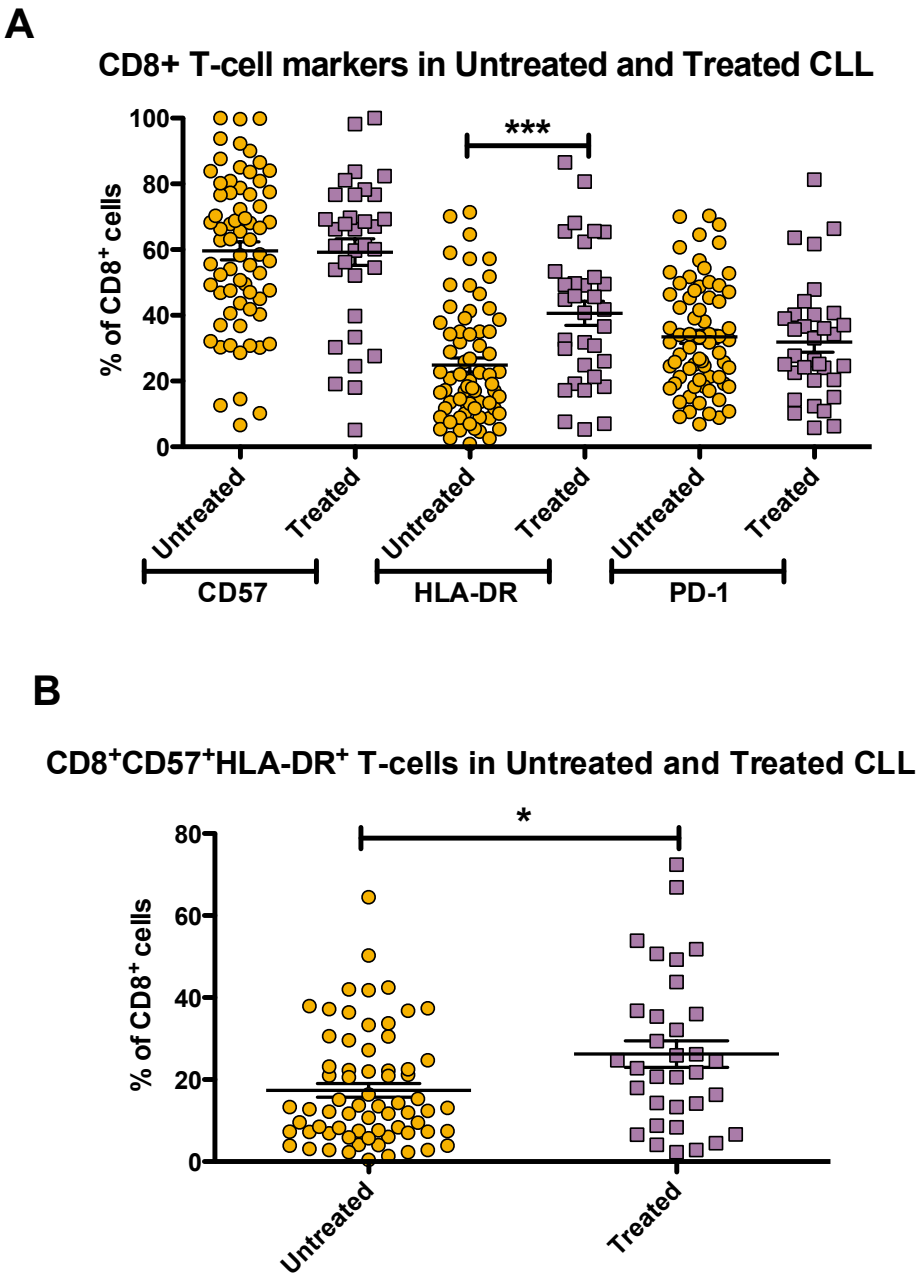

Figure 5.3. Frequency of $CD8^+$ T-cell phenotypes in untreated (n = 68) and treated (n = 33) CLL patients. Cells were collected using flow cytometry (FACS CantoII, BD FACSDiva) and analysed using FlowJo (v.9). Lymphocytes were gated based on forward and side scatter profile; forward scatter area and height were used for exclusion of doublet cells. $CD8^+$ T-cells were identified by gating first on $CD3^+$ then $CD8^+$ cells. (A) $CD57^+$, $HLA\text{-}DR^+$ and $PD\text{-}1^+$ single frequencies within the $CD8^+$ compartment of untreated and treated patients. (B) $CD57^+HLA\text{-}DR^+$ frequency of $CD8^+$ T-cells was shown to be of prognostic relevance in Chapter 3, and so frequency of $CD8^+CD57^+HLA\text{-}DR^+$ T-cells untreated and treated CLL patients is shown. Pairwise statistical analysis (HD vs CLL) was performed using the non-parametric Mann-Whitney test. Significant results were included on the graph (* = $p \leq 0.05$; ** = $p \leq 0.01$; *** = $p \leq 0.001$).

Previous multivariate analysis gave $CD8^+CD57^+HLA\text{-}DR^+$ as the $CD8^+$ phenotype with the most prognostic potential from within the $CD8^+$ compartment (Chapter 3). Here, $CD8^+CD57^+HLA\text{-}DR^+$ T-cell frequencies were higher in the treated subgroup ($p = 0.0211$, Figure 5.3B). Additional multivariate and survival analyses performed in Chapter 3 identified an optimal prognostic cut-off for this variable of 25%. To identify whether this prognostic threshold had any link with treatment, patients were stratified based on $CD8^+CD57^+HLA\text{-}DR^+$ frequency of $<25\%$ or $\geq 25\%$ within the untreated or treated groups: 42.4% of the treated subgroup (14/33) were above this threshold, compared to 23.5% of untreated (16/68). Fisher's exact revealed no significant difference ($p = 0.0641$) between the distributions of patients with $<25\%$ or $\geq 25\%$ (Figure 5.4).

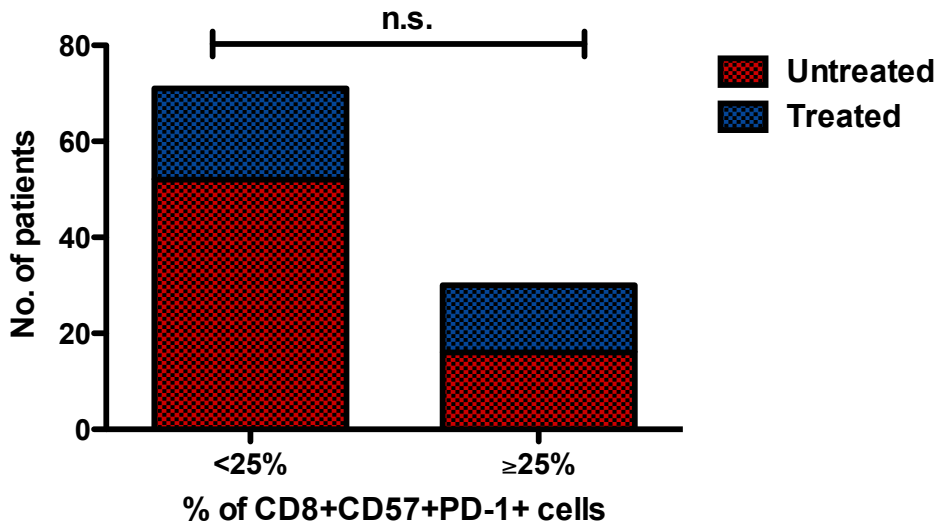

Figure 5.4. Distribution of untreated and treated patients and $CD8^+CD57^+HLA\text{-}DR^+$ frequency. Multivariate analyses performed in this thesis (Chapter 3) demonstrated $CD8^+CD57^+HLA\text{-}DR^+$ as the most prognostic $CD8^+$ phenotype within the study. Further analyses suggested an optimum cut-off approximately 25%, with patients who have 25% or more $CD8^+CD57^+HLA\text{-}DR^+$ having poorer prognosis. Untreated and treated patients were stratified based on this threshold to produce four subgroups: <25% untreated (n = 52), <25% treated (n = 19), ≥25% untreated (n = 16) and ≥25% treated (n = 14). Fisher's exact test was used for analysis. Significant results were included on the graph (* = $p \leq 0.05$; ** = $p \leq 0.01$; *** = $p \leq 0.001$).

5.1.3. $CD4^+$ memory T-cell phenotypes in treated CLL patients

Work in Chapter 4 demonstrated that the $CD4^+$ T-cell compartment of CLL patients is significantly enriched with memory T-cells and identified phenotypic subsets with potential prognostic value. Therefore, the distribution of $CD4^+$ memory subsets was also compared in the treated and untreated patient subgroups.

Looking at the $CD4^+$ T-cell memory subsets (Figure 5.5), a dramatic reduction (more than 4-fold) was observed in the $CD4^+$ naïve frequency in previously treated CLL patients compared to the untreated patient subgroup (9.7% versus 40.8%, $p < 0.0001$). Conversely, the treated subgroup had a significantly higher frequency of $CD4^+$ EM compared to the untreated patients ($p < 0.0001$). This was a similar pattern to that observed when comparing $CD4^+$ T-cell subsets between untreated CLL patients and age-matched healthy donors, suggesting that treatment is associated with depletion in the proportion of naïve T-cells and a relative increase in the proportion of EM T-cells. This pattern was also seen in the $CD8^+$ T-cell compartment in the previous section (5.1.2), suggesting that both the $CD4^+$ and $CD8^+$ T-cell compartments in CLL manifest similar changes in the distribution of T-cell subsets, which are more pronounced in the treated subgroup.

The expression of CD57, HLA-DR and PD-1 markers in different combinations in the $CD4^+$ compartment, were associated with the inverted CD4:CD8 ratio (Chapters 3 and 4). The proportions of T-cells expressing these markers in the $CD4^+$ T-cell compartment of treated CLL patients were all higher when compared to the untreated CLL patients (Figure 5.6A). There were significantly higher frequencies of $CD57^+$, HLA-DR^+ and PD-1^+ T-cells in the $CD4^+$ compartment of treated CLL patients ($p = 0.0004$, $p < 0.0001$ and $p < 0.0001$, respectively).

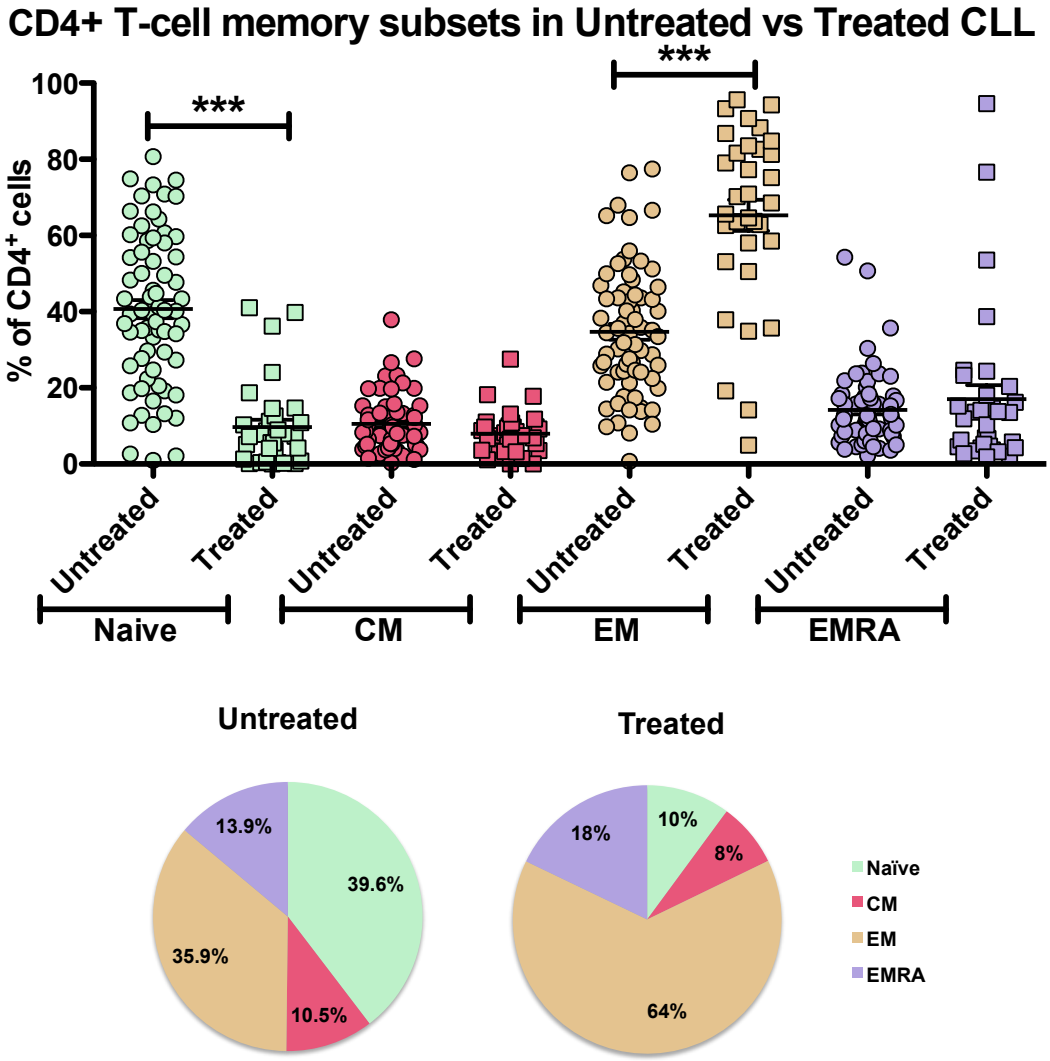

Figure 5.5. CD4⁺ T-cell memory subsets in untreated (n = 68) and treated (n = 33) CLL patients. Cells were collected using flow cytometry (FACS CantoII, BD FACSDiva) and analysed using FlowJo (v.9). Lymphocytes were gated based on forward and side scatter profile; forward scatter area and height were used for exclusion of doublet cells. $CD4^+$ T-cells were identified by gating on $CD3^+$ and then $CD4^+$ cells. Memory subsets were defined using CCR7 and CD45RO memory markers: naïve ($CCR7^+CD45RO^-$), Central Memory (CM, $CCR7^+CD45RO^+$), Effector Memory (EM, $CCR7^-CD45RO^+$) and EMRA ($CCR7^-CD45RO^-$). Pairwise statistical analysis (HD vs CLL) was performed using the non-parametric Mann-Whitney test. Significant results were included on the graph (* = $p \leq 0.05$; ** = $p \leq 0.01$; *** = $p \leq 0.001$).

The multivariate analyses described in Chapter 4 demonstrated that $CD4^+HLA\text{-}DR^+PD\text{-}1^+$ was not only the most prognostically significant $CD4^+$ phenotype in CLL patients, but was also the strongest phenotype of all the parameters analysed. This phenotype was therefore investigated in relation to treatment status (Figure 5.6B). The median $CD4^+HLA\text{-}DR^+PD\text{-}1^+$ T-cell frequency was more than 2-fold higher in the treated subgroup when compared with the untreated subgroup (20.3% versus 7.9%, $p = <0.0001$). Using the optimal $CD4^+HLA\text{-}DR^+PD\text{-}1^+$ prognostic cut-off of 15% (identified in Chapter 4), treated and untreated patients were stratified based on this indicator. 57.1% (19/33) of treated patients had ≥15% $CD4^+HLA\text{-}DR^+PD\text{-}1^+$ T-cells, associated with an inferior prognosis, versus 16.2% (11/68) in the untreated group. Fisher's exact test, based on this stratification, supported a significant bias of patients within the treated subgroup possessing ≥15% $CD4^+HLA\text{-}DR^+PD\text{-}1^+$ ($p <0.0001$, Figure 5.7).

The multivariate analyses in Chapter 4 also revealed that patients who had <5% of $HLA\text{-}DR^+PD\text{-}1^+$ within the $CD4^+$ compartment uniformly showed no disease progression: 47.1% (32/68) of untreated patients fell within this category, versus only 18.2% (6/33) of treated patients ($p = 0.0080$, Figure 5.7B). Conversely, results from the multivariate suggested that the CLL patients with $CD4^+HLA\text{-}DR^+PD\text{-}1^+$ frequencies above 31.5% had the poorest prognosis, although patient numbers within this cohort were relatively small. Only the treated population contained patients with $CD4^+HLA\text{-}DR^+PD\text{-}1^+$ frequencies above the 31.5% threshold (9/33 treated patients; 27.3%), suggesting significant skewing of $CD4^+HLA\text{-}DR^+PD\text{-}1^+$ within the treated subset ($p <0.0001$, Figure 5.7C). Taken together, these results show that patients with higher levels of the prognostic $CD4^+HLA\text{-}DR^+PD\text{-}1^+$ are disproportionately represented in the treated subgroup, suggesting a potential link between the $CD4^+HLA\text{-}DR^+PD\text{-}1^+$ phenotype and patients who undergo treatment.

These results give potential that the $CD4^+HLA\text{-}DR^+PD\text{-}1^+$ phenotype bears some association with patients who are treated and untreated: more specifically, higher $CD4^+HLA\text{-}DR^+PD\text{-}1^+$ frequencies that are congruent with poorer prognosis appear to be more prevalent in the treated subgroup. However, it is uncertain whether having increased frequencies of this phenotype is indicative of patients who have poorer prognosis and require treatment, or that the patients with poorer prognosis receive treatment that then results in the higher $CD4^+HLA\text{-}DR^+PD\text{-}1^+$ frequencies.

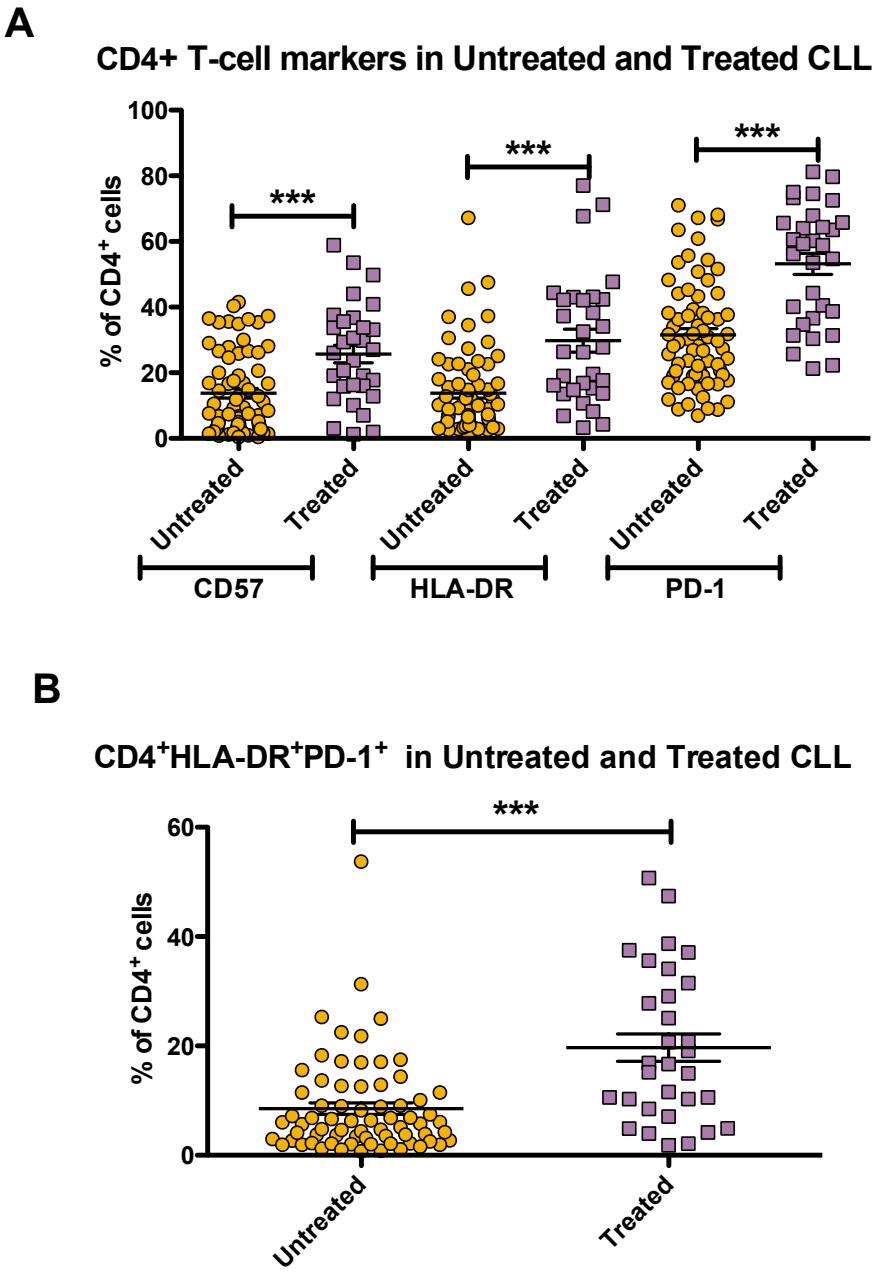

Figure 5.6. Frequency of $CD4^+$ T-cell phenotypes in untreated (n = 68) and treated (n = 33) CLL patients. Cells were collected using flow cytometry (FACS CantoII, BD FACSDiva) and analysed using FlowJo (v.9). Lymphocytes were gated based on forward and side scatter profile; forward scatter area and height were used for exclusion of doublet cells. $CD4^+$ T-cells were identified by gating first on $CD3^+$ then $CD4^+$ cells. (A) $CD57^+$, $HLA\text{-}DR^+$ and $PD\text{-}1^+$ single frequencies within the $CD8^+$ compartment of untreated and treated patients. (B) $HLA\text{-}DR^+PD\text{-}1^+$ frequency of $CD4^+$ T-cells was shown to be of prognostic relevance in Chapter 4 and to be the strongest prognostic marker to arise from that study, and so frequency of $CD4^+HLA\text{-}DR^+PD\text{-}1^+$ T-cells Untreated and Treated CLL patients is shown. Pairwise statistical analysis (HD vs CLL) was performed using the non-parametric Mann-Whitney test. Significant results were included on the graph (* = $p \leq 0.05$; ** = $p \leq 0.01$; *** = $p \leq 0.001$).

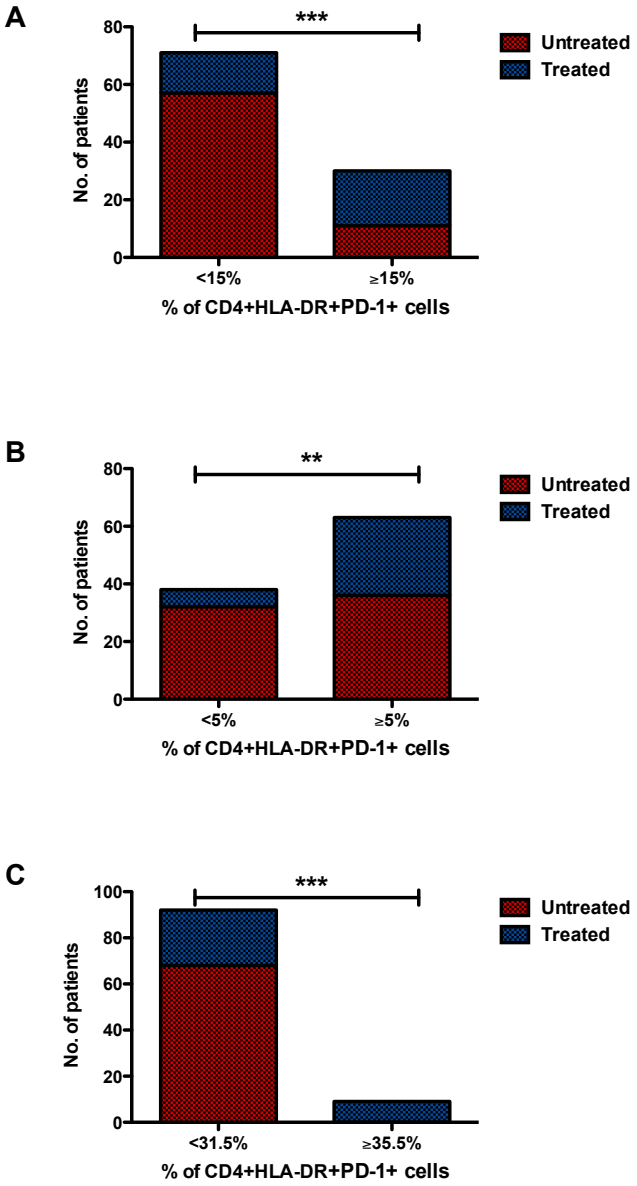

Figure 5.7. Distribution of untreated and treated patients and $CD4^+HLA\text{-}DR^+PD\text{-}1^+$ frequency. Multivariate analyses performed in this thesis (Chapter 3) demonstrated $CD4^+HLA\text{-}DR^+PD\text{-}1^+$ as the most prognostic $CD4^+$ phenotype within the study, and the strongest prognostic variable overall: further analyses suggested optimum prognostic thresholds. Untreated and treated patients were stratified into four subgroups based on these thresholds. (A) Stratification based on a threshold of 15% $CD4^+HLA\text{-}DR^+PD\text{-}1^+$ (<15% untreated [n = 57], <15% treated [n = 14], ≥15% untreated [n = 11] and ≥15% treated [n = 19]). (B) Stratification based on a threshold of 5% $CD4^+HLA\text{-}DR^+PD\text{-}1^+$ (<5% untreated [n = 32], <5% treated [n = 6], ≥5% untreated [n = 36] and ≥5% treated [n = 27]). (A) Stratification based on a threshold of 31.5% $CD4^+HLA\text{-}DR^+PD\text{-}1^+$ (<31.5% untreated [n = 68], <31.5% treated [n = 24], ≥31.5% untreated [n = 0] and ≥31.5% treated [n = 9]). Fisher's exact test was used for analysis. Significant results were included on the graph (* = p ≤0.05; ** = p ≤0.01; *** = p ≤0.001).

5.2. Longitudinal observations of treated and untreated CLL patients

During the immunophenotypic analysis of treated patients, where possible, repeat sampling was performed with the aim of determining: a) whether the prognostic phenotypes changed over time, including during/after treatment, b) whether the prognostic markers were unchanged after treatment and c) whether the prognostic phenotypes were transient and reverted upon disease relapse. Longitudinal samples obtained at several time points were obtained for 9 treated and 6 untreated patients (Figure 5.8 and Figure 5.9). If data had been collected from the same patients as part of the main immunophenotyping study (Chapters 3 and 4), they were also included as additional data points. Due to the limited patient numbers, varying treatment regimens and inconsistent time intervals, analyses of the total cohort was not performed. However, the data collected was examined on an individual patient basis to look for potential trends. Since CD4:CD8 ratio, $CD4^+$HLA-$DR^+$$PD\text{-}1^+$ and $CD8^+CD57^+$HLA-DR^+ were previously identified (Chapters 3 and 4) as having potential prognostic value, the analysis focussed on these phenotypes at the different time points, and where available, the specific treatment received by the patient recorded.

CD4:CD8 ratio status changed in 2/9 treated patients: Patient 8 changed from inverted (0.86) to a normal ratio of 1.23 prior to treatment, whereas Patient 9 had an initial ratio of 4.84 that became inverted (0.54) 20 months after treatment. A decrease in $CD4^+$HLA-$DR^+$$PD\text{-}1^+$ frequency was observed following treatment in five of the treated patients (Patients 1-3, 5 and 6) and remained consistent in three others (Patient 4, 7 and 9). The frequency of $CD8^+CD57^+$HLA-DR^+ also reduced following treatment (Patients 1, 3, 5, 6, 7 and 9) or remained constant (Patients 2 and 4). In Patient 8 both $CD4^+$HLA-$DR^+$$PD\text{-}1^+$ and $CD8^+CD57^+$HLA-DR^+ and ratio increase over a single month, prior to treatment initiation.

CD4:CD8 ratio appeared consistent across the time points for 3/6 untreated patients (Patient 2, 3 and 6); 2 patients retained a normal ratio despite showing either an increase (Patient 5) or a decrease (Patient 1) over time. 1 patient observed a change in ratio status, from inverted (0.73) to normal (2.87 and 3.74). The frequency of $CD4^+$HLA-$DR^+$$PD\text{-}1^+$ changed very little across the time points in most patients, and frequencies were below the poor prognosis threshold suggested in the previous chapters (<15%), except for Patient 4 who had 17.1% $CD4^+$HLA-$DR^+$$PD\text{-}1^+$ at primary analysis that then reduced to 9.6% at the next sampling. $CD8^+CD57^+$HLA-DR^+ was more

variable but overall appeared to decrease over time. Overall, the markers observed were more consistent in the untreated group, particularly $CD4^{+}HLA\text{-}DR^{+}PD\text{-}1^{+}$, which supports this phenotype as having the strongest potential as a prognostic marker.

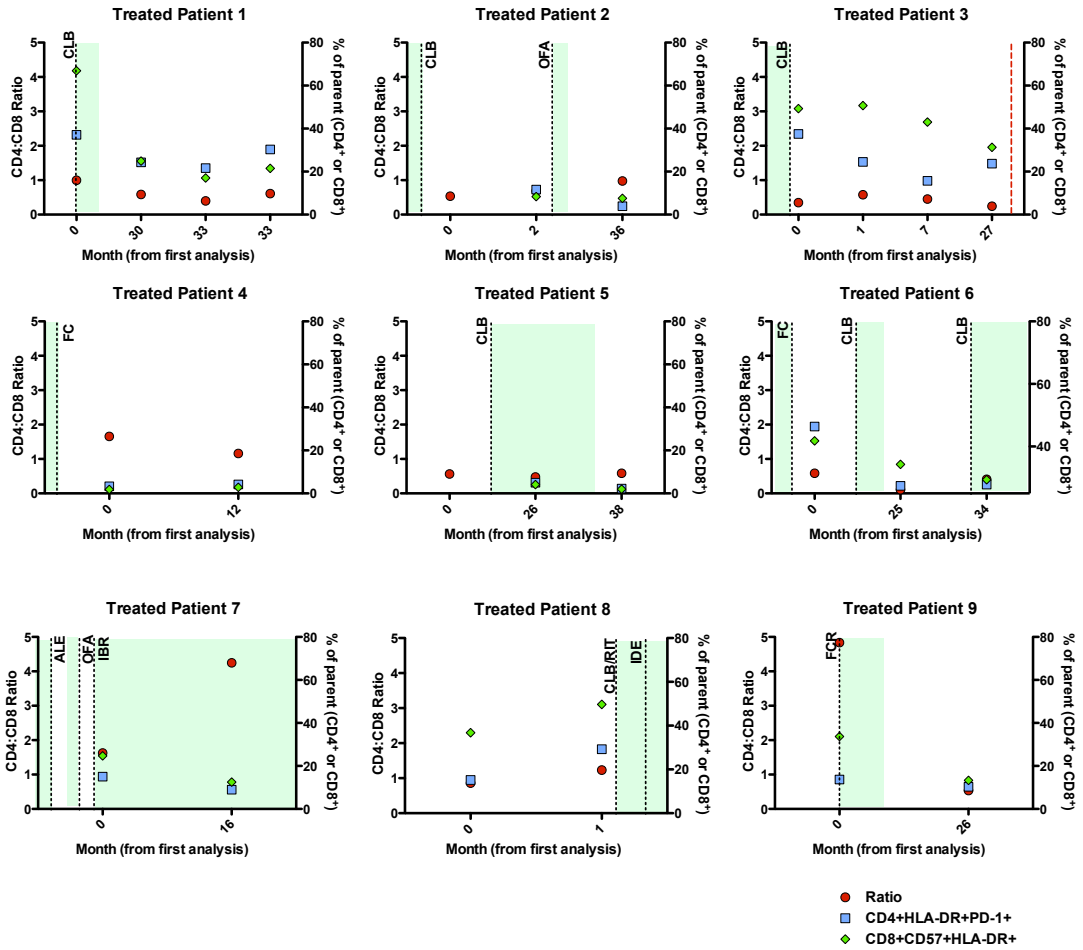

Figure 5.8. Change in the frequency of T-cell phenotypes at different time points in the treated patient subgroup. Cells were collected using flow cytometry (FACS CantoII, BD FACSDiva) and analysed using FlowJo (v.9). Lymphocytes were gated based on forward and side scatter profile; forward scatter area and height were used for exclusion of doublet cells. $CD4^+$ and $CD8^+$ T-cells were identified by gating first on $CD3^+$ then $CD4^+$ cells. The number of events in $CD4^+$ and $CD8^+$ gates were used to calculate CD4:CD8 ratio. Sampling was performed at various time points. (---- and green shading: treatment; ----: death; CLB: chlorambucil; OFA: ofatumumab; FC: fludarabine/cyclophosphamide; ALE: alemtuzumab; IBR: ibrutinib; RIT: rituximab; IDE: idelalisib; FCR; fludarabine/cyclophosphamide/rituximab)

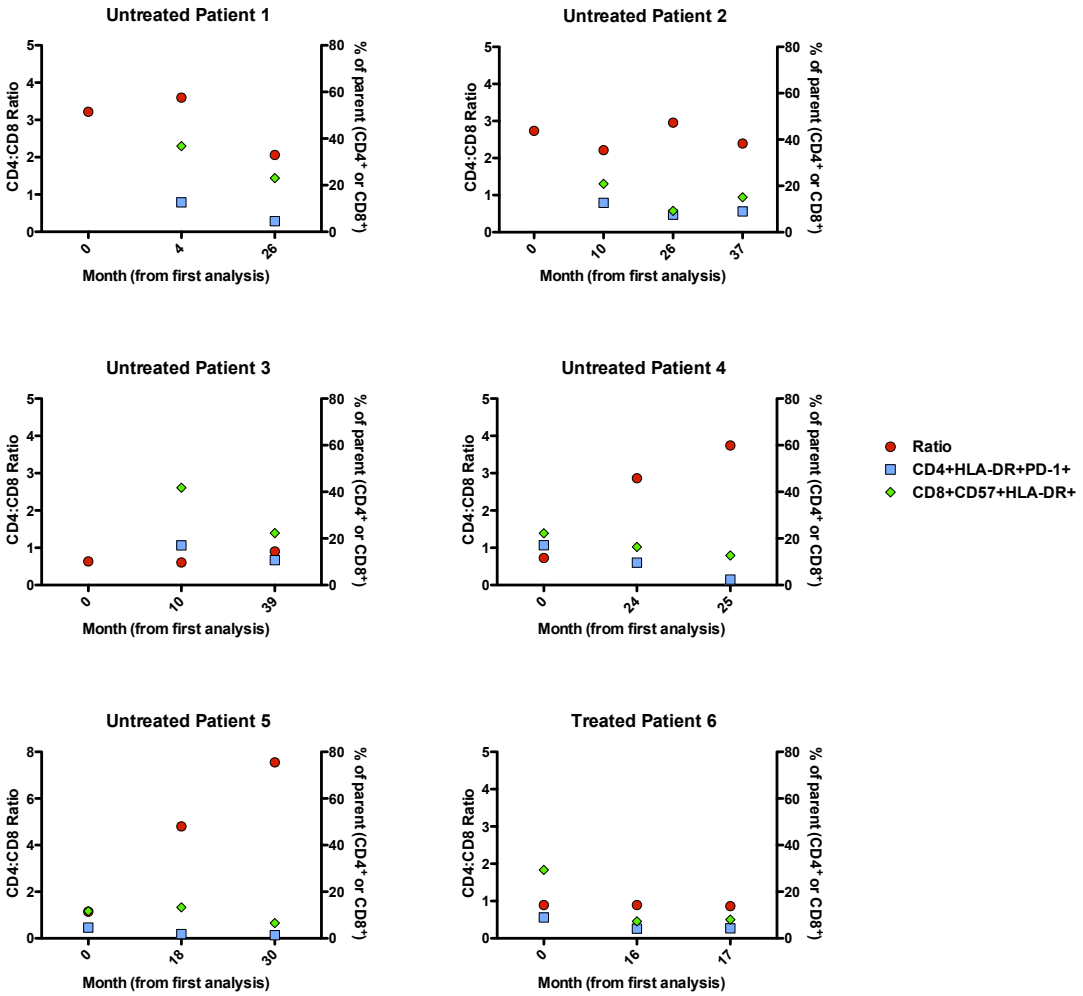

Figure 5.9. Change in T-cell phenotypes at different time points in the treated patient subgroup. Cells were collected using flow cytometry (FACS CantoII, BD FACSDiva) and analysed using FlowJo (v.9). Lymphocytes were gated based on forward and side scatter profile; forward scatter area and height were used for exclusion of doublet cells. $CD4^+$ and $CD8^+$ T-cells were identified by gating first on $CD3^+$ then $CD4^+$ cells. The number of events in $CD4^+$ and $CD8^+$ gates were used to calculate CD4:CD8 ratio. Sampling was performed at various time points.

5.3. Discussion

Due to the heterogeneity of CLL, at early diagnosis CLL patients are subjected to a 'watch and wait' approach until disease progression and subsequent need for treatment. The application of appropriate prognostic markers could aid in the stratification and identification of patients who will have progressive disease and/or relapse following treatment. The aim of this chapter was to investigate CD4:CD8 ratio in treated patients to further explore its prognostic value, with the hypothesis being that an inverted ratio would be more prevalent in the treated patient group. In addition, the relationship between the potential prognostic markers $CD4^+HLA\text{-}DR^+PD\text{-}1^+$ and $CD8^+CD57^+HLA\text{-}DR^+$ was explored. Another aim was to assess longitudinal change in CD4:CD8 ratio and the prognostic phenotypes over time, including following treatment. Whether alterations in the CD4:CD8 ratio or phenotype frequency could be used as a way of monitoring disease relapse/need for further treatment was also considered. Unfortunately, limitations on sample acquisition meant that only preliminary longitudinal assessment could be performed (discussed below in more detail).

This study revealed that treated CLL patients overall have lower CD4:CD8 ratios than the untreated CLL, with a significant increase in the proportion of patients with inverted CD4:CD8 ratios in the treated subgroup. Stratification of treated and untreated patients based on normal and inverted ratio also suggested a potential association between inversion of the CD4:CD8 ratio and treatment. This supports the previous assessment that this ratio is associated with poorer prognosis (Zenz et al. 2010; Nunes et al. 2012; Oscier et al. 2012). However, this study did not account for the effect of additional clinical factors such as age and gender; future additional analyses should include these clinical factors to correct this. The preliminary assessment of patients at different time points, however, did not reveal any discernible pattern of ratio improvement either shortly after or during treatment; nor was there any apparent ratio inversion prior to the need for treatment. In most patients, ratio status did not change and appeared relatively consistent across the time points measured, regardless of treatment status. Some patients did have more variation in the ratio, but this again was observed in both treated and untreated patients.

Due to limitations on time and sample acquisition, it was not possible to pursue a true longitudinal analysis. This assessment was therefore limited by inconsistent time-points between patients, varying from 1-30 months between sample collections. These

variations restricted the comparisons that can be made and the changes that could be observed throughout a patient's timeline. A larger, prospective study with samples collected at standardised intervals would allow a more accurate assessment of the relationships between T-cell prognostic markers in treated CLL by allowing for more consistent monitoring of changes over time. Detailed patient follow-up would be needed to assess the prognostic potential of these markers in the prediction of untreated patients who need treatment, and in relation to relapse of previously treated patients with need for additional treatment. The additional investigation of absolute counts at each time point would also help in interpreting changes in the proportions or percentages of T-cell phenotypes in conjunction with disease.

A distinct skewing towards the EM phenotype in the treated subgroup was associated with an inverted CD4:CD8 ratio. It is possible that the larger proportion of inverted ratio patients in the treated subgroup (60.6% compared to the 27.9% in untreated patients) is a confounding factor that contributes to the altered memory phenotype seen overall. Interestingly, the shift to EM was far more prominent in the $CD4^+$ T-cell compartment. This, along with increased frequencies of $CD57^+$ and PD-1^+ in $CD4^+$ and not the $CD8^+$ T-cell population, would suggest that $CD4^+$ T-cells have increased senescence/exhaustion within the treated compartment. However, both $CD4^+$ and $CD8^+$ T-cells displayed higher HLA-DR frequencies, implying that there is also increased T-cell activation in treated patients. Furthermore, the $CD4^+$ compartment comprises of various functional subsets, including Tregs. Therefore, future work should include additional parameters to identify these populations.

Previous work noted that PD-1 expression on $CD4^+$ and $CD8^+$ T-cells in CLL patients is particularly higher in patients who have relapsed or refractory disease, with the highest number of $CD8^+$PD-1^+ observed in patients with active disease and during relapse (Tinhofer et al. 2006; Novák et al. 2015; Gonzalez-Rodriguez et al. 2010; Nunes et al. 2012; Serrano et al. 1997). Nunes et al. (2012) also associated $CD8^+$PD-1^+ with inverted CD4:CD8 ratio and disease progression. Similarly, a higher proportion of inverted ratios in the treated subgroup was observed in this chapter. However, this study observed no difference in $CD8^+$PD-1^+ frequency when comparing treated and untreated patient subgroups. This is in-line with the lack of differences observed between normal and inverted ratio patients in the previous chapters. Based on the available information, it was unclear whether the patients had active disease or relapsed

disease at time of sampling. This could be addressed with a longitudinal study over a longer time frame that recorded specific patient stages (active disease/remission/relapse etc.) at the point each sample was taken.

Following multivariate and survival analyses, $CD8^+CD57^+HLA\text{-}DR^+$ was shown to be the $CD8^+$ phenotype with the strongest prognostic effect, whereas $CD4^+HLA\text{-}DR^+PD\text{-}1^+$ was shown to be the strongest prognostic factor overall. Both phenotypes were considered to have stronger prognostic potential than CD4:CD8 ratio within that study, and so frequencies of these phenotypes were investigated. Both $CD8^+CD57^+HLA\text{-}DR^+$ and $CD4^+HLA\text{-}DR^+PD\text{-}1^+$ frequencies were significantly higher in treated CLL patients compared to untreated. The biggest, more significant increase was seen with the $CD4^+HLA\text{-}DR^+PD\text{-}1^+$ phenotype (7.9% in untreated patients versus 20.3% in treated) than the $CD8^+CD57^+HLA\text{-}DR^+$ (17.4% versus 26.2%, respectively). In addition, Fisher's exact tests showed that the higher frequency $CD4^+HLA\text{-}DR^+PD\text{-}1^+$ phenotypes significantly skewed to the treated subgroup. As stated previously for the CD4:CD8 ratio, this test did not take other cofounding clinical factors into account; however, as treatment is initiated in CLL patients with progressive disease (Hallek et al. 2008), the presence of a phenotype associated with inferior prognosis within a treated cohort is not wholly unexpected.

Some treated patients observed a decrease in the $CD8^+CD57^+HLA\text{-}DR^+$ subset following treatment, but levels of this phenotype appeared sporadic in both treated and untreated patients. On the other hand, $CD4^+HLA\text{-}DR^+PD\text{-}1^+$ demonstrated potential to remain more consistent within the untreated patients, with a decrease in frequency often observed following treatment. Furthermore, $CD4^+HLA\text{-}DR^+PD\text{-}1^+$ began to increase in some patients in the treated cohort during periods without treatment, including one patient who died after their final sample collection. It is possible that there is an accumulation of this phenotype as disease progresses, which is then depleted either directly or indirectly following treatment. Taken together with the skewed $CD4^+HLA\text{-}DR^+PD\text{-}1^+$ in the treated cohort, this suggests that the $CD4^+HLA\text{-}DR^+PD\text{-}1^+$ phenotype may be a superior potential marker for not only patients at risk of more aggressive disease, but may also be a potential marker of disease progression/relapse and need for further treatment. Whether higher frequencies of $CD4^+HLA\text{-}DR^+PD\text{-}1^+$ T-cells identifies poor prognosis patients that will eventually require treatment, or whether the treatment itself results in exacerbated $CD4^+HLA\text{-}DR^+PD\text{-}1^+$ frequencies,

could not be fully determined here due to the study limitations described above. Furthermore, there is inherent difficulty in separating treatment from inferior prognosis, as the inferior prognosis patients are ones with progressive disease and who are undergoing treatment, or have received treatment prior to assessment. However, from the limited longitudinal patient data studied in this chapter, some treatment-naïve patients possessed high $CD4^+HLA\text{-}DR^+PD\text{-}1^+$ frequencies ($\geq$14.4%) that decreased after treatment was initiated, suggesting that high $CD4^+HLA\text{-}DR^+PD\text{-}1^+$ is present prior to therapeutics. Further comprehensive longitudinal studies that follow larger patient cohorts from diagnosis through to disease progression and treatment are needed to allow further assessment and confirm the prognostic value of $CD4^+HLA\text{-}DR^+PD\text{-}1^+$.

In conclusion, this preliminary study of treated CLL patients demonstrates associations with the previously identified CD4:CD8 ratio as a prognostic marker, but also two phenotypic markers that have been identified in this thesis as having a strong prognostic effect in CLL. The presence of these phenotypes in higher frequencies in treated patients suggests that these T-cells have a role in disease, but their prognostic role is unknown without further investigation. $CD4^+HLA\text{-}DR^+PD\text{-}1^+$ has demonstrated good potential to be used for prognostic assessment in identifying patients with poorer clinical outcome. It could also provide a means for monitoring disease relapse, but additional, more comprehensive longitudinal studies are needed to fully assess the usefulness of this phenotype. Assessment by flow cytometry, particularly if limited to a few selected markers on a small panel would be a relatively simple and cheaper technique compared to more expensive and labour-intensive assessments, such as genotyping for prognostic genetic aberrations (Orchard et al. 2004). Therefore, if further work established the prognostic use of $CD4^+HLA\text{-}DR^+PD\text{-}1^+$, this could prove a valuable tool to guide the treatment of CLL patients.

Chapter 6
Single telomere length analysis (STELA) of T-cell memory subsets in CLL

Telomeres are repetitive nucleoside -TTAGGG- sequences that 'cap' the end of chromosomes to protect loss of the important chromosomal DNA (Buggert et al. 2014; Baird 2005; Trautmann et al. 2006; Champagne et al. 2001; Pawelec and Gouttefangeas 2013): each time a cell division occurs the telomeres shorten (L. Zhang et al. 2003; Sanders and Newman 2013; Sato et al. 2005; Woo et al. 2002; Nunes et al. 2012). Telomeric length has therefore been recognised as a way to establish the replicative age and senescence of a cell population.

Prior studies have shown links between telomere lengths of peripheral blood cells and the prognosis of solid tumours, including head, neck, breast and renal cancer, although studies are conflicting on whether poorer prognosis is associated with longer or shorter telomeres (Zenz et al. 2010; Wu et al. 2003; Oscier et al. 2012; Shao et al. 2007; Svenson et al. 2008; Svenson et al. 2013). Telomere shortening specifically within the T-cell compartment has been associated with worse clinical status in lung cancer and Alzheimer's disease (Tinhofer et al. 2006; Qian et al. 2016; Gonzalez-Rodriguez et al. 2010; Panossian et al. 2003; Nunes et al. 2012; Serrano et al. 1997; Novák et al. 2015). The telomere length of adoptively transferred T-cells can also influence clinical outcome; melanoma patients who received tumour-infiltrating lymphocytes (TIL) with longer telomeres demonstrated higher persistence of TIL and this was associated with clinical response (Zhou et al. 2005). Therefore, it is possible that telomere length of T-cells could be linked to immunological response to disease and disease progression.

Research focusing on telomere length of malignant B-cells in CLL patients has demonstrated that critically short telomeres are associated with disease progression, genomic instability and poorer prognosis (Grabowski et al. 2005; T. T. Lin et al. 2010b; T. T. Lin et al. 2014). Naïve ($CD45RA^+$) and memory ($CD45RA^-$) T-cells in poor prognosis Zap-70^+/$CD38^+$ CLL patients have been shown to possess significantly shorter telomeres than Zap-70^-/$CD38^-$ patients. However, telomere length distributions of the $CD8^+$ T-cell memory compartment in CLL patients, and telomeric differences based on CD4:CD8 ratio, have not been fully explored.

Chapter 3 investigated phenotypic abnormalities in CLL patients based on previous research in our group, which identified a poor prognosis subgroup of CLL patients with an expanded $CD8^+$ T-cell compartment skewed to a more differentiated memory phenotype (Nunes et al. 2012). As well as supporting the increased presence of more differentiated phenotypes in CLL, we also identified 'active differentiated' phenotypes that were more prevalent in CLL patients with inverted CD4:CD8 ratios, and this was linked to inferior prognosis.

The underlying reasons for this expanded population of $CD8^+$ T-cells are not yet understood. One possibility is that chronic antigenic stimulation has led to an accumulation of long-lived, highly differentiated mature T-cells that have undergone continual stimulation and proliferation; these T-cells would have shorter telomeres due to extensive cell division coupled with reduced variation in telomere length distribution due to clonal expansion. A second possibility is that the origin of the expansion is activation of T-cells from the naïve compartment that then skew towards more differentiated phenotypes in response to continual antigenic stimulation.

This study aims to investigate the telomere length distributions of the $CD8^+$ T-cells in CLL patients in order to establish the proliferative age of $CD8^+$ memory subsets in CLL^{IR} patients. In order to achieve this, we will employ single telomere length analysis (STELA) to determine whether there are telomeric length differences within the $CD8^+$ T-cell population within CLL^{NR} and CLL^{IR} patients. This will allow assessment of the replicative history of the expanded $CD8^+$ population of inverted ratio patients.

STELA is a multistep process that provides high-resolution measurement of telomere lengths at a specific chromosome end (in this case, the XpYp chromosome)(Baird 2005). A brief outline of the experimental process can be seen in Figure 6.1. This study focused on the $CD4^+$ and $CD8^+$ T-cell compartment as a whole, and the $CD8^+$ memory subsets; Figure 6.2 shows the gating strategy applied to isolate these populations via FACS.

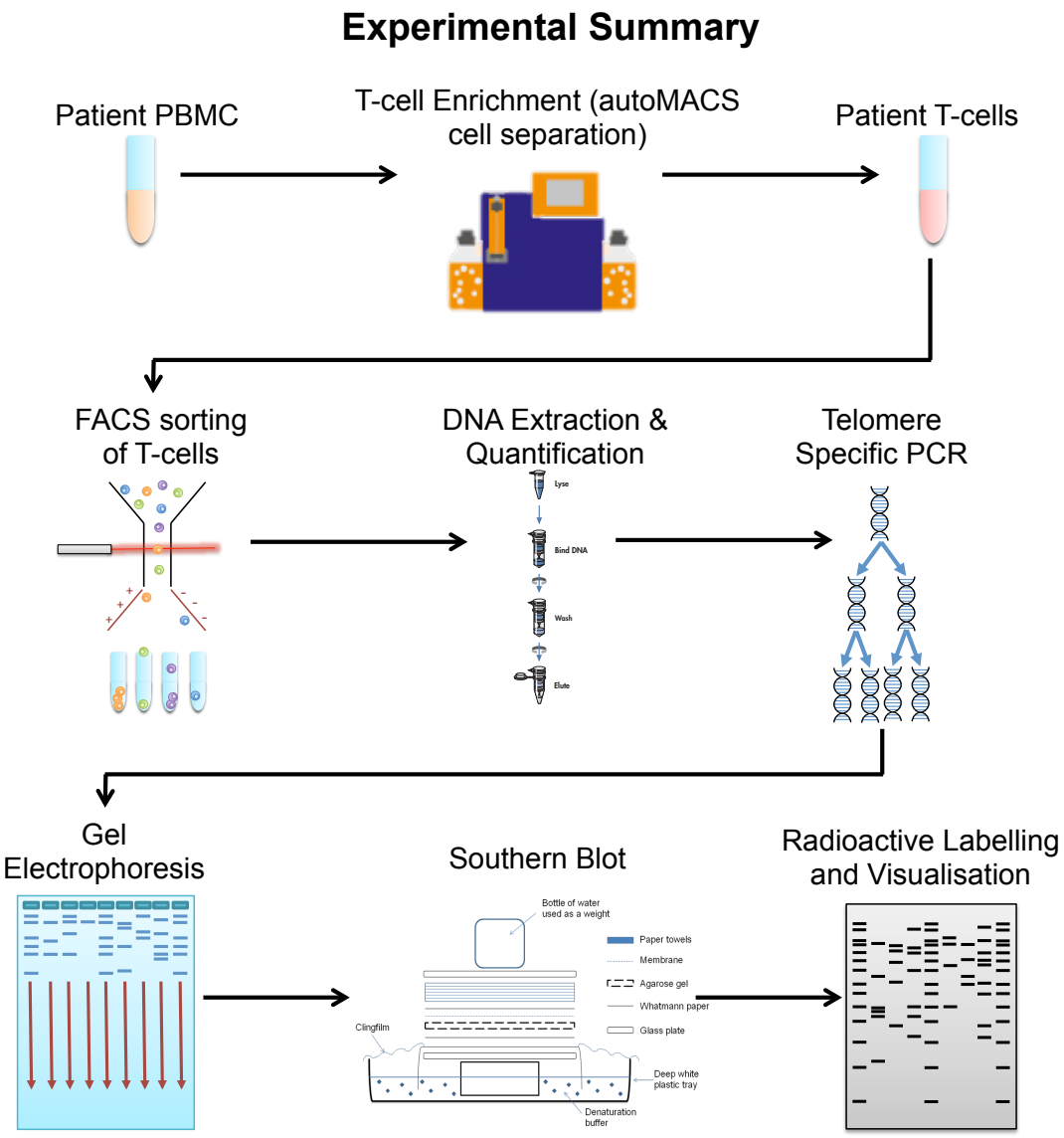

Figure 6.1. Experimental outline of the sample acquisition and single telomere length analysis (STELA) of T-cell populations in CLL. Peripheral blood mononuclear cells (PBMCs) were isolated from CLL patient blood samples by density centrifugation. T-cell subsets of interest were isolated first via enrichment using autoMACS cell separation (negative selection using $CD19^+$ magnetic beads) and then via fluorescence-activated cell sorting (FACS) using BD FACS Aria. DNA was extracted from samples of interest (Qiagen QIAamp DNA Micro Kit) and quantified. STELA was then performed: telomere-specific ($XpYpE_2$) PCR was performed and resolved via gel electrophoresis. DNA was then transferred to a membrane using Southern blotting and visualised via radioactive DNA-labelling of the membrane. Telomere length and distribution was calculated using Phoretix software: mean telomere lengths were calculated using Excel. Figure is a composite of diagrams including diagrams from Miltenyi Biotech and Qiagen[3]

[3] Diagrams obtained from:
Miltenyi Biotech: http://www.miltenyibiotec.com/en/products-and-services/macs-cell-separation/macs-technology/whole-blood-microbeads.aspx
Qiagen: https://www.qiagen.com/gb/resources/resourcedetail?id=085e6418-1ec0-45f2-89eb-62705f86f963&lang=en

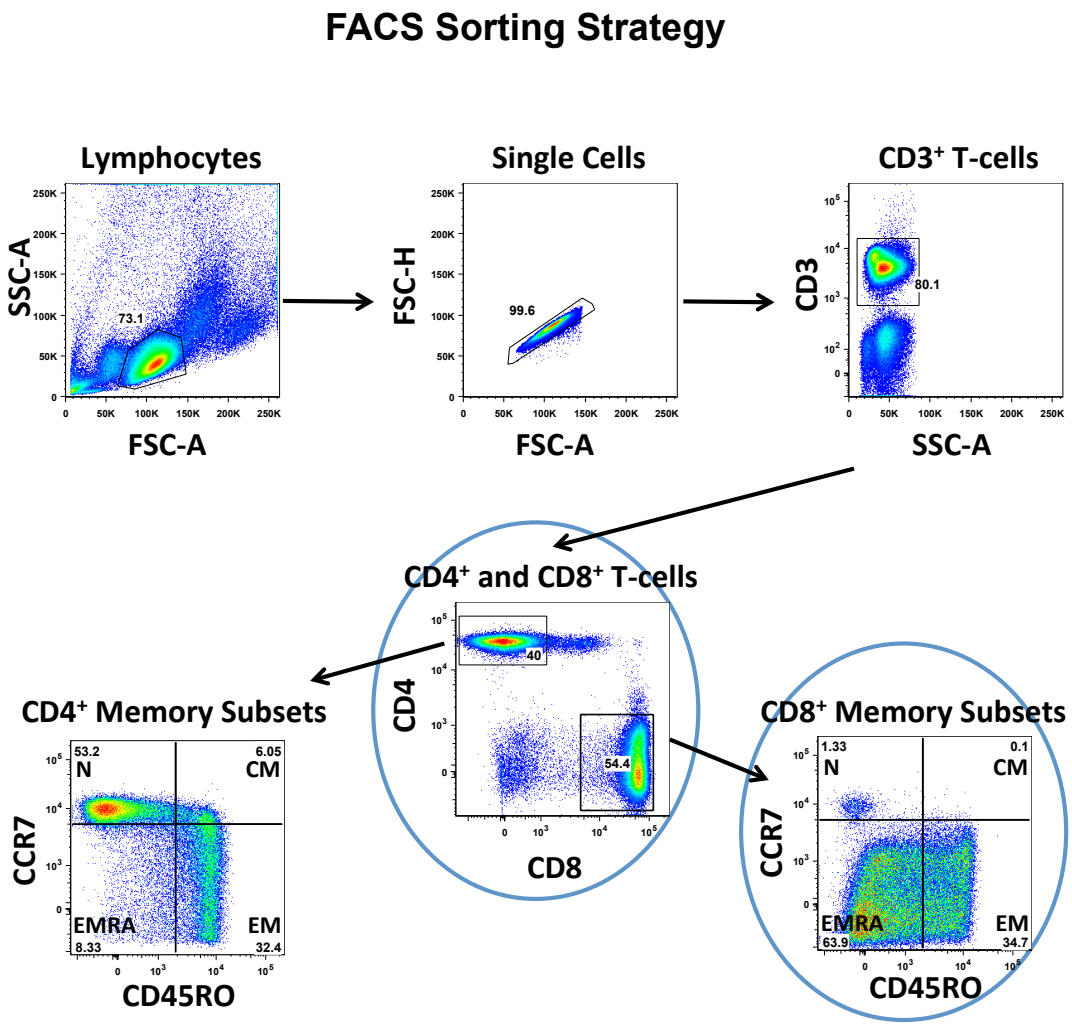

Figure 6.2. Representative gating strategy used for FACS of T-cell subsets for single telomere length analysis (STELA). Fluorescence-activated cell sorting (FACS) was performed (BD Aria, BD FACSDiva) on purified PBMC samples. Lymphocytes were gated based on forward and side scatter profile; single cells were gated by forward scatter area and height. T-cells were identified by gating first on $CD3^+$ then either $CD4^+$ or $CD8^+$ populations. $CD8^+$ memory subsets were defined within the $CD8^+$ gate using CCR7 and CD45RO memory markers: naïve (N, $CCR7^+CD45RO^-$), Central Memory (CM, $CCR7^+CD45RO^+$), Effector Memory (EM, $CCR7^-CD45RO^+$) and EMRA ($CCR7^-CD45RO^-$). Circled (blue) are the T-cell populations that were FACS sorted and taken forward for STELA. Post-sorting analysis of T-cells was performed using FlowJo (v.9).

6.1. Preservation of T-cell compartment during enrichment

CLL is characterised by the lymphoproliferative expansion of $CD5^+CD19^+$ malignant B-CLL cells (Zenz et al. 2010). Therefore, when PBMCs are isolated from CLL patient blood samples, the majority of the sample is comprised of B-cells and the relative proportion of T-cells within the patient sample is much smaller. For example, the CLL cohort used in the previous phenotyping chapters of this thesis (Chapters 3 and 4) had a median of 6.25% $CD3^+$ cells in isolated PBMCs. Attempting to isolate T-cell subsets via FACS directly from PBMC samples would therefore be time consuming, and carries a higher risk of sorting error and contamination of the T-cell fractions with B-cells.

To optimise the isolation of T-cell populations the PBMCs were enriched for T-cells via magnetic-activated cell sorting (MACS). PBMCs were labelled with $CD19^+$ magnetic beads and run through an autoMACS machine (Miltenyi Biotech) allowing the isolation of a $CD19^+$ and $CD19^-$ fractions. As $CD19^+$ is a well-documented marker for B-cells this process therefore separated CLL cells from the rest of the sample and the negative fraction contained T-cell enriched PBMCs. The enrichment process is shown in Figure 6.3, which highlights the $CD3^+$ frequency of a patient before and after $CD19^+$ isolation. AutoMACS enrichment resulted in much higher proportions of $CD3^+$ cells in the samples that were taken forward to FACS.

Adding the autoMACS step introduced additional treatment of cells that could pose a risk to delicate T-cell populations and it was important that the phenotypic composition of the T-cell compartment was preserved for STELA analysis. Therefore, the memory subset distribution was compared before and after the autoMACS process (Figure 6.4). Both the $CD4^+$ and $CD8^+$ T-cell compartments as a whole and the memory subsets were maintained pre- and post-T-cell enrichment. The autoMACS process was therefore a useful method to obtain samples for FACS sorting that were enriched for T-cells. Furthermore, the distribution of the T-cell populations appears to be retained following autoMACS sorting.

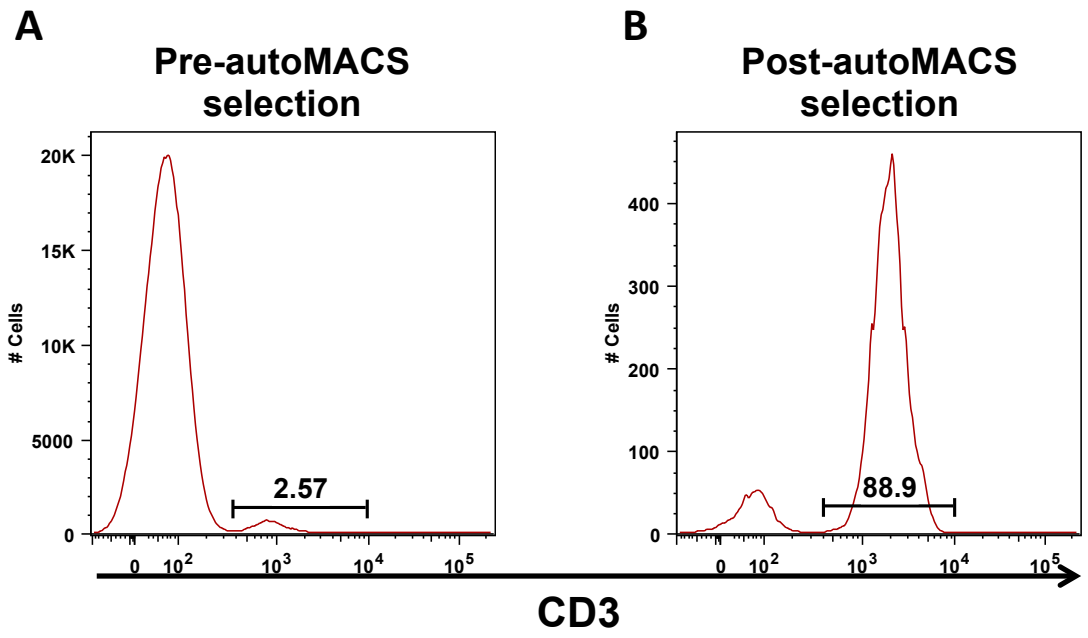

Figure 6.3. Representative CLL patient demonstrating T-cell enrichment using automagnetic-activated cell sorting (autoMACS, Miltenyi Biotech). T-cells were enriched from isolated PMBC samples via negative selection. PBMCs were labelled with $CD19^+$ magnetic beads and then passed through magnetic columns to allow the positive isolation of B-cells (CLL cells). The $CD19^-$ negative fraction was enriched with T-cells and retained fluorescence activated cell sorting of T-cell subsets and single telomere length analysis (STELA). (A) $CD3^+$ T-cell frequency in PBMC of an example CLL patient. (B) $CD3^+$ T-cell frequency within the $CD19^-$ (T-cell enriched) fraction following CD19 autoMACS selection.

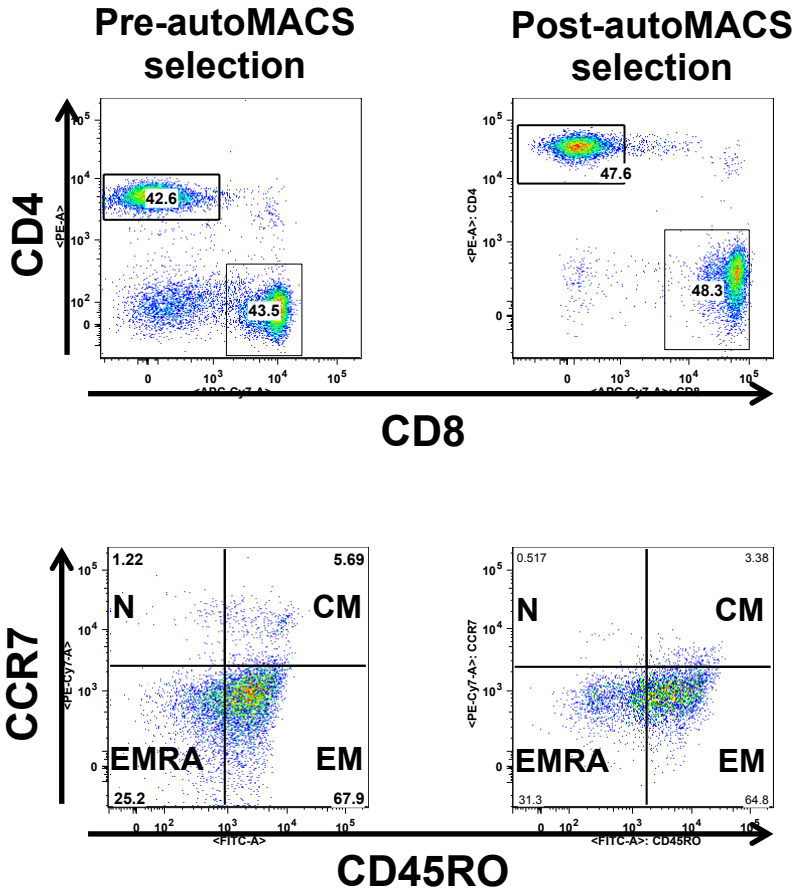

Figure 6.4. Representative CLL patient showing phenotypic composition of T-cells pre- and post- autoMACS selection. Gating was performed as described in Figure 6.2. (A) Percentage of $CD4^+$ and $CD8^+$ T-cells before and after T-cell enrichment with autoMACS. (B) Percentage of $CD8^+$ T-cell memory subsets before and after T-cell enrichment with autoMACS. Pre-autoMACS phenotyping data was collected using BD Canto II and BD FACSDiva. Post-autoMACS phenotyping data was collected during fluorescence-activated cell sorting (FACS) of sample (BD Aria, BD FACSDiva). Post-sorting analysis was performed using FlowJo (v.9).

6.2. T-cell memory subsets of STELA cohort

Flow cytometric data showing T-cell subsets composition was recorded during FACS for $CD4^+$, $CD8^+$ and $CD8^+$ memory subsets fractions. This data was subsequently analysed to assess whether the distribution of $CD8^+$ T-cell memory subsets of the CLL patients in the STELA cohort fairly represented the results observed in the phenotyping cohort (Chapter 3).

As shown in Figure 5.5A, the STELA cohort of CLL patients demonstrated a significant reduction in the $CD8^+$ naïve T-cells when compared to healthy donors ($p = 0.0116$). Both the $CD8^+$ EM and $CD8^+$ EMRA cohorts demonstrated a trend towards increase in frequency in the CLL patients of the STELA study when compared to healthy donors, although this was not statistically significant. The $CD8^+$ T-cell memory subset composition within the CLL patients of the STELA cohort is therefore similar to that observed previously.

Parallels were also observed between the cohort from the phenotyping study (Chapter 3) and that of the STELA cohort when patients were stratified by CD4:CD8 ratio. The reduction of $CD8^+$ naïve T-cells was exacerbated in the CLL^{IR} subgroup when compared against both CLL^{NR} patients and healthy donors ($p \leq 0.05$ and $p \leq 0.01$, respectively). There was also a trend towards increased frequency of the $CD8^+$ EMRA subset of CLL^{IR} patients versus CLL^{NR} and healthy donors. Interestingly, the same pattern was not seen in the $CD8^+$ EM compartment.

Overall, the composition of $CD8^+$ T-cell memory subsets in the STELA cohort reflects that observed in the phenotypic study in Chapter 3: a clear skewing from naïve to differentiated memory.

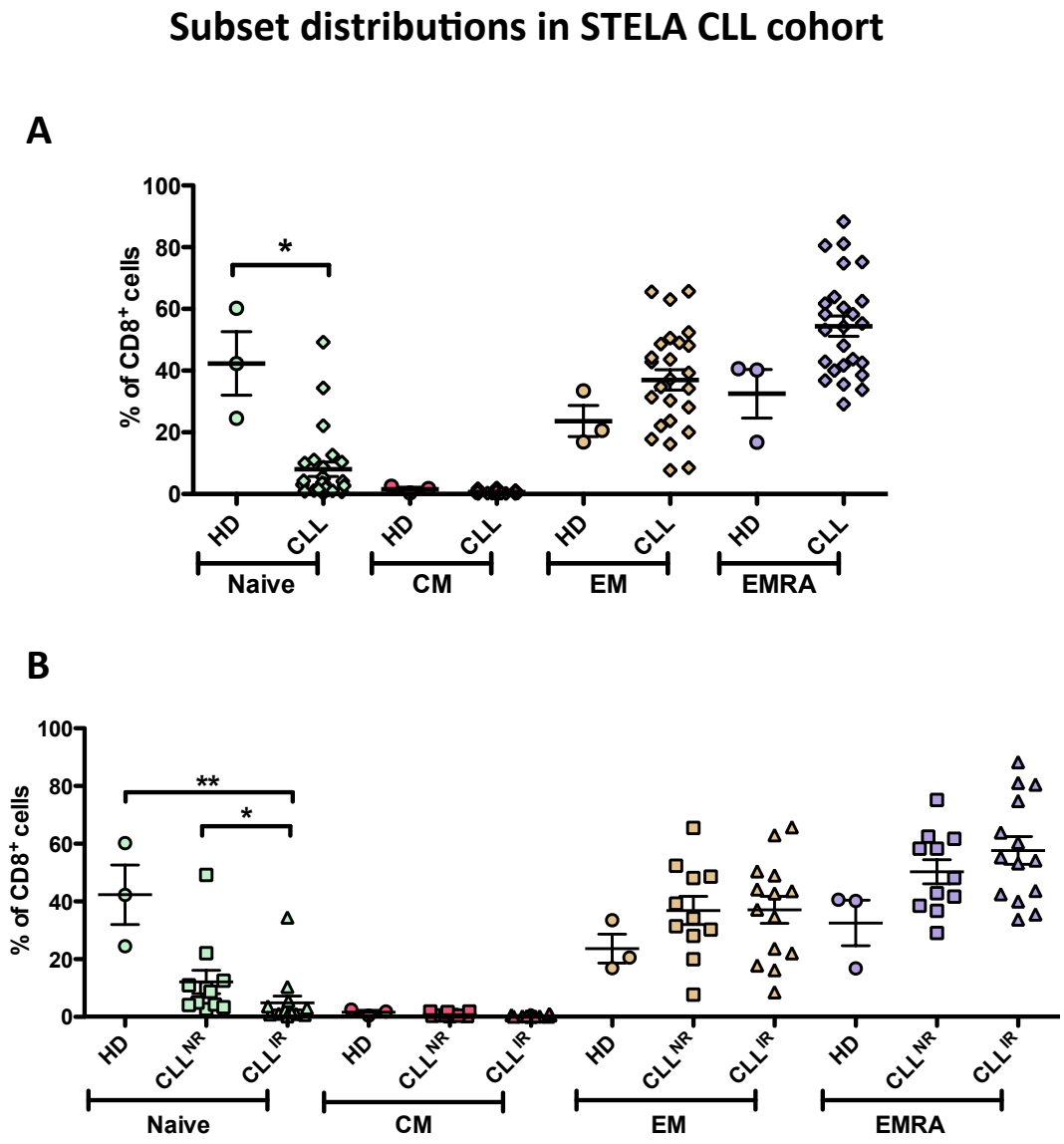

Figure 6.5. Frequency of CD8$^+$ T-cell memory subsets in CLL patients (n = 25) versus healthy donors (n = 3). Fluorescence-activated cell sorting (FACS) was performed (BD Aria, BD FACSDiva) using gating as described in Figure 6.2. (A) Subset composition of CLL patients (n = 25) versus healthy donors (n = 3). Pairwise statistical analysis (HD vs CLL) was performed using the non-parametric Mann-Whitney test. Patients were stratified based on CD4:CD8 T-cell ratio: patients with a CD4:CD8 ratio <1.0 were considered inverted (CLL^{IR}) and patients with a ratio ≥1.0 were considered 'normal' (CLL^{NR}). (B) Subset frequencies of healthy donors versus CLL^{NR} (n = 11) and CLL^{IR} (n = 14) patients. Three-way ANOVA statistical analysis was performed using Kruskal-Wallis test (HD vs CLL^{NR} vs CLL^{IR}), with all pairs of data assessed using the Dunn's post-test. Significant results were included on the graph (* = p ≤0.05; ** = p ≤0.01; *** = p ≤0.001).

6.3. $CD4^+$ and $CD8^+$ telomere lengths

Initially, STELA was performed on the entire $CD4^+$ and $CD8^+$ T-cell populations to identify any overall change in telomere length within the T-cell compartments between healthy donors and CLL patients.

Within the CLL cohort neither $CD4^+$ nor $CD8^+$ T-cell telomere lengths differed from the healthy donor counterparts (Figure 6.6A). However, due to the number of healthy donors analysed (n = 3), this puts limitations on the comparisons between healthy donors and CLL patients. Statistical analysis comparing the CLL $CD4^+$ and $CD8^+$ T-cell compartments against one another also showed that there was no significant difference in mean telomere lengths between the two T-cell populations.

Further stratification within the CLL cohort based on CD4:CD8 ratio was performed (Figure 6.6B): patients with a ratio <1.0 were considered to have an inverted ratio. The $CD8^+$ compartment of CLL^{IR} patients demonstrated numerically longer telomeres on average, particularly compared to the CLL^{NR} subgroup (4.17 kb versus 3.57 kb; versus 3.84 kb for age-matched healthy donors): however, this did not reach significance. The same pattern was observed in the $CD4^+$ T-cell compartment, with $CD4^+$ T-cells in the CLL^{IR} subgroup having longer telomeres than the CLL^{NR} (4.44 kb versus 3.80 kb) and healthy donors (4.44 kb versus 3.97 kb); again, these differences were not deemed significant. Further to this, there was no change in telomere lengths when comparing CD4 against CD8 within the CLL^{NR} or within the CLL^{IR} patient groups.

Overall, the CLL cohort used within this study demonstrated no discernible differences in telomere length between $CD4^+$ and $CD8^+$ T-cells. Furthermore, the telomere lengths in these populations did not appear to differ in CLL patients compared to their healthy counterparts, although there is a trend for inverted ratio patients to have longer telomeres.

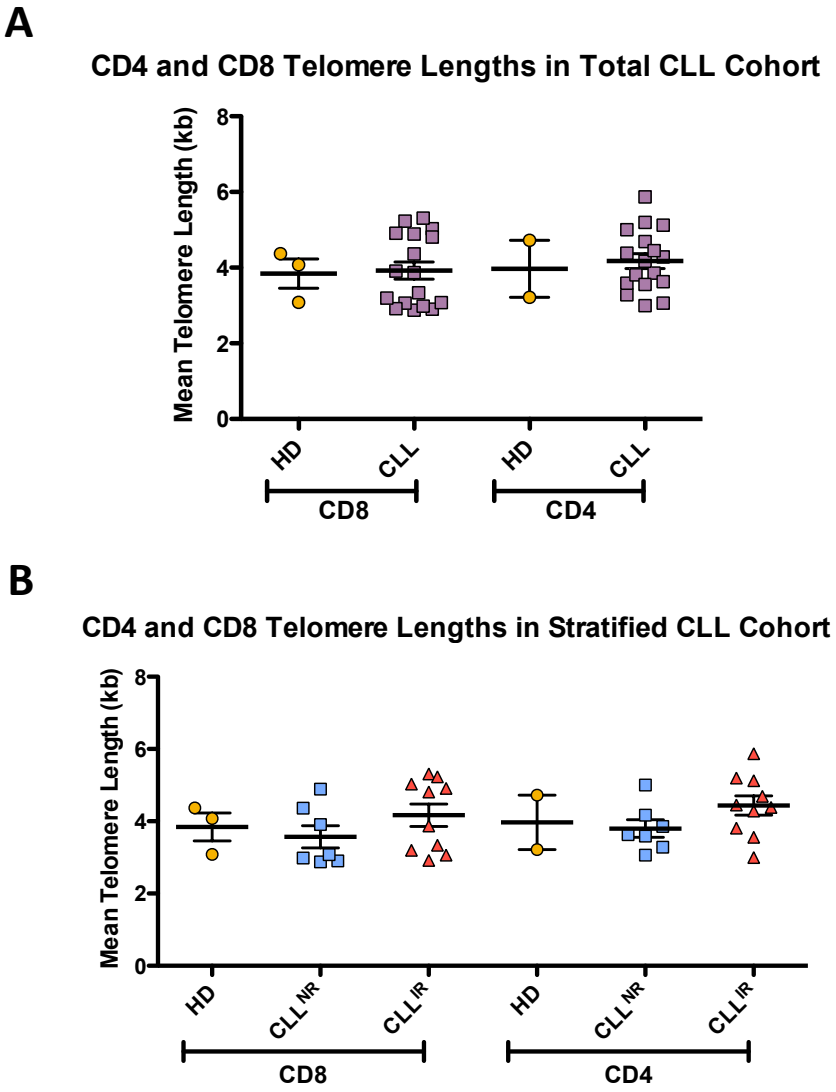

Figure 6.6. Telomere length of CD8$^+$ and CD4$^+$ T-cells in CLL versus age-matched healthy donors. Fluorescence-activated cell sorting (FACS) was performed (BD Aria, BD FACSDiva) using gating as described in Figure 6.2. DNA was extracted from CD4$^+$ and CD8$^+$ T-cells isolated from PBMCs of CLL patients and XpYp specific STELA was performed. Telomere length and distribution was calculated using Phoretix software: mean telomere lengths were calculated using excel. (A) Telomere lengths of CD8$^+$ and CD4$^+$ T-cells in healthy donors (n = 3) and CLL patients (n = 17). Pairwise statistical analysis (HD vs CLL) was performed using the non-parametric Mann-Whitney test. Patients were stratified based on CD4:CD8 T-cell ratio: patients with a CD4:CD8 ratio <1.0 were considered inverted (CLL^{IR}) and patients with a ratio ≥1.0 were considered 'normal' (CLL^{NR}). (B) Telomere lengths of CD8$^+$ and CD4$^+$ T-cells in healthy donors (n = 3) versus CLL^{NR} (n = 6) and CLL^{IR} (n = 10). Three-way ANOVA statistical analysis was performed using Kruskal-Wallis test (HD vs CLL^{NR} vs CLL^{IR}), with all pairs of data assessed using the Dunn's post-test. Significant results were included on the graph (* = p ≤0.05; ** = p ≤0.01; *** = p ≤0.001).

6.4. Analysis of telomere length between CD8$^+$ T-cell subsets

The expansion of CD8$^+$ T-cells in CLL^{IR} patients resulted in a skewing to a more differentiated memory phenotype (Chapter 3). Therefore, further analysis was performed within the CD8$^+$ T-cell compartment to analyse telomere lengths of the memory subsets of CLL patients. Due to the relatively small patient sample size and the low frequency of central memory CD8$^+$ T-cells, the CM population was not routinely analysed.

A representative STELA blot of the telomere length distributions of CD8$^+$ T-cell memory subsets is shown in Figure 6.7. In the CLL CD8$^+$ compartment, mean telomere length appears to decrease as the T-cells become more differentiated: naïve T-cells have the longest telomeres on average, followed sequentially by the CM and EM compartment, with the EMRA population having the shortest telomeres.

This reduction in telomere length is consistent with previous work (Weng et al. 1995), and the suggestion that the T-cell populations further down the memory/differentiation pathway have undergone further replication and are therefore more 'aged'. In this representative patient, the EMRA cells also had the lowest standard deviation of all the memory subsets. This implies that the CD8$^+$ EMRA subset is less heterogeneous in terms of telomere length and is potentially either more clonal than the other memory subsets, or that the T-cells are stimulated by a diverse antigen repertoire and driven to similar telomere lengths as they become highly differentiated. The mean telomere lengths within the CD8$^+$ population as a whole are much lower than those observed in the naïve, CM and EM population, and are closer to the EMRA population. Therefore, it is possible that the EMRA population makes up a large proportion of the CD8$^+$ T-cell compartment in this patient, therefore skewing the mean telomere length.

These patterns in telomere lengths are carried through to the whole CLL cohort. Collectively CD8$^+$ EM and EMRA populations possess significantly shorter telomeres than the CD8$^+$ naïve population (Figure 6.8A, $p \leq 0.01$ for both). The same pattern is observed when using standard deviation of the memory populations as a surrogate measure of clonality, as naïve T-cells demonstrated a significantly larger standard deviation than the EM and EMRA subsets (Figure 6.8B, $p \leq 0.01$ versus EM and $p \leq 0.05$ versus EMRA).

Reduced telomere length and reduced telomere standard deviation appears to occur within the same T-cell population; it could be that the two are proportionally linked, i.e. that as telomere length shortens, variability is also reduced. To address this correlation analyses were performed to assess whether telomere shortening was associated with the telomere variability of a CLL T-cell population (Figure 6.9). A strong relationship between the mean telomere length and telomere length variability was observed in both $CD4^+$ ($r^2 = 0.5543$, $p = 0.0003$; Figure 6.9A) and $CD8^+$ T-cells ($r^2 = 0.7728$, $p = 0.0010$; Figure 6.9B), with the $CD8^+$ compartment having the stronger association. $CD8^+$ memory subsets followed this pattern: $CD8^+$ naïve T-cells demonstrated the widest range and variance in telomere lengths (Section 6.4, Figure 6.8) and here they showed weakest relationship between telomere length and variability ($r^2 = 0.5836$, $p = 0.0038$; Figure 6.9C). Both $CD8^+$ EM and $CD8^+$ EMRA T-cells showed strong links between the mean telomere lengths and variability ($r^2 = 0.7233$, $p < 0.0001$; $r^2 = 0.7996$, $p < 0.0001$). Overall, a reduction in telomere length appeared to be associated with reduced variability.

Overall, this suggests that the naïve T-cell population has undergone less proliferation (less aged) and is more heterogeneous, whereas the more differentiated memory subsets have undergone more proliferation (aged) and have become more clonal in nature. Furthermore, increased replicative age (shortened telomeres) is correlated with reduced variance within the T-cell subsets, implying that CLL patients with shorter T-cell telomeres have reduced T-cell clonality.

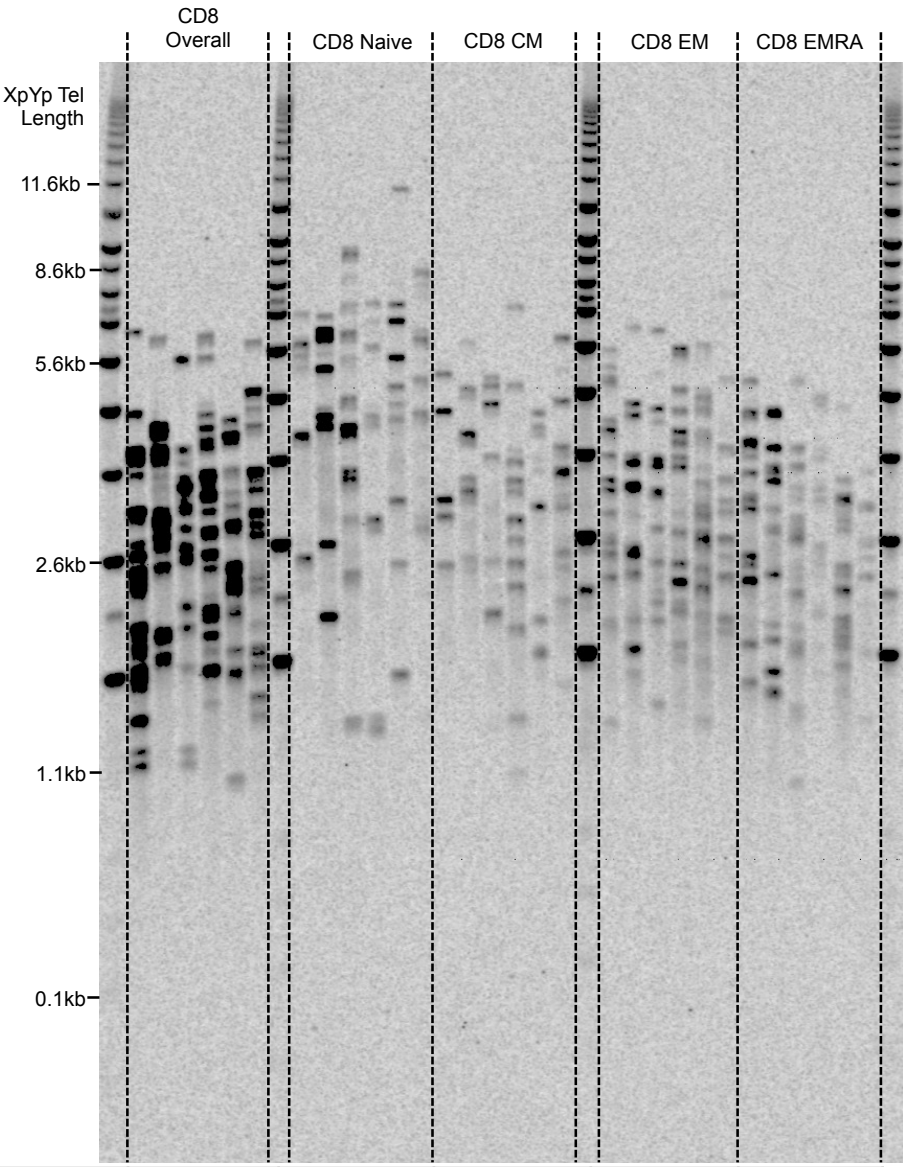

	CD8 Overall	Naïve	CM	EM	EMRA
Mean Telomere length (kb)	2.92	4.62	3.25	3.17	2.60
Standard Deviation	1.29	2.29	1.25	1.31	0.97

Figure 6.7. Representative STELA profile of the CD8$^+$ T-cell subsets of a CLL patient. Fluorescence activated cell-sorting (FACS) was performed (BD Aria, BD FACSDiva using gating as described in Figure 6.2. DNA was extracted from CD8$^+$ T-cells isolated from PBMCs of CLL patients and XpYp specific STELA was performed. Telomere length and distribution was calculated using Phoretix software: mean telomere lengths were calculated using Excel.

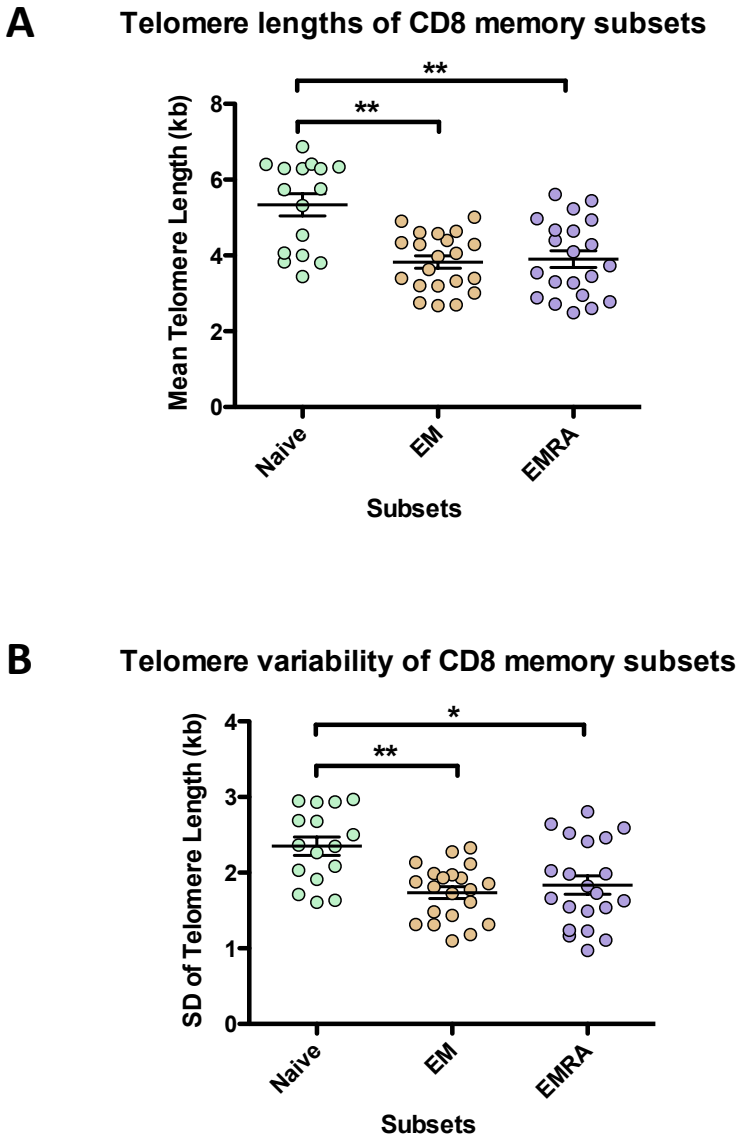

Figure 6.8. Telomere length and variability of CD8$^+$ T-cell subsets of CLL patients. Fluorescence-activated cell sorting (FACS) was performed (BD Aria, BD FACSDiva) using gating as described in Figure 6.2. DNA was extracted from CD8$^+$ T-cells isolated from PBMCs of CLL patients and XpYp specific STELA was performed. Telomere length and distribution was calculated using Phoretix software: mean telomere lengths were calculated using excel. (A) Mean telomere lengths of CD8$^+$ T-cells in the naïve (n = 16), EM (n = 21) and EMRA (n = 21) subsets of CLL patients. (B) Standard deviation (SD) of telomere lengths of CD8$^+$ T-cells in the naïve EM and EMRA subsets of CLL patients. Three-way ANOVA statistical analysis was performed using Kruskal-Wallis test (HD vs CLL^{NR} vs CLL^{IR}), with all pairs of data assessed using the Dunn's post-test. Significant results were included on the graph (* = p ≤0.05; ** = p ≤0.01; *** = p ≤0.001).

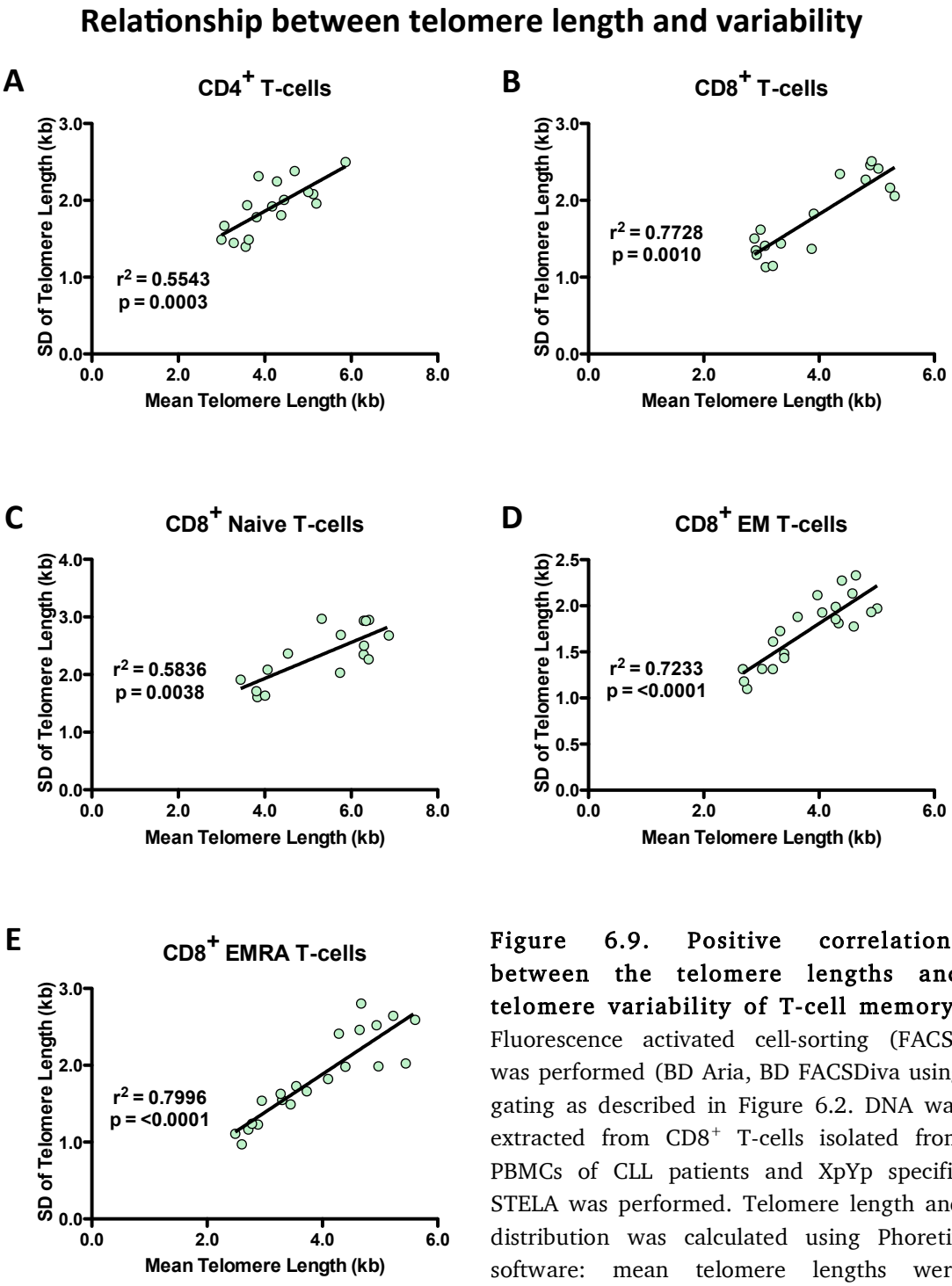

Figure 6.9. Positive correlations between the telomere lengths and telomere variability of T-cell memory. Fluorescence activated cell-sorting (FACS) was performed (BD Aria, BD FACSDiva using gating as described in Figure 6.2. DNA was extracted from $CD8^+$ T-cells isolated from PBMCs of CLL patients and XpYp specific STELA was performed. Telomere length and distribution was calculated using Phoretix software: mean telomere lengths were calculated using Excel. Correlation between mean telomere lengths and standard deviation of telomere lengths for (A) Total $CD4^+$ T-cell compartment, (B) Total $CD8^+$ T-cell compartment, (C) $CD8^+$ naive T-cell subset, (D) $CD8^+$ EM T-cell subset, and (E) $CD8^+$ EMRA T-cell subset. Spearman's correlation analyses were used to determine significance.

6.5. Telomere length of CD8$^+$ T-cell memory subsets in CLL

Phenotyping analyses revealed that CLL patients were much more skewed to a differentiated CD8$^+$ T-cell EM/EMRA phenotype when compared to age-matched healthy donors ((Nunes et al. 2012) and Chapter 3). STELA was employed to investigate whether the skewing to increased differentiation was linked to an accumulation of replicatively-aged cells, or a conversion of newly activated T-cells moving down the differentiation pathway.

Although CLL patients showed a trend for longer telomeres, the mean telomere length of naïve, EM and EMRA subsets did not differ significantly between the total CLL cohort and healthy donors (Figure 6.10). These preliminary results could imply that overall the CD8$^+$ T-cell subsets of CLL patients have not undergone additional proliferation compared to CD8$^+$ T-cells in healthy donors, and therefore do not appear to be any more aged in CLL pathology.

Previous results (Chapter 3) demonstrated that phenotypic skewing was exacerbated in patients with inverted CD4:CD8 ratio (CLL^{IR}), and the inverted ratio was predominantly due to an expansion within the CD8$^+$ T-cell compartment. The STELA CLL cohort was therefore stratified into CLL^{NR} and CLL^{IR} subgroups for further analysis. In contrast to the phenotyping results, this did not result in any significant differences in mean telomere lengths either between the two CLL subgroups (CLL^{IR} vs CLL^{NR}) or between these subgroups and the healthy donors (Figure 6.11).

Overall, telomere length does not appear to be different in CLL patients when stratified by CD4:CD8 ratio.

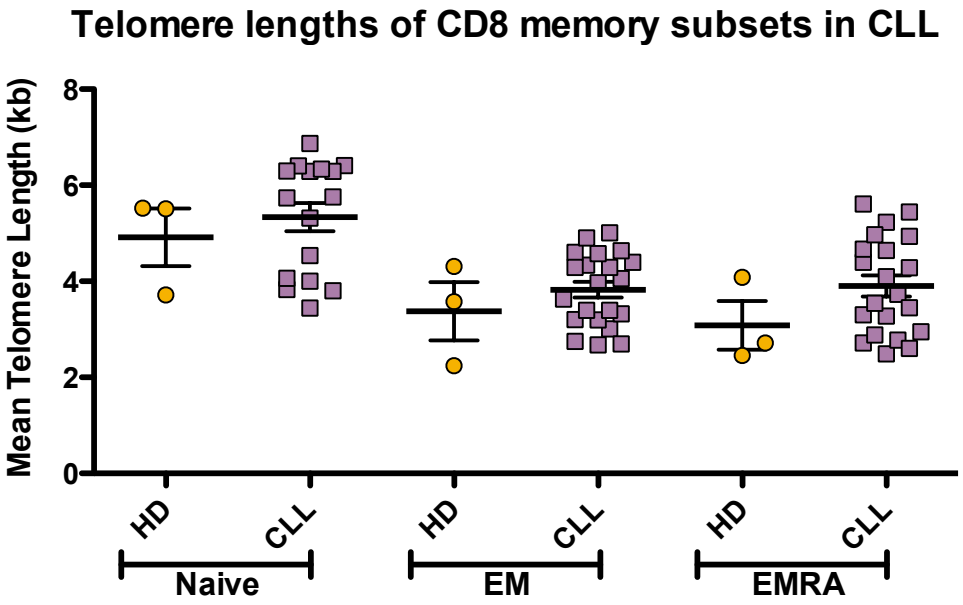

Figure 6.10. Mean telomere lengths of CD8$^+$ T-cell memory subsets in CLL patients and healthy donors (n = 3). Fluorescence-activated cell sorting (FACS) was performed (BD Aria, BD FACSDiva). Lymphocytes were gated based on forward and side scatter profile; single cells were gated by forward scatter area and height. T-cells were identified by gating first on CD3$^+$ then either CD4$^+$ or CD8$^+$ populations. CD8$^+$ memory subsets were defined within the CD8$^+$ gate using CCR7 and CD45RO memory markers: naïve (CCR7$^+$CD45RO$^-$, n = 16), Central Memory (CM, CCR7$^+$CD45RO$^+$), Effector Memory (EM, CCR7$^-$CD45RO$^+$, n = 21) and EMRA (CCR7$^-$CD45RO$^-$, n = 21). DNA was extracted from CD8$^+$ T-cells isolated from PBMCs of CLL patients and XpYp specific STELA was performed. Telomere length and distribution was calculated using Phoretix software: mean telomere lengths were calculated using Excel. Pairwise statistical analysis (HD vs CLL) was performed using the non-parametric Mann-Whitney test. Significant results were included on the graph (* = p ≤0.05; ** = p ≤0.01; *** = p ≤0.001).

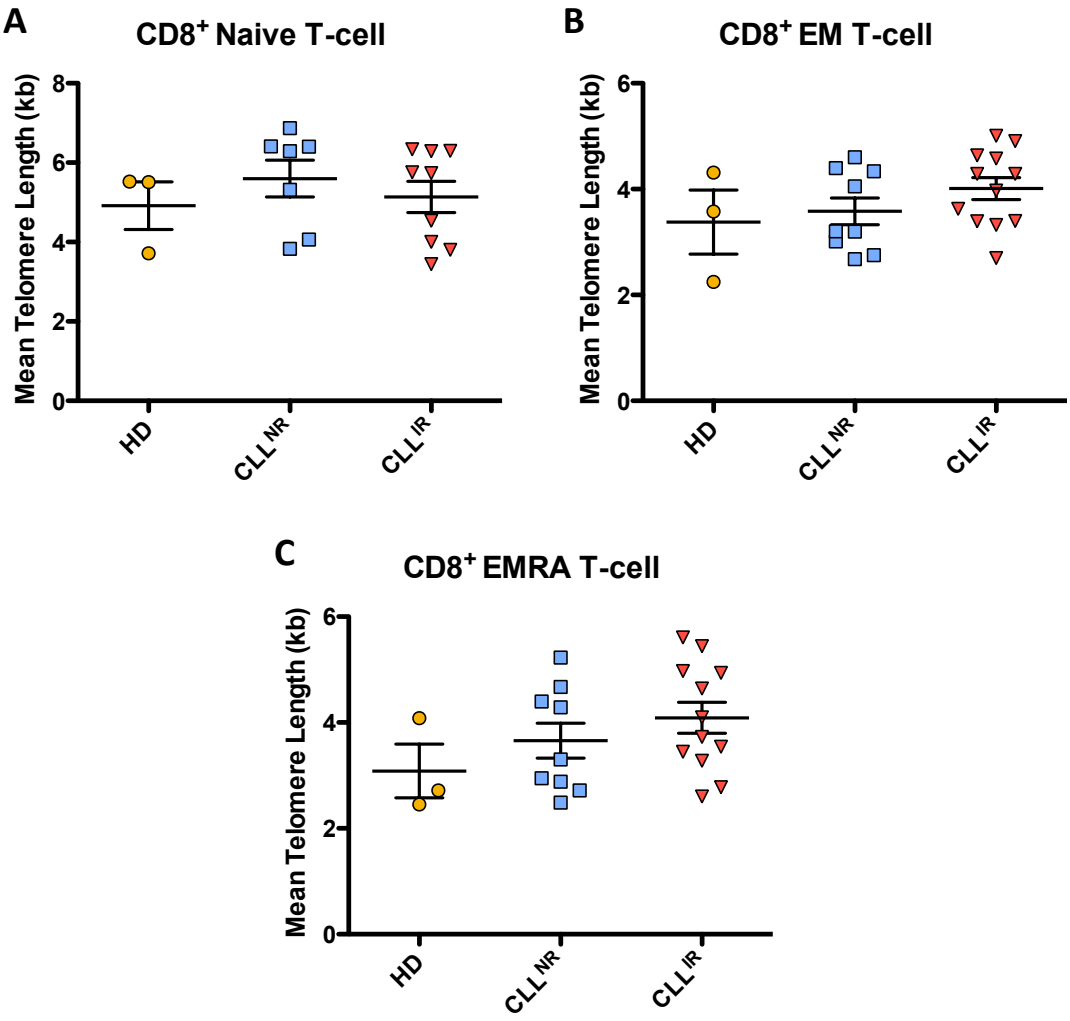

Figure 6.11. Mean telomere lengths of CD8$^+$ T-cell memory subsets in CLL^{NR} patients, CLL^{IR} patients and healthy donors (n = 3). Fluorescence-activated cell sorting (FACS) was performed (BD Aria, BD FACSDiva) using gating as described in Figure 6.2. DNA was extracted from CD8$^+$ T-cells isolated from PBMCs of CLL patients and XpYp specific STELA was performed. Telomere length and distribution was calculated using Phoretix software: mean telomere lengths were calculated using excel. (A) Telomere length of CD8$^+$ naïve T-cells in healthy donor, CLL^{NR} (n = 7) and CLL^{IR} (n = 9) patients. (B) Telomere length of CD8$^+$ EM T-cells in healthy donor, CLL^{NR} (n = 9) and CLL^{IR} (n = 12) patients. (C) Telomere length of CD8$^+$ EMRA T-cells in healthy donor, CLL^{NR} (n = 9) and CLL^{IR} (n = 12) patients. Three-way ANOVA statistical analysis was performed using Kruskal-Wallis test (HD vs CLL^{NR} vs CLL^{IR}), with all pairs of data assessed using the Dunn's post-test. Significant results were included on the graph (* = p ≤0.05; ** = p ≤0.01; *** = p ≤0.001).

6.6. $CD8^+$ naïve populations with abnormally short telomere length

In line with previous work (Weng et al. 1995), this study observed that $CD8^+$ naïve T-cells in CLL patients possessed significantly longer telomeres than the more differentiated memory subsets (EM/EMRA; see Figure 6.8, Section 6.4). However, one interesting observation that arose from this analysis was the presence of a subgroup of CLL patients (6/16 patients) with abnormally short telomeres within the $CD8^+$ naïve subset. This was first apparent when visualising the STELA blots as a clear telomere shortening could be observed for certain patients (see representative Figure 6.12). This was confirmed when data was analysed in a scatter plot: there appeared to be a distinct division where the CLL patients appeared to cluster in either a long or short telomere length subgroup (Figure 6.10).

When stratified into $CD8^+$ naïve long- and short- telomere subgroups, the short-telomere subgroup possessed an average telomere length of 3.95 kb within the naïve subset, versus 6.17 kb in the patients with longer telomeres. The abnormally short $CD8^+$ naïve telomere length was similar to the average telomere lengths observed in the EM and EMRA subsets of the total CLL cohort (3.83 and 3.90, respectively), suggesting that the naïve population of these patients possess a replicative age similar to that of a more differentiated memory T-cell.

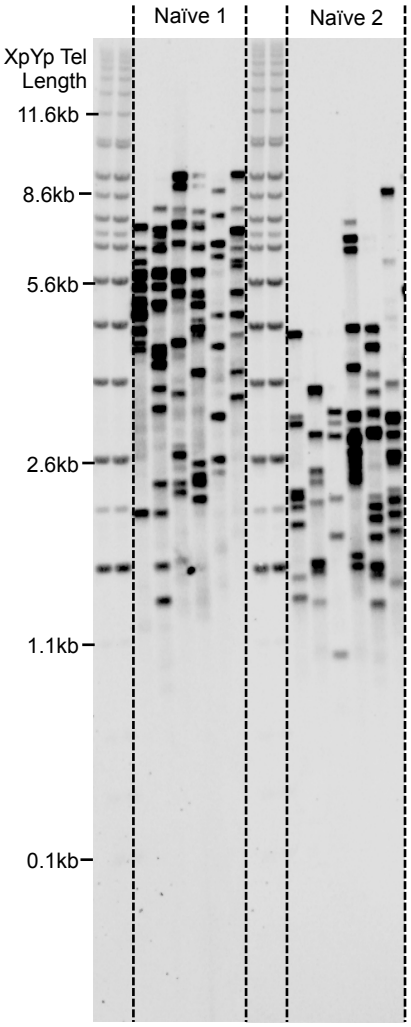

	Naïve 1	Naïve 2
Mean Telomere length (kb)	4.52	3.44
Standard Deviation	2.25	1.91

Figure 6.12. CD8$^+$ naïve populations with longer and shorter telomere length, shown in representative CLL patients. Fluorescence-activated cell sorting (FACS) was performed (BD Aria, BD FACSDiva) using gating as described in Figure 6.2. DNA was extracted from CD8$^+$ T-cells isolated from PBMCs of CLL patients and XpYp specific STELA was performed. Telomere length and distribution was calculated using Phoretix software: mean telomere lengths were calculated using excel. Presented in this figure a representative CLL patients of the long and short telomere length subgroups.

6.7. CLL patient subgroups with long or short telomeres

The more differentiated $CD8^+$ memory subsets' telomeres are shorter and possess less variation than their naïve counterparts (Section 6.4, Figure 6.8), but there is still some level of telomere length heterogeneity within these memory subsets and patient-to-patient variability.

Following the observation that some patients possessed particularly short telomeres within the naïve $CD8^+$ population (see previous section), analysis was performed to investigate any potential trend between long and short telomere subgroups within the other memory subsets of the CLL patient cohort. Patient data was collated from patients where STELA data was available for any three out of the four $CD8^+$ populations of interest: $CD8^+$ as a whole, $CD8^+$ naïve, $CD8^+$ EM and $CD8^+$ EMRA. If telomere lengths for a patient were consistently above (long telomere) or below average (short telomere) of the T-cell population, they were assigned a specific colour (within the red spectrum for long telomere; blue spectrum for short telomeres). Results are displayed in Figure 6.13.

Overall, it appeared that there were subgroups within the study cohort who had consistently longer than average telomeres in the $CD8^+$ naïve, EM and EMRA subsets. Conversely, there was a subgroup of CLL patients who consistently demonstrated shorter than average telomeres in naïve, EM and EMRA $CD8^+$ T-cell subsets.

This interesting observation suggests that telomere length of $CD8^+$ T-cells in CLL patients can have a consistent trend across subsets; therefore, replicative age between the T-cell subsets in an individual patient may be linked.

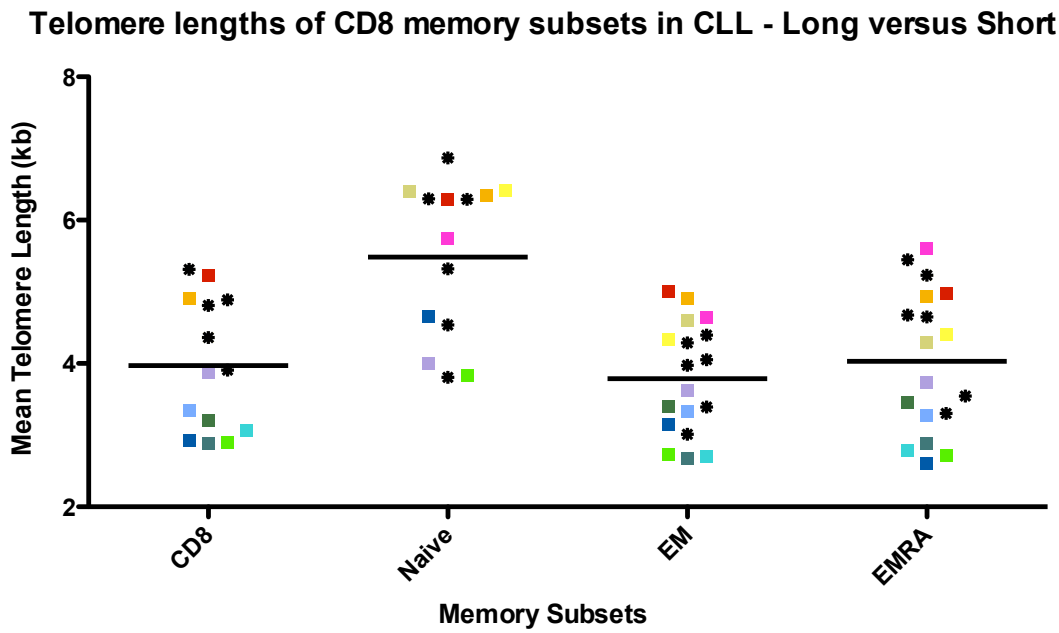

Figure 6.13. CLL patient comparison for long and short telomere length sub-groups. Fluorescence-activated cell sorting (FACS) was performed (BD Aria, BD FACSDiva) using gating as described in Figure 6.2. DNA was extracted from $CD8^+$ T-cells isolated from PBMCs of CLL patients and XpYp specific STELA was performed. Telomere length and distribution was calculated using Phoretix software: mean telomere lengths were calculated using excel. If a patient's mean telomere length was consistently longer than average in multiple subsets, they were assigned a colour in the red spectrum. If a patient's mean telomere length was consistently shorter than average in multiple subsets, they were assigned a colour in the blue spectrum. Black stars represent patients who do not fit within the 'all long' or 'all short' subgroups.

6.8. Correlation between subset telomere length

Patient subgroups were identified with a pattern of 'longer' or 'shorter' telomere lengths in all memory subsets. To assess whether there was an association with telomeres of proportional length across the $CD8^+$ memory subsets, correlation analyses were performed.

Strong positive associations were found between telomere lengths of the whole $CD8^+$ fraction and that of the $CD8^+$ EM subset ($r^2 = 0.5927$, $p = 0.0012$; Figure 6.14A). A similar relationship was observed between $CD8^+$ whole fraction and the $CD8^+$ EMRA subset ($r^2 = 0.7012$, $p = 0.0001$; Figure 6.14B). These relationships are perhaps not that surprising: as CLL patients have demonstrated that a significant proportion of the $CD8^+$ T-cell compartment consists of EM/EMRA cells, the telomere lengths of the whole $CD8^+$ fraction would therefore be strongly influenced by the telomere lengths of the EM/EMRA memory subsets. The strongest relationship was found between the $CD8^+$ EM and $CD8^+$ EMRA T-cell subsets, which demonstrated a significant positive relationship ($r^2 = 0.7852$, $p < 0.0001$; Figure 6.14C). This strongly suggests that the replicative age of EM and EMRA subsets are linked.

In summary: correlations between telomere lengths of the whole $CD8^+$ compartment against the EM and EMRA subsets is consistent with the previously observed compartmental skew to these more differentiated phenotypes, and such strong associations between the EM and EMRA telomere length lends strength to a linked replicative history between the two subsets.

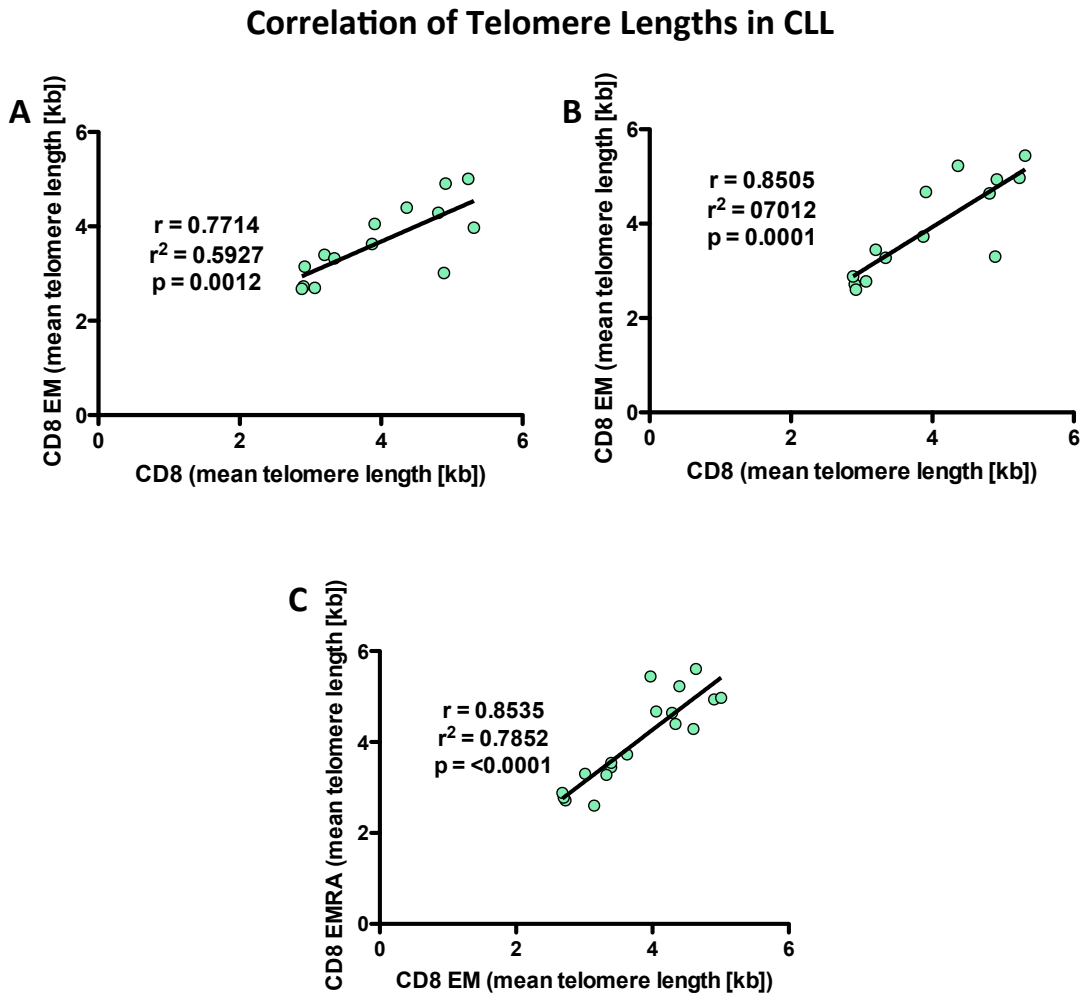

Figure 6.14. Positive correlations between the telomere lengths of CD8$^+$ T-cell memory subsets. Fluorescence-activated cell sorting (FACS) was performed (BD Aria, BD FACSDiva) using gating as described in Figure 6.2. DNA was extracted from CD8$^+$ T-cells isolated from PBMCs of CLL patients and XpYp specific STELA was performed. Telomere length and distribution was calculated using Phoretix software: mean telomere lengths were calculated using excel. Correlation between mean telomere lengths were analysed for (A) Total CD8$^+$ compartment versus CD8$^+$ EM subset, (B) Total CD8$^+$ compartment versus CD8$^+$ EMRA subset, and (C) CD8$^+$ EM subset versus CD8$^+$ EMRA subset. Spearman's correlation analyses were used to determine significance.

6.9. Discussion

This Chapter aimed to explore the replicative history of the T-cells in CLL patients, with a focus on the $CD8^+$ T-cell compartment. Specifically, to test the hypothesis that the expansion of $CD8^+$ T-cells in patients with inverted CD4:CD8 ratio was a result of excessive cell division. A prediction of this hypothesis would be that $CD8^+$ T-cells in the CLL^{IR} cohort would have shorter telomeres than $CD8^+$ T-cells in the CLL^{NR} cohort.

Due to the low frequency of T-cells usually observed in CLL PBMC fractions, further purification of T-cells was performed using $CD19^+$ magnetic bead sorting. Preliminary analysis of $CD4^+$ and $CD8^+$ populations demonstrated no detrimental effect on the $CD4^+/CD8^+$ frequencies or the memory subsets. However, there were limitations on size of patient samples (<5mls of blood) that meant detailed phenotyping (2 antibody panels, Chapters 3 and 4) and STELA could not be performed on the same patient samples. Phenotypic comparison between this CLL STELA cohort and the larger CLL cohort analysed in previous phenotyping analyses (Chapter 3) demonstrated that the STELA cohort displayed similar $CD8^+$ T-cell memory composition, i.e. CLL patients skewed to a more differentiated memory phenotype compared to healthy donors that was exacerbated in CLL^{IR} patients. However, for the most part the trend was non-significant and only the reduction in $CD8^+$ naïve frequency reached significance in either the total or stratified CLL cohort. Furthermore, Chapter 3 observed increased frequencies of $CD8^+$ EM T-cells in the CLL^{IR} subgroup compared to the healthy donors: this was not reflected in the STELA cohort, but the lack of significance could be due to the smaller cohort size of the STELA study. Further analysis with a larger patient cohort would give greater strength and understanding to the results, particularly in comparisons between healthy donor and CLL patient groups. However, overall the STELA cohort followed the expected skewing of subset distributions and therefore could provide insight into the replicative history of CLL T-cells.

The primary aims of this study were to compare whether the telomere lengths of $CD8^+$ subsets could provide insight on the expanded $CD8^+$ compartment of CLL^{IR} patients. This study did not observe any differences in telomere length of $CD8^+$ T-cells of CLL patients compared against healthy donors. This was the same within the $CD8^+$ compartment as a whole as well as the naïve, EM and EMRA memory subsets. However, due to the limitation in sample sizes, particularly in the healthy donor group, these

results are preliminary. An expanded telomere length analysis in a larger cohort would address this limitation.

Using telomere length as a sign for proliferative age and senescence of cells is well documented (Allsopp et al. 1992; Vaziri et al. 1994; J. Lin et al. 2010a; Sanders and Newman 2013), as is the association of shortened telomeres with poorer disease prognosis and mortality (Willeit et al. 2010; Wu et al. 2003; Han et al. 2009; Shao et al. 2007). This study used STELA to assess telomere length to allow a high resolution analysis of the telomeres lengths of a specific chromosome (XpYp), in addition to a key advantage of being able to detect telomeres at much shorter lengths than other techniques (Britt-Compton et al. 2011; Baird 2005). As the inverted CD4:CD8 ratio in CLL patients results from an expanded $CD8^+$ compartment (Nunes et al. 2012), it could be expected that there would be a marked shortening in telomeric length of $CD8^+$ T-cells in the CLL^{IR} population, particularly within the EM and EMRA subsets. However, overall this study observed no $CD8^+$ telomere shortening in the CLL^{IR} subgroup, suggesting that there was no proliferative expansion. Instead, telomere lengths of $CD8^+$ T-cells did not appear to differ between CLL^{IR}, CLL^{NR} and healthy donor patients. Although we expected CLL^{IR} patients to demonstrate telomere shortening to reflect $CD8^+$ T-cell expansion, there was instead a trend towards longer telomeres in CLL^{IR} patients, although this was not significant.

Rather than a clonal expansion of chronically stimulated, highly differentiated 'aged' $CD8^+$ T-cells, the $CD8^+$ T-cell expansion in CLL could originate from newly differentiated EM/EMRA T-cells converted from the naïve T-cell compartment. Newly formed memory T-cells possess a longer telomere length profile, similar to that observed in the healthy donors and CLL^{NR} patients, and would accumulate via continuous turnover from the naïve pool. Related to this, Svenson et al. (2013) observed correlations between longer peripheral blood T-cell telomeres and increased levels of regulatory T-cells in renal cell carcinoma patients with poorer prognosis. This could suggest that the $CD8^+$ expansion might not arise from a clonal expansion of highly differentiated T-cells that have undergone multiple rounds of division, but is rather an accumulation of 'younger' T-cells that are chronically stimulated but are under active immunological suppression from factors such as T_{reg} cells. Accumulation of regulatory $CD4^+$ T-cells in CLL patients has been reported previously (Piper et al. 2011; Nunes et al. 2012), and it is possible CLL cells themselves play an immunoregulatory role, as CLL

B-cells have been previously shown to demonstrate immunosuppressive functions (DiLillo et al. 2013; Ramsay et al. 2008).

Another consideration is the involvement of telomerase contributing to $CD8^+$ telomere length maintenance, either by conserving telomeres and preventing telomere shortening during proliferation, or by lengthening telomeres that have already shortened during multiple rounds of division. Aberrant upregulation of telomerase is often identified in malignant cells, including CLL cells (Rampazzo et al. 2011; Damle 2002). However, telomerase activity has also been reported in non-malignant hematopoietic cells, including T-cells, with an increase in telomerase activity during T-cell activation (Broccoli et al. 1995; Weng et al. 1996; Bodnar et al. 1996). Studies have observed induced telomerase activity and preserved telomere lengths in clonally expanded virus-specific $CD8^+$ memory T-cell populations during acute infections (Hathcock et al. 2003; Plunkett et al. 2001; Maini et al. 1999). It could be possible that a similar situation is taking place in the expanded $CD8^+$ T-cells of CLL^{IR} patients, whereby the expanded EM/EMRA population are proliferating in response to antigen, but do not display a loss of telomere length due to the up-regulation of telomerase within these cells. However, T-cell telomerase activity has been shown to decrease over time, and it is unable to overcome telomere shortening during long-term stimulations (Valenzuela and Effros 2002; Bodnar et al. 1996). Therefore, the accumulation of T-cells that already possess longer telomeres seems more likely, perhaps with short-term rather than long-term telomerase maintenance. Further work investigating the presence of telomerase within the $CD8^+$ T-cell compartment of CLL would help further elucidate the origin of the $CD8^+$ T-cell expansion in CLL^{IR} patients. Furthermore, parallel analysis of CLL cell telomere lengths and telomerase activity in CLL patient samples could help identify links between T-cell and CLL cell relationships within the tumour microenvironment.

Prior work analysing telomere lengths of human T-cell memory subsets have shown naïve T-cells have the longest telomeres, where EM/EMRA telomere lengths are much shorter by comparison (Rufer et al. 1998; Weng et al. 1995): this was also observed in CLL patients in this study. Adding to this, STELA also demonstrated that the EM and EMRA subsets were less heterogeneous and more clonal than the naïve population. This is to be somewhat expected, as the memory T-cell are longer-lived cells that will have undergone more division than naïve T-cells.

Some CLL patients exhibited much shorter telomeres than others within the naïve compartment. Aging can have an effect on immune capacity in patients, including skewing to a more differentiated phenotype, increased senescence and a significant reduction in telomeres (Koch et al. 2008; Weiskopf et al. 2009). These characteristics are not fixed; immunological factors continue to worsen with age, including within the naïve T-cell population (Ferrando-Martínez et al. 2011). CLL is a predominantly a disease of the elderly and it is possible that the patients identified with shorter naïve telomeres were the more elderly patients within the cohort. However, preliminary retrospective correlation analysis suggests that age and naïve telomere length were not linked within the STELA cohort (Appendix VIII). This was based on limited data and small patient numbers, however, so further research including associations with age and other clinical factors would be beneficial.

Another interesting pattern identified was a subgroup of CLL patients who had shorter telomeres (based on the patient average) across the $CD8^+$ subsets (i.e. shorter telomeres in naïve, EM and EMRA). Inversely, a subgroup of patients who had longer telomeres in naïve $CD8^+$ T-cells also had longer telomeres in the EM/EMRA subset. This was particularly apparent with the EM/EMRA subsets and draws an interesting link across the $CD8^+$ compartment. Telomere length in peripheral blood lymphocytes has been associated with prognosis for various cancers (Svenson et al. 2008; Svenson et al. 2013; Duggan et al. 2014; Qian et al. 2016). Furthermore, there was strong correlation between the telomere lengths of the $CD8^+$ EM and EMRA subsets, suggesting a relationship between their replicative history driven by the same stimulatory environment and potentially are clonotypes at different stages of the T-cell memory pathway. Stratification of CLL patients into these 'long' and 'short' T-cell telomere subgroups could have potential prognostic value in CLL. This study also observed a direct relationship with mean telomere length and the telomere length distribution, suggesting that in CLL patients where T-cell populations have undergone more replication have, they have also become more clonal. Unfortunately, comparisons were limited as prognostic data for each subset was not available for each patient. Additional telomere analysis of the $CD8^+$ T-cell compartment in a larger cohort of patients and healthy donors could be used to compare telomere length against clinical data such as PFS applying survival analyses and shed further light on the relationship of telomere lengths across the T-cell subsets and whether there is any role in CLL prognosis.

One of the biggest limitations within this study was the acquisition of appropriate samples. The majority of PBMCs from CLL patients are malignant B-CLL lymphocytes. Therefore, larger samples are required in order to obtain an appropriate amount of T-cells suitable for sorting and DNA extraction. This limited the number of appropriate samples available, and could have introduced bias to the study as it restricted sampling to patients with larger numbers of lymphocytes per ml of blood, which is usually a signifier for CLL patients with higher pathology (i.e. higher numbers of circulating CLL cells). This may account for why the STELA cohort skewed even more towards the $CD8^+$ EMRA subset than the cohort analysed in Chapter 3 as previously mentioned. In future work, it would be desirable to obtain a larger sample of blood from patients, to allow a more representative cohort to be used for analysis and to reduce bias. A larger patient cohort may also be better powered for the phenotypic skewing and telomere length trends demonstrated here to show significant differences within CLL patients. Furthermore, if larger numbers of T-cells could be acquired, this could give the opportunity for expansive phenotypic analysis to tunnel further into the T-cell compartment and isolate additional, phenotypes alongside STELA analysis within the same patient. As an example, this study was only able to perform STELA on the $CD4^+$ compartment as a whole, whereas additional sample could allow for telomere length analysis of the $CD4^+$ memory subsets and subtypes (Tregs, Th1, Th17). Additional sample could also give an opportunity to isolate smaller T-cell populations, such as the phenotypes of prognostic interest identified in the previous chapters. Further STELA analysis acquiring larger blood samples and/or collecting samples over a longer period could give rise to a larger cohort and more opportunity for additional analyses, for example investigating the links to CLL prognosis. It could also allow for longitudinal analysis of CLL patients to observe changes in T-cell/CLL cell telomere length over time or as a consequence of treatment.

This study has given novel insight into T-cell telomere length of CLL patients. Somewhat unexpectedly and contrary to our hypothesis, telomere lengths in CLL^{IR} patients were similar to CLL^{NR} patients and healthy donors, despite the presence of the expanded $CD8^+$ population. Further work is needed to establish how telomere length of the $CD8^+$ expansion is maintained, whether it is due to the expansion originating from newly converted memory T-cells, or telomere lengthening processes such as telomerase. Additionally, this study identified subgroups of CLL patients with short or long telomeres that could be used to stratify future CLL cohorts and investigate the relevance

of this discovery, if any, on CLL pathogenesis and prognosis. Regardless, no loss of telomere length in CLL^{IR} patients supports the assessment that the expanded $CD8^{+}$ T-cells have not reached a stage of irreversible replicative senescence or terminal differentiation.

Chapter 7
Final discussion

The primary overall objective of this thesis was to gain further insight into the $CD8^+$ expansion observed in a subgroup of CLL patients that resulted in an inversion of the CD4:CD8 ratio (CLL^{IR}, ratio <1.0). One of the major factors that drove interest into this subgroup was that CLL^{IR} patients had significantly poorer prognosis than their normal ratio (CLL^{NR}) counterparts. Nunes et al. (2012) established that CLL^{IR} patients were 3.4 times as likely to experience disease progression (PFS HR = 3.4, p = 0.005). The CLL cohort used for the phenotyping study of Chapters 3 and 4 demonstrated similar results (HR 5.5, 95% CI 2.25-13.62, p = 0.0002) and showed a potential increased risk in patients with a ratio of approximately 0.5 or lower, suggesting that the lower the ratio, the more inferior the prognosis. Thus it may be possible to stratify patients into those with higher and lower risk of progression based on CD4:CD8 ratio alone.

Both the multivariate and univariate analyses applied in Chapter 3 confirmed that CD4:CD8 ratio does have some prognostic link to CLL; however, the analyses revealed additional T-cell phenotypes that conferred a much stronger effect on PFS. The strongest phenotype to derive from this analysis was $CD4^+HLA\text{-}DR^+PD\text{-}1^+$, which was present at much higher frequencies in CLL (particularly within CLL^{IR} patients). $CD4^+PD\text{-}1^+$ T-cells have previously been shown to be higher in CLL and associated with poorer prognosis (Novák et al. 2015; Rusak et al. 2015), but the $CD4^+HLA\text{-}DR^+PD\text{-}1^+$ phenotype has not been previously reported in CLL.

This phenotype has been described previously on TILs in melanoma for both the $CD4^+$ and $CD8^+$subsets, including tumour-antigen specific $CD8^+$ T-cells (Ahmadzadeh et al. 2009). In CLL we also reported increased frequencies of $HLA\text{-}DR^+PD\text{-}1^+$ in both $CD4^+$ and $CD8^+$ compartments, but it was the $CD4^+$ phenotypes that showed the greatest prognostic potential. Like melanoma, the increase in this phenotype within CLL could be related to the tumour microenvironment and tumour-specific T-cells. The $HLA\text{-}DR^+PD\text{-}1^+$ markers could define primed/activated T-cells that have impaired function. They may be unable to respond effectively due to the immunosuppressive effects of CLL cells: dysfunction between the PD-1/PD-1L axis between T-cells and CLL cells has been reported previously (Brusa et al. 2013), as well as expansions of $CD8^+$

T-cells expressing PD-1 that have impaired cytotoxic activity but retain cytokine production (Riches et al. 2013). Blockade of PD-1 has demonstrated a reversion of T-cell function and prevention of CLL progression in murine models (McClanahan et al. 2015), supporting an immunosuppressive role for this molecule.

This prompts the immunotherapeutic potential of anti-PD-1 therapy, and at the time of writing there is an ongoing clinical trial investigating dual therapy of ibrutinib with anti-PD-1 monoclonal antibody (Freeman and Gribben 2016). The results obtained in this thesis reinforce the relevance of the immunosuppressive phenotypes within CLL but further work is needed to assess any functional or prognostic importance behind the co-expression of HLA-DR. If indeed the PD-1^{+}HLA-DR^{+} T-cells are reacting to tumour antigen, it is possible that PD-1 blockade treatment would be superior in patients with high frequencies of CD4^{+}HLA-DR^{+}PD-1^{+} T-cells, due to the prevalence of tumour specific T-cells. A suggested study to address this would be to compare anti-PD-1 antibody treatment in HLA-DR^{+}PD-1^{+} versus HLA-DR^{-}PD-1^{+} CLL samples *in vitro*.

CD8^{+} T-cell frequency was included second in the list of significant prognostic variables, suggesting that rather than an inverted CD4:CD8 ratio as the prognostic factor, the CD8^{+} expansion itself should be the focus, regardless of ratio i.e. regardless of CD4^{+} T-cell numbers. Confounding CLL patients with CD8^{+} expansions, but not CD4:CD8 inversion and therefore characterised as CLL^{NR}, may explain why significant changes in telomere lengths were not observed in Chapter 6. Furthermore, there appeared to be some overlap between the prognostic phenotypes (CD4^{+}HLA-DR^{+}PD-1^{+} and CD8^{+}CD57^{+}HLA-DR^{+}) and CD4:CD8 ratio, as these phenotypes were exacerbated within the CLL^{IR} subgroup. It is possible, therefore, that the T-cells expressing these markers contribute to the CD8^{+} expansion that can then cause CD4:CD8 ratio inversion; hence the phenotypes (and the CD8^{+} compartment as a whole) are more direct prognostic factors. Analysis of a CLL cohort stratified by CD8^{+} T-cell frequency (with a threshold of approximately 30% as suggested by the multivariate analyses) or absolute CD8^{+} T-cell numbers rather than CD4:CD8 ratio may yield more significant associations with prognosis.

With regards to the CD4:CD8 ratio, what can be summarised from the phenotypic analysis of this study confirms the already reported increase in senescence within the CLL^{IR} subgroup (Nunes et al. 2012) in the form of CD57^{+} and KLRG-1^{+} T-cells making

up a significant proportion of the $CD8^+$ compartment, with approximately 50% of $CD8^+$ T-cells expressing $CD57^+KLRG\text{-}1^+$. However, we also observed a similar proportion of $CD8^+$ T-cells with an activated phenotype and $CD8^+$ T-cell subtypes identified as presenting an 'activated senescent' $CD57^+HLA\text{-}DR^+$ phenotype that were more frequent in the patients with inverted CD4:CD8 ratio (CLL^{IR}). Interestingly, the $CD4^+$ compartment exhibited similar trends with exacerbated $CD57^+HLA\text{-}DR^+$ and $HLA\text{-}DR^+PD\text{-}1^+$ frequencies in CLL^{IR} patients, although these phenotypes comprised a smaller proportion of the total $CD4^+$ compartment. That all these phenotypes occur in CLL^{IR} patients and are strongly related to one another (as demonstrated in Chapter 4) would imply interrelated T-cell activation and subsequent differentiation in response to antigen(s). Furthermore, with both $CD4^+HLA\text{-}DR^+PD\text{-}1^+$ and (to a lesser effect) $CD8^+CD57^+HLA\text{-}DR^+$ identified as significant prognostic phenotypes, their potential importance in CD4:CD8 ratio and CLL pathology. With regard to the latter, it would be useful to ascertain whether these phenotypes are solely prognostic markers for these conditions or whether they play a direct role in CLL pathology, i.e. if they are tumour promoting T-cell populations, or tumour-reactive T-cells that accumulate under chronic antigenic conditions but are unable to respond in the immunosuppressive tumour microenvironment. If the latter, these phenotypes could prove to be a good target for immunotherapy, whether that be as a monotherapy or as a combination therapy with other CLL treatments. Further work to address this would be to explore the functional capabilities of T-cells expressing these phenotypes, such as proliferation assays (using mitogens or CLL-specific stimulation) and cytokine assays.

One major confounding factor when investigating the immune dysfunction of an elderly population is the persistence of common latent viral infections that have accumulated during ones lifetime and dominate the T-cell repertoire (Fülöp et al. 2013). As the majority of CLL diagnoses occur in the elderly, it could be speculated that T-cell dysfunction in CLL is due to virus-specific T-cell clonotypes forming the majority of the T-cell pool, which may contribute to an impaired immune response against the CLL cells themselves. CMV can be found in approximately 90% of the elderly population and has been shown to drive both $CD4^+$ and $CD8^+$ T-cells to a highly differentiated, immunosenescent phenotype (Vasto et al. 2007). Adding to this, CMV-specific T-cells have been reported to form 5-30% of the $CD8^+$ T-cell pool (Klenerman and Oxenius 2016). Through the CMV serotyping of CLL patients, this study determined that CMV was not associated with the CD4:CD8 ratio, nor T-cell memory skewing observed in

both the $CD4^+$ and $CD8^+$ T-cell pools. Furthermore, the prognostic phenotypes of interest within this study ($CD4^+HLA\text{-}DR^+PD\text{-}1^+$ and $CD8^+CD57^+HLA\text{-}DR^+$) were significantly more prevalent within the CLL^{IR} subgroup and seemed to originate from the EM memory compartment; this suggests that these phenotypes are also not CMV-driven.

A large cohort study (n = 347) did show that CMV^+ CLL patients experienced poorer prognosis than their CMV^- counterparts: however, when exposed to multivariate analysis and taking confounding clinical factors such as age into account, this prognostic difference was lost (Parry et al. 2016). This not only lends further strength to the prognostic phenotypes of this study being CMV-independent, but also reinforces the value of performing multivariate analyses to establish valuable prognostic markers, as was done for this thesis. Due to the limited number of CMV^- individuals in the cohort, CMV seropositivity could not be included in the multivariate analyses, and chi-squared analysis of $CD4^+HLA\text{-}DR^+PD\text{-}1^+$ and $CD8^+CD57^+HLA\text{-}DR^+$ could not be performed. Therefore, future studies with larger cohorts are needed to fully rule out CMV as a confounding factor.

EBV is another latent virus found in the majority of adults, residing in B-cells (Visco et al. 2015). In healthy individuals EBV latency is controlled by CTLs, but in cases of immune T-cell dysfunction there is a risk of EBV reactivation and replication. CLL is not normally considered an EBV associated disease; EBV has low detection rate in CLL patients, EBV markers are only detectible on certain CLL subpopulations, and immortalisation of a CLL cell line using EBV has proved challenging (Visco et al. 2015; Dolcetti and Carbone 2010), though perhaps not impossible (Hertlein et al. 2013). Interestingly, recent work investigating EBV in CLL reported significantly higher EBV DNA load in CLL patients versus healthy donors, but concluded no relationship between EBV-load and disease state (Visco et al. 2015). However, high EBV load was identified as an independent prognostic variable following multivariate analysis, raising the question of whether EBV could be associated with the T-cell dysfunction reported in this thesis. This is enhanced by the fact that EBV-specific T-cells typically present a EM phenotype that is less differentiated than with CMV (Fülöp et al. 2013).

Interestingly, EBV-specific $CD8^+$ cells in CLL are highly differentiated memory cells compared to healthy donors, and present markers associated with exhaustion, (Hofland

et al. 2015). Additionally, considering the high prevalence of EBV reported in other immunological malignancies, including B, T and NK cell lymphomas (Dolcetti and Carbone 2010), the lack of similar evidence for CLL argues that there is low involvement of EBV within the disease. Taken together, this suggests that EBV is less likely to be a driving factor of the T-cell abnormalities reported in this thesis. Further work is needed to eliminate viral persistence as the driver for the $CD4^+HLA\text{-}DR^+PD\text{-}1^+$. However, the reporting of $CD4^+PD\text{-}1^+HLA\text{-}DR^+$ in melanoma as discussed above (Ahmadzadeh et al. 2009) lends support to the $CD4^+HLA\text{-}DR^+PD\text{-}1^+$ phenotype being tumour-driven, rather than the result of chronic viral stimulation.

In most studies analysing the telomere lengths of T-cells in cancer, it is a shorter telomere length that ties with poor prognosis (Wu et al. 2003; Shao et al. 2007). Opposing results are reported here in CLL where no significant change in telomere length was observed in CLL^{IR} patients, which is somewhat unexpected in light of the observed $CD8^+$ T-cell expansion. Lack of change in $CD8^+$ T-cell telomere lengths within the CLL^{IR} cohort, particularly within the EM/EMRA cohort, could be attributed to continuous turnover from the naïve $CD8^+$ T-cell pool. These could be continuously driven down the T-cell differentiation pathway where they accumulate as EM and EMRA cells. This in turn may cause the reduction in $CD8^+$ naïve frequency and skewing to the more differentiated memory phenotype as observed in Chapter 3, supporting the theory that the expanded $CD8^+$ T-cells in CLL^{IR} patients is driven by CLL-specific T-cells. Furthermore, unlike the other cancer studies where shorter T-cell telomeres were associated with poorer prognosis, CLL cells are accumulated malignant B-cells, meaning that B-cell:T-cell interactions within CLL can result in the 'accidental' promotion of CLL cells by Th cells (Os et al. 2013), which in turn can exert immunosuppressive effects upon the effector functions of the activated T-cells, including the impairment of T-cell proliferation (Ramsay et al. 2008). This could therefore result in the continual T-cell accumulation of T-cells that do not proliferate and therefore do not experience telomeric shortening. If this conversion from the naïve pool is indeed the case observed here, a gradual reduction of naïve T-cell numbers would be expected; however, this was not the case after analysis of the preliminary counts of Chapter 3. Furthermore, this study identified patients with abnormally short telomeres in their $CD8^+$ naïve T-cells with mean telomere lengths similar to those observed in more differentiated memory subsets (Chapter 6). T-cell memory stem cells (Tscms) are reported to display the naïve memory phenotype (Gattinoni et al. 2011), as do a recently identified memory T-cell

population, termed Tmnps (memory T-cells with a naïve phenotype)(Pulko et al. 2016). It is possible, therefore, that a reduction in naïve T-cells was not observed in this study due to the confounding presence of alternative $CCR7^{+}CD45RO^{+}$ populations. Inclusion of additional characterising markers within future phenotypic analyses would help identify the truly naïve T-cells and the changes that occur within this subset.

The application of T-cell immunotherapy in CLL has growing interest, particularly the development of chimeric antigen receptor (CAR) T-cells – autologous T-cells that are harvested from patients and genetically modified to recognise tumour specific antigen, before being expanded and adoptively transferred back into the patient (Freeman and Gribben 2016). CD19-specific CAR T-cells have demonstrated immunotherapeutic potential in CLL patients (Porter et al. 2015; Porter et al. 2013; Brentjens et al. 2011), with increased efficacy observed in the generation of CAR T-cells following ibrutinib therapy (Fraietta et al. 2016). However, using CAR T-cells directed to $CD19^{+}$ cells would also include targeting of 'normal' B-cells; B-cell aplasia has been reported in CLL patients treated with CD19-specific CAR T-cells (Davila and Brentjens 2013). Therefore, optimising adoptive T-cell therapy by engineering the T-cells to recognise additional tumour-specific antigens could be of further therapeutic benefit. Further analysis into the clonality and specificity of the expanded T-cell populations identified in this thesis could help identify novel CLL specific antigens and the TCR that recognise them. High affinity versions of those TCRs could then be engineered into T-cells from CLL patients for therapy.

One aspect for future work in the phenotypic characterisation of CLL patients with regards to CD4:CD8 ratio would be rather than looking at CLL^{IR} related phenotypes and their link to inferior prognosis/CLL progression, to instead consider focusing on CLL^{NR} occurring phenotypes. It is possible that the $CD8^{+}$ expansion and phenotypes within CLL^{IR} patients actually relate to the 'normal' T-cell pathology in CLL, and that perhaps with a focus on T-cell patterns in CLL^{NR} one could identify T-cell attributes within CLL pathology that directly confer superior prognosis. Alternatively, further stratification of the CLL^{IR} subsets based on disease progression could be used to assess differences between these patients. The contribution of additional clinical characteristics upon patient prognosis must also be taken into account (age, gender, etc.) and considered in any future analyses in order to ascertain whether any prognostic association is indeed due to T-cells.

A limitation with the phenotypic analysis and STELA applied in this thesis is that although it can provide insight into T-cell subset distributions and their molecular age, it only provides a snapshot of the T cell population at the time the patient sample was acquired. There is potential for phenotypic data to be transient even in normal individuals, particularly when observing immunological cell types such as T-cells that could become activated and expand in number due to transient infections that patients may encounter. This is apparent in the preliminary study of Chapter 5 where even some untreated patients demonstrated phenotypic variability over time. It could be argued that CD4:CD8 ratio could be more prone to variability due to T-cell responses in acute infections, whereas disease-specific T-cell phenotypes may hold more stability and only incur changes due to disease pathology. It would therefore be prudent to argue that focusing on $CD4^+HLA\text{-}DR^+PD\text{-}1^+$, for example, rather than CD4:CD8 ratio or $CD8^+$ frequency/numbers, may provide a more successful, stable means of prognostic evaluation in CLL. This is supported by the observations in treated patients, where $CD4^+HLA\text{-}DR^+PD\text{-}1^+$ appeared more stable among the majority of untreated patients, and large frequency changes between time points occurred more often in treated patients. Ideally, analysis of both phenotype and telomere length would be undertaken in expansive longitudinal analyses. Unfortunately, the ability to perform such longitudinal assessment for the thesis was limited due to time and sample restrictions. Longitudinal analysis of untreated CLL over an extended time period (e.g. minimum of two years with standardised time points) would also be beneficial to identify T-cell changes that occur due to disease progression or effect of treatment. Such analyses would also be of similar benefit in observing CD4:CD8 ratio fluctuations over longer time periods to investigate disease related changes versus 'normal' ratio variations, i.e. during acute infections.

In conclusion, the thesis has confirmed that CD4:CD8 ratio inversion is linked to more aggressive clinical disease. The combination of high-resolution flow cytometry and multivariate analysis revealed that this ratio inversion is linked to a complex array of $CD8^+$ and $CD4^+$ T-cell subsets. Importantly, two T-cell subsets, $CD8^+CD57^+HLA\text{-}DR^+$ and $CD4^+PD\text{-}1^+HLA\text{-}DR^+$, were shown to be stronger predictors of poor prognosis than the CD4:CD8 ratio and would be suitable for testing on larger UK wide cohorts. Further functional and genetic characterisation of these novel T-cell subsets may give insight

into role of T-cells within CLL disease, but may also provide simpler and more specific prognostic markers that will benefit CLL patients.

Appendices

Appendix I. Statistical analyses of $CD8^+$ marker distributions using SPICE

Table 1. T-test analyses comparing $CD8^+$ markers in CLL versus healthy donors (HD).

Phenotype	HD vs CLL
Panel 1	
$CD57^+HLA\text{-}DR^+PD\text{-}1^+$	<0.0001
$CD57^+HLA\text{-}DR^+PD\text{-}1^-$	0.0012
$CD57^+HLA\text{-}DR^-PD\text{-}1^+$	0.0003
$CD57^+HLA\text{-}DR^-PD\text{-}1^-$	0.3548
$CD57^-HLA\text{-}DR^+PD\text{-}1^+$	<0.0001
$CD57^-HLA\text{-}DR^+PD\text{-}1^-$	0.4538
$CD57^-HLA\text{-}DR^-PD\text{-}1^+$	0.1002
$CD57^-HLA\text{-}DR^-PD\text{-}1^-$	<0.0001
Panel 2	
$CD57^+CD38^+CD127^+KLRG\text{-}1^+$	<0.0001
$CD57^+CD38^+CD127^+KLRG\text{-}1^-$	0.0002
$CD57^+CD38^+CD127^-KLRG\text{-}1^+$	0.0012
$CD57^+CD38^+CD127^-KLRG\text{-}1^-$	0.0049
$CD57^+CD38^-CD127^+KLRG\text{-}1^+$	0.0001
$CD57^+CD38^-CD127^+KLRG\text{-}1^-$	0.3528
$CD57^+CD38^-CD127^-KLRG\text{-}1^+$	0.3258
$CD57^+CD38^-CD127^-KLRG\text{-}1^-$	0.0646
$CD57^-CD38^+CD127^+KLRG\text{-}1^+$	0.3530
$CD57^-CD38^+CD127^+KLRG\text{-}1^-$	0.7257
$CD57^-CD38^+CD127^-KLRG\text{-}1^+$	0.0098
$CD57^-CD38^+CD127^-KLRG\text{-}1^-$	0.0910
$CD57^-CD38^-CD127^+KLRG\text{-}1^+$	0.2011
$CD57^-CD38^-CD127^+KLRG\text{-}1^-$	0.0204
$CD57^-CD38^-CD127^-KLRG\text{-}1^+$	0.6178
$CD57^-CD38^-CD127^-KLRG\text{-}1^-$	0.0086

Table 2. T-test analyses comparing $CD8^+$ markers in CLL^{IR} versus CLL^{NR} and healthy donors (HD).

Phenotype	HD vs CLL^{IR}	CLL^{NR} vs CLL^{IR}
Panel 1		
$CD57^+HLA\text{-}DR^+PD\text{-}1^+$	<0.0001	0.2436
$CD57^+HLA\text{-}DR^+PD\text{-}1^-$	<0.0001	0.0010
$CD57^+HLA\text{-}DR^-PD\text{-}1^+$	0.0066	0.8927
$CD57^-HLA\text{-}DR^+PD\text{-}1^+$	0.0032	0.9157
$CD57^+HLA\text{-}DR^-PD\text{-}1^-$	0.1581	0.2088
$CD57^-HLA\text{-}DR^+PD\text{-}1^-$	0.1255	0.0618
$CD57^-HLA\text{-}DR^-PD\text{-}1^+$	0.5626	0.0029
$CD57^-HLA\text{-}DR^-PD\text{-}1^-$	<0.0001	<0.0001
Panel 2		
$CD57^+CD38^+CD127^+KLRG\text{-}1^+$	0.0006	0.0550
$CD57^+CD38^+CD127^+KLRG\text{-}1^-$	0.0019	0.1184
$CD57^+CD38^+CD127^-KLRG\text{-}1^+$	0.0002	0.0026
$CD57^+CD38^+CD127^-KLRG\text{-}1^+$	0.0672	0.3527
$CD57^+CD38^-CD127^+KLRG\text{-}1^+$	0.0049	0.7243
$CD57^+CD38^-CD127^+KLRG\text{-}1^-$	0.5705	0.5897
$CD57^+CD38^-CD127^-KLRG\text{-}1^+$	0.1450	0.1691
$CD57^+CD38^-CD127^-KLRG\text{-}1^-$	0.1076	0.4745
$CD57^-CD38^+CD127^+KLRG\text{-}1^+$	0.3258	0.5207
$CD57^-CD38^+CD127^+KLRG\text{-}1^-$	0.2181	0.0750
$CD57^-CD38^+CD127^-KLRG\text{-}1^+$	0.0106	0.0366
$CD57^-CD38^+CD127^-KLRG\text{-}1^-$	0.0142	0.0691
$CD57^-CD38^-CD127^+KLRG\text{-}1^+$	0.0338	0.0031
$CD57^-CD38^-CD127^+KLRG\text{-}1^-$	0.0002	0.0001
$CD57^-CD38^-CD127^-KLRG\text{-}1^+$	0.8962	0.5739
$CD57^-CD38^-CD127^-KLRG\text{-}1^-$	0.0031	0.0728

Appendix II. Phenotypic analyses of CD8$^+$ T-cells in CLL: additional data for CD57, KLRG-1 and CD127

Figure 1: Co-expression of CD57 and CD127 in (A) Whole CD8$^+$ T-cell compartment (B) CD8$^+$ EM and (C) CD8$^+$ EMRA memory subsets of CLL patients.

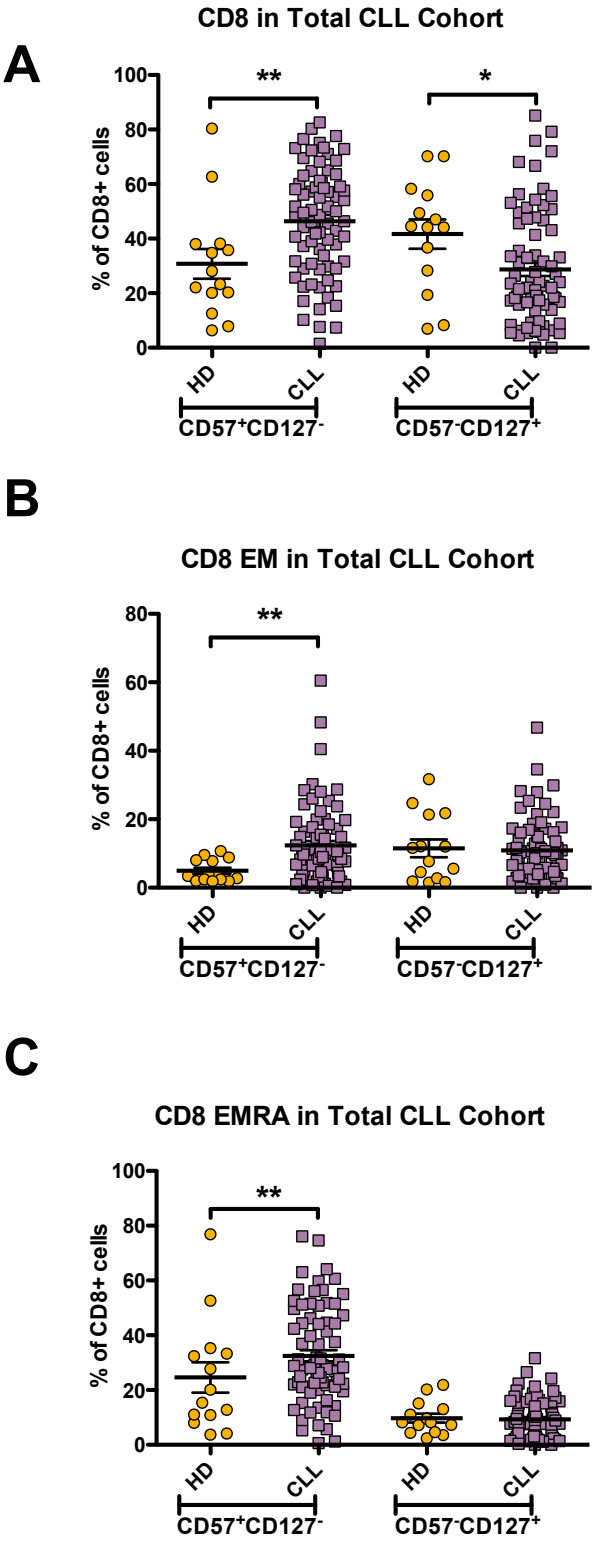

Figure 2: Co-expression of CD57 and CD127 in (A) Whole $CD8^+$ T-cell compartment (B) $CD8^+$ EM and (C) $CD8^+$ EMRA memory subsets of CLL^{NR}, CLL^{IR} and healthy donors.

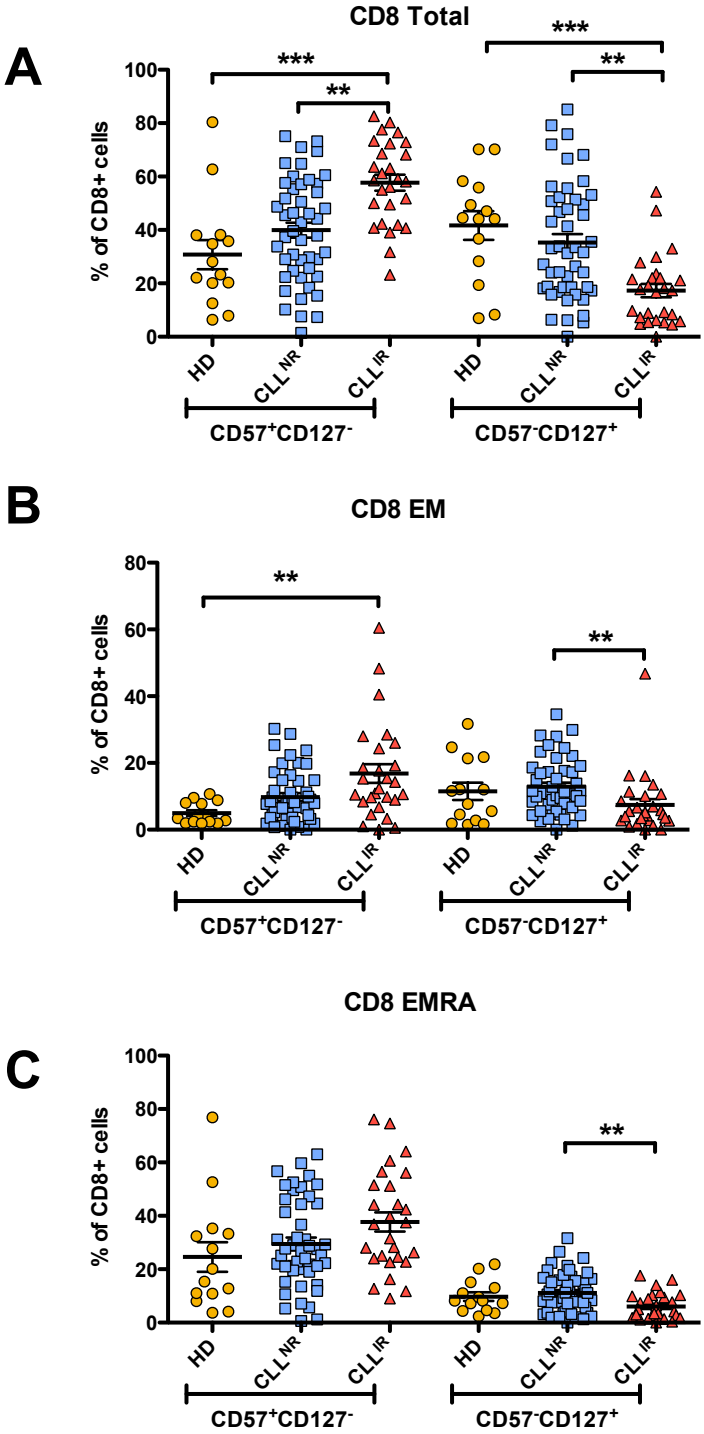

Figure 3: Expression of CD57, KLRG-1 and CD127 in $CD8^+$ EM T-cell memory subsets of (A) CLL patients and age-matched healthy donors, and (B) CLL^{NR}, CLL^{IR} and healthy donors.

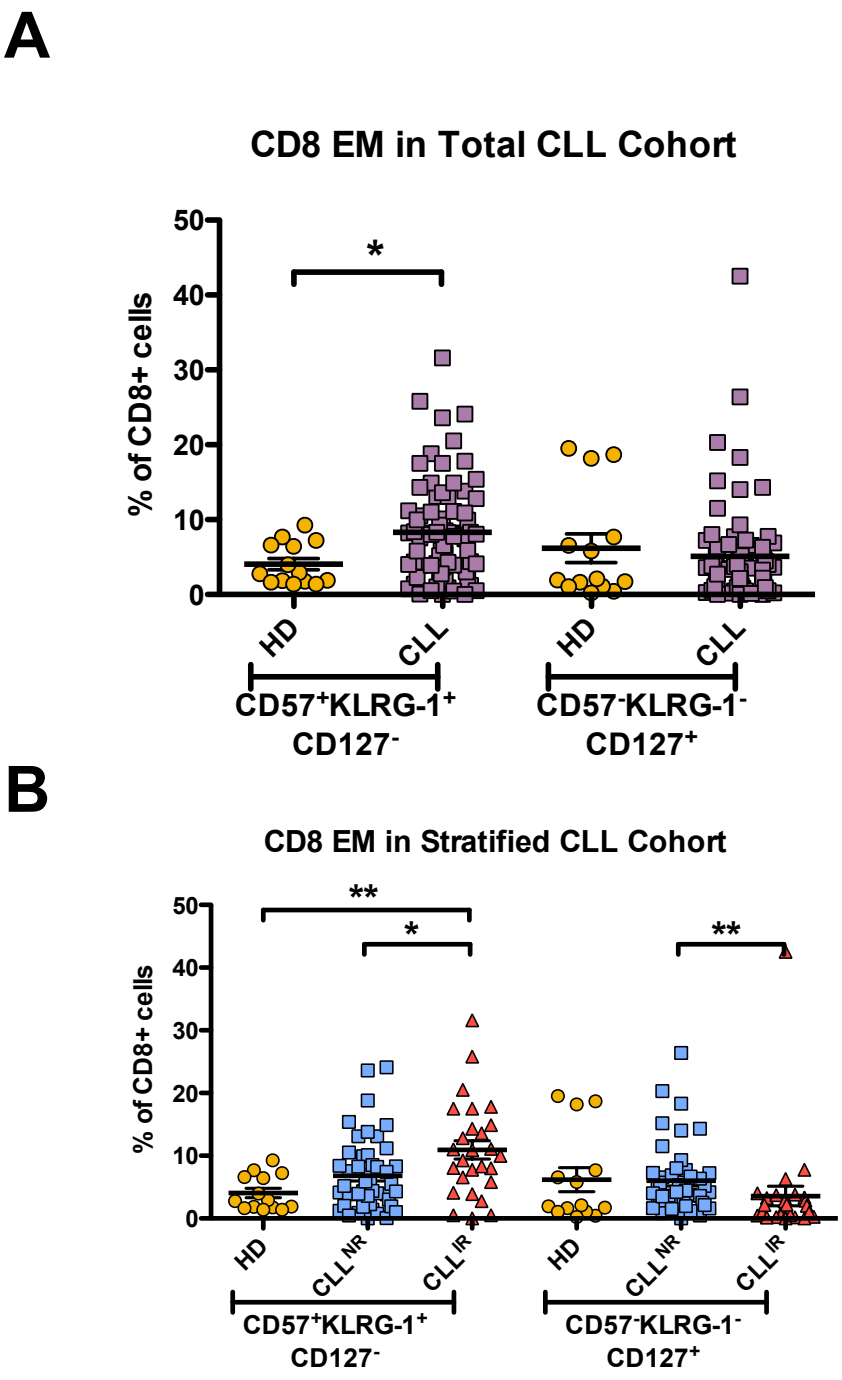

Figure 4: Expression of CD57, KLRG-1 and CD127 in $CD8^+$ EMRA T-cell memory subsets of (A) CLL patients and age-matched healthy donors, and (B) CLL^{NR}, CLL^{IR} and healthy donors.

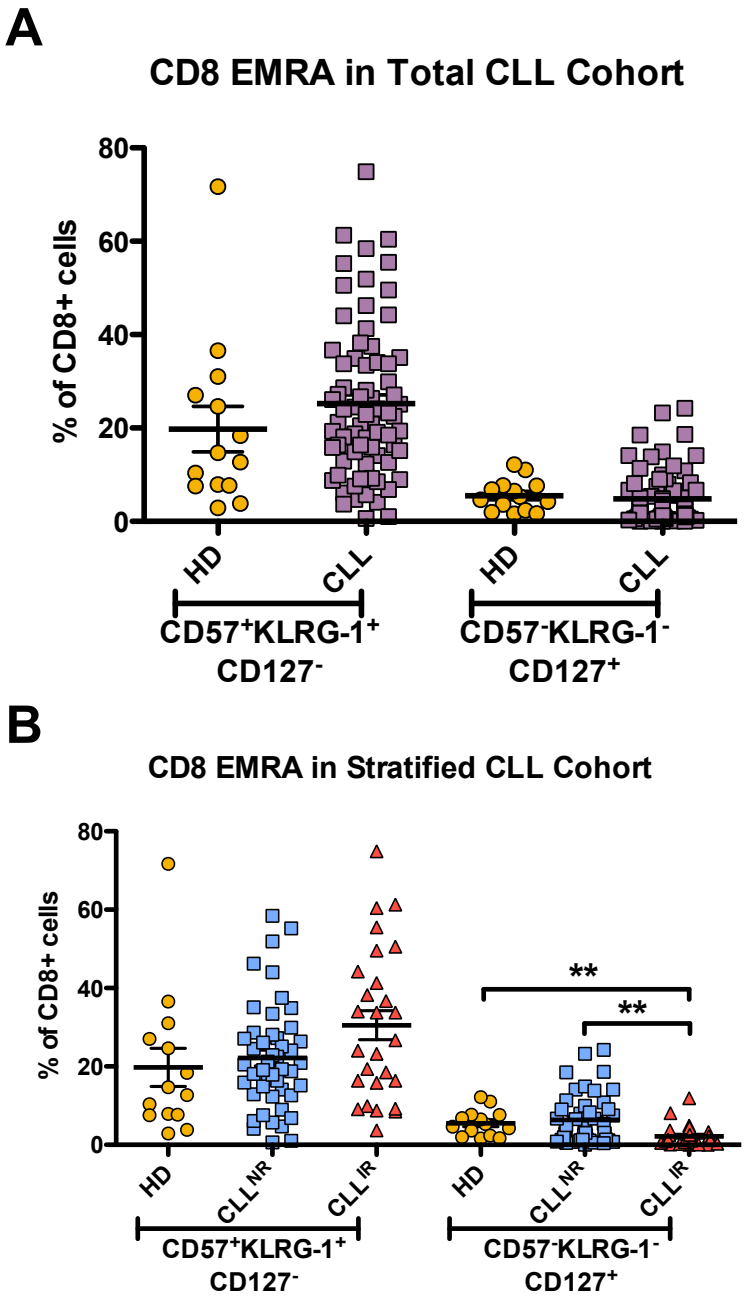

Appendix III. Phenotypic analyses of CD8$^+$ T-cells in CLL: additional data for CD57, KLRG-1 and CD38

Figure 1: KLRG-1 and CD38 co-expression in CD8$^+$ T-cell memory subsets of (A) CLL patients and age-matched healthy donors, and (B) CLL^{NR}, CLL^{IR} and healthy donors.

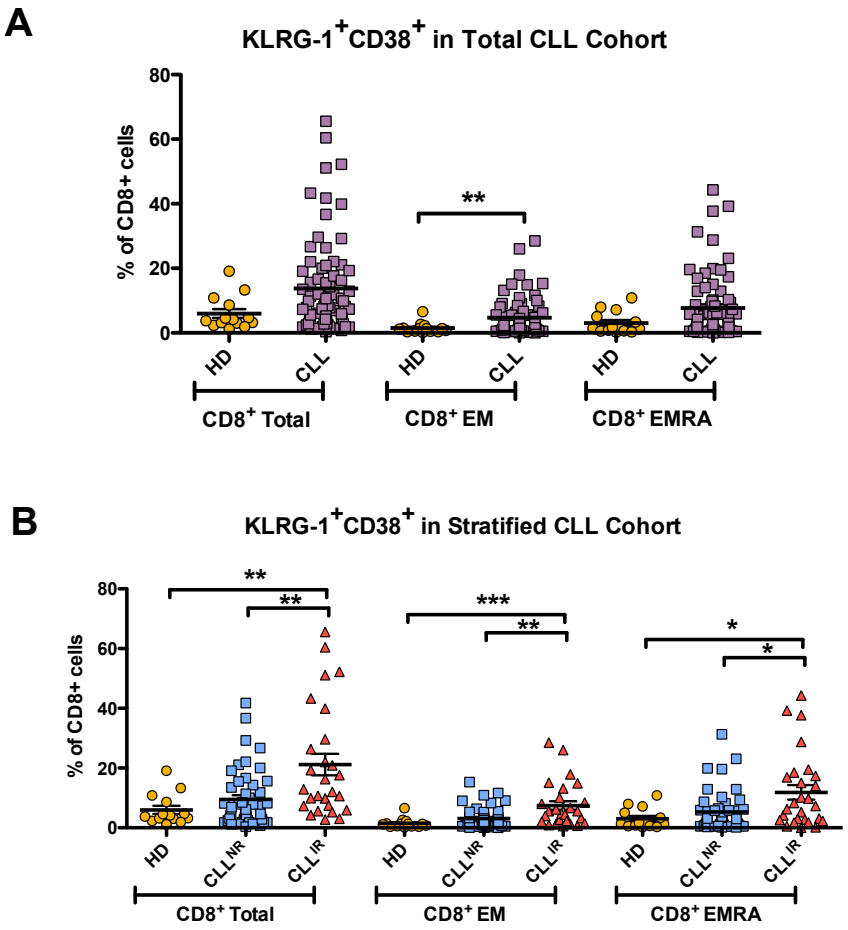

Figure 2: Expression of CD57, KLRG-1 and CD38 in $CD8^+$ T-cells of CLL patients and age-matched healthy donors.

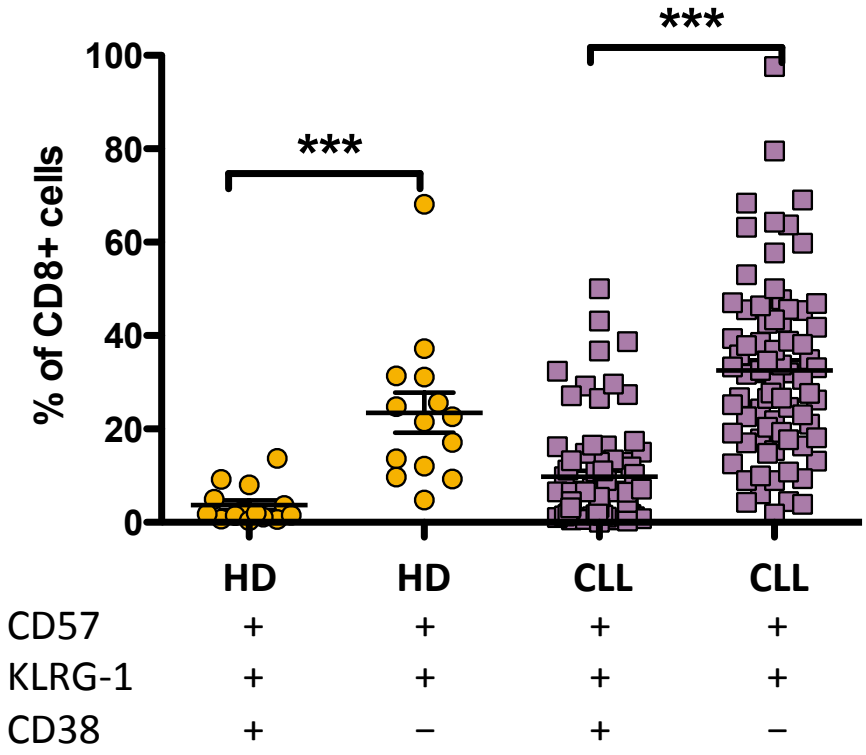

Appendix IV. Outputs from multivariate analysis

Table 1. Simple statistics (mean, standard deviation, median, minimum and maximum) calculated during multivariate analysis.

Variable	Mean	Std Dev	Median	Minimum	Maximum
CD4:CD8 RATIO	2.36	3.02	1.33	0.29	21.86
$CD3^+$	9.83	14.33	5.26	0.60	83.50
$CD8^+$	33.12	15.89	32.50	4.07	67.40
$CD8^+Naïve^+$	10.68	12.78	5.10	0.02	46.60
$CD8^+CM^+$	1.93	2.05	1.13	0.01	8.84
$CD8^+EM^+$	29.74	15.80	27.15	0.23	63.80
$CD8^+EMRA^+$	57.64	17.01	60.70	27.30	97.40
$CD4^+$	46.56	18.81	43.35	10.20	88.90
$CD4^+Naïve^+$	32.28	22.57	33.05	0.01	80.70
$CD4^+CM^+$	10.18	7.40	8.14	0.06	37.90
$CD4^+EM^+$	41.04	22.85	35.65	0.65	95.60
$CD4^+EMRA^+$	16.50	13.49	13.70	2.03	76.60
$CD8^+CD57^+$	58.07	23.67	61.20	4.20	100.00
$CD8^+HLA\text{-}DR^+$	35.07	20.34	34.65	2.61	86.50
$CD8^+PD\text{-}1^+$	33.99	17.33	31.25	6.30	81.30
$CD8^+EM^+CD57^+$	17.72	14.97	12.20	0.00	58.40
$CD8^+EM^+HLA\text{-}DR^+$	13.30	11.51	9.23	0.00	54.00
$CD8^+EM^+PD\text{-}1^+$	15.91	11.22	14.20	0.00	58.50
$CD8^+EMRA^+CD57^+$	38.34	19.67	35.25	0.00	97.50
$CD8^+EMRA^+HLA\text{-}DR^+$	19.48	13.35	17.80	0.00	48.80
$CD8^+EMRA^+PD\text{-}1^+$	15.63	11.24	13.10	0.00	62.20
$CD4^+CD57^+$	18.94	15.05	16.80	0.48	58.90
$CD4^+HLA\text{-}DR^+$	21.43	17.28	16.40	2.59	77.00
$CD4^+PD\text{-}1^+$	39.34	20.60	34.90	6.99	81.20
$CD4^+EM^+CD57^+$	12.05	11.83	7.26	0.25	57.70
$CD4^+EM^+HLA\text{-}DR^+$	14.34	15.03	8.85	0.16	74.50
$CD4^+EM^+PD\text{-}1^+$	26.72	17.11	21.50	0.61	72.80

Variable	Mean	Std Dev	Median	Minimum	Maximum
$CD4^+EMRA^+CD57^+$	5.89	8.95	2.16	0.00	41.60
$CD4^+EMRA^+HLA\text{-}DR^+$	4.26	6.50	1.81	0.00	36.30
$CD4^+EMRA^+PD\text{-}1^+$	6.87	9.80	4.11	0.00	61.10
$CD8^+CD57^+HLA\text{-}DR^+$	24.10	16.80	21.90	1.81	72.40
$CD8^+CD57^+PD\text{-}1^+$	20.38	13.94	16.65	3.09	60.70
$CD8^+HLA\text{-}DR^+PD\text{-}1^+$	14.92	11.56	10.90	1.49	53.80
$CD8^+CD57^+HLA\text{-}DR^+PD\text{-}1^+$	9.42	8.49	6.90	0.30	40.20
$CD8^+EM^+CD57^+HLA\text{-}DR^+$	9.27	9.54	6.62	0.02	50.00
$CD8^+EM^+CD57^+PD\text{-}1^+$	9.84	8.95	7.50	0.18	40.10
$CD8^+EM^+HLA\text{-}DR^+PD\text{-}1^+$	7.67	7.40	5.67	0.00	46.00
$CD8^+EM^+CD57^+HLA\text{-}DR^+PD\text{-}1^+$	4.94	5.51	2.92	0.00	32.30
$CD8^+EMRA^+CD57^+HLA\text{-}DR^+$	14.31	10.68	11.85	0.30	47.50
$CD8^+EMRA^+CD57^+PD\text{-}1^+$	10.33	8.65	8.11	0.64	37.50
$CD8^+EMRA^+HLA\text{-}DR^+PD\text{-}1^+$	6.27	6.23	4.96	0.00	33.20
$CD8^+EMRA^+CD57^+HLA\text{-}DR^+PD\text{-}1^+$	3.14	3.35	2.30	0.00	19.00
$CD4^+CD57^+HLA\text{-}DR^+$	9.29	9.08	6.41	0.17	39.80
$CD4^+CD57^+PD\text{-}1^+$	11.56	9.89	9.08	0.29	46.70
$CD4^+HLA\text{-}DR^+PD\text{-}1^+$	13.89	12.33	9.08	0.85	50.70
$CD4^+CD57^+HLA\text{-}DR^+PD\text{-}1^+$	6.06	6.02	3.95	0.11	25.90
$CD4^+EM^+CD57^+HLA\text{-}DR^+$	6.34	7.50	3.31	0.04	38.70
$CD4^+EM^+CD57^+PD\text{-}1^+$	8.30	7.69	5.79	0.17	30.40
$CD4^+EM^+HLA\text{-}DR^+PD\text{-}1^+$	10.24	10.67	6.22	0.16	46.50
$CD4^+EM^+CD57^+HLA\text{-}DR^+PD\text{-}1^+$	4.55	5.03	2.85	0.04	23.80
$CD8^+CD38^+$	21.50	18.53	15.25	1.51	75.80
$CD8^+CD57^+$	55.78	22.08	58.70	2.86	99.90
$CD8^+CD127^+$	38.10	20.36	33.20	6.08	86.50
$CD8^+KLRG\text{-}1^+$	63.98	23.22	69.10	12.90	99.60
$CD8^+EM^+CD38^+$	7.71	9.64	3.97	0.01	59.30
$CD8^+EM^+CD57^+$	16.89	12.91	14.05	0.11	64.00
$CD8^+EM^+CD127^+$	14.97	10.28	13.15	0.06	53.20

Variable	Mean	Std Dev	Median	Minimum	Maximum
$CD8^+EM^+KLRG\text{-}1^+$	20.43	12.26	18.85	0.11	57.80
$CD8^+EMRA^+CD38^+$	10.39	10.39	7.26	0.36	47.50
$CD8^+EMRA^+CD57^+$	37.36	20.89	31.15	1.27	98.20
$CD8^+EMRA^+CD127^+$	14.14	9.11	12.90	0.65	49.90
$CD8^+EMRA^+KLRG\text{-}1^+$	40.15	22.08	38.40	4.38	96.90
$CD4^+CD38^+$	29.42	16.17	25.00	5.75	74.30
$CD4^+CD57^+$	23.09	17.00	20.75	0.60	75.50
$CD4^+CD127^+$	60.78	21.28	63.35	12.50	93.50
$CD4^+KLRG\text{-}1^+$	35.01	23.70	33.05	0.49	99.20
$CD4^+EM^+CD38^+$	8.32	10.84	4.64	0.01	65.10
$CD4^+EM^+CD57^+$	11.32	11.01	7.88	0.03	56.30
$CD4^+EM^+CD127^+$	26.43	16.22	23.50	0.09	76.70
$CD4^+EM^+KLRG\text{-}1^+$	16.17	16.04	9.95	0.12	61.20
$CD4^+EMRA^+CD38^+$	5.89	6.72	2.89	0.44	30.40
$CD4^+EMRA^+CD57^+$	7.34	8.90	3.89	0.12	47.10
$CD4^+EMRA^+CD127^+$	7.93	9.36	5.07	0.33	61.70
$CD4^+EMRA^+KLRG\text{-}1^+$	9.63	13.92	6.14	0.14	83.30
$CD8^+CD38^+KLRG\text{-}1^+$	13.77	14.65	8.22	0.35	65.60
$CD8^+CD38^+CD57^+$	13.31	13.52	9.59	0.00	65.50
$CD8^+CD38^+CD127^+$	4.81	7.14	2.19	0.00	35.50
$CD8^+CD57^+KLRG\text{-}1^+$	42.29	21.22	39.90	1.75	99.50
$CD8^+CD57^+CD127^+$	9.37	7.91	8.06	0.12	53.40
$CD8^+CD127^+KLRG\text{-}1^+$	19.56	11.65	18.25	3.42	58.20
$CD8^+CD38^+CD57^+KLRG\text{-}1^+$	9.76	11.04	5.63	0.00	50.00
$CD8^+EM^+CD38^+KLRG\text{-}1^+$	4.69	5.61	2.62	0.00	28.50
$CD8^+EM^+CD38^+CD57^+$	5.09	7.80	2.48	0.00	56.20
$CD8^+EM^+CD38^+CD127^+$	1.41	1.91	0.64	0.00	9.22
$CD8^+EM^+CD57^+KLRG\text{-}1^+$	11.30	8.48	9.30	0.00	33.30
$CD8^+EM^+CD57^+CD127^+$	3.95	3.51	3.44	0.00	21.30
$CD8^+EM^+CD127^+KLRG\text{-}1^+$	8.76	6.97	7.27	0.00	40.20
$CD8^+EMRA^+CD38^+KLRG\text{-}1^+$	7.68	9.73	3.45	0.00	44.30

Variable	Mean	Std Dev	Median	Minimum	Maximum
$CD8^+EMRA^+CD38^+CD57^+$	7.45	8.46	3.98	0.00	41.00
$CD8^+EMRA^+CD38^+CD127^+$	1.30	2.22	0.48	0.00	11.20
$CD8^+EMRA^+CD57^+KLRG\text{-}1^+$	29.50	20.19	26.20	0.80	96.90
$CD8^+EMRA^+CD57^+CD127^+$	4.88	7.10	3.29	0.06	49.80
$CD8^+EMRA^+CD127^+KLRG\text{-}1^+$	8.74	7.84	6.62	0.24	49.60
$CD4^+CD38^+KLRG\text{-}1^+$	10.79	10.82	6.54	0.06	48.00
$CD4^+CD38^+CD57^+$	6.34	7.38	4.04	0.23	33.50
$CD4^+CD38^+CD127^+$	17.84	15.14	16.00	0.27	69.20
$CD4^+CD57^+KLRG\text{-}1^+$	14.26	13.57	9.39	0.19	60.30
$CD4^+CD57^+CD127^+$	7.77	6.97	6.29	0.23	30.70
$CD4^+CD127^+KLRG\text{-}1^+$	20.97	17.34	15.80	0.30	72.80
$CD4^+EM^+CD38^+KLRG\text{-}1^+$	3.86	6.96	1.54	0.00	46.20
$CD4^+EM^+CD38^+CD57^+$	3.32	5.02	1.77	0.00	30.60
$CD4^+EM^+CD38^+CD127^+$	3.75	5.57	1.52	0.01	29.70
$CD4^+EM^+CD57^+KLRG\text{-}1^+$	7.66	9.38	3.61	0.02	44.80
$CD4^+EM^+CD57^+CD127^+$	5.43	5.98	3.06	0.02	30.60
$CD4^+EM^+CD127^+KLRG\text{-}1^+$	10.27	11.21	6.33	0.09	53.20
$CD4^+EMRA^+CD38^+KLRG\text{-}1^+$	2.63	4.56	0.96	0.01	20.80
$CD4^+EMRA^+CD38^+CD57^+$	1.93	3.68	0.81	0.02	22.90
$CD4^+EMRA^+CD38^+CD127^+$	2.68	4.26	0.87	0.01	22.50
$CD4^+EMRA^+CD57^+KLRG\text{-}1^+$	2.06	3.16	1.01	0.00	16.60
$CD4^+EMRA^+CD57^+CD127^+$	5.37	6.51	2.62	0.07	30.40
$CD4^+EMRA^+CD127^+KLRG\text{-}1^+$	3.47	3.43	2.34	0.12	18.00

Table 2. Correlation of phenotypic variables against CD4:CD8 ratio

Variable	r	p-value
$CD3^+$	0.01182	0.9204
$CD8^+$	-0.85023	<0.0001
$CD8^+Naïve^+$	0.71172	<0.0001
$CD8^+CM^+$	-0.0712	0.5466
$CD8^+EM^+$	-0.34253	0.0028
$CD8^+EMRA^+$	-0.09578	0.4169
$CD4^+$	0.87022	<0.0001
$CD4^+Naïve^+$	0.57513	<0.0001
$CD4^+CM^+$	0.03129	0.7913
$CD4^+EM^+$	-0.46058	<0.0001
$CD4^+EMRA^+$	-0.09769	0.4077
$CD8^+CD57^+$	-0.51858	<0.0001
$CD8^+HLA\text{-}DR^+$	-0.38528	0.0007
$CD8^+PD\text{-}1^+$	0.10998	0.3509
$CD8^+EM^+CD57^+$	-0.48736	<0.0001
$CD8^+EM^+HLA\text{-}DR^+$	-0.44627	<0.0001
$CD8^+EM^+PD\text{-}1^+$	-0.06893	0.5595
$CD8^+EMRA^+CD57^+$	-0.21366	0.0676
$CD8^+EMRA^+HLA\text{-}DR^+$	-0.25504	0.0283
$CD8^+EMRA^+PD\text{-}1^+$	0.1388	0.2383
$CD4^+CD57^+$	-0.52054	<0.0001
$CD4^+HLA\text{-}DR^+$	-0.54439	<0.0001
$CD4^+PD\text{-}1^+$	-0.48144	<0.0001
$CD4^+EM^+CD57^+$	-0.57537	<0.0001
$CD4^+EM^+HLA\text{-}DR^+$	-0.54785	<0.0001
$CD4^+EM^+PD\text{-}1^+$	-0.45261	<0.0001
$CD4^+EMRA^+CD57^+$	-0.30921	0.0073
$CD4^+EMRA^+HLA\text{-}DR^+$	-0.38201	0.0008
$CD4^+EMRA^+PD\text{-}1^+$	-0.22333	0.0558
$CD8^+CD57^+HLA\text{-}DR^+$	-0.45455	<0.0001
$CD8^+CD57^+PD\text{-}1^+$	-0.11104	0.3462
$CD8^+HLA\text{-}DR^+PD\text{-}1^+$	-0.13432	0.2539
$CD8^+CD57^+HLA\text{-}DR^+PD\text{-}1^+$	-0.19634	0.0936
$CD8^+EM^+CD57^+HLA\text{-}DR^+$	-0.44996	<0.0001
$CD8^+EM^+CD57^+PD\text{-}1^+$	-0.17731	0.1307
$CD8^+EM^+HLA\text{-}DR^+PD\text{-}1^+$	-0.24554	0.035
$CD8^+EM^+CD57^+HLA\text{-}DR^+PD\text{-}1^+$	-0.30524	0.0082
$CD8^+EMRA^+CD57^+HLA\text{-}DR^+$	-0.32098	0.0053
$CD8^+EMRA^+CD57^+PD\text{-}1^+$	0.01128	0.924
$CD8^+EMRA^+HLA\text{-}DR^+PD\text{-}1^+$	-0.06482	0.5832
$CD8^+EMRA^+CD57^+HLA\text{-}DR^+PD\text{-}1^+$	-0.12214	0.2999
$CD4^+CD57^+HLA\text{-}DR^+$	-0.61185	<0.0001

Variable	r	p-value
$CD4^+CD57^+PD\text{-}1^+$	-0.60481	<0.0001
$CD4^+HLA\text{-}DR^+PD\text{-}1^+$	-0.55478	<0.0001
$CD4^+CD57^+HLA\text{-}DR^+PD\text{-}1^+$	-0.5868	<0.0001
$CD4^+EM^+CD57^+HLA\text{-}DR^+$	-0.634	<0.0001
$CD4^+EM^+CD57^+PD\text{-}1^+$	-0.61579	<0.0001
$CD4^+EM^+HLA\text{-}DR^+PD\text{-}1^+$	-0.5718	<0.0001
$CD4^+EM^+CD57^+HLA\text{-}DR^+PD\text{-}1^+$	-0.6013	<0.0001
$CD8^+CD38^+$	-0.25587	0.0278
$CD8^+CD57^+$	-0.47144	<0.0001
$CD8^+CD127^+$	0.43507	0.0001
$CD8^+KLRG\text{-}1^+$	-0.33109	0.004
$CD8^+EM^+CD38^+$	-0.24609	0.0346
$CD8^+EM^+CD57^+$	-0.24472	0.0356
$CD8^+EM^+CD127^+$	0.41851	0.0002
$CD8^+EM^+KLRG\text{-}1^+$	-0.06604	0.5762
$CD8^+EMRA^+CD38^+$	-0.26348	0.0233
$CD8^+EMRA^+CD57^+$	-0.27029	0.0199
$CD8^+EMRA^+CD127^+$	0.29147	0.0117
$CD8^+EMRA^+KLRG\text{-}1^+$	-0.2355	0.0434
$CD4^+CD38^+$	0.18795	0.1088
$CD4^+CD57^+$	-0.48414	<0.0001
$CD4^+CD127^+$	0.3234	0.0049
$CD4^+KLRG\text{-}1^+$	-0.26241	0.0239
$CD4^+EM^+CD38^+$	-0.25102	0.031
$CD4^+EM^+CD57^+$	-0.36741	0.0013
$CD4^+EM^+CD127^+$	-0.04415	0.7088
$CD4^+EM^+KLRG\text{-}1^+$	-0.27273	0.0187
$CD4^+EMRA^+CD38^+$	0.07578	0.521
$CD4^+EMRA^+CD57^+$	-0.29755	0.01
$CD4^+EMRA^+CD127^+$	0.1539	0.1905
$CD4^+EMRA^+KLRG\text{-}1^+$	-0.17546	0.1348
$CD8^+CD38^+KLRG\text{-}1^+$	-0.43485	0.0001
$CD8^+CD38^+CD57^+$	-0.47965	<0.0001
$CD8^+CD38^+CD127^+$	0.07399	0.531
$CD8^+CD57^+KLRG\text{-}1^+$	-0.41236	0.0003
$CD8^+CD57^+CD127^+$	-0.11734	0.3194
$CD8^+CD127^+KLRG\text{-}1^+$	0.12842	0.2755
$CD8^+CD38^+CD57^+KLRG\text{-}1^+$	-0.51862	<0.0001
$CD8^+EM^+CD38^+KLRG\text{-}1^+$	-0.32938	0.0042
$CD8^+EM^+CD38^+CD57^+$	-0.36299	0.0015
$CD8^+EM^+CD38^+CD127^+$	-0.08357	0.479
$CD8^+EM^+CD57^+KLRG\text{-}1^+$	-0.23681	0.0422
$CD8^+EM^+CD57^+CD127^+$	-0.02168	0.8545

Variable	r	p-value
$CD8^+EM^+CD127^+KLRG\text{-}1^+$	0.3152	0.0062
$CD8^+EMRA^+CD38^+KLRG\text{-}1^+$	-0.42402	0.0002
$CD8^+EMRA^+CD38^+CD57^+$	-0.40365	0.0004
$CD8^+EMRA^+CD38^+CD127^+$	0.0808	0.4937
$CD8^+EMRA^+CD57^+KLRG\text{-}1^+$	-0.28491	0.0139
$CD8^+EMRA^+CD57^+CD127^+$	-0.09619	0.4149
$CD8^+EMRA^+CD127^+KLRG\text{-}1^+$	0.01231	0.9171
$CD4^+CD38^+KLRG\text{-}1^+$	-0.23216	0.0465
$CD4^+CD38^+CD57^+$	-0.51012	<0.0001
$CD4^+CD38^+CD127^+$	0.28742	0.013
$CD4^+CD57^+KLRG\text{-}1^+$	-0.43188	0.0001
$CD4^+CD57^+CD127^+$	-0.39756	0.0005
$CD4^+CD127^+KLRG\text{-}1^+$	-0.14371	0.2219
$CD4^+EM^+CD38^+KLRG\text{-}1^+$	-0.427	0.0001
$CD4^+EM^+CD38^+CD57^+$	-0.4548	<0.0001
$CD4^+EM^+CD38^+CD127^+$	-0.13151	0.264
$CD4^+EM^+CD57^+KLRG\text{-}1^+$	-0.4066	0.0003
$CD4^+EM^+CD57^+CD127^+$	-0.35631	0.0018
$CD4^+EM^+CD127^+KLRG\text{-}1^+$	-0.18797	0.1088
$CD4^+EMRA^+CD38^+KLRG\text{-}1^+$	-0.21077	0.0715
$CD4^+EMRA^+CD38^+CD57^+$	-0.31009	0.0072
$CD4^+EMRA^+CD38^+CD127^+$	0.24082	0.0387
$CD4^+EMRA^+CD57^+KLRG\text{-}1^+$	-0.14347	0.2226
$CD4^+EMRA^+CD57^+CD127^+$	-0.26926	0.0203
$CD4^+EMRA^+CD127^+KLRG\text{-}1^+$	0.25809	0.0264

Table 3. Summary of Cox-proportional hazard regression model with forward selection (0.05 level entry)

Variable	Number in	Chi-square	p-value
$CD4^+HLA\text{-}DR^+PD\text{-}1^+$	1	23.4347	<.0001
$CD8^+$	2	5.5428	0.0186
$CD8^+CD57^+HLA\text{-}DR^+$	3	4.7188	0.0298
$CD8^+EMRA^+CD57^+HLA\text{-}DR^+PD\text{-}1^+$	4	5.2623	0.0218

Table 4. Summary of Cox-proportional hazard regression model with forward selection (0.99 level entry)

Variable	Number in	Chi-square	p-value
$CD4^+HLA\text{-}DR^+PD\text{-}1^+$	1	23.4347	<0.0001
$CD8^+$	2	5.5428	0.0186
$CD8^+CD57^+HLA\text{-}DR^+$	3	4.7188	0.0298
$CD8^+EMRA^+CD57^+HLA\text{-}DR^+PD\text{-}1^+$	4	5.2623	0.0218
$CD4^+CD57^+PD\text{-}1^+$	5	3.2936	0.0695
$CD8^+EMRA^+CD57^+HLA\text{-}DR^+$	6	3.4165	0.0645
$CD4^+EMRA^+CD38^+KLRG\text{-}1^+$	7	8.0052	0.0047
$CD4^+CD127^+$	8	6.6548	0.0099
CD4:CD8 RATIO	9	31.6757	<0.0001
$CD4^+EMRA^+CD57^+KLRG\text{-}1^+$	10	11.8763	0.0006
$CD4^+CD38^+CD127^+$	11	6.6349	0.0100
$CD8^+EMRA^+CD57^+$	12	22.6099	<0.0001

Figure 1: Prognosis of CLL patients stratified based on median frequencies of prognostic markers determined by multivariate analysis: (A) $CD4^+HLA\text{-}DR^+PD\text{-}1^+$ (B) $CD8^+$ (C) $CD8^+CD57^+HLA\text{-}DR^+$ and (D) $CD8^+$ EMRA $CD57^+HLA\text{-}DR^+PD\text{-}1^+$.

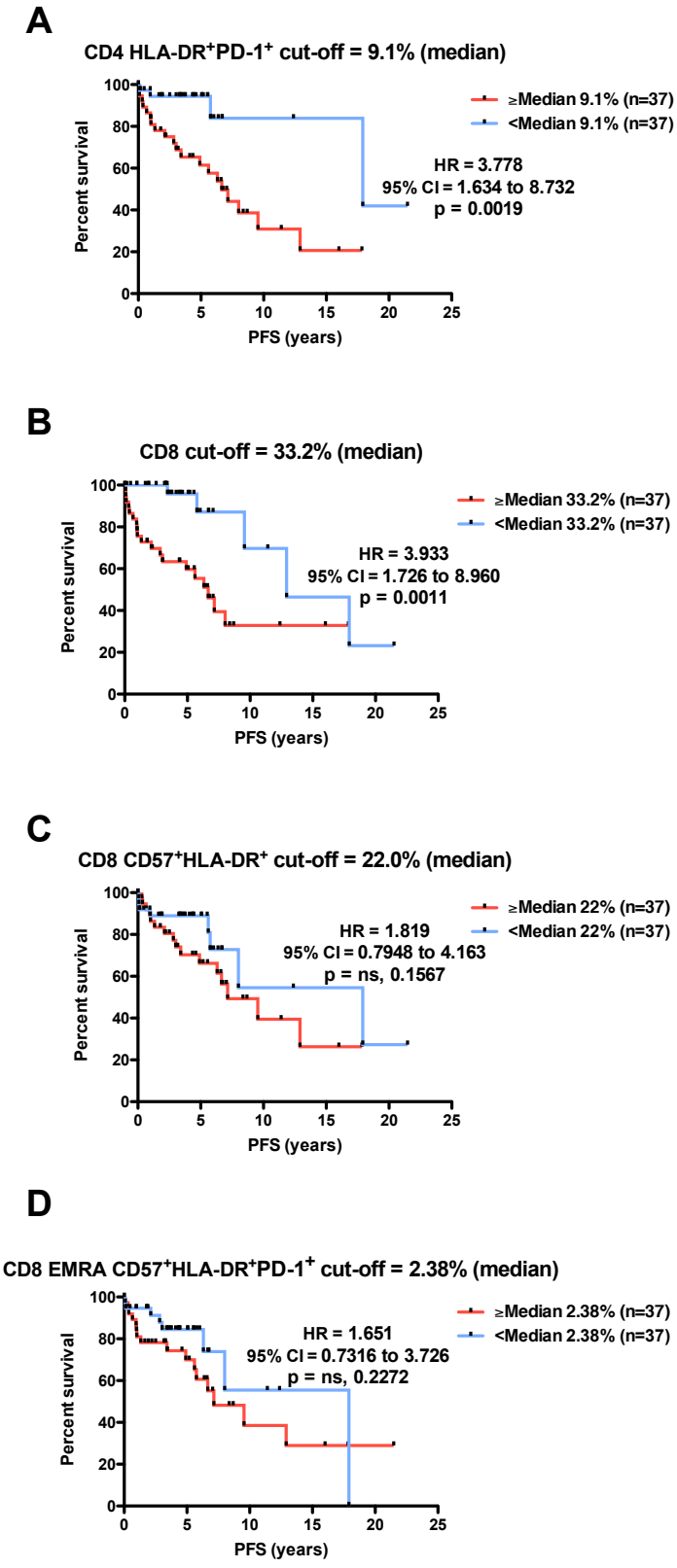

Table 5. CD4:CD8 ratio cut-offs determined by multivariate analysis.

Ratio	Number in	Chi-square	p-value
0.521	1	41.3074	<0.0001
1.009	2	8.2603	0.0041
0.951	3	24.1866	<0.0001
0.995	4	9.8197	0.0017
0.504	5	9.2847	0.0023
0.804	5	6.538	0.0106

Figure 2: Prognosis of CLL patients stratified by CD4:CD8 ratio using cut-offs determined by multivariate analyses (Table 5)

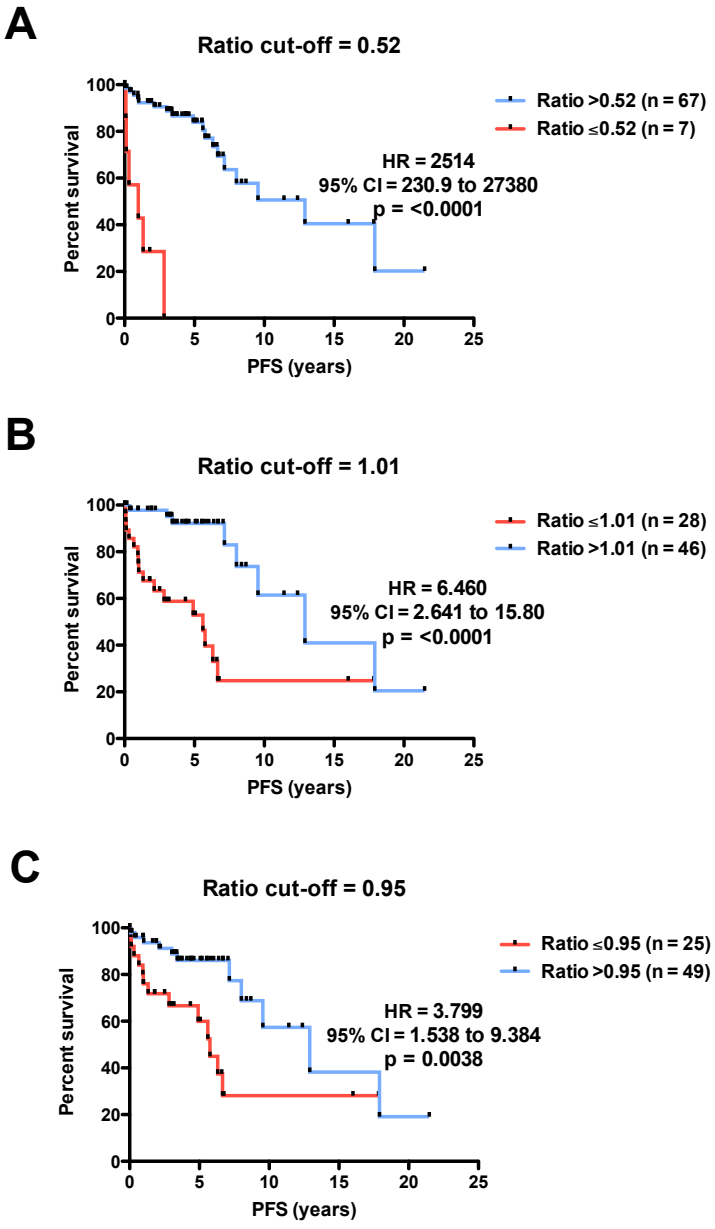

E

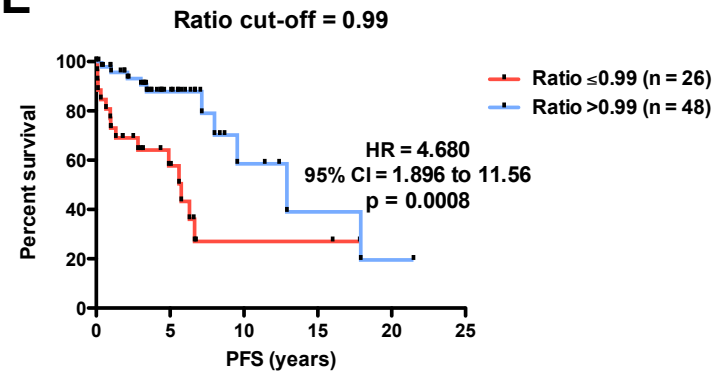
Ratio cut-off = 0.99
Percent survival
PFS (years)
Ratio ≤0.99 (n = 26)
Ratio >0.99 (n = 48)
HR = 4.680
95% CI = 1.896 to 11.56
p = 0.0008

F

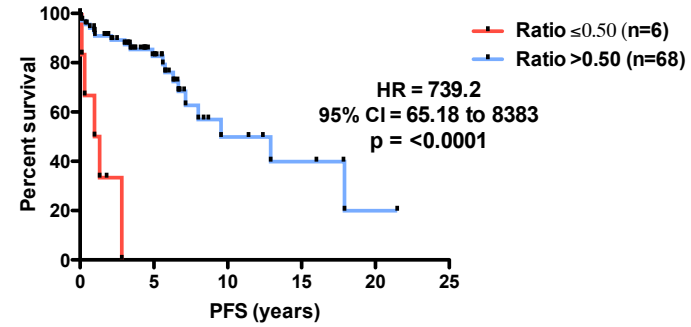
Ratio cut-off = 0.50
Percent survival
PFS (years)
Ratio ≤0.50 (n=6)
Ratio >0.50 (n=68)
HR = 739.2
95% CI = 65.18 to 8383
p = <0.0001

G

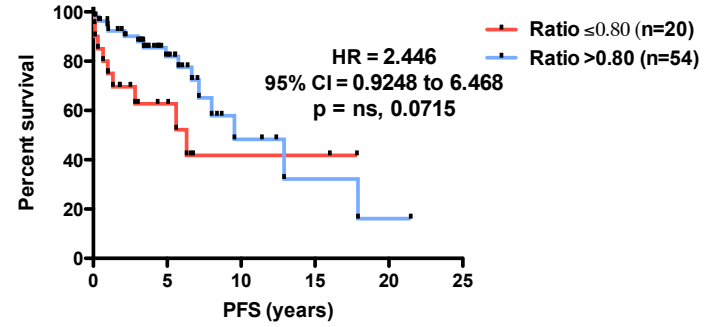
Ratio cut-off = 0.80
Percent survival
PFS (years)
Ratio ≤0.80 (n=20)
Ratio >0.80 (n=54)
HR = 2.446
95% CI = 0.9248 to 6.468
p = ns, 0.0715

Table 6. $CD4^+HLA\text{-}DR^+PD\text{-}1^+$ cut-offs determined by multivariate analysis.

$CD4^+HLA\text{-}DR^+PD\text{-}1^+$ (% of CD4)	Number in	Chi-square	p
47.4	1	35.2552	<0.0001
31.5	2	27.076	<0.0001
14.4	3	8.0021	0.0047
16.7	4	13.6212	0.0002
4.69	5	4.3964	0.036
4.95	5	89.8294	<0.0001
37.5	7	4.5554	0.0328
46.4	8	10.5532	0.0012

Figure 3: Prognosis of CLL patients stratified by $CD4^+HLA\text{-}DR^+PD\text{-}1^+$ using cut-offs determined by multivariate analyses (Table 6)

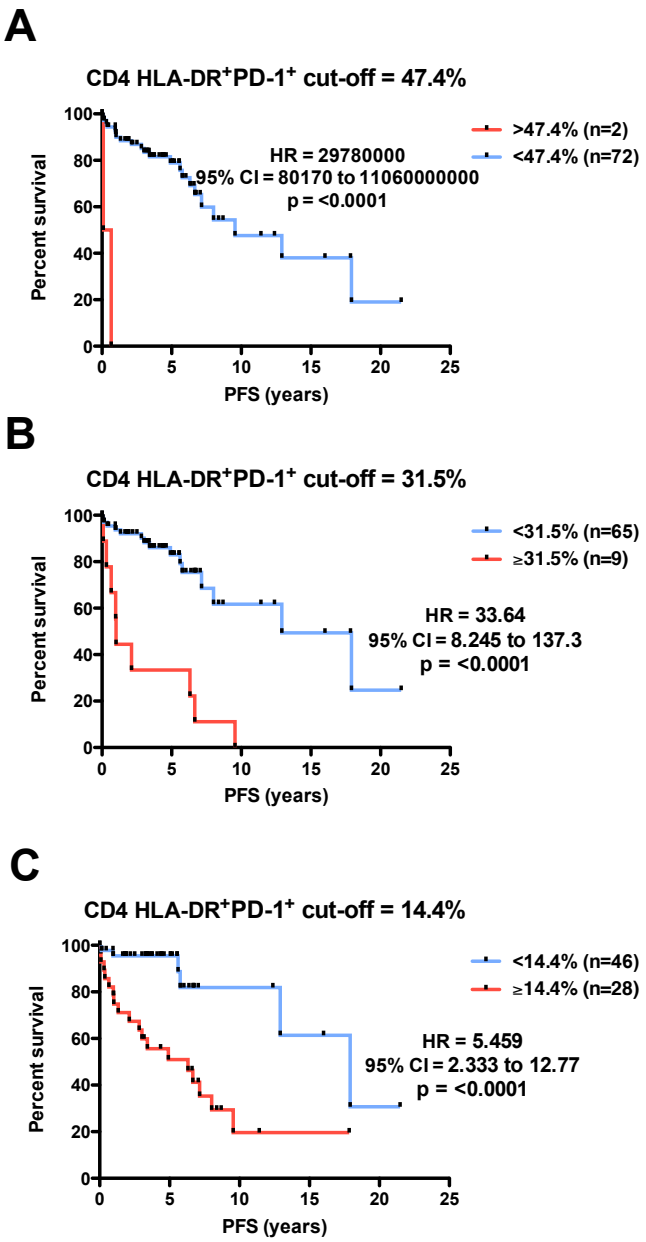

D

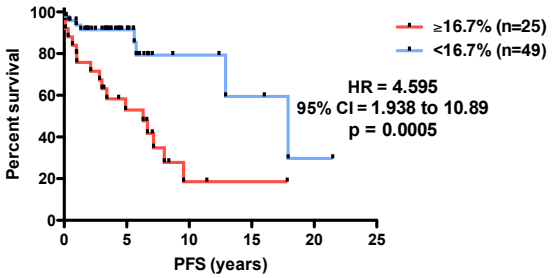
CD4 HLA-DR+PD-1+ cut-off = 16.7%
≥16.7% (n=25)
<16.7% (n=49)
HR = 4.595
95% CI = 1.938 to 10.89
p = 0.0005
Percent survival
PFS (years)

E

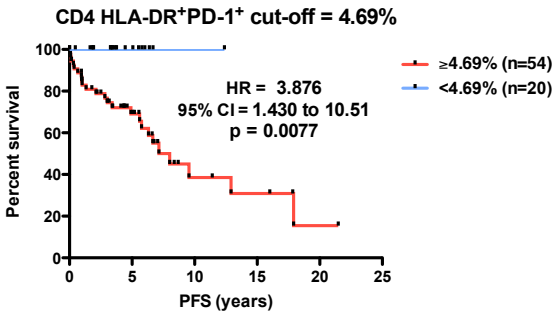
CD4 HLA-DR+PD-1+ cut-off = 4.69%
≥4.69% (n=54)
<4.69% (n=20)
HR = 3.876
95% CI = 1.430 to 10.51
p = 0.0077
Percent survival
PFS (years)

F

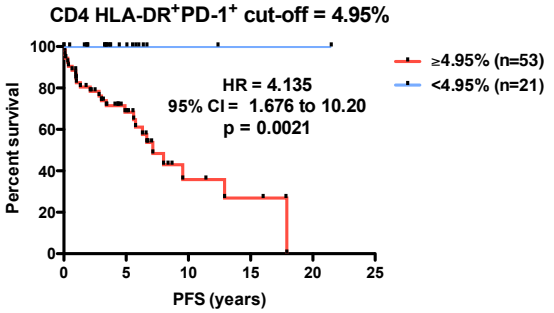
CD4 HLA-DR+PD-1+ cut-off = 4.95%
≥4.95% (n=53)
<4.95% (n=21)
HR = 4.135
95% CI = 1.676 to 10.20
p = 0.0021
Percent survival
PFS (years)

G

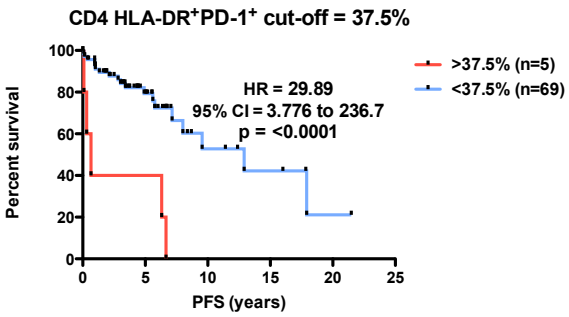
CD4 HLA-DR+PD-1+ cut-off = 37.5%
>37.5% (n=5)
<37.5% (n=69)
HR = 29.89
95% CI = 3.776 to 236.7
p = <0.0001
Percent survival
PFS (years)

H

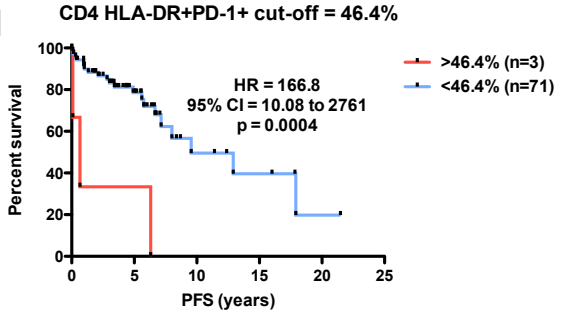
CD4 HLA-DR+PD-1+ cut-off = 46.4%
>46.4% (n=3)
<46.4% (n=71)
HR = 166.8
95% CI = 10.08 to 2761
p = 0.0004
Percent survival
PFS (years)

Table 7. $CD8^+$ cut-offs determined by multivariate analysis.

CD8 (%)	Number in	Chi-square	p-value
56.9	1	29.6995	<0.0001
58.5	2	8.1732	0.0043
31.0	3	7.9394	0.0048
33.2	4	9.1904	0.0024
65.1	5	5.9365	0.0148

Figure 4: Prognosis of CLL patients stratified by $CD8^+$ using cut-offs determined by multivariate analyses (Table 7)

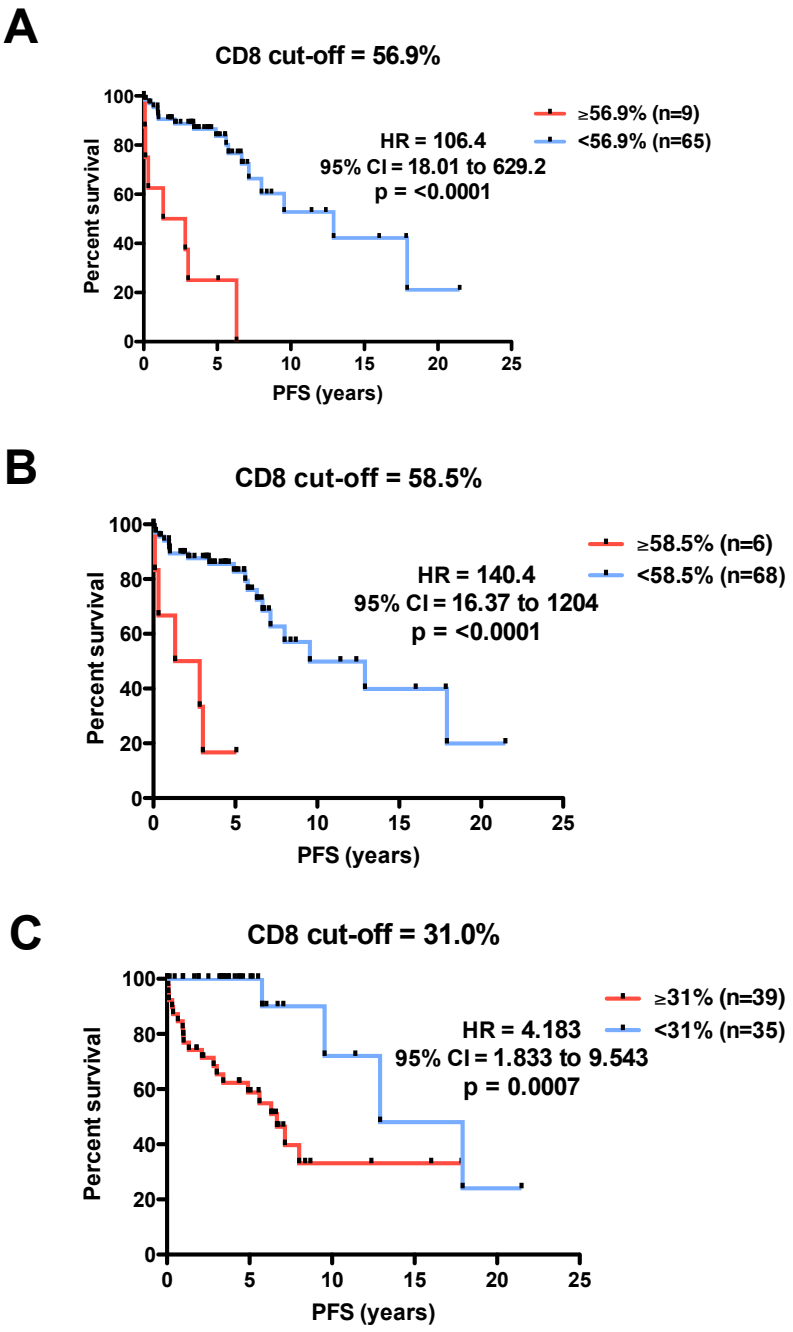

D

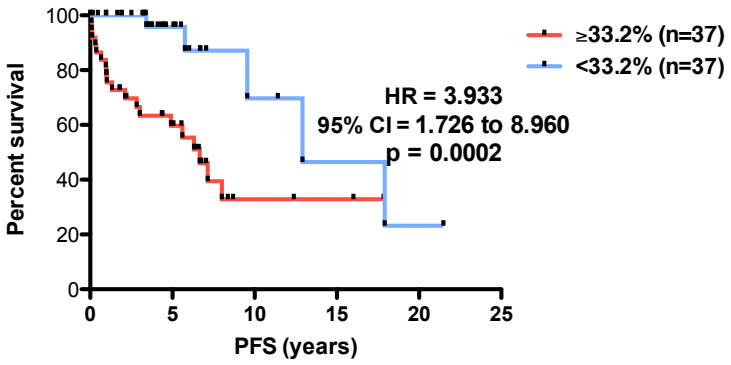
CD8 cut-off = 33.2%
Percent survival
PFS (years)
HR = 3.933
95% CI = 1.726 to 8.960
p = 0.0002
≥33.2% (n=37)
<33.2% (n=37)

E

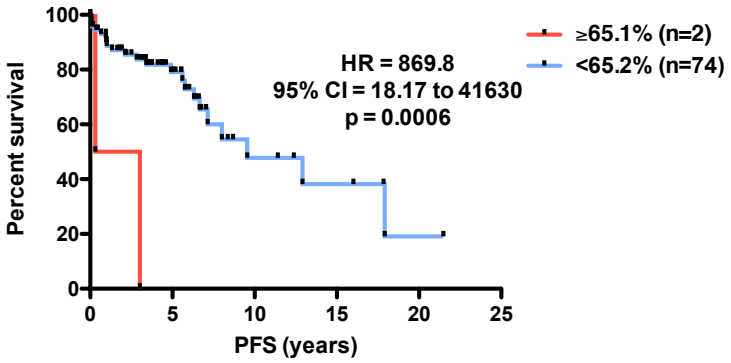
CD8 cut-off = 65.1%
Percent survival
PFS (years)
HR = 869.8
95% CI = 18.17 to 41630
p = 0.0006
≥65.1% (n=2)
<65.2% (n=74)

Table 8. $CD8^+CD57^+HLA\text{-}DR^+$ cut-offs determined by multivariate analysis.

$CD8\ CD57^+HLA\text{-}DR^+$ (% of CD8)	Number in	Chi-square	p
64.5	1	15.0336	0.0001
24.7	2	4.8578	0.0275
24.7	3	10.0683	0.0015
26.2	4	4.1445	0.0418

Figure 5: Prognosis of CLL patients stratified by $CD8^+CD57^+HLA\text{-}DR^+$ using cut-offs determined by multivariate analyses (Table 8)

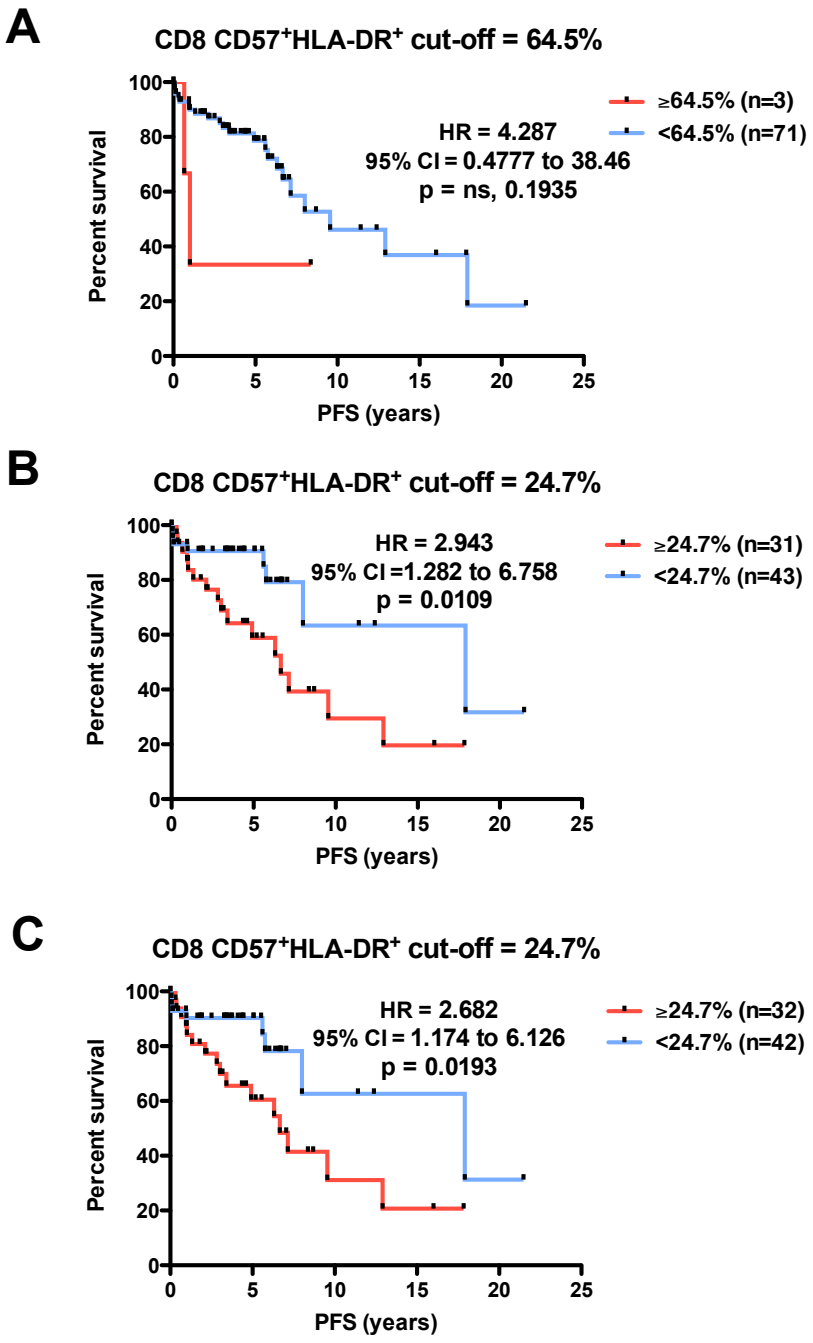

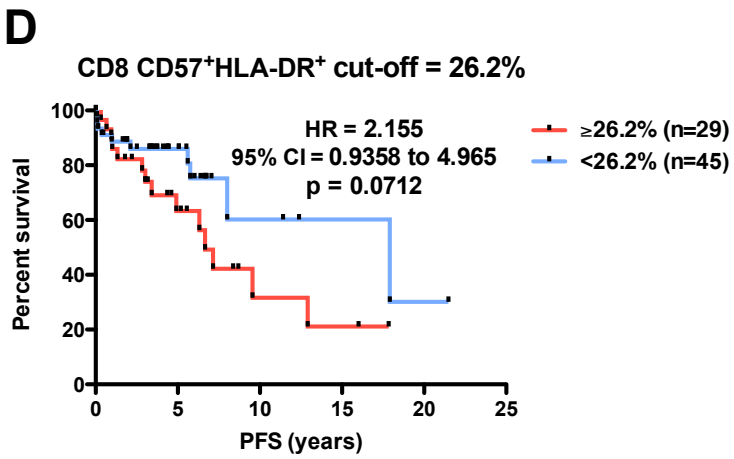

Table 9. $CD8^+$ EMRA $CD57^+HLA\text{-}DR^+PD\text{-}1^+$ cut-offs determined by multivariate analysis.

CD8 EMRA $CD57^+HLA\text{-}DR^+PD\text{-}1^+$ (% of CD8)	Number in	Chi-square	p
6.45	1	6.3376	0.0118
6.86	2	4.4215	0.0355

Figure 6: Prognosis of CLL patients stratified by $CD8^+CD57^+HLA\text{-}DR^+$ using cut-offs determined by multivariate analyses (Table 9)

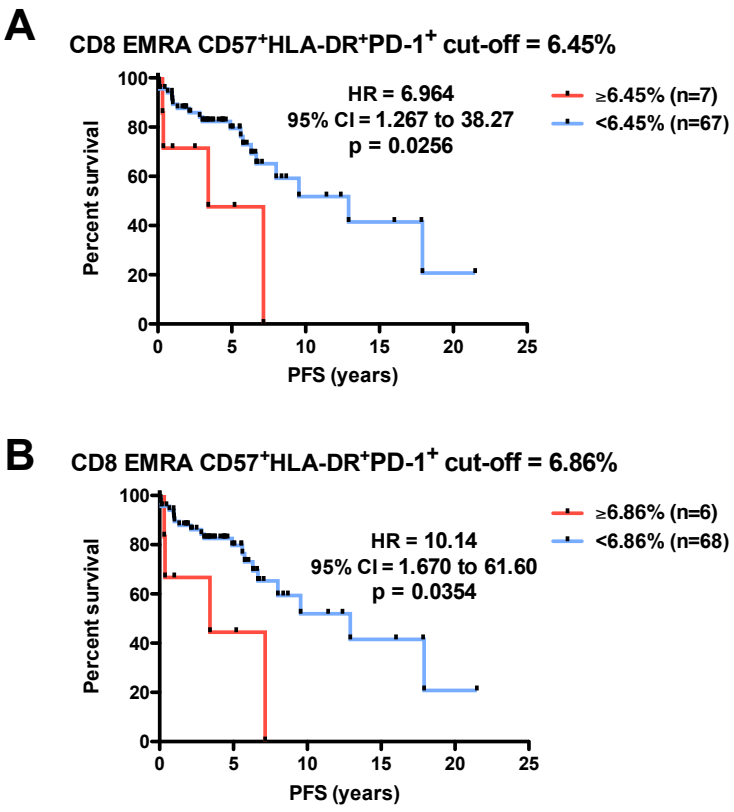

Appendix V. Correlation analysis of $CD8^+$ naïve T-cells and $CD8^+CD127^+$ T-cells.

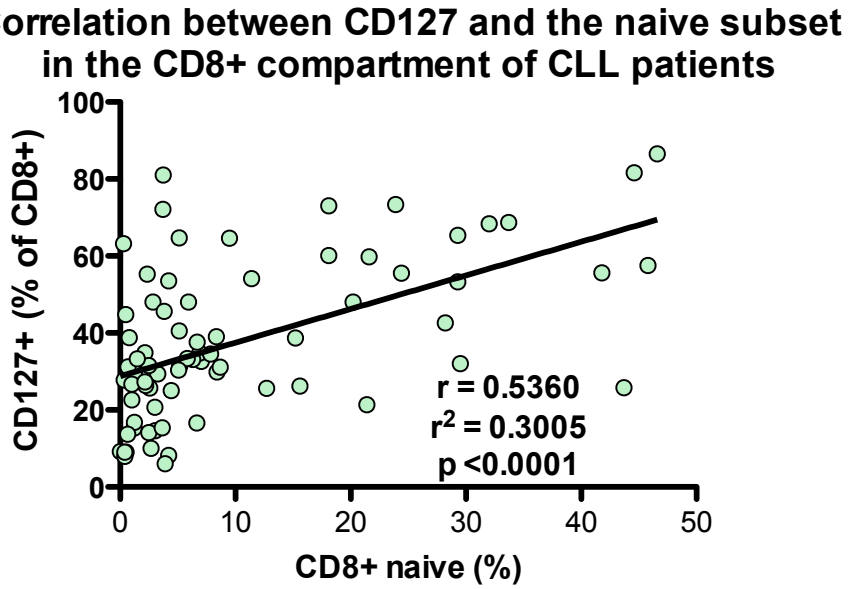

Appendix VI. Statistical analyses of $CD8^+$ marker distributions using SPICE

Table 1. T-test analyses comparing $CD4^+$ markers in CLL versus healthy donors (HD).

Phenotype	HD vs CLL
Panel 1	
$CD57^+HLA\text{-}DR^+PD\text{-}1^+$	<0.0001
$CD57^+HLA\text{-}DR^+PD\text{-}1^-$	0.0026
$CD57^+HLA\text{-}DR^-PD\text{-}1^+$	<0.0001
$CD57^+HLA\text{-}DR^-PD\text{-}1^-$	0.1080
$CD57^-HLA\text{-}DR^+PD\text{-}1^+$	<0.0001
$CD57^-HLA\text{-}DR^+PD\text{-}1^-$	0.8249
$CD57^-HLA\text{-}DR^-PD\text{-}1^+$	<0.0001
$CD57^-HLA\text{-}DR^-PD\text{-}1^-$	<0.0001
Panel 2	
$CD57^+CD38^+CD127^+KLRG\text{-}1^+$	0.0004
$CD57^+CD38^+CD127^+KLRG\text{-}1^-$	0.0007
$CD57^+CD38^+CD127^-KLRG\text{-}1^+$	0.0020
$CD57^+CD38^+CD127^-KLRG\text{-}1^+$	0.0009
$CD57^+CD38^-CD127^+KLRG\text{-}1^+$	0.0004
$CD57^+CD38^-CD127^+KLRG\text{-}1^-$	0.0143
$CD57^+CD38^-CD127^-KLRG\text{-}1^+$	0.0449
$CD57^+CD38^-CD127^-KLRG\text{-}1^-$	0.0003
$CD57^-CD38^+CD127^+KLRG\text{-}1^+$	0.0812
$CD57^-CD38^+CD127^+KLRG\text{-}1^-$	0.7101
$CD57^-CD38^+CD127^-KLRG\text{-}1^+$	0.0068
$CD57^-CD38^+CD127^-KLRG\text{-}1^-$	0.0088
$CD57^-CD38^-CD127^+KLRG\text{-}1^+$	0.0362
$CD57^-CD38^-CD127^+KLRG\text{-}1^-$	0.4206
$CD57^-CD38^-CD127^-KLRG\text{-}1^+$	0.8258
$CD57^-CD38^-CD127^-KLRG\text{-}1^-$	0.6961

Table 2. T-test analyses comparing $CD4^+$ markers in CLL^{IR} versus CLL^{NR} and healthy donors (HD)

Phenotype	HD vs CLLIR	CLLNR vs CLLIR
Panel 1		
$CD57^+HLA\text{-}DR^+PD\text{-}1^+$	0.0015	<0.0001
$CD57^+HLA\text{-}DR^+PD\text{-}1^-$	0.0090	0.0012
$CD57^+HLA\text{-}DR^-PD\text{-}1^+$	0.0208	<0.0001
$CD57^+HLA\text{-}DR^-PD\text{-}1^-$	0.3620	0.1115
$CD57^-HLA\text{-}DR^+PD\text{-}1^+$	0.0120	<0.0001
$CD57^-HLA\text{-}DR^+PD\text{-}1^-$	0.0274	0.2205
$CD57^-HLA\text{-}DR^-PD\text{-}1^+$	0.8160	<0.0001
$CD57^-HLA\text{-}DR^-PD\text{-}1^-$	0.0004	<0.0001
Panel 2		
$CD57^+CD38^+CD127^+KLRG\text{-}1^+$	0.0021	0.0099
$CD57^+CD38^+CD127^+KLRG\text{-}1^-$	0.0144	0.2567
$CD57^+CD38^+CD127^-KLRG\text{-}1^+$	0.0010	0.0187
$CD57^+CD38^+CD127^-KLRG\text{-}1^+$	0.0125	0.1604
$CD57^+CD38^-CD127^+KLRG\text{-}1^+$	0.0009	0.4462
$CD57^+CD38^-CD127^+KLRG\text{-}1^-$	0.0104	0.4596
$CD57^+CD38^-CD127^-KLRG\text{-}1^+$	0.0422	0.4340
$CD57^+CD38^-CD127^-KLRG\text{-}1^-$	0.0077	0.0420
$CD57^-CD38^+CD127^+KLRG\text{-}1^+$	0.4361	0.5358
$CD57^-CD38^+CD127^+KLRG\text{-}1^-$	0.0436	0.0085
$CD57^-CD38^+CD127^-KLRG\text{-}1^+$	0.4337	0.0811
$CD57^-CD38^+CD127^-KLRG\text{-}1^-$	0.0018	0.1485
$CD57^-CD38^-CD127^+KLRG\text{-}1^+$	0.0627	0.9830
$CD57^-CD38^-CD127^+KLRG\text{-}1^-$	0.0109	0.0034
$CD57^-CD38^-CD127^-KLRG\text{-}1^+$	0.4813	0.1433
$CD57^-CD38^-CD127^-KLRG\text{-}1^-$	0.7562	0.9659

Appendix VII. Correlation analysis of CD38 and HLA-DR in $CD4^+$ naïve T-cells of CLL patients.

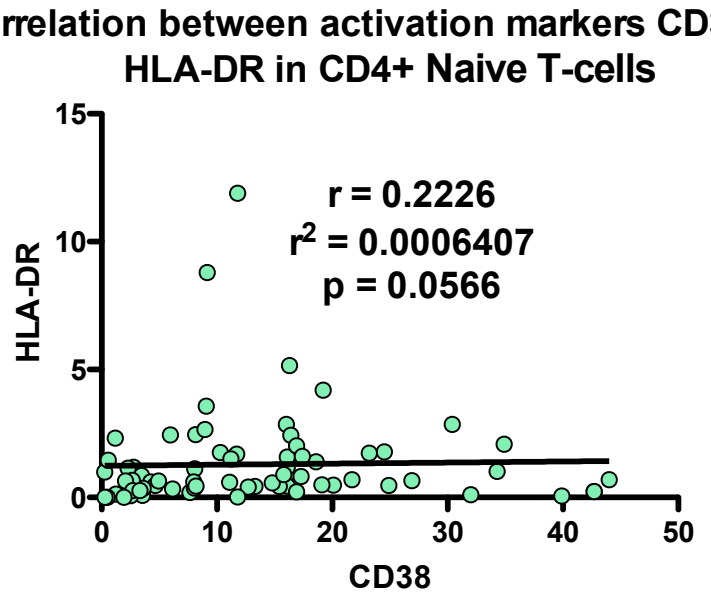

Appendix VIII. Correlation analysis of $CD8^+$ naïve T-cell telomere length and patients age.

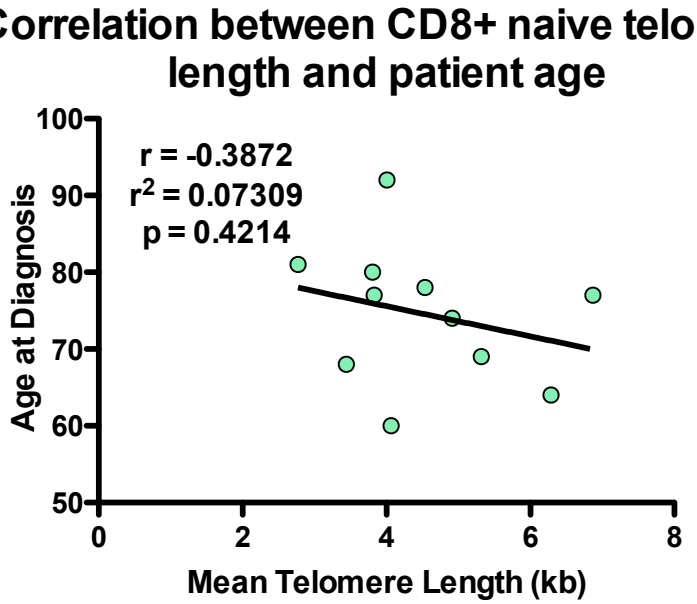

Appendix IX. Patient Characteristics.

Table 1. Clinical characteristics of phenotyping cohort (Chapters 3 and 4)

Characteristic		Total cohort (n = 74)
Age (years)	Mean	62.9
	Median	64.5
	Range	29.3-86.6
Binet stage, n (%)	A	62 (83.8%)
	B	7 (9.5%)
	C	4 (5.4%)
	Unknown	1 (1.4%)
CD38 status, n (%)	+ (>20%)	20 (27.0%)
	– (<20%)	24 (32.4%)
	Unknown	30 (40.5%)
Lymphocyte doubling time (LDT), n (%)	<12 months	9 (12.2%)
	>12 months	48 (64.9%)
	Unknown	17 (23.0%)
IGHV status, n (%)	Unmutated	18 (24.3%)
	Mutated	5 (6.8%)
	Unknown	51 (68.9%)
TTFT status, n (%)	Treated	22 (29.7%)
	Untreated	52 (70.3%)

Table 2. Clinical characteristics of merged untreated/treated cohort (Chapter 5)

		Total cohort (n = 42)	Treated (n = 19)	Untreated (n = 23)
Age (years)	Mean	70.6	69.2	72
	Median	71	70	74
	Range	44-90	44-87	47-90
Binet stage, n (%)	A	32	11	21
	B	3	3	0
	C	3	3	0
	Unknown	4	2	2
CD38 status, n (%)	+ (>20%)	5	5	0
	– (<20%)	17	6	11
	Unknown	20	8	12
LDT, n (%)	<12 months	5	3	2
	>12 months	22	7	15
	Unknown	15	9	6

IGHV status, n (%)	Unmutated	2	2	0
	Mutated	6	4	2
	Unknown	34	13	21
TTFT status, n (%)	Treated	19	-	-
	Untreated	23	-	-

Table 2. Treatment history of treated cohort (Chapter 5)

Treated Patient	Treatment history
Longitudinal patients	
1	CLB: Apr 2013-Aug 2013
2	CLB: Oct 2010-Mar 2011 Ofatumumab: Apr -Oct 2013
3	CLB: Feb 2007-Sep 2007 CLB: 2012
4	FC: Jan 2008-Jun 2008
5	CLB: Nov 2014-Oct 2015
6	FC: Jan 2010-Feb 2010 CLB: Oct 2013-Mar 2014 CLB: Oct 2015-ongoing
7	FCR: Sep 2009-Mar 2010 Alemtuzumab: Jan-Apr 2012 Ofatumumab: Feb 2013-Jan 2014 Ibrutinib: Jan 2014-ongoing
8	CLB/Rituximab: Apr 2006-Sep 2016 Idelalsisib: Sep 2016
9	FCR: Sep 2013-Mar 2014
Other treated patients	
10	Idelalisib/Rituximab: Jan 2016-Apr 2016
11	CLB/Obinutuzumab: Aug 2010-Sep 2010 BR: Oct 2011-Feb 2012
12	CLB: Jul 2006-Jan 2007 CLB: Jan 2009-May 2009 FCR: Sep 2011-Feb 2012
13	BR: Feb 2008-Apr 2008 RCHOP, Alemtuzumab, BR again, GS 4059 and finally idelalsib/Rituximab: dates unknown
14	Alemtuzumab: Oct 2008-Jan 2009 Stem cell allograft: Jul 2009 Idelalisib: May 2015-Sep 2016
15	CLB: May 1993-Apr 1994 CLB: Aug 2010-Feb 2011
16	Ibrutinib/rituximab: Aug 2015-ongoing

17	BR: Feb 2014-Jul 2014
18	CLB: Jul 2009-Feb 2010 CLB: Dec 2015-Mar 2016
19	CLB: Jul 2013-Apr 2014
20	FC: Jan-Jul 2004 Alemtuzumab: Sep-Dec 2008 BR: date unknown.

References

Ahmadzadeh, M., Johnson, L.A., Heemskerk, B., Wunderlich, J.R., Dudley, M.E., White, D.E. and Rosenberg, S.A. 2009. Tumor antigen-specific CD8 T cells infiltrating the tumor express high levels of PD-1 and are functionally impaired. *Blood* 114(8), pp. 1537–1544.

Akagi, J. and Baba, H. 2008. Prognostic value of CD57(+) T lymphocytes in the peripheral blood of patients with advanced gastric cancer. *International journal of clinical oncology* 13(6), pp. 528–535.

Allsopp, R.C., Vaziri, H., Patterson, C., Goldstein, S., Younglai, E.V., Futcher, A.B., Greider, C.W., et al. 1992. Telomere length predicts replicative capacity of human fibroblasts. *Proceedings of the National Academy of Sciences of the United States of America* 89(21), pp. 10114–10118.

Angelosanto, J.M., Blackburn, S.D., Crawford, A. and Wherry, E.J. 2012. Progressive loss of memory T cell potential and commitment to exhaustion during chronic viral infection. *Journal of virology* 86(15), pp. 8161–8170.

Anichini, A., Molla, A., Vegetti, C., Bersani, I., Zappasodi, R., Arienti, F., Ravagnani, F., et al. 2010. Tumor-reactive CD8+ early effector T cells identified at tumor site in primary and metastatic melanoma. *Cancer research* 70(21), pp. 8378–8387.

Aref, S., Azmy, E., Hakim, H., Khodary, El, T., Menshawy, El, N. and Ebrahim, L. 2014. Regulatory T cells in chronic lymphocytic leukemia. *AGE* 24(3), pp. 649–652.

Bachmann, M.F., Wolint, P., Schwarz, K., Jäger, P. and Oxenius, A. 2005. Functional properties and lineage relationship of CD8+ T cell subsets identified by expression of IL-7 receptor alpha and CD62L. *Journal of immunology (Baltimore, Md. : 1950)* 175(7), pp. 4686–4696.

Baird, D.M. 2005. New developments in telomere length analysis. *Experimental gerontology* 40(5), pp. 363–368.

Banchereau, J. and Steinman, R.M. 1998. Dendritic cells and the control of immunity. *Nature* 392(6673), pp. 245–252.

Banham, A.H. 2006. Cell-surface IL-7 receptor expression facilitates the purification of FOXP3+ regulatory T cells. *Trends in immunology* 27(12), pp. 541–544.

Basham, T.Y. and Merigan, T.C. 1983. Recombinant interferon-gamma increases HLA-DR synthesis and expression. *Journal of immunology (Baltimore, Md. : 1950)* 130(4), pp. 1492–1494.

Baumgarth, N. 2011. The double life of a B-1 cell: self-reactivity selects for protective effector functions. *Nature reviews. Immunology* 11(1), pp. 34–46.

Bechter, O.E., Eisterer, W., Pall, G., Hilbe, W., Kühr, T. and Thaler, J. 1998. Telomere length and telomerase activity predict survival in patients with B cell chronic lymphocytic leukemia. *Cancer research* 58(21), pp. 4918–4922.

Bendall, S.C., Nolan, G.P., Roederer, M. and Chattopadhyay, P.K. 2012. A deep profiler's guide to cytometry. *Trends in immunology* 33(7), pp. 323–332.

Bengsch, B., Seigel, B., Ruhl, M., Timm, J., Kuntz, M., Blum, H.E., Pircher, H., et al. 2010. Coexpression of PD-1, 2B4, CD160 and KLRG1 on exhausted HCV-specific CD8+ T cells is linked to antigen recognition and T cell differentiation. *PLoS pathogens* 6(6), p. e1000947.

Bengsch, B., Spangenberg, H.C., Kersting, N., Neumann-Haefelin, C., Panther, E., Weizsäcker,

von, F., Blum, H.E., et al. 2007. Analysis of CD127 and KLRG1 expression on hepatitis C virus-specific CD8+ T cells reveals the existence of different memory T-cell subsets in the peripheral blood and liver. *Journal of virology* 81(2), pp. 945–953.

Binet, J.L., Auquier, A., Dighiero, G., Chastang, C., Piguet, H., Goasguen, J., Vaugier, G., et al. 1981. A new prognostic classification of chronic lymphocytic leukemia derived from a multivariate survival analysis. *Cancer* 48(1), pp. 198–206.

Bodnar, A.G., Kim, N.W., Effros, R.B. and Chiu, C.P. 1996. Mechanism of telomerase induction during T cell activation. *Experimental cell research* 228(1), pp. 58–64.

Boehmer, von, H. 2005. Mechanisms of suppression by suppressor T cells. *Nature immunology* 6(4), pp. 338–344.

Born, W.K., Kemal Aydintug, M. and O'Brien, R.L. 2012. Diversity of γδ T-cell antigens. *Cellular & molecular immunology* 10(1), pp. 13–20.

Bossi, G. and Griffiths, G.M. 1999. Degranulation plays an essential part in regulating cell surface expression of Fas ligand in T cells and natural killer cells. *Nature medicine* 5(1), pp. 90–96.

Brenchley, J.M., Karandikar, N.J., Betts, M.R., Ambrozak, D.R., Hill, B.J., Crotty, L.E., Casazza, J.P., et al. 2003. Expression of CD57 defines replicative senescence and antigen-induced apoptotic death of CD8+ T cells. *Blood* 101(7), pp. 2711–2720.

Brentjens, R.J., Riviere, I., Park, J.H., Davila, M.L., Wang, X., Stefanski, J., Taylor, C., et al. 2011. Safety and persistence of adoptively transferred autologous CD19-targeted T cells in patients with relapsed or chemotherapy refractory B-cell leukemias. *Blood* 118(18), pp. 4817–4828.

Britt-Compton, B., Lin, T.T., Ahmed, G., Weston, V., Jones, R.E., Fegan, C., Oscier, D.G., et al. 2011. Extreme telomere erosion in ATM-mutated and 11q-deleted CLL patients is independent of disease stage. *Leukemia* 26(4), pp. 826–830.

Broccoli, D., Young, J.W. and de Lange, T. 1995. Telomerase activity in normal and malignant hematopoietic cells. *Proceedings of the National Academy of Sciences of the United States of America* 92(20), pp. 9082–9086.

Brown, J.R. 2014. Inherited predisposition to chronic lymphocytic leukemia. *Expert review of hematology* 1(1), pp. 51–61.

Brusa, D., Serra, S., Coscia, M., Rossi, D., D'Arena, G., Laurenti, L., Jaksic, O., et al. 2013. The PD-1/PD-L1 axis contributes to T-cell dysfunction in chronic lymphocytic leukemia. *Haematologica* 98(6), pp. 953–963.

Buggert, M., Frederiksen, J., Noyan, K., Svärd, J., Barqasho, B., Sönnerborg, A., Lund, O., et al. 2014. Multiparametric bioinformatics distinguish the CD4/CD8 ratio as a suitable laboratory predictor of combined T cell pathogenesis in HIV infection. *Journal of immunology (Baltimore, Md. : 1950)* 192(5), pp. 2099–2108.

Buggins, A.G.S., Levi, A., Gohil, S., Fishlock, K., Patten, P.E.M., Calle, Y., Yallop, D., et al. 2011. Evidence for a macromolecular complex in poor prognosis CLL that contains CD38, CD49d, CD44 and MMP-9. *British journal of haematology* 154(2), pp. 216–222.

Bulian, P., Shanafelt, T.D., Fegan, C., Zucchetto, A., Cro, L., Nuckel, H., Baldini, L., et al. 2014. CD49d Is the Strongest Flow Cytometry-Based Predictor of Overall Survival in Chronic Lymphocytic Leukemia. *Journal of Clinical Immunology* 32(9), pp. 897–904.

Burnet, M. 1957. Cancer—a biological approach: I. The processes of control. II. The significance of somatic mutation. *British medical journal*.

Carroll, M.C. 2004. The complement system in regulation of adaptive immunity. *Nature immunology* 5(10), pp. 981–986.

Cerutti, A., Cols, M. and Puga, I. 2012. Activation of B cells by non-canonical helper signals. *EMBO reports* 13(9), pp. 798–810.

Cerwenka, A. and Lanier, L.L. 2001. Ligands for natural killer cell receptors: redundancy or specificity. *Immunological reviews* 181, pp. 158–169.

Champagne, P., Ogg, G.S., King, A.S., Knabenhans, C., Ellefsen, K., Nobile, M., Appay, V., et al. 2001. Skewed maturation of memory HIV-specific CD8 T lymphocytes. *Nature* 410(6824), pp. 106–111.

Characiejus, D., Pasukoniene, V., Jonusauskaite, R., Azlauskaite, N., Aleknavicius, E., Mauricas, M. and Otter, W.D. 2008. Peripheral blood CD8highCD57+ lymphocyte levels may predict outcome in melanoma patients treated with adjuvant interferon-alpha. *Anticancer research* 28(2B), pp. 1139–1142.

Chattopadhyay, P.K., Betts, M.R., Price, D.A., Gostick, E., Horton, H., Roederer, M. and De Rosa, S.C. 2008. The cytolytic enzymes granyzme A, granzyme B, and perforin: expression patterns, cell distribution, and their relationship to cell maturity and bright CD57 expression. *Journal of Leukocyte Biology* 85(1), pp. 88–97.

Cheng, G., Yuan, X., Tsai, M.S., Podack, E.R., Yu, A. and Malek, T.R. 2012. IL-2 receptor signaling is essential for the development of Klrg1+ terminally differentiated T regulatory cells. *Journal of immunology (Baltimore, Md. : 1950)* 189(4), pp. 1780–1791.

Chikuma, S. 2016. Basics of PD-1 in self-tolerance, infection, and cancer immunity. *International journal of clinical oncology* 21(3), pp. 448–455.

Chiorazzi, N. and Ferrarini, M. 2011. Cellular origin(s) of chronic lymphocytic leukemia: cautionary notes and additional considerations and possibilities. *Blood* 117(6), pp. 1781–1791.

Chong, L.K., Aicheler, R.J., Llewellyn-Lacey, S., Tomasec, P., Brennan, P. and Wang, E.C.Y. 2008. Proliferation and interleukin 5 production by CD8hi CD57+ T cells. *European journal of immunology* 38(4), pp. 995–1000.

Chow, J.C., Young, D.W., Golenbock, D.T., Christ, W.J. and Gusovsky, F. 1999. Toll-like receptor-4 mediates lipopolysaccharide-induced signal transduction. *The Journal of biological chemistry* 274(16), pp. 10689–10692.

Cobaleda, C., Schebesta, A., Delogu, A. and Busslinger, M. 2007. Pax5: the guardian of B cell identity and function. *Nature immunology* 8(5), pp. 463–470.

Cockerham, L.R., Jain, V., Sinclair, E., Glidden, D.V., Hartogenesis, W., Hatano, H., Hunt, P.W., et al. 2014. Programmed death-1 expression on $CD4^+$ and $CD8^+$ T cells in treated and untreated HIV disease. *AIDS (London, England)* 28(12), pp. 1749–1758.

Coiffier, B., Lepretre, S., Pedersen, L.M., Gadeberg, O., Fredriksen, H., van Oers, M.H.J., Wooldridge, J., et al. 2008. Safety and efficacy of ofatumumab, a fully human monoclonal anti-CD20 antibody, in patients with relapsed or refractory B-cell chronic lymphocytic leukemia: a phase 1-2 study. *Blood* 111(3), pp. 1094–1100.

Collin, M., McGovern, N. and Haniffa, M. 2013. Human dendritic cell subsets. *Immunology* 140(1), pp. 22–30.

CRUK 2016. Chronic lymphocytic leukaemia (CLL) statistics. [Online]. Available at: http://www.cancerresearchuk.org/health-professional/cancer-statistics/statistics-by-cancer-

type/leukaemia-cll [Accessed: 1 December 2016].

Damle, R.N. 2002. B-cell chronic lymphocytic leukemia cells express a surface membrane phenotype of activated, antigen-experienced B lymphocytes. *Blood* 99(11), pp. 4087–4093.

Damle, R.N., Wasil, T., Fais, F., Ghiotto, F., Valetto, A., Allen, S.L., Buchbinder, A., et al. 1999. Ig V gene mutation status and CD38 expression as novel prognostic indicators in chronic lymphocytic leukemia. *Blood* 94(6), pp. 1840–1847.

Davila, M.L. and Brentjens, R. 2013. Chimeric antigen receptor therapy for chronic lymphocytic leukemia: what are the challenges? *Hematology/oncology clinics of North America* 27(2), pp. 341–353.

Day, C.L., Kaufmann, D.E., Kiepiela, P., Brown, J.A., Moodley, E.S., Reddy, S., Mackey, E.W., et al. 2006. PD-1 expression on HIV-specific T cells is associated with T-cell exhaustion and disease progression. *Nature* 443(7109), pp. 350–354.

de Lafaille, M.A.C. and Lafaille, J.J. 2009. Natural and Adaptive Foxp3+ Regulatory T Cells: More of the Same or a Division of Labor? *Immunity* 30(5), pp. 626–635.

Defrance, T., Vanbervliet, B., Brière, F., Durand, I., Rousset, F. and Banchereau, J. 1992. Interleukin 10 and transforming growth factor beta cooperate to induce anti-CD40-activated naive human B cells to secrete immunoglobulin A. *The Journal of experimental medicine* 175(3), pp. 671–682.

Di Mitri, D., Azevedo, R.I., Henson, S.M., Libri, V., Riddell, N.E., Macaulay, R., Kipling, D., et al. 2011. Reversible senescence in human CD4+CD45RA+CD27- memory T cells. *Journal of immunology (Baltimore, Md. : 1950)* 187(5), pp. 2093–2100.

Dianzani, U., Funaro, A., DiFranco, D., Garbarino, G., Bragardo, M., Redoglia, V., Buonfiglio, D., et al. 1994. Interaction between endothelium and CD4+CD45RA+ lymphocytes. Role of the human CD38 molecule. *Journal of immunology (Baltimore, Md. : 1950)* 153(3), pp. 952–959.

DiLillo, D.J., Weinberg, J.B., Yoshizaki, A., Horikawa, M., Bryant, J.M., Iwata, Y., Matsushita, T., et al. 2013. Chronic lymphocytic leukemia and regulatory B cells share IL-10 competence and immunosuppressive function. *Leukemia* 27(1), pp. 170–182.

Dillon, S.M., Rogers, L.M., Howe, R., Hostetler, L.A., Buhrman, J., McCarter, M.D. and Wilson, C.C. 2010. Human Intestinal Lamina Propria CD1c+ Dendritic Cells Display an Activated Phenotype at Steady State and Produce IL-23 in Response to TLR7/8 Stimulation. *Journal of immunology (Baltimore, Md. : 1950)* 184(12), pp. 6612–6621.

Dolcetti, R. and Carbone, A. 2010. Epstein-Barr virus infection and chronic lymphocytic leukemia: a possible progression factor? *Infectious Agents and Cancer* 5(1), p. 22.

Dranoff, G. 2004. Cytokines in cancer pathogenesis and cancer therapy. *Nature reviews. Cancer* 4(1), pp. 11–22.

Duggan, C., Risques, R., Alfano, C., Prunkard, D., Imayama, I., Holte, S., Baumgartner, K., et al. 2014. Change in peripheral blood leukocyte telomere length and mortality in breast cancer survivors. *Journal of the National Cancer Institute* 106(4), p. dju035.

Dunkle, A., Dzhagalov, I., Gordy, C. and He, Y.-W. 2013. Transfer of CD8+ T cell memory using Bcl-2 as a marker. *Journal of immunology (Baltimore, Md. : 1950)* 190(3), pp. 940–947.

Dunn, G.P., Old, L.J. and Schreiber, R.D. 2004. The Three Es of Cancer Immunoediting. *Annual review of immunology* 22(1), pp. 329–360.

Dürig, J., Naschar, M., Schmücker, U., Renzing-Köhler, K., Hölter, T., Hüttmann, A. and Dührsen, U. 2002. CD38 expression is an important prognostic marker in chronic lymphocytic leukaemia. *Leukemia* 16(1), pp. 30–35.

Eichhorst, B., Dreyling, M., Robak, T., Montserrat, E., Hallek, M.On behalf of the ESMO Guidelines Working Group 2011. Chronic lymphocytic leukemia: ESMO Clinical Practice Guidelines for diagnosis, treatment and follow-up. *Annals of Oncology* 22(Supplement 6), pp. vi50–vi54.

Ferlazzo, G., Pack, M., Thomas, D., Paludan, C., Schmid, D., Strowig, T., Bougras, G., et al. 2004. Distinct roles of IL-12 and IL-15 in human natural killer cell activation by dendritic cells from secondary lymphoid organs. *Proceedings of the National Academy of Sciences* 101(47), pp. 16606–16611.

Ferrando-Martínez, S., Ruiz-Mateos, E., Hernández, A., Gutiérrez, E., Rodríguez-Méndez, M.D.M., Ordoñez, A. and Leal, M. 2011. Age-related deregulation of naive T cell homeostasis in elderly humans. *AGE* 33(2), pp. 197–207.

Focosi, D., Bestagno, M., Burrone, O. and Petrini, M. 2010. CD57+ T lymphocytes and functional immune deficiency. *Journal of Leukocyte Biology* 87(1), pp. 107–116.

Fraietta, J.A., Beckwith, K.A., Patel, P.R., Ruella, M., Zheng, Z., Barrett, D.M., Lacey, S.F., et al. 2016. Ibrutinib enhances chimeric antigen receptor T-cell engraftment and efficacy in leukemia. *Blood* 127(9), pp. 1117–1127.

Freeman, C.L. and Gribben, J.G. 2016. Immunotherapy in Chronic Lymphocytic Leukaemia (CLL). *Current Hematologic Malignancy Reports* 11(1), pp. 29–36.

Funaro, A., De Monte, L.B., Dianzani, U., Forni, M. and Malavasi, F. 1993. Human CD38 is associated to distinct molecules which mediate transmembrane signaling in different lineages. *European journal of immunology* 23(10), pp. 2407–2411.

Funaro, A., Spagnoli, G.C., Ausiello, C.M., Alessio, M., Roggero, S., Delia, D., Zaccolo, M., et al. 1990. Involvement of the multilineage CD38 molecule in a unique pathway of cell activation and proliferation. *Journal of immunology (Baltimore, Md. : 1950)* 145(8), pp. 2390–2396.

Furman, R.R., Sharman, J.P., Coutre, S.E., Cheson, B.D., Pagel, J.M., Hillmen, P., Barrientos, J.C., et al. 2014. Idelalisib and Rituximab in Relapsed Chronic Lymphocytic Leukemia. *New England Journal of Medicine* 370(11), pp. 997–1007.

Fülöp, T., Larbi, A. and Pawelec, G. 2013. Human T cell aging and the impact of persistent viral infections. *Frontiers in immunology* 4, p. 271.

Galon, J., Costes, A., Sanchez-Cabo, F., Kirilovsky, A., Mlecnik, B., Lagorce-Pagès, C., Tosolini, M., et al. 2006. Type, density, and location of immune cells within human colorectal tumors predict clinical outcome. *Science* 313(5795), pp. 1960–1964.

Garaud, S., Morva, A., Lemoine, S., Hillion, S., Bordron, A., Pers, J.-O., Berthou, C., et al. 2011. CD5 promotes IL-10 production in chronic lymphocytic leukemia B cells through STAT3 and NFAT2 activation. *Journal of immunology (Baltimore, Md. : 1950)* 186(8), pp. 4835–4844.

Gattei, V., Bulian, P., Del Principe, M.I., Zucchetto, A., Maurillo, L., Buccisano, F., Bomben, R., et al. 2008. Relevance of CD49d protein expression as overall survival and progressive disease prognosticator in chronic lymphocytic leukemia. *Blood* 111(2), pp. 865–873.

Gattinoni, L., Lugli, E., Ji, Y., Pos, Z., Paulos, C.M., Quigley, M.F., Almeida, J.R., et al. 2011. A human memory T cell subset with stem cell-like properties. *Nature medicine* 17(10), pp. 1290–1297.

Geginat, J. 2003. Proliferation and differentiation potential of human CD8+ memory T-cell subsets in response to antigen or homeostatic cytokines. *Blood* 101(11), pp. 4260–4266.

Germain, R.N. 2002. T-cell development and the CD4-CD8 lineage decision. *Nature reviews. Immunology* 2(5), pp. 309–322.

Gitelson, E., Hammond, C., Mena, J., Lorenzo, M., Buckstein, R., Berinstein, N.L., Imrie, K., et al. 2003. Chronic lymphocytic leukemia-reactive T cells during disease progression and after autologous tumor cell vaccines. *Clinical cancer research : an official journal of the American Association for Cancer Research* 9(5), pp. 1656–1665.

Golden-Mason, L., Burton, J.R., Castelblanco, N., Klarquist, J., Benlloch, S., Wang, C. and Rosen, H.R. 2006. Loss of IL-7 receptor alpha-chain (CD127) expression in acute HCV infection associated with viral persistence. *Hepatology (Baltimore, Md.)* 44(5), pp. 1098–1109.

Gonzalez-Rodriguez, A.P., Contesti, J., Huergo-Zapico, L., Lopez-Soto, A., Fernández-Guizán, A., Acebes-Huerta, A., Gonzalez-Huerta, A.J., et al. 2010. Prognostic significance of CD8 and CD4 T cells in chronic lymphocytic leukemia. *Leukemia & lymphoma* 51(10), pp. 1829–1836.

Gordon, S. and Taylor, P.R. 2005. Monocyte and macrophage heterogeneity. *Nature reviews. Immunology* 5(12), pp. 953–964.

Görgün, G., Holderried, T.A.W., Zahrieh, D., Neuberg, D. and Gribben, J.G. 2005. Chronic lymphocytic leukemia cells induce changes in gene expression of CD4 and CD8 T cells. *The Journal of clinical investigation* 115(7), pp. 1797–1805.

Göthert, J.R., Eisele, L., Klein-Hitpass, L., Weber, S., Zesewitz, M.-L., Sellmann, L., Röth, A., et al. 2013. Expanded CD8+ T cells of murine and human CLL are driven into a senescent KLRG1+ effector memory phenotype. *Cancer immunology, immunotherapy : CII* 62(11), pp. 1697–1709.

Grabowski, P., Hultdin, M., Karlsson, K., Tobin, G., Aleskog, A., Thunberg, U., Laurell, A., et al. 2005. Telomere length as a prognostic parameter in chronic lymphocytic leukemia with special reference to VH gene mutation status. *Blood* 105(12), pp. 4807–4812.

Hallek, M., Cheson, B.D., Catovsky, D., Caligaris-Cappio, F., Dighiero, G., Dohner, H., Hillmen, P., et al. 2008. Guidelines for the diagnosis and treatment of chronic lymphocytic leukemia: a report from the International Workshop on Chronic Lymphocytic Leukemia updating the National Cancer Institute-Working Group 1996 guidelines. *Blood* 111(12), pp. 5446–5456.

Hamblin, A.D. and Hamblin, T.J. 2008. The immunodeficiency of chronic lymphocytic leukaemia. *British medical bulletin* 87, pp. 49–62.

Hamblin, T.J., Davis, Z., Gardiner, A., Oscier, D.G. and Stevenson, F.K. 1999. Unmutated Ig V(H) genes are associated with a more aggressive form of chronic lymphocytic leukemia. *Blood* 94(6), pp. 1848–1854.

Hamblin, T.J., Orchard, J.A., Ibbotson, R.E., Davis, Z., Thomas, P.W., Stevenson, F.K. and Oscier, D.G. 2002. CD38 expression and immunoglobulin variable region mutations are independent prognostic variables in chronic lymphocytic leukemia, but CD38 expression may vary during the course of the disease. *Blood* 99(3), pp. 1023–1029.

Hammond, M.E., Lapointe, G.R., Feucht, P.H., Hilt, S., Gallegos, C.A., Gordon, C.A., Giedlin, M.A., et al. 1995. IL-8 induces neutrophil chemotaxis predominantly via type I IL-8 receptors. *Journal of immunology (Baltimore, Md. : 1950)* 155(3), pp. 1428–1433.

Han, J., Qureshi, A.A., Prescott, J., Guo, Q., Ye, L., Hunter, D.J. and De Vivo, I. 2009. A prospective study of telomere length and the risk of skin cancer. *The Journal of investigative dermatology* 129(2), pp. 415–421.

Hanahan, D. and Weinberg, R.A. 2011. Hallmarks of cancer: the next generation. *Cell* 144(5), pp. 646–674.

Hand, T.W., Morre, M. and Kaech, S.M. 2007. Expression of IL-7 receptor alpha is necessary but not sufficient for the formation of memory CD8 T cells during viral infection. *Proceedings of the National Academy of Sciences of the United States of America* 104(28), pp. 11730–11735.

Harty, J.T. and Badovinac, V.P. 2008. Shaping and reshaping CD8+ T-cell memory. *Nature reviews. Immunology* 8(2), pp. 107–119.

Hathcock, K.S., Kaech, S.M., Ahmed, R. and Hodes, R.J. 2003. Induction of telomerase activity and maintenance of telomere length in virus-specific effector and memory CD8+ T cells. *Journal of immunology (Baltimore, Md. : 1950)* 170(1), pp. 147–152.

Hayakawa, K., Formica, A.M., Brill-Dashoff, J., Shinton, S.A., Ichikawa, D., Zhou, Y., Morse, H.C., et al. 2016. Early generated B1 B cells with restricted BCRs become chronic lymphocytic leukemia with continued c-Myc and low Bmf expression. *The Journal of experimental medicine* 213(13), pp. 3007–3023.

Henson, S.M., Franzese, O., Macaulay, R., Libri, V., Azevedo, R.I., Kiani-Alikhan, S., Plunkett, F.J., et al. 2009. KLRG1 signaling induces defective Akt (ser473) phosphorylation and proliferative dysfunction of highly differentiated CD8+ T cells. *Blood* 113(26), pp. 6619–6628.

Herman, S.E.M., Mustafa, R.Z., Gyamfi, J.A., Pittaluga, S., Chang, S., Chang, B., Farooqui, M., et al. 2014. Ibrutinib inhibits BCR and NF-κB signaling and reduces tumor proliferation in tissue-resident cells of patients with CLL. *Blood* 123(21), pp. 3286–3295.

Hertlein, E., Beckwith, K.A., Lozanski, G., Chen, T.L., Towns, W.H., Johnson, A.J., Lehman, A., et al. 2013. Characterization of a New Chronic Lymphocytic Leukemia Cell Line for Mechanistic In Vitro and In Vivo Studies Relevant to Disease. *PloS one* 8(10), p. e76607.

Hoffman, W., Lakkis, F.G. and Chalasani, G. 2016. B Cells, Antibodies, and More. *Clinical Journal of the American Society of Nephrology* 11(1), pp. 137–154.

Hofland, T., de Weerdt, I., Terpstra, S., Remmerswaal, E.B.M., Berge, ten, I.J.M., Kater, A.P. and Tonino, S.H. 2015. EBV-Specific CD8+ T-Cells Are Not Functionally Impaired in Chronic Lymphocytic Leukemia. *Blood* 126(23), pp. 1723–1723.

Holling, T.M., van der Stoep, N., Quinten, E. and van den Elsen, P.J. 2002. Activated Human T Cells Accomplish MHC Class II Expression Through T Cell-Specific Occupation of Class II Transactivator Promoter III. *Journal of immunology (Baltimore, Md. : 1950)* 168(2), pp. 763–770.

Hori, S., Nomura, T. and Sakaguchi, S. 2003. Control of regulatory T cell development by the transcription factor Foxp3. *Science* 299(5609), pp. 1057–1061.

Hukelmann, J.L., Anderson, K.E., Sinclair, L.V., Grzes, K.M., Murillo, A.B., Hawkins, P.T., Stephens, L.R., et al. 2016. The cytotoxic T cell proteome and its shaping by the kinase mTOR. *Nature Publishing Group* 17(1), pp. 104–112.

Ibegbu, C.C., Xu, Y.-X., Harris, W., Maggio, D., Miller, J.D. and Kourtis, A.P. 2005. Expression of killer cell lectin-like receptor G1 on antigen-specific human CD8+ T lymphocytes during active, latent, and resolved infection and its relation with CD57. *Journal of immunology (Baltimore, Md. : 1950)* 174(10), pp. 6088–6094.

Iwasaki, A. and Medzhitov, R. 2015. Control of adaptive immunity by the innate immune system. *Nature immunology* 16(4), pp. 343–353.

Janeway, C.A., Travers, P., Walport, M. and Shlomchik, M. 2001. *Immunobiology*. Fifth edition. New York: Garland Publishin.

Joffre, O.P., Segura, E., Savina, A. and Amigorena, S. 2012. Cross-presentation by dendritic cells. *Nature reviews. Immunology*, pp. 1–13.

Josefowicz, S.Z., Lu, L.-F. and Rudensky, A.Y. 2012. Regulatory T Cells: Mechanisms of Differentiation and Function. *Annual review of immunology* 30(1), pp. 531–564.

Kaech, S.M., Tan, J.T., Wherry, E.J., Konieczny, B.T., Surh, C.D. and Ahmed, R. 2003. Selective expression of the interleukin 7 receptor identifies effector CD8 T cells that give rise to long-lived memory cells. *Nature immunology* 4(12), pp. 1191–1198.

Keir, M.E., Butte, M.J., Freeman, G.J. and Sharpe, A.H. 2008. PD-1 and Its Ligands in Tolerance and Immunity. *Annual review of immunology* 26(1), pp. 677–704.

Khan, N., Shariff, N., Cobbold, M., Bruton, R., Ainsworth, J.A., Sinclair, A.J., Nayak, L., et al. 2002. Cytomegalovirus seropositivity drives the CD8 T cell repertoire toward greater clonality in healthy elderly individuals. *Journal of immunology (Baltimore, Md. : 1950)* 169(4), pp. 1984–1992.

Kim, J., Kim, A.-R. and Shin, E.-C. 2015. Cytomegalovirus Infection and Memory T Cell Inflation. *Immune Network* 15(4), p. 186.

Kindt, T.J., Goldsby, R.A. and Osborne, B.A. 2007. *Kuby Immunology*. Sixth Edition. New York: W. H. Freeman and Company.

Klebanoff, C.A., Gattinoni, L. and Restifo, N.P. 2006. CD8+ T-cell memory in tumor immunology and immunotherapy. *Immunological reviews* 211(1), pp. 214–224.

Klenerman, P. and Oxenius, A. 2016. T cell responses to cytomegalovirus. *Nature reviews. Immunology* 16(6), pp. 367–377.

Koch, S., Larbi, A., Derhovanessian, E., Ozcelik, D., Naumova, E. and Pawelec, G. 2008. Multiparameter flow cytometric analysis of CD4 and CD8 T cell subsets in young and old people. *Immunity & Ageing* 5, p. 6.

Kolaczkowska, E. and Kubes, P. 2013. Neutrophil recruitment and function in health and inflammation. *Nature reviews. Immunology* 13(3), pp. 159–175.

Kurtulus, S., Tripathi, P., Moreno-Fernandez, M.E., Sholl, A., Katz, J.D., Grimes, H.L. and Hildeman, D.A. 2011. Bcl-2 allows effector and memory CD8+ T cells to tolerate higher expression of Bim. *Journal of immunology (Baltimore, Md. : 1950)* 186(10), pp. 5729–5737.

LeBien, T.W. and Tedder, T.F. 2008. B lymphocytes: how they develop and function. *Blood* 112(5), pp. 1570–1580.

Li, Y., Hofmann, M., Wang, Q., Teng, L., Chlewicki, L.K., Pircher, H. and Mariuzza, R.A. 2009. Structure of natural killer cell receptor KLRG1 bound to E-cadherin reveals basis for MHC-independent missing self recognition. *Immunity* 31(1), pp. 35–46.

Li, Z., Woo, C.J., Iglesias-Ussel, M.D., Ronai, D. and Scharff, M.D. 2004. The generation of antibody diversity through somatic hypermutation and class switch recombination. *Genes & development* 18(1), pp. 1–11.

Lin, J., Epel, E., Cheon, J., Kroenke, C., Sinclair, E., Bigos, M., Wolkowitz, O., et al. 2010a. Analyses and comparisons of telomerase activity and telomere length in human T and B cells: insights for epidemiology of telomere maintenance. *Journal of Immunological Methods* 352(1-2),

pp. 71–80.

Lin, T.T., Letsolo, B.T., Jones, R.E., Rowson, J., Pratt, G., Hewamana, S., Fegan, C., et al. 2010b. Telomere dysfunction and fusion during the progression of chronic lymphocytic leukemia: evidence for a telomere crisis. *Blood* 116(11), pp. 1899–1907.

Lin, T.T., Norris, K., Heppel, N.H., Pratt, G., Allan, J.M., Allsup, D.J., Bailey, J., et al. 2014. Telomere dysfunction accurately predicts clinical outcome in chronic lymphocytic leukaemia, even in patients with early stage disease. *British journal of haematology* 167(2), pp. 214–223.

Lin, X., Chen, M., Liu, Y., Guo, Z., He, X., Brand, D. and Zheng, S.G. 2013. Advances in distinguishing natural from induced Foxp3(+) regulatory T cells. *International journal of clinical and experimental pathology* 6(2), pp. 116–123.

Ma, A., Koka, R. and Burkett, P. 2006. Diverse functions of IL-2, IL-15, and IL-7 in lymphoid homeostasis. *Annual review of immunology* 24, pp. 657–679.

Ma, C.S., Deenick, E.K., Batten, M. and Tangye, S.G. 2012. The origins, function, and regulation of T follicular helper cells. *The Journal of experimental medicine* 209(7), pp. 1241–1253.

Ma, C.S., Suryani, S., Avery, D.T., Chan, A., Nanan, R., Santner-Nanan, B., Deenick, E.K., et al. 2009. Early commitment of naïve human CD4(+) T cells to the T follicular helper (T(FH)) cell lineage is induced by IL-12. *Immunology and cell biology* 87(8), pp. 590–600.

Mahnke, Y.D., Brodie, T.M., Sallusto, F., Roederer, M. and Lugli, E. 2013. The who's who of T-cell differentiation: Human memory T-cell subsets. *European journal of immunology* 43(11), pp. 2797–2809.

Maini, M.K., Soares, M.V., Zilch, C.F., Akbar, A.N. and Beverley, P.C. 1999. Virus-induced CD8+ T cell clonal expansion is associated with telomerase up-regulation and telomere length preservation: a mechanism for rescue from replicative senescence. *Journal of immunology (Baltimore, Md. : 1950)* 162(8), pp. 4521–4526.

Malavasi, F., Deaglio, S., Funaro, A., Ferrero, E., Horenstein, A.L., Ortolan, E., Vaisitti, T., et al. 2008. Evolution and Function of the ADP Ribosyl Cyclase/CD38 Gene Family in Physiology and Pathology. *Physiological Reviews* 88(3), pp. 841–886.

Mantovani, A., Sica, A., Sozzani, S., Allavena, P., Vecchi, A. and Locati, M. 2004. The chemokine system in diverse forms of macrophage activation and polarization. *Trends in immunology* 25(12), pp. 677–686.

Marshall, J.S. 2004. Mast-cell responses to pathogens. *Nature reviews. Immunology* 4(10), pp. 787–799.

Martinez, F.O. and Gordon, S. 2014. The M1 and M2 paradigm of macrophage activation: time for reassessment. *F1000prime reports* 6, p. 13.

Martín-Fontecha, A., Thomsen, L.L., Brett, S., Gerard, C., Lipp, M., Lanzavecchia, A. and Sallusto, F. 2004. Induced recruitment of NK cells to lymph nodes provides IFN-γ for TH1 priming. *Nature immunology* 5(12), pp. 1260–1265.

McClanahan, F., Hanna, B., Miller, S., Clear, A.J., Lichter, P., Gribben, J.G. and Seiffert, M. 2015. PD-L1 checkpoint blockade prevents immune dysfunction and leukemia development in a mouse model of chronic lymphocytic leukemia. *Blood* 126(2), pp. 203–211.

Medzhitov, R. 2007. Recognition of microorganisms and activation of the immune response. *Nature* 449(7164), pp. 819–826.

Meeusen, E.N. and Balic, A. 2000. Do eosinophils have a role in the killing of helminth parasites? *Parasitology today (Personal ed.)* 16(3), pp. 95–101.

Mills, C.D. 2015. Anatomy of a discovery: m1 and m2 macrophages. *Frontiers in immunology*.

Mittag, D., Proietto, A.I., Loudovaris, T., Mannering, S.I., Vremec, D., Shortman, K., Wu, L., et al. 2011. Human dendritic cell subsets from spleen and blood are similar in phenotype and function but modified by donor health status. *Journal of immunology (Baltimore, Md. : 1950)* 186(11), pp. 6207–6217.

Monserrat, J., Sánchez, M.Á., de Paz, R., Díaz, D., Mur, S., Reyes, E., Prieto, A., et al. 2013. Distinctive patterns of naïve/memory subset distribution and cytokine expression in CD4 T lymphocytes in ZAP-70 B-chronic lymphocytic patients. *Cytometry Part A* 86(1), pp. 32–43.

Morandi, B., Bougras, G., Muller, W.A., Ferlazzo, G. and Münz, C. 2006. NK cells of human secondary lymphoid tissues enhance T cell polarizationvia IFN-γ secretion. *European journal of immunology* 36(9), pp. 2394–2400.

Moreno, C. and Montserrat, E. 2008. New prognostic markers in chronic lymphocytic leukemia. *Blood Reviews* 22(4), pp. 211–219.

Morita, C.T., Beckman, E.M., Bukowski, J.F., Tanaka, Y., Band, H., Bloom, B.R., Golan, D.E., et al. 1995. Direct presentation of nonpeptide prenyl pyrophosphate antigens to human γδ T cells. *Immunity* 3(4), pp. 495–507.

Moser, M. and Murphy, K.M. 2000. Dendritic cell regulation of TH1-TH2 development. *Nature immunology* 1(3), pp. 199–205.

Motta, M., Wierda, W.G. and Ferrajoli, A. 2009. Chronic lymphocytic leukemia. *Cancer* 115(17), pp. 3830–3841.

Murray, P.J. and Wynn, T.A. 2011. Protective and pathogenic functions of macrophage subsets. *Nature reviews. Immunology* 11(11), pp. 723–737.

Nackiewicz, D., Dan, M., He, W., Kim, R., Salmi, A., Rütti, S., Westwell-Roper, C., et al. 2014. TLR2/6 and TLR4-activated macrophages contribute to islet inflammation and impair beta cell insulin gene expression via IL-1 and IL-6. *AGE* 57(8), pp. 1645–1654.

NICE 2015a. TA343. Obinutuzumab in combination with chlorambucil for untreated chronic lymphocytic leukaemia.

NICE 2015b. TA344. Ofatumumab in combination with chlorambucil or bendamustine for untreated chronic lymphocytic leukaemia.

Niu, N. and Qin, X. 2013. New insights into IL-7 signaling pathways during early and late T cell development. *Cellular & molecular immunology* 10(3), pp. 187–189.

Nosari, A. 2012. Infectious complications in chronic lymphocytic leukemia. *Mediterranean journal of hematology and infectious diseases* 4(1), p. e2012070.

Novák, M., Procházka, V., Turcsányi, P. and Papajík, T. 2015. Numbers of CD8+PD-1+ and CD4+PD-1+ Cells in Peripheral Blood of Patients with Chronic Lymphocytic Leukemia Are Independent of Binet Stage and Are Significantly Higher Compared to Healthy Volunteers. *Acta haematologica* 134(4), pp. 208–214.

Nunes, C., Wong, R., Mason, M., Fegan, C., Man, S. and Pepper, C. 2012. Expansion of a CD8(+)PD-1(+) replicative senescence phenotype in early stage CLL patients is associated with inverted CD4:CD8 ratios and disease progression. *Clinical cancer research : an official journal of*

the American Association for Cancer Research 18(3), pp. 678–687.

Nutt, S.L., Hodgkin, P.D., Tarlinton, D.M. and Corcoran, L.M. 2015. The generation of antibody-secreting plasma cells. *Nature reviews. Immunology* 15(3), pp. 160–171.

Oltval, Z.N., Milliman, C.L. and Korsmeyer, S.J. 1993. Bcl-2 heterodimerizes in vivo with a conserved homolog, Bax, that accelerates programed cell death. *Cell* 74(4), pp. 609–619.

Orchard, J.A., Ibbotson, R.E., Davis, Z., Wiestner, A., Rosenwald, A., Thomas, P.W., Hamblin, T.J., et al. 2004. ZAP-70 expression and prognosis in chronic lymphocytic leukaemia. *Lancet (London, England)* 363(9403), pp. 105–111.

Os, A., Bürgler, S., Ribes, A.P., Funderud, A., Wang, D., Thompson, K.M., Tjønnfjord, G.E., et al. 2013. Chronic Lymphocytic Leukemia Cells Are Activated and Proliferate in Response to Specific T Helper Cells. *CellReports* 4(3), pp. 566–577.

Oscier, D., Dearden, C., Eren, E., Erem, E., Fegan, C., Follows, G., Hillmen, P., et al. 2012. Guidelines on the diagnosis, investigation and management of chronic lymphocytic leukaemia. *British journal of haematology* 159(5), pp. 541–564.

Oscier, D., Fegan, C., Hillmen, P., Illidge, T., Johnson, S., Maguire, P., Matutes, E., et al. 2004. Guidelines on the diagnosis and management of chronic lymphocytic leukaemia. *British journal of haematology* 125(3), pp. 294–317.

Panossian, L.A., Porter, V.R., Valenzuela, H.F., Zhu, X., Reback, E., Masterman, D., Cummings, J.L., et al. 2003. Telomere shortening in T cells correlates with Alzheimer's disease status. *Neurobiology of aging* 24(1), pp. 77–84.

Park, H., Li, Z., Yang, X.O., Chang, S.H., Nurieva, R., Wang, Y.-H., Wang, Y., et al. 2005. A distinct lineage of CD4 T cells regulates tissue inflammation by producing interleukin 17. *Nature immunology* 6(11), pp. 1133–1141.

Parry, H.M., Damery, S., Hudson, C., Maurer, M.J., Cerhan, J.R., Pachnio, A., Begum, J., et al. 2016. Cytomegalovirus infection does not impact on survival or time to first treatment in patients with chronic lymphocytic leukemia. *American journal of hematology* 91(8), pp. 776–781.

Pawelec, G. and Gouttefangeas, C. 2013. T-cell dysregulation caused by chronic antigenic stress: the role of CMV in immunosenescence? *Aging clinical and experimental research* 18(2), pp. 171–173.

Pålsson-McDermott, E.M. and O'Neill, L.A.J. 2004. Signal transduction by the lipopolysaccharide receptor, Toll-like receptor-4. *Immunology* 113(2), pp. 153–162.

Pillai, S. and Cariappa, A. 2009. The follicular versus marginal zone B lymphocyte cell fate decision. *Nature reviews. Immunology* 9(11), pp. 767–777.

Pillay, J., Braber, den, I., Vrisekoop, N., Kwast, L.M., de Boer, R.J., Borghans, J.A.M., Tesselaar, K., et al. 2010. In vivo labeling with 2H2O reveals a human neutrophil lifespan of 5.4 days. *Blood* 116(4), pp. 625–627.

Piper, K.P., Karanth, M., McLarnon, A., Kalk, E., Khan, N., Murray, J., Pratt, G., et al. 2011. Chronic lymphocytic leukaemia cells drive the global CD4+ T cell repertoire towards a regulatory phenotype and leads to the accumulation of CD4+ forkhead box P3+ T cells. *Clinical and experimental immunology* 166(2), pp. 154–163.

Pita-Lopez, M.L., Gayoso, I., DelaRosa, O., Casado, J.G., Alonso, C., Muñoz-Gomariz, E., Tarazona, R., et al. 2009. Effect of ageing on CMV-specific CD8 T cells from CMV seropositive healthy donors. *Immunity & Ageing* 6, p. 11.

Plunkett, F.J., Soares, M.V., Annels, N., Hislop, A., Ivory, K., Lowdell, M., Salmon, M., et al. 2001. The flow cytometric analysis of telomere length in antigen-specific CD8+ T cells during acute Epstein-Barr virus infection. *Blood* 97(3), pp. 700–707.

Porter, D.L., Hwang, W.T., Frey, N.V., Lacey, S.F., Shaw, P.A., Loren, A.W., Bagg, A., et al. 2015. Chimeric antigen receptor T cells persist and induce sustained remissions in relapsed refractory chronic lymphocytic leukemia. *Science Translational Medicine* 7(303), pp. 303ra139–303ra139.

Porter, D.L., Kalos, M., Frey, N.V., Grupp, S.A., Loren, A.W., Jemision, C., Gilmore, J., et al. 2013. Randomized, Phase II Dose Optimization Study Of Chimeric Antigen Receptor Modified T Cells Directed Against CD19 (CTL019) In Patients With Relapsed, Refractory CLL. *Blood* 122(21), pp. 873–873.

Pourgheysari, B., Bruton, R., Parry, H., Billingham, L., Fegan, C., Murray, J. and Moss, P. 2010. The number of cytomegalovirus-specific CD4+ T cells is markedly expanded in patients with B-cell chronic lymphocytic leukemia and determines the total CD4+ T-cell repertoire. *Blood* 116(16), pp. 2968–2974.

Pourgheysari, B., Khan, N., Best, D., Bruton, R., Nayak, L. and Moss, P.A.H. 2007. The cytomegalovirus-specific CD4+ T-cell response expands with age and markedly alters the CD4+ T-cell repertoire. *Journal of virology* 81(14), pp. 7759–7765.

Puiggros, A., Blanco, G. and Espinet, B. 2014. Genetic Abnormalities in Chronic Lymphocytic Leukemia: Where We Are and Where We Go. *BioMed Research International* 2014(21), pp. 1–13.

Pulko, V., Davies, J.S., Martinez, C., Lanteri, M.C., Busch, M.P., Diamond, M.S., Knox, K., et al. 2016. Human memory T cells with a naive phenotype accumulate with aging and respond to persistent viruses. *Nature Publishing Group* 17(8), pp. 966–975.

Qian, Y., Ding, T., Wei, L., Cao, S. and Yang, L. 2016. Shorter telomere length of T-cells in peripheral blood of patients with lung cancer. *OncoTargets and therapy* 9, pp. 2675–2682.

Raa, te, G.D., Pascutti, M.F., Garcia-Vallejo, J.J., Reinen, E., Remmerswaal, E.B.M., Berge, ten, I.J.M., van Lier, R.A.W., et al. 2014. CMV-specific CD8+ T-cell function is not impaired in chronic lymphocytic leukemia. *Blood* 123(5), pp. 717–724.

Rai, K.R., Sawitsky, A., Cronkite, E.P., Chanana, A.D., Levy, R.N. and Pasternack, B.S. 1975. Clinical staging of chronic lymphocytic leukemia. *Blood* 46(2), pp. 219–234.

Rampazzo, E., Bonaldi, L., Trentin, L., Visco, C., Keppel, S., Giunco, S., Frezzato, F., et al. 2011. Telomere length and telomerase levels delineate subgroups of B-cell chronic lymphocytic leukemia with different biological characteristics and clinical outcomes. *Haematologica* 97(1), pp. 56–63.

Ramsay, A.G., Johnson, A.J., Lee, A.M., Görgün, G., Le Dieu, R., Blum, W., Byrd, J.C., et al. 2008. Chronic lymphocytic leukemia T cells show impaired immunological synapse formation that can be reversed with an immunomodulating drug. *The Journal of clinical investigation* 118(7), pp. 2427–2437.

Read, S., Mauze, S., Asseman, C., Bean, A., Coffman, R. and Powrie, F. 1998. CD38+ CD45RBlow CD4+ T cells: a population of T cells with immune regulatory activities in vitro. *European journal of immunology* 28(11), pp. 3435–3447.

Redaelli, A., Laskin, B.L., Stephens, J.M., Botteman, M.F. and Pashos, C.L. 2004. The clinical and epidemiological burden of chronic lymphocytic leukaemia. *European journal of cancer care* 13(3), pp. 279–287.

Ribeiro, D., Melão, A. and Barata, J.T. 2012. IL-7R-mediated signaling in T-cell acute

lymphoblastic leukemia. *Advances in biological regulation*.

Riches, J.C., Davies, J.K., McClanahan, F., Fatah, R., Iqbal, S., Agrawal, S., Ramsay, A.G., et al. 2013. T cells from CLL patients exhibit features of T-cell exhaustion but retain capacity for cytokine production. *Blood* 121(9), pp. 1612–1621.

Roederer, M., Nozzi, J.L. and Nason, M.C. 2011. SPICE: exploration and analysis of post-cytometric complex multivariate datasets. *Cytometry. Part A : the journal of the International Society for Analytical Cytology* 79(2), pp. 167–174.

Rosenblum, M.D., Way, S.S. and Abbas, A.K. 2015. Regulatory T cell memory. *Nature reviews. Immunology* 16(2), pp. 90–101.

Rosén, A., Bergh, A.-C., Gogok, P., Evaldsson, C., Myhrinder, A.L., Hellqvist, E., Rasul, A., et al. 2012. Lymphoblastoid cell line with B1 cell characteristics established from a chronic lymphocytic leukemia clone by in vitro EBV infection. *Oncoimmunology* 1(1), pp. 18–27.

Rossmann, E.D., Lewin, N., Jeddi-Tehrani, M., Osterborg, A. and Mellstedt, H. 2002. Intracellular T cell cytokines in patients with B cell chronic lymphocytic leukaemia (B-CLL). *European Journal of Haematology* 68(5), pp. 299–306.

Rufer, N., Dragowska, W., Thornbury, G., Roosnek, E. and Lansdorp, P.M. 1998. Telomere length dynamics in human lymphocyte subpopulations measured by flow cytometry. *Nature biotechnology* 16(8), pp. 743–747.

Rusak, M., Eljaszewicz, A., Bołkun, Ł., Łuksza, E., Łapuć, I., Piszcz, J., Singh, P., et al. 2015. Prognostic significance of PD-1 expression on peripheral blood CD4+ T cells in patients with newly diagnosed chronic lymphocytic leukemia. *Polskie Archiwum Medycyny Wewnętrznej* 125(7-8), pp. 553–559.

Russ, B.E., Prier, J.E., Rao, S. and Turner, S.J. 2013. T cell immunity as a tool for studying epigenetic regulation of cellular differentiation. *Frontiers in genetics* 4, p. 218.

Sakaguchi, S., Sakaguchi, N., Asano, M., Itoh, M. and Toda, M. 1995. Immunologic self-tolerance maintained by activated T cells expressing IL-2 receptor alpha-chains (CD25). Breakdown of a single mechanism of self-tolerance causes various autoimmune diseases. *Journal of immunology (Baltimore, Md. : 1950)* 155(3), pp. 1151–1164.

Salgado, F.J., Lojo, J., Fernández-Alonso, C.M., Viñuela, J., Cordero, O.J. and Nogueira, M. 2002. Interleukin-dependent modulation of HLA-DR expression on CD4and CD8 activated T cells. *Immunology and cell biology* 80(2), pp. 138–147.

Sallusto, F., Geginat, J. and Lanzavecchia, A. 2004. Central memory and effector memory T cell subsets: function, generation, and maintenance. *Annual review of immunology* 22, pp. 745–763.

Sancho, D., Joffre, O.P., Keller, A.M., Rogers, N.C., Martínez, D., Hernanz-Falcón, P., Rosewell, I., et al. 2009. Identification of a dendritic cell receptor that couples sensing of necrosis to immunity. *Nature* 458(7240), pp. 899–903.

Sanders, J.L. and Newman, A.B. 2013. Telomere length in epidemiology: a biomarker of aging, age-related disease, both, or neither? *Epidemiologic reviews* 35, pp. 112–131.

Sanin, D.E. and Pearce, E.J. 2016. The cell identity of cytotoxic T lymphocytes. *Nature immunology*.

Sarkar, S., Kalia, V., Haining, W.N., Konieczny, B.T., Subramaniam, S. and Ahmed, R. 2008. Functional and genomic profiling of effector CD8 T cell subsets with distinct memory fates. *The Journal of experimental medicine* 205(3), pp. 625–640.

Sato, E., Olson, S.H., Ahn, J., Bundy, B., Nishikawa, H., Qian, F., Jungbluth, A.A., et al. 2005. Intraepithelial CD8+ tumor-infiltrating lymphocytes and a high CD8+/regulatory T cell ratio are associated with favorable prognosis in ovarian cancer. *Proceedings of the National Academy of Sciences* 102(51), pp. 18538–18543.

Sauce, D., Almeida, J.R., Larsen, M., Haro, L., Autran, B., Freeman, G.J. and Appay, V. 2007. PD-1 expression on human CD8 T cells depends on both state of differentiation and activation status. *AIDS (London, England)* 21(15), pp. 2005–2013.

Schauber, J. and Gallo, R.L. 2009. Antimicrobial peptides and the skin immune defense system. *The Journal of allergy and clinical immunology* 124(3 Suppl 2), pp. R13–8.

Schroers, R., Griesinger, F., Trümper, L., Haase, D., Kulle, B., Klein-Hitpass, L., Sellmann, L., et al. 2005. Combined analysis of ZAP-70 and CD38 expression as a predictor of disease progression in B-cell chronic lymphocytic leukemia. *Leukemia* 19(5), pp. 750–758.

Seddiki, N., Santner-Nanan, B., Martinson, J., Zaunders, J., Sasson, S., Landay, A., Solomon, M., et al. 2006. Expression of interleukin (IL)-2 and IL-7 receptors discriminates between human regulatory and activated T cells. *The Journal of experimental medicine* 203(7), pp. 1693–1700.

Seder, R.A. and Ahmed, R. 2003. Similarities and differences in CD4+ and CD8+ effector and memory T cell generation. *Nature immunology* 4(9), pp. 835–842.

Serrano, D., Monteiro, J., Allen, S.L., Kolitz, J., Schulman, P., Lichtman, S.M., Buchbinder, A., et al. 1997. Clonal expansion within the CD4+CD57+ and CD8+CD57+ T cell subsets in chronic lymphocytic leukemia. *Journal of immunology (Baltimore, Md. : 1950)* 158(3), pp. 1482–1489.

Shao, L., Wood, C.G., Zhang, D., Tannir, N.M., Matin, S., Dinney, C.P. and Wu, X. 2007. Telomere dysfunction in peripheral lymphocytes as a potential predisposition factor for renal cancer. *The Journal of urology* 178(4 Pt 1), pp. 1492–1496.

Shi, C. and Pamer, E.G. 2011. Monocyte recruitment during infection and inflammation. *Nature reviews. Immunology* 11(11), pp. 762–774.

Silva-Santos, B., Serre, K. and Norell, H. 2015. γδ T cells in cancer. *Nature reviews. Immunology* 15(11), pp. 683–691.

Smyth, M.J., Dunn, G.P. and Schreiber, R.D. 2006. Cancer immunosurveillance and immunoediting: the roles of immunity in suppressing tumor development and shaping tumor immunogenicity. *Advances in immunology* 90, pp. 1–50.

Sprent, J. and Surh, C.D. 2002. T cell memory. *Annual review of immunology* 20, pp. 551–579.

Steinman, R.M. and Hemmi, H. 2006. Dendritic cells: translating innate to adaptive immunity. *Current topics in microbiology and immunology* 311, pp. 17–58.

Strioga, M., Pasukoniene, V. and Characiejus, D. 2011. CD8+ CD28− and CD8+ CD57+ T cells and their role in health and disease. *Immunology* 134(1), pp. 17–32.

Suvas, S., Singh, V., Sahdev, S., Vohra, H. and Agrewala, J.N. 2002. Distinct role of CD80 and CD86 in the regulation of the activation of B cell and B cell lymphoma. *The Journal of biological chemistry* 277(10), pp. 7766–7775.

Svenson, U., Grönlund, E., Söderström, I., Sitaram, R.T., Ljungberg, B. and Roos, G. 2013. Telomere length in relation to immunological parameters in patients with renal cell carcinoma. *PloS one* 8(2), p. e55543.

Svenson, U., Nordfjäll, K., Stegmayr, B., Manjer, J., Nilsson, P., Tavelin, B., Henriksson, R., et al.

2008. Breast cancer survival is associated with telomere length in peripheral blood cells. *Cancer research* 68(10), pp. 3618–3623.

Swain, S.L., Weinberg, A.D., English, M. and Huston, G. 1990. IL-4 directs the development of Th2-like helper effectors. *Journal of immunology (Baltimore, Md. : 1950)* 145(11), pp. 3796–3806.

Tanaka, Y., Morita, C.T., Tanaka, Y., Nieves, E., Brenner, M.B. and Bloom, B.R. 1995. Natural and synthetic non-peptide antigens recognized by human gamma delta T cells. *Nature* 375(6527), pp. 155–158.

Tenca, C., Merlo, A., Zarcone, D., Saverino, D., Bruno, S., De Santanna, A., Ramarli, D., et al. 2003. Death of T cell precursors in the human thymus: a role for CD38. *International immunology* 15(9), pp. 1105–1116.

Thimme, R., Appay, V., Koschella, M., Panther, E., Roth, E., Hislop, A.D., Rickinson, A.B., et al. 2005. Increased expression of the NK cell receptor KLRG1 by virus-specific CD8 T cells during persistent antigen stimulation. *Journal of virology* 79(18), pp. 12112–12116.

Thomas, M.D., Srivastava, B. and Allman, D. 2006. Regulation of peripheral B cell maturation. *CELLULAR IMMUNOLOGY* 239(2), pp. 92–102.

Tinhofer, I., Rubenzer, G., Holler, C., Hofstaetter, E., Stoecher, M., Egle, A., Steurer, M., et al. 2006. Expression levels of CD38 in T cells predict course of disease in male patients with B-chronic lymphocytic leukemia. *Blood* 108(9), pp. 2950–2956.

Tinhofer, I., Weiss, L., Gassner, F., Rubenzer, G., Holler, C. and Greil, R. 2009. Difference in the relative distribution of CD4+ T-cell subsets in B-CLL with mutated and unmutated immunoglobulin (Ig) VH genes: implication for the course of disease. *Journal of immunotherapy (Hagerstown, Md. : 1997)* 32(3), pp. 302–309.

Tötterman, T.H., Carlsson, M., Simonsson, B., Bengtsson, M. and Nilsson, K. 1989. T-cell activation and subset patterns are altered in B-CLL and correlate with the stage of the disease. *Blood* 74(2), pp. 786–792.

Trautmann, L., Janbazian, L., Chomont, N., Said, E.A., Gimmig, S., Bessette, B., Boulassel, M.-R., et al. 2006. Upregulation of PD-1 expression on HIV-specific CD8+ T cells leads to reversible immune dysfunction. *Nature medicine* 12(10), pp. 1198–1202.

Valenzuela, H.F. and Effros, R.B. 2002. Divergent telomerase and CD28 expression patterns in human CD4 and CD8 T cells following repeated encounters with the same antigenic stimulus. *Clinical immunology (Orlando, Fla.)* 105(2), pp. 117–125.

Van den Hove, L.E., Vandenberghe, P., Van Gool, S.W., Ceuppens, J.L., Demuynck, H., Verhoef, G.E. and Boogaerts, M.A. 1998. Peripheral blood lymphocyte subset shifts in patients with untreated hematological tumors: evidence for systemic activation of the T cell compartment. *Leukemia Research* 22(2), pp. 175–184.

Vantourout, P. and Hayday, A. 2013. Six-of-the-best: unique contributions of γδ T cells to immunology. *Nature reviews. Immunology* 13(2), pp. 88–100.

Vasto, S., Colonna-Romano, G., Larbi, A., Wikby, A., Caruso, C. and Pawelec, G. 2007. Role of persistent CMV infection in configuring T cell immunity in the elderly. *Immunity & Ageing* 4, p. 2.

Vaziri, H., Dragowska, W., Allsopp, R.C., Thomas, T.E., Harley, C.B. and Lansdorp, P.M. 1994. Evidence for a mitotic clock in human hematopoietic stem cells: loss of telomeric DNA with age. *Proceedings of the National Academy of Sciences of the United States of America* 91(21), pp. 9857–9860.

Villadangos, J.A. and Schnorrer, P. 2007. Intrinsic and cooperative antigen-presenting functions of dendritic-cell subsets in vivo. *Nature reviews. Immunology* 7(7), pp. 543–555.

Visco, C., Falisi, E., Young, K.H., Pascarella, M., Perbellini, O., Carli, G., Novella, E., et al. 2015. Epstein-Barr virus DNA load in chronic lymphocytic leukemia is an independent predictor of clinical course and survival. *Oncotarget* 6(21), pp. 18653–18663.

Vivier, E., Tomasello, E., Baratin, M., Walzer, T. and Ugolini, S. 2008. Functions of natural killer cells. *Nature immunology* 9(5), pp. 503–510.

Voehringer, D., Koschella, M. and Pircher, H. 2002. Lack of proliferative capacity of human effector and memory T cells expressing killer cell lectinlike receptor G1 (KLRG1). *Blood* 100(10), pp. 3698–3702.

Wallin, R.P.A., Screpanti, V., Michaëlsson, J., Grandien, A. and Ljunggren, H.-G. 2003. Regulation of perforin-independent NK cell-mediated cytotoxicity. *European journal of immunology* 33(10), pp. 2727–2735.

Wardlaw, A.J., Brightling, C., Green, R., Woltmann, G. and Pavord, I. 2000. Eosinophils in asthma and other allergic diseases. *British medical bulletin* 56(4), pp. 985–1003.

Wartha, F., Beiter, K., Normark, S. and Henriques-Normark, B. 2007. Neutrophil extracellular traps: casting the NET over pathogenesis. *Current Opinion in Microbiology* 10(1), pp. 52–56.

Weaver, C.T., Harrington, L.E., Mangan, P.R., Gavrieli, M. and Murphy, K.M. 2006. Th17: An Effector CD4 T Cell Lineage with Regulatory T Cell Ties. *Immunity* 24(6), pp. 677–688.

Weiskopf, D., Weinberger, B. and Grubeck-Loebenstein, B. 2009. The aging of the immune system. *Transplant international : official journal of the European Society for Organ Transplantation* 22(11), pp. 1041–1050.

Weng, N.P., Levine, B.L., June, C.H. and Hodes, R.J. 1995. Human naive and memory T lymphocytes differ in telomeric length and replicative potential. *Proceedings of the National Academy of Sciences of the United States of America* 92(24), pp. 11091–11094.

Weng, N.P., Levine, B.L., June, C.H. and Hodes, R.J. 1996. Regulated expression of telomerase activity in human T lymphocyte development and activation. *The Journal of experimental medicine* 183(6), pp. 2471–2479.

Whelan, C.A., Willoughby, R. and McCann, S.R. 1982. T-cell function in chronic lymphocytic leukaemia. *British journal of haematology* 50(1), pp. 111–121.

Wherry, E.J. and Ahmed, R. 2004. Memory CD8 T-Cell Differentiation during Viral Infection. *Journal of virology* 78(11), pp. 5535–5545.

Willeit, P., Willeit, J., Brandstätter, A., Ehrlenbach, S., Mayr, A., Gasperi, A., Weger, S., et al. 2010. Cellular aging reflected by leukocyte telomere length predicts advanced atherosclerosis and cardiovascular disease risk. *Arteriosclerosis, thrombosis, and vascular biology* 30(8), pp. 1649–1656.

Wojciechowski, S., Tripathi, P., Bourdeau, T., Acero, L., Grimes, H.L., Katz, J.D., Finkelman, F.D., et al. 2007. Bim/Bcl-2 balance is critical for maintaining naive and memory T cell homeostasis. *The Journal of experimental medicine* 204(7), pp. 1665–1675.

Woo, E.Y., Yeh, H., Chu, C.S., Schlienger, K., Carroll, R.G., Riley, J.L., Kaiser, L.R., et al. 2002. Cutting edge: Regulatory T cells from lung cancer patients directly inhibit autologous T cell proliferation. *Journal of immunology (Baltimore, Md. : 1950)* 168(9), pp. 4272–4276.

Wood, P. 2006. *Understanding Immunology*. Second Edition. Pearson Education Limited.

Wu, X., Amos, C.I., Zhu, Y., Zhao, H., Grossman, B.H., Shay, J.W., Luo, S., et al. 2003. Telomere dysfunction: a potential cancer predisposition factor. *Journal of the National Cancer Institute* 95(16), pp. 1211–1218.

Yang, Z.-Z., Grote, D.M., Ziesmer, S.C., Xiu, B., Novak, A.J. and Ansell, S.M. 2015. PD-1 expression defines two distinct T-cell sub-populations in follicular lymphoma that differentially impact patient survival. *Blood cancer journal* 5, p. e281.

Ye, F., Turner, J. and Flaño, E. 2012. Contribution of pulmonary KLRG1(high) and KLRG1(low) CD8 T cells to effector and memory responses during influenza virus infection. *Journal of immunology (Baltimore, Md. : 1950)* 189(11), pp. 5206–5211.

Yuzefpolskiy, Y., Baumann, F.M., Kalia, V. and Sarkar, S. 2015. Early CD8 T-cell memory precursors and terminal effectors exhibit equipotent in vivo degranulation. *Cellular & molecular immunology* 12(4), pp. 400–408.

Zenz, T., Mertens, D., Küppers, R., Döhner, H. and Stilgenbauer, S. 2010. From pathogenesis to treatment of chronic lymphocytic leukaemia. *Nature reviews. Cancer* 10(1), pp. 37–50.

Zhang, L., Conejo-Garcia, J.R., Katsaros, D., Gimotty, P.A., Massobrio, M., Regnani, G., Makrigiannakis, A., et al. 2003. Intratumoral T cells, recurrence, and survival in epithelial ovarian cancer. *New England Journal of Medicine* 348(3), pp. 203–213.

Zhang, N. and Bevan, M.J. 2011. CD8+ T Cells: Foot Soldiers of the Immune System. *Immunity* 35(2), pp. 161–168.

Zhou, J., Shen, X., Huang, J., Hodes, R.J., Rosenberg, S.A. and Robbins, P.F. 2005. Telomere length of transferred lymphocytes correlates with in vivo persistence and tumor regression in melanoma patients receiving cell transfer therapy. *Journal of immunology (Baltimore, Md. : 1950)* 175(10), pp. 7046–7052.

Zhu, J., Yamane, H. and Paul, W.E. 2010. Differentiation of Effector CD4 T Cell Populations *. *Annual review of immunology* 28(1), pp. 445–489.

Zucchetto, A., Sonego, P., Degan, M., Bomben, R., Dal Bo, M., Russo, S., Attadia, V., et al. 2005. Surface-antigen expression profiling (SEP) in B-cell chronic lymphocytic leukemia (B-CLL): Identification of markers with prognostic relevance. *Journal of Immunological Methods* 305(1), pp. 20–32.